INVESTIGATING THE THYMUS MEDULLA'S CONTROL OF THE POST-SELECTION MATURATION AND THYMIC EGRESS OF CD4 AND CD8 THYMOCYTES

By

Callum Michael Moore

A thesis submitted to the University of Birmingham

For the Degree of DOCTOR OF PHILOSOPHY

Institute of Immunity and Immunotherapy

College of Medical and Dental Science

University of Birmingham

September 2022

ABSTRACT

Following thymic selection, thymocytes progress through a controlled maturation as they gain functional maturity before undergoing an ordered egress into the periphery. Whilst this maturation and egress is well defined in conventional $CD4^+$ (cSP4) thymocytes, such definition in conventional $CD8^+$ (cSP8) thymocytes is lacking. Using extensive flow cytometric analysis, we looked to bring the definition of these processes in cSP8 in line with that of cSP4, before using this to explore how they are impacted by structural changes in the thymus following bone marrow transplantation (BMT). Through defining true cSP8 for the first time we were able to compare cSP4 and cSP8 side-by-side and show that both lineages use the conveyor-belt mechanism of maturation and egress. Furthermore, we identified the earliest SP8-committed thymocytes within a subpopulation of double-positive (DP) thymocytes. We utilised analysis of this population to highlight thymic selection as the determining factor is the CD4:CD8 T-cell ratio. Our analysis of BMT mice showed that the failure in mTEC recovery in this model does not disrupt the maturation of cSP4 or cSP8 thymocytes. In addition, we report a failure in recovery in thymic portal endothelial cells (TPEC), that control thymic entry and egress, resulting in an accumulation of mature thymocytes in BMT mice. Finally, we were able to utilise our comprehensive definition of cSP8 thymocyte to isolate and analyse the non-conventional $Eomes^+$ SP8 population, highlighting their difference from the cSP8 population and the importance of removing this population from conventional analysis. Collectively our findings define a new approach to defining cSP8 thymocytes, subsequently highlighting a new role for thymic selection in establishing the CD4:CD8 ratio. Additionally we describe further failures in recovery following BMT, with a loss of TPEC rather than mTEC limiting thymic egress.

ACKNOWLEDGMENTS

Firstly, I would like to express my gratitude to my supervisor, Professor Graham Anderson, for his support and guidance throughout my PhD. This comes particularly through a prolonged period of remote work and study, a new challenge to all of us. Without him, to achieve this PhD would not have been possible, let alone with the level of enjoyment I have had throughout my time here. I would also like to thank my second supervisor, Dr. Will Jenkinson, for all his of help throughout the last 3 years in helping me to complete my PhD.

I am also incredibly thankful to all the members of the Anderson Lab for their warm welcome, continued support (and patience!), and constant supply of cookies, cakes, and food recommendations around Birmingham. It has been a pleasure to be a member of the lab over the last 3 years thanks to everyone's kindness and friendliness, and I will really miss being a part of it.

I also owe a sincere thank you my family, my friends, and Amanda for supporting me throughout my study. Their unwavering love and encouragement have pushed me through the tough times and allowed me to enjoy the good times, all with them by my side. I would like to reserve a final, special thank you for John. Without his drive to see me achieve I would have struggled to believe I had the capability to undertake and complete a PhD.

TABLE OF CONTENTS

LIST OF FIGURES

LIST OF TABLES

LIST OF ABBREVIATIONS

3PP	Third Pharyngeal Pouch
Aire	Autoimmune Regulator
APC	Antigen Presenting Cells
Bcl	B-Cell Lymphoma
Bcl-xL	B-Cell Lymphoma Extra-Large
BMC	Bone Marrow Chimeras
BMSU	Biomedical Services Unit
BMT	Bone Marrow Transplantation
CCL	C-C Chemokine Ligand
CCR	C-C Chemokine Receptor
CD	Cluster of Differentiation
cDC	Conventional DC
CDR	Complementary Determining Region
Cld	Claudin
CLIP	MHC Class II – Associated Invariant Chain Peptide
CLP	Common Lymphoid Progenitors
cSP	Conventional Single Positive
cTEC	Cortical TEC
CTLA-4	Cytotoxic T-Lymphocyte-Associated Protein 4
CXCL	CXC Chemokine Ligand
CXCR	CXC Chemokine Receptor
DC	Dendritic Cells
DLL4	Delta-Like Ligand 4
DN	Double-Negative
DP	Double Positive
Eomes	Eomesodermin
ERK	Extracellular Signal Regulated Kinase
ETP	Early T-Cell Progenitors
eYFP	Enhanced Yellow Fluorescent Protein
FCS	Fetal Calf Serum
Fezf2	FEZ Family Zinc Finger 2
FOXN1	Forkhead-Box N1
Foxo1	Forkhead Box Protein O1
Foxp3	Forkhead Box P3
Gcm2	Glial Cell Missing 2
GFP	Green Fluorescent Protein
HSC	Haematopoietic Stem-Cells

I.V.	Intravenous
ICAM-1	Intracellular Adhesion Molecule 1
ICOS	Inducible T-Cell Costimulatory
ICOS-L	ICOS-Ligand
IEL	Intraepithelial Lymphocytes
IFNγ	Interferon-γ
Ig	Immunoglobulin
IL	Interleukin
iNKT	Invariant Natural Killer Cells
iTreg	Inducible Treg
Klf-2	Krüpple-Like Factor 2
Lpp3	Lipid Phosphate Phosphatase 3
LSK	Lineage$^-$ Sca1$^+$ C-Kit$^+$
LTi	Lymphoid Tissue Induced Cell
LTβR	Lymphotoxic β Receptor
M1	Mature 1
M2	Mature 2
MAC	Membrane Attack Complex
MAPK	Mitogen Activated Protein Kinase
MFI	Mean Fluorescence Intensity
MHC	Major Histocompatibility Complex
MPP	Multipotential Progenitor Cells
mTEC	Medullary TEC
NF-κB	Nuclear Factor Kappa-Light-Chain-Enhancer
nTreg	Natural Treg
OPG	Osteoprotegerin
PAMP	Pathogen-Associated Molecular Pattern
PBS	Phosphate Buffered Saline
pDC	Plasmacytoid DC
PDL1/2	Programmed Death Ligand 1/2
PRR	Pathogen Recognition Receptors
PSLG-1	P-Selectin Glycoprotein Ligand 1
PVS	Perivascular Space
RAG	Recombinase Activating Gene
RANK	Receptor Activator For NF-κB
RF10	Rpmi-1640 Hepes Medium
RORγT	Retinoic Acid-Related Orphan Receptor-γT
RTE	Recent Thymic Emigrants
S1P	Sphingosine-1-Phosphate

S1PR1	Sphingosine-1-Phosphate Receptor 1
SCF	Stem Cell Factor
SCZ	Subcapsular Zone
SM	Semi-Mature
SP	Single Positive
Sphk	Sphingosine Kinase
SPL	S1P Lyase
SSEA-1	Stage-Specific Embryonic Antigen 1
TAP	Transporter Associated with Antigen Processing
TCR	T-Cell Receptor
TEC	Thymic Epithelial Cells
TEPC	Thymic Epithelial Progenitor Cells
Tfh	T Follicular Helper Cells
TGFβ	Transforming Growth Factor β
Th	T-Helper
TLR	Toll-Like Receptor
TNC	Thymic Nurse Cells
TNFRSF	Tumour Necrosis Factor Receptor Super Family
TPEC	Thymic Portal Endothelial Cells
TRA	Tissue Restricted Antigen
Treg	Regulatory T-Cells
TSP	Thymus Settling Progenitors
TSSP	Thymus Specific Serine Protease
VCAM-1	Vascular Cellular Adhesion Molecule 1
VDJ	Variable Diverse Joining
WT	Wildtype
γc	Common Cytokine Receptor γ Chain

CHAPTER 1: INTRODUCTION

1.1 OVERVIEW OF THE IMMUNE SYSTEM

1.1.1 The Innate and Adaptive Immune System

The body is constantly exposed to threats of external pathogens invading and causing harm. It is the role of the immune system to protect the host from these pathogens and the damage they may cause. The key role of the immune system in the maintenance of health and ultimately survival is shown by the vast array of immunodeficiencies whereby the host immune response is insufficient, with individuals succumbing to severe infection and disease manifestation (1). In keeping with the crucial role of the immune system, it exhibits enormous complexity within the host, with numerous different cell types and humoral factors working in conjunction to orchestrate an immune response that limits the effect of invading pathogens. The immune system can be separated into the initial, rapid, and nonspecific innate immune response, and the longer-lived, targeted adaptive immune response.

The innate immune system is the frontline of defence following bypass of the physical barriers to foreign pathogens and is antigen non-specific, recognising and subsequently responding to highly conserved factors associated with pathogenic infection. These pathogen-associated molecular patterns (PAMPs) are recognised through germline-encoded pathogen recognition receptors (PRRs) (2,3) expressed within the innate immune system. These PRRs are expressed both by cells involved in the innate response, and as soluble receptors within the plasma. Cells of the innate immune system such as macrophages, neutrophils, and dendritic cells (DC), as well as cells found at host barriers such as epithelial cells, can express certain PRRs on their surface to detect external PAMPs, as well as internally to detect cytosolic

pathogens that have invaded the cell (3,4). A number of different receptor families exist; the Toll-like receptor (TLR) family has members expressed both externally, such as TLR 5 to detect bacterial flagellin (5), and internally, such as TLR 7 which recognises viral single stranded RNA (6,7).

The major component of soluble PRR recognition of PAMPs comes from the complement system. The complement system consists of a series of soluble proteins that are triggered in a cascade following recognition of PAMPs. Upon recognition, one of three different pathways can be triggered, the classical, alternative, or mannose binding pathways, all of which ultimately lead to the activation of a C3 convertase which promotes the lysis of C3 protein into C3a and C3b (8). Activation of the complement cascade can lead to the opsonisation of the recognised pathogen, promoting it for phagocytosis by macrophages and neutrophils, as well as the formation of membrane attack complexes (MACs), which actively perforate the membrane of pathogens leading to death (8,9).

Both recognition by soluble PRRs in the blood plasma and those expressed by cells promote inflammation, release of both cytokines and chemokines, and recruitment of innate immune cells to the site of infection (10). The recruitment of neutrophils precedes their phagocytosis of pathogens and cytotoxic granule release to promote death of pathogens (4,11,12). Macrophages also carry out this phagocytosis following recruitment, whilst also clearing apoptotic cells and further releasing inflammatory cytokines (4,12). Whilst these innate cell types play key roles in the initial response following the recognition of foreign pathogen, a fundamental part of the innate immune response is carried out by DC. Following their recruitment, DC have the ability to process antigen from the specific invading pathogen and present this to cells of the

adaptive immune system, inducing a specific adaptive immune response to the infection (13).

The adaptive immune response is antigen-specific, crafting targeted immune responses through the generation and optimisation of receptors specific for a single given antigen expressed by the infecting pathogen. Two specific cell subsets comprise the adaptive arm, B-lymphocytes (B-cells) and T-lymphocytes (T-cells). As this thesis centres on $\alpha\beta$T-cells and, more specifically their development, they will be discussed further in *1.1.2.*

B-cells develop from haematopoietic stem cells in the bone marrow. They develop though a series of populations in the bone marrow before gaining maturity and leaving the bone marrow as naïve B-cells (14). Key to this development in the acquisition of the B-cell receptor that enables recognition and response to specific pathogenic antigens the B-cells will encounter. In a process that underpins the wide-ranging variance and specificity of the adaptive immune response to a given antigen, these cells will undergo rearrangement of the variable, diverse, and joining (VDJ) regions of the immunoglobulin (Ig) genes, supported by the recombinase activating genes 1 and 2 (Rag1/2). This rearrangement allows for the diverse repertoire of surface expressed Ig between developing B-cells, recognising a multitude of potential antigens (14,15). B-cells leave the bone marrow expressing surface IgM, a defining feature of immature B-cells, before migrating to the secondary lymphoid organs in the periphery where they gain expression of IgD (16). Here they may encounter their cognate antigen where upon interaction, B-cells have two fates. They may transition to marginal zone B-cells and then further to short-lived plasma cells capable of producing IgM or IgD antibody specific to the invading pathogen (14). Alternatively, B-cells can enter germinal centres

following interaction with their antigen, whereby interacting with T-cells they undergo class switching to generate plasma cells capable of producing IgA, IgE, or IgG (17,18). As well as changes to the constant region and subsequently class switching of expressed Ig, the antigen-recognising heavy and light chains undergo somatic hypermutation, with nucleotide substitutions altering and optimising affinity for cognate antigen in a process known as affinity maturation (19). As well as both generating a targeted response to specific pathogens and optimising this through the course of the infection, the B-cell response also generates long-lived memory B-cells that produce high-affinity antibodies as a result of affinity maturation in germinal centres and can persist for years without re-exposure to cognate antigen (14). The ability of the adaptive immune response to maintain immunological memory is another key feature of this arm of the immune system that allows for a strong and targeted immune response upon re-exposure to pathogens.

1.1.2 T-Cells

1.1.2.1 $\alpha\beta$ and $\gamma\delta$ T-cells

Just as the expression of a unique B-cell receptor is key to a B-cell's role within adaptive immunity, the T-cell receptor (TCR) is a defining property of the T-cell. The recombination of the TCR to give a vast array of antigen specificity within the T-cell pool mirrors that described in B-cells, however the development of T-cells, and subsequently the rearrangement and selection of appropriate TCR, occurs within its own organ distinct for this role: the thymus. T-cell development in the thymus is the focus of this thesis, and hence will be discussed further in *1.3.*

As the TCR defines T-cells as such, two different types of TCR and therefore T-cell exist: the αβ T-cell and the γδ T-cell. Whilst both are produced by and exported from the thymus, diverging early in development (20), αβ T-cells represent a more conventional lineage, circulating in the periphery and secondary lymphoid organs where they encounter cognate antigen. These cells require antigen to be processed and presented by specialised antigen presenting cells (APC) such as DC (21). αβ T-cells will express either the cluster of differentiation 4 (CD4) or CD8 co-receptor alongside their TCR, allowing the recognition of antigen presented on either major histocompatibility complex (MHC) class II or MHC class I respectively. Interaction with their cognate antigen alongside stimulation by the presenting cell leads to naïve αβ T-cells differentiating into their effector subsets and contributing towards the adaptive immune response to a given pathogen (22).

γδ T-cells however display clear differences in their function and role in the immune system. Rather than circulating through peripheral lymphoid tissues, γδ T-cells appear to remain resident in the epithelium of tissues such as the skin following their thymic export (23). Furthermore, γδ T-cell appear to not recognise processed and MHC-presented antigen, instead recognising a multitude of antigens associated with stress, damage, and infection (24). As such, γδ T-cells appear to exhibit a role more similar to cells of the innate immune system compared to the αβ T-cells they are produced alongside. Owing to their more conventional role within the adaptive immune system, focus from herein will be on αβ T-cells.

1.1.2.2 CD4 T-cells

Their expression of the CD4 co-receptor means that CD4 T-cells can interact with antigen expressed in the context of MHC class II via their TCR. This antigen is processed and presented in conjunction with costimulatory molecules CD80 and CD86 by specific APC such as DC and macrophages which interact with CD28 on the surface of T-cells (21), discussed further in *1.2.2.4,* to promote the maturation of naïve CD4 T-cells into one of a number of different T-helper (Th) subsets. These different subsets have different roles within the immune response, with the differentiation to each subset requiring specific cytokine release by the APC with which the T-cell is interacting (25).

Th1 cells are involved in cellular immunity, supporting the killing of intracellular pathogens through the production of interferon-γ (IFNγ) and its effect on cells of the innate immune system such as macrophages (26,27). Differentiation towards the Th1 lineage comes through response to IL-12 during stimulation leading to the upregulation of the key transcription factor in Th1 cells, T-bet (28). GATA-3, promoted through response to interleukin-4 (IL-4), is the key transcription factor in Th2 cells, with this leading to further production of IL-4 alongside IL-5 and IL-13. This cytokine production acts to promote Ig class-switching and B-cell proliferation, therefore targeting extracellular pathogens (26,29,30). Th17 differentiation is controlled by the transcription factor retinoic acid-related orphan receptor-γt (RORγT) following exposure to both transforming growth factor β (TGFβ) and IL-6 and promotes the production of IL-17, again supporting the killing of extracellular pathogens such as bacteria and fungi (25,31). Whilst Th1, Th2, and Th17 CD4 T-cells have direct roles in their support of pathogen killing, T follicular helper cells (Tfh) represent T helper cells with a significantly different role. Controlled by the expression of the transcription factor B-

cell lymphoma-6 (Bcl-6), Tfh are crucial for the formation of germinal centres, expressing CXC chemokine receptor 5 (CXCR5) to localise to the B-cell follicles of the lymph nodes (32), these cells interact with B-cells responding to infection and promote class switching, somatic hypermutation, and differentiation to plasma and memory cells as described previously (25,33).

The above Th subsets represent conventional CD4 T-cells, but non-conventional regulatory T-cells (Treg) also exist within the CD4 T-cell compartment. These cells act to supress autoreactive immune responses, ensuring the immune response is regulated and reducing the risk of half to self (34). Natural Treg (nTreg) are produced in the thymus alongside conventional CD4 T-cells. The generation of nTreg is covered further in *1.3.4*, however a key point about their development is their higher affinity for self-peptide than conventional T-cells (35). As well as nTreg exported from the thymus, inducible Treg (iTreg) can be formed in the periphery from naïve CD4 T-cells receiving TCR signals alongside TGFβ (36). Forkhead box P3 (Foxp3) is the key transcription factor controlling Treg, shaping these cells to be suited for their regulatory function (37). Similar to Th subsets, Treg produce specific cytokines, however these take the form of inhibitory cytokines TGFβ and IL-10 (38,39). Treg also express cytotoxic T-lymphocyte-associated protein 4 (CTLA-4), a surface receptor that acts to downregulate CD80/86 on antigen presenting DC to inhibit costimulation of naïve T-cells, dampening the T-cell response (40). Finally, expression of granzyme B allows Treg to directly interact with T-cells in the periphery, promoting cell death to again further limit the T-cell response (41). The key role of Treg in the immune response is shown in scurfy mice lacking functional Foxp3. These mice widespread autoimmunity and organ infiltrations, ultimately leading to early death (42).

1.1.2.3 CD8 T-cells

CD8 expression on cytotoxic CD8 T-cells allows for interaction with antigens presented by MHC class I molecules. MHC I is expressed on the surface of all cells, presenting antigen that is processed intracellularly (43). As such, CD8 T-cells have a key role in the viral immune response following intracellular infection, and are also involved in anti-tumour immunity (44), responding to their antigen with cytolytic activity such as the release of granzymes and perforin to induce cell death (45). Ability to respond to antigen in the periphery relies on the CD8 T-cell being activated, requiring antigen-presentation combined with costimulation provided by APC in secondary lymphoid tissues, also leading to expansion of the activated cells (46,47). Crucially, effector function in CD8 T-cells also requires further signalling via IL-12, with cells provided with antigen and costimulation activating and expanding but lacking cytolytic activity without this third signal (48,49). This effector function is reportedly controlled by the transcription factor *Eomesodermin* (Eomes), whilst T-bet is also thought to be involved, perhaps explaining the capability of these cells to produce IFNγ similar to Th1 CD4 T-cells (49,50).

The expression of Eomes leads to a complex diversity within the CD8 T-cell pool. Whilst Eomes expression can define both effector and memory T-cells that have been activated following response to their antigen, a population of memory-like CD8 T-cells exist that express Eomes without encountering their cognate antigen (51). Furthermore, these are seen to exist in different environments, being present in response to lymphopenia, in response to increased IL-4 availability, and in the steady state (51). Recent work has looked to define a portion of these Eomes expressing CD8 T-cell that are newly produced from the thymus, attributing their presence to specific

TCR repertoires that drive their divergence from conventional CD8 T-cell development (52). Despite this, the role of these cells remains poorly understood, perhaps owing to the lack of clear markers to separate these non-conventional populations, however it does show and interesting level of heterogeneity within the CD8 T-cell pool, similar to that seen within CD4 T-cells.

1.1.2.4 Antigen Presentation and Co-stimulation

The activation and effector function of T-cells in response to antigen relies upon interaction between the TCR and antigen exclusively in the context of MHC/peptide complexes. To enable this process, cells will process antigen to be presented by surface MHC molecules for T-cells to recognise and respond to. MHC class I presents endogenous antigens that are subsequently recognised by CD8 T-cells, whilst MHC class II is expressed exclusively by specialist APC capable of endocytosing and presenting exogenous proteins to CD4 T-cells (53).

MHC I presentation of endogenous peptides makes these molecules key in the response to viral infection where the virus invades the host cell, as well as in anti-tumour immunity, and as such MHC I is expressed on the surface of most cells in the body (43). These peptides are formed from proteasomal degradation of endogenous proteins and can associate with transporter associated with antigen processing (TAP), a peptide transporter located within the endoplasmic reticulum, which will form the peptide loading complex (54). In conjunction with other chaperone proteins within this complex, TAP transports peptides towards empty MHC I molecules to be presented on the surface of cells (55). Whilst CD8 T-cells will be tolerised in the thymus and hence do not respond to endogenous self-peptide/MHC complexes presented on the

surface of cells (56), non-self-peptides, such as that from a virus infecting the host cell, will be recognised and induce a cytotoxic response against the infected cell.

Unlike MHC I, MHC II is exclusively expressed by specialised immune cells such as macrophages, B-cells, and DC, and specialises in the presentation of exogenous proteins that are subsequently degraded by the endosomal pathway (53,55). MHC II molecules are formed in the endoplasmic reticulum where they will bind the invariant chain, acting as a pseudopeptide associating with the peptide-binding groove (55). As this complex moves through the endosomal pathway, the invariant chain is cleaved by various proteases to leave the MHC class II – associated invariant chain peptide (CLIP) bound to MHC II, which is in turn displaced by higher affinity antigenic peptides processed and present in the same endosomal compartment (57). Peptide-bound MHC II molecules are then transported to be expressed on the cell surface to present antigen to CD4 T-cells.

As well as being crucial in guiding and targeting T-cell effector function, antigen presentation is also key in the activation of both CD4 and CD8 T-cells. Specialised APC such as DC will circulate to secondary lymphoid organs such as the lymph nodes to present antigen to naïve T-cells. DC will process and present exogenous antigen on MHC II to activate naïve CD4 T-cells in the same way as previously discussed, however specialised presentation is required to present MHC I peptide that is not endogenous to the cell. Cross-presentation is a specialised function of DC that allows for antigen from other cells at a site of infection to be taken up and presented in the context of MHC I to naïve CD8 T-cells, activating them in the immune response (53,58). As well as supplying MHC/peptide complexes to engage naïve T-cells' TCR, APC such as DC also provide co-stimulatory signals crucial for naïve T-cell activation. DC

express a number of different co-stimulatory molecules, instructing the T-cell response following recognition of the cognate antigen by TCR. The key interaction in this process is CD80/86 on DC interacting with CD28 expressed on T-cells promoting IL-2 production which in turn supports the survival and expansion of the T-cells (59). Other molecules have roles in this process, such as inducible T-cell costimulatory (ICOS) expressed by CD4 T-cells binding to ICOS-ligand (ICOS-L) on DC, again promoting survival and proliferation (60). Not always is this a positive stimulation of the naïve T-cells, with factors such as programmed death ligand 1/2 (PDL1/2) on DC interacting with PD1 on T-cells and promoting apoptosis, inhibiting a response (61). Interestingly, other co-stimulatory factors can show both a stimulatory and tolerising effect. CD40 and OX40L are expressed by DC, binding to CD40L and OX40 respectively on T-cells, with this resulting in either a promotion of a T-cell response through survival and expansion, or impairing the T-cell response and hence having a tolerogenic effect (62).

1.2 THE THYMUS AS THE SITE OF T-CELL DEVELOPMENT

1.2.1 Thymus Organogenesis

The thymus is a primary lymphoid organ that is responsible for the development of T-cells, controlling this process from the recruitment of progenitor cells, selection of those capable of recognising foreign MHC-bound antigen, supporting their maturation through a series of developmental stages, and ultimately through to their export into the periphery. Interestingly, despite its clear importance in establishing a key arm of the immune system, its function was only relatively recently understood by studies in the 1960's showing that mice thymectomised after birth had a reduced survival rate owing to a loss of lymphocyte numbers (63).

The thymus itself develops from the third pharyngeal pouch (3PP) formed from the endoderm around E9.5 - E10.5 (64,65). These epithelial cells are surrounded by mesenchymal cells derived from the neural crest which produce soluble factors that guide the formation of the 3PP (66). As well as the thymus, the parathyroid emerges from the 3PP, being separated by glial cell missing 2 (Gcm2) marking the development of the parathyroid and forkhead-box n1 (FOXN1) being expressed in thymic organogenesis (67). FOXN1 plays a crucial role in the development of thymic epithelial cells (TEC), specialised stromal cells found within the thymus that are fundamental to the support of T-cell development (65). Fitting with their key role, the development and further specialisation of different TEC subsets is complex and will be discussed further in *1.2.2* and *1.2.3*.

1.2.2 Thymic Epithelial Cell Development

TEC are subdivided into two further cell types, cortical TEC (cTEC) and medullary TEC (mTEC), representing specialised subsets that possess separate roles in the sequential development of thymocytes. Whilst cTEC support the early stages of thymic T-cell development, including progenitor recruitment and positive selection during TCR-rearrangement, mTEC support the induction of tolerance and the maturation and egress of thymocytes in the latter stages of their development (68). These differing but crucial roles for both cell types is underpinned by both a differential expression pattern that makes these cells specialised for their role, and also the distinct anatomical regions within the thymus that both can be found, with clear cortical and medullary regions constituting the three-dimensional structure of the thymus (69,70).

Despite the fundamental differences between cTEC and mTEC, their emergence during embryonic development of the thymus has long been considered to result from the same population of cells. Initial evidence of these bipotent progenitors came from two separate studies. Work by *Rossi et al.* used microinjection of $CD45^{-}EpCAM1^{+}$ TEC from an E12 enhanced yellow fluorescent protein (eYFP) mouse into host thymi to show that these single cells were capable of producing both cTEC and mTEC progeny, with $eYFP^{+}$ cells of both lineages being present (71). Presence of a bipotent progenitor was also shown using a mouse model containing a revertible null allele of Foxn1 in Foxn1-deficient *nude* mice. Induction of the Foxn1 allele showed that single cells were capable of forming structures containing both cTEC and mTEC (72). Interestingly, the model used in the latter study both shows that differentiation of bipotent progenitors into their progeny requires Foxn1 (72), but also that Foxn1-independent thymic epithelial progenitor cells (TEPC) exist upstream. Foxn1 has long been known to be crucial to the development of TEC, with *nude* mice lacking this gene failing to develop a functional thymus capable of supporting T-cell development, and instead displaying a basic thymic rudiment (73). Despite this, these Foxn1-independent TEPC are present within the thymic rudiment of *nude* mice, although they are not capable of further differentiation (72–75). This therefore exhibits further steps in the generation of TEC, dependant on different factors.

Following the identification of a bipotent TEC progenitor, further work looked to define the distinct phenotype of these cells within the thymus. As candidates for these progenitors emerged, it became clear that cells expressing typical cTEC markers have the potential to differentiate into both mature cTEC and mTEC. β5t is a proteasomal subunit encoded by the *Psmb11* gene, and expressed by cTEC and not mTEC (76),

however use of a β5t-Cre green fluorescent protein (GFP) -reporter mouse showed that mTEC emerge from a population of β5t expressing cells (77). Similarly, expression of IL-7 has been shown to be restricted to cTEC, but was capable of giving rise to mTEC, albeit seemingly through an IL-7$^-$ intermediary population (78). A sequential progression from a cTEC-like expression pattern towards mTEC was shown using cTEC associated marker CD205, and mTEC associated CD40 (68,79). Isolation of CD205$^+$ cells from the embryonic thymus showed that they were able to generate both cTEC and mTEC *in vivo*, with typical markers of cTEC, including CD205, and mTEC being restricted to the cortical and medullary regions respectively. Furthermore, during embryonic thymic development these CD205$^+$ CD40$^-$ cTEC phenotype cells were shown to generate CD205$^-$ CD40$^+$ mTEC via a CD205$^+$ CD40$^+$ intermediate population (79). The combination of the above studies therefore lead to a 'serial progression' model of TEC development, where bipotent progenitor cells with a cTEC phenotype can continue towards commitment to the cTEC lineage, or divert towards an mTEC phenotype through differential gene expression (80).

Whilst the existence of a cTEC-like bipotent TEC progenitor was clearly shown to be present in embryonic thymus development, such a population capable of producing and maintaining cTEC and mTEC progeny does not appear to be present in the adult thymus. Two studies utilising an inducible β5t-Cre reporter model throughout different stages in embryonic, neonatal, and adult mouse development showed that whilst embryonic and early neonatal β5t expressing cells are capable of giving rise to cTEC and mTEC, the capability of these cells to produce mTEC progeny reduced with age (81,82). Although this data showed that adult β5t expressing cells do not contain a bipotent progenitor, it also highlighted that almost all adult mTEC originate from

embryonic β5t expressing bipotent progenitors (81). As such, this suggests a role for unipotent cTEC and mTEC progenitors that are responsible for the maintenance of adult TEC populations.

Unipotent mTEC progenitors have been identified by the expression of cell adhesion molecules claudin 3 and 4 (Cld3/4) (83) and later additionally by stage-specific embryonic antigen 1 (SSEA-1) (84). Identified in the embryonic thymus, these cells were shown to be a self-renewing population with the capacity to generate mTEC progeny capable of carrying out their role in the induction of thymic tolerance (84). Whilst these cells can be identified in the adult thymus, they do not possess the progenitor potential capable of producing mature mTECs like their embryonic counterparts (83,84). Importantly these progenitors were present independent of both Foxn1, and Relb, a part of the nuclear factor kappa-light-chain-enhancer (NF-κB) complex that is shown to be crucial for the development of mTEC in the thymus medulla (85,86). This study also identified a further subset of mTEC progenitors downstream of Cld3/4^{+} SSEA-1^{+} cells identified through expression of tumour necrosis factor receptor super family (TNFRSF) member receptor activator for NF-κB (RANK) and loss of SSEA-1 expression, with this population reliant of Relb and therefore NF-κB signalling (85). Identification of this population interestingly displays requirement for different factors throughout mTEC ontogeny, but also the importance of TNFRSF signalling for the development of mature, functional mTEC populations (87).

TNSFRSF signalling in mTEC is provided by a number of different receptors and their ligands ultimately resulting in the activation of NF-κB signalling required for development (68). RANK/RANK-L interactions comprise one of these key

combinations required for mTEC development, with RANK being expressed on mTEC populations and precursors (85). RANK-L is provided by a number of different cell types, with $CD4^+$ $CD3^-$ lymphoid tissue induced cell (LTi) expression of RANK-L being crucial to the embryonic development of mTEC (88), whilst a number of different thymocyte populations are the main suppliers of RANK-L that contribute to continued mTEC development in the adult thymus (89). The provision of RANK signalling to promote mTEC development by those thymocytes also receiving developmental cues from thymic stroma is termed 'thymic cross-talk' and is also displayed by non-conventional Treg (90) and CD1d-restricted invariant natural killer cells (iNKT) (91) produced by the thymus, alongside immature conventional populations (89). Working cooperatively with RANK, CD40, another TNFRSF member, is also key to mTEC development. Mice deficient for both RANK and CD40 display severe medullary disorganisation and breakdown in tolerance (92), with RANK signalling subsequently being shown to be key for CD40 upregulation before CD40-L is provided through conventional thymocyte cross-talk (90). Also working in conjunction with RANK is osteoprotegerin (OPG). Acting as a decoy receptor for RANK-L, OPG negatively regulates mTEC numbers, shown by larger medullary areas and increased mTEC populations in $Opg^{-/-}$ mice (89,93).

Lymphotoxin β receptor (LTβR) is another TNFRSF member heavily linked with mTEC development, shown by a loss of mTEC numbers, medullary organisation, and capability to support the induction of tolerance and thymocyte egress in germline knockout (KO) mice (94). Specific deletion of LTβR on TEC showed that it is LTβR expression by TEC themselves that control the numbers of mTEC (95,96), with $Cld3/4^+$ $SSEA\text{-}1^+$ mTEC progenitors also being reduced, suggesting a requirement of LTβR

upstream of this progenitor (95). Importantly, although loss of LTβR significantly disrupts the mTEC compartment, expression of the autoimmune regulator (Aire), key to the induction of tolerance by mTEC, is unaffected (97). Subsequently, the breakdown in tolerance seen with a loss of LTβR is reported to be attributed to a loss of thymic DC, also key to negative selection in the thymus (96). Similarly, failure to effectively support thymic egress in LTβR deficient mice was shown to be independent of LTβR expression by TEC, and instead a result of LTβR loss on endothelial cells (98), discussed in more detail in *1.3.6*. Together, while this shows a key role of mTEC-expressed LTβR in the regulation of mTEC numbers, T-cell development can function effectively in its absence.

Although Cld3/4^{+} SSEA-1^{+} mTEC progenitors identified in embryo fail to replicate their progenitor capacity in the adult thymus, precursor-product relationships between subpopulations within adult mTEC have been reported. MHCII^{LO} CD80^{LO} mTEC^{LO} populations give rise to MHCII^{HI} CD80^{HI} mTEC^{HI}, which contain Aire^{+} cells (99). Despite a clear progression from mTEC^{LO} to mTEC^{HI}, problems exist with defining the former solely as an adult mTEC progenitor. Within mTEC^{LO} exist mature, functional cells expressing CCL21, crucial for intrathymic transport of cells (100,101). Furthermore, a complex relationship between mTEC^{LO} and mTEC^{HI} exists, with a subpopulation of mTEC^{LO} being shown to previously express Aire, hence originating from the mTEC^{HI} population (102). More recently, these post-Aire mTEC^{LO} are now known to contain a unique subset of mTEC termed thymic tuft cells, implicated in the availability of IL-4 within the thymus (103). This is thought to be through their provision of IL-25 to iNKT2 which produce IL-4 (104), exhibiting another functional role for mTEC^{LO}. Interestingly, this study also showed a key role for LTβR in the regulation of this heterogenous

mTEC^{LO} population (104). The heterogeneity seen within the mTEC^{LO} population combined with the complex relationship with mTEC^{HI} therefore suggests a model where mTEC^{LO} contain both mature functional cells, and a small population of progenitor cells capable of producing mTEC^{HI}.

The complex process of TEC development forms a highly specialised and compartmentalised thymus capable of supporting the development of T-cells. Whilst this development will be covered from a T-cell perspective in *1.3*, the unique specialisations of both cTEC and mTEC that make them uniquely fit for their purpose are vast and important to understanding the interplay between thymocytes and the thymic stroma.

1.2.3 The Role of TEC

1.2.3.1 Cortical Thymic Epithelial Cells

cTEC are defined within the thymus as Ly51^{+} CD205^{+} MHC II^{+} TEC and represent one of the first stromal populations that developing thymocytes encounter. As such, they have key roles in supporting the development of early thymocytes, namely the recruitment on bone-marrow derived thymocyte progenitors, and induction of thymocyte positive selection.

The initial role of cTEC in T-cell development is the recruitment of thymocyte progenitors to seed the thymus and undergo thymopoiesis. This recruitment is controlled through the expression of chemokines CXC chemokine ligand 12 (CXCL12) and CC chemokine ligand 25 (CCL25), with these interacting with their respective receptors CXCR4 and CC chemokine receptor 9 (CCR9) on the surface of thymocyte progenitors (105–107). Loss of such interactions through ablation of either the cTEC-

expressed ligand, or progenitor-expressed receptor, results in a reduction of progenitor recruitment (105,106). Interestingly, although CCL21 is not expressed by cTEC, recruitment via its receptor, CCR7 expressed on progenitor cells is also shown to be key for this progenitor recruitment (106,108). cTEC are proposed to still regulate this process, however, with expression of atypical chemokine receptor CCRL1, which is reported to regulate the bioavailability of CCL19, CCL21, and CCL25 within the thymus (109) as it does in the lymph nodes (110,111), although this has been shown to not simply be through levels of protein (112). Following the recruitment of progenitors, cTEC also provide these cells with signals promoting their survival and commitment to the T-cell lineage through expression of a series of factors including delta-like ligand 4 (DLL4) (113), stem cell factor (SCF) (114), and IL-7 (115). As well as its role in recruitment, CXCL12-CXCR4 interactions provided by cTEC have also been shown to be key to the survival of early developing thymocytes, with cells failing to progress through key stages in development when the interaction was blocked (116).

Following this process, cTEC carry out perhaps their most distinct function, positive selection. Described further in *1.3.2.2*, summarised this process involves the selective survival of those thymocytes with a rearranged TCR capable of recognising MHC/peptide complexes, and therefore fit-for-purpose (56). These peptide/MHC complexes are presented on the surface of cTEC, with these cells having specialised features involved in antigen processing and presentation to optimise positive selection. One such feature is the expression of β5t, exclusive to cTEC enabling the formation of the thymoproteosome (117,118). This specialised proteosome enables cTEC to produce a unique array of MHC I restricted antigens capable of selecting $CD8^+$ thymocytes with low affinity to antigen. Its importance in the positive selection of CD8

thymocytes is shown through its loss resulting in a significant reduction of CD8 but not CD4 T-cells (117,118). Furthermore, those CD8 T-cells capable of passing through positive selection in the absence of β5t showed a limited TCR repertoire and functionality (118,119).

Similarly, cTEC possess specific proteases that aid the processing of peptides for MHC II expression to positively select CD4 thymocytes. Cathepsin L (120), and thymus specific serine protease (TSSP) (121,122) are both exclusively expressed by cTEC. It has been shown that separate loss of either cathepsin L or TSSP leads to a reduction in selection of CD4 thymocytes (120,122). cTEC also have the ability to break down and express intracellular proteins through their unique expression of the autophagosome (123). This autophagy was shown to be key to the selection of CD4 thymocytes, with *Atg*$^{-/-}$ mice, lacking the autophagosome, showing a reduction in CD4 thymocyte selection in MHC II restricted models (123). The lack of autophagy also resulted in autoimmunity in these mice (123), suggesting a role for this process in tolerising thymocytes to the self-peptide it generates. As well as the processing of MHC II antigen, cTEC regulate their expression of MHC II molecules through the expression of CD83. CD83 antagonises MARCH 8, an E3 ubiquitin ligase involved in controlling MHC II trafficking, therefore regulating the level of MHC II expression by cTEC (124). As such, loss of CD83 results in reduced CD4 thymocyte selection and ultimately fewer CD4 T-cells (124).

Further supporting the positive selection of thymocytes are multi-cellular complexes known as thymic nurse cells (TNC). Initially described as cells that engulf developing thymocytes, thought to support their development and potentially both positive and negative selection (125), more recent studies have characterised these cells as a

subset of cTEC (126). These cTEC are capable of engulfing and interacting with numerous double positive (DP) thymocytes undergoing positive selection, and promote secondary TCRα rearrangements, supporting and optimising the positive selection of these thymocytes (126).

1.2.3.2 Medullary Thymic Epithelial Cells

Within the TEC population, mTEC are defined as Ly-51^{-}UEA1^{+} cells. As described earlier, subpopulations termed mTEC^{LO} and mTEC^{HI} based on expression of CD80 and MHCII exist further within this population. This phenotypic heterogeneity within mTEC is underpinned by key functional heterogeneity between these subpopulations. The characteristic function of mTEC is the induction of tolerance through negative selection of self-reactive thymocytes and generation of nTreg, although mTEC also possess different roles within the thymus medulla, such as recruitment and organisation of medullary thymocyte populations, all of which are key to orchestrating the latter stages of T-cell development.

For developing thymocytes to encounter mTEC and undergo negative selection, mTEC must recruit them from the cortex where their early development takes place. A subset of CCL21^{+} mTEC^{LO} are responsible for this, promoting the corticomedullary translocation of positively selected CCR7-expressing thymocytes (100,101,127). The importance of CCL21 expression and the subsequent interaction with its thymocyte-expressed receptor is shown with loss of either CCL21 or CCR7 resulting in a failure of thymocytes to enter the medulla (100,127). More recently, the importance of CCL21^{+} mTEC mediated translocation to negative selection in the medulla was emphasised,

showing signs of autoimmunity with absence of CCL21 and a failure in negative selection in CCL21$^{-/-}$ RIP m-OVA mice (127).

mTEC also have the vital role of inducing tolerance during thymocyte development, promoting generation of nTreg and subjecting cells to negative selection. This process is covered further in *1.3.4*, and essentially involves the screening of developing thymocytes' TCR against an array of self-antigens to remove self-reactive thymocytes (56). The ability of mTEC carry out this screening is made possible by their unique expression of tissue restricted antigen (TRA), a variety of peptides otherwise confined to specific peripheral tissues (128,129). Effective negative selection covering all peripheral antigens that T-cells may encounter is achieved through what has been described as a 'mosaic' expression (130), with up to 90% of all TRA genes expressed by mTEC (129), but any given antigen only being expressed by around 2% of mTEC (131). TRA expression by mTEC was first shown to be controlled by the transcription factor Aire within the mTEC^{HI} subset, with mice lacking this gene showing severe autoimmune disease (132,133). Accordingly, the human autoimmune disease APECED is also shown to be resulting from a loss of Aire expression (133,134). Aire is thought to work in combination with protein deacetylase Sirt-1 which promotes deacetylation of Aire allowing for its promotion and transcription of target genes (135). Whilst a number of genes are referred to as Aire-dependant, Aire-independent TRA are also expressed by mTEC (136), with the transcription factor FEZ family zinc finger 2 (Fezf2) reported to have a role in TRA expression beyond Aire (137). Fezf2 can be expressed by mTEC in conjunction with, or separate from Aire, shown to work co-operatively but non-redundantly, as loss of Fezf2 also leads to autoimmunity (96,137).

Whilst having key roles in the localisation and negative selection of thymocytes, mTEC also interact with other cell types in the medulla to regulate medullary processes. The recently identified $mTEC^{LO}$ subset of thymic tuft cells described earlier have been shown to be key in supplying IL-25 to thymic iNKT2 (104). NKT2 are known to be key providers of IL-4 within the thymus, and as such a loss of tuft cells has shown to affect populations regulated by IL-4 in the thymus, such as the presence of $Eomes^{+}$ SP8 (103), and activation status of intrathymic DC (104). Furthermore, mTEC are also shown to directly control the localisation of thymic DC within the medulla through expression of XCL1 (138). XCL1 expression was shown to be restricted to $Aire^{+}$ $mTEC^{HI}$, and its loss was shown to result in a failure of DC to accumulate in medullary areas, a loss of nTreg production, and ultimately autoimmunity (138), exhibiting another mechanism by which $Aire^{+}$ mTEC regulate thymic tolerance.

1.2.4 Dendritic Cells

Alongside the epithelial populations, also abundant within the thymus medulla, and working cooperatively with TEC populations are DC. Within these DC lie three subpopulations which can be subdivided into two groups: intrathymic DC consisting of conventional DC-1 (cDC-1), and extrathymic DC that are recruited to the thymus, made up of cDC-2 and plasmacytoid DC (pDC) (139,140).

cDC-1 represent the population of DC that emerge from and remain resident within the thymus. As such it was initially proposed that these cells develop from the same precursor population that is responsible for developing thymocytes (141). Subsequently, however, it was shown that these two populations are developmentally separate from one another, with fluorescent IL-7 reporter mice labelling thymocytes

but not thymic DC progeny of an upstream IL-7^{+} lymphoid progenitor (142). Instead cDC-1 are shown to arise from the progenitor pre-cDC population. Having previously been described in other lymphoid tissues (143), these pre-cDC have more recently been shown to seed the thymic population of cDC-1, being recruited through thymic CCL21 and pre-cDC expression of CCR7 (144). cDC-1 contribute to the induction of tolerance in the medulla through presentation of TRA to developing thymocytes. Given that DC are not capable of generating TRA in the way that mTEC are, their presentation relies on cross presentation, whereby DC are capable of presenting antigen that is generated by mTEC. The capability of haematopoietic cells resident to the thymus to carry out cross presentation was initially identified through the grafting of OT-I bone marrow into RIP-mOVA mice lacking MHC I expression on mTEC. Despite the fact mTEC could not present MHC I restricted antigen, OT-I thymocytes were deleted, showing that presentation of mTEC derived antigen could be presented by bone marrow-derived cells (145). This was later shown to mainly be carried out through cDC-1, with donor cDC-1 showing to have acquired GFP from host-mTEC, displaying their capability to present mTEC-derived antigens (146). Consistent with their key interplay with mTEC, intrathymic DC also express XCR1, interacting with mTEC-expressed XCL1 to aid localisation and organisation of medullary DC (138).

Both cDC-2 and pDC are peripheral DC that migrate to the thymus carrying peripheral antigen to present within the medulla, increasing the repertoire of antigens by which thymocytes are exposed to (139,147). Their ability to do this has been shown via their ability to thymically present and tolerise thymocytes against antigen they have been exposed to following intravenous (I.V.) injection (139,148), as well as antigen exclusively expressed in peripheral tissue (149). This recruitment by the thymus is

shown to differ between the two DC populations, with cDC-2 migrating to the thymus via CCR2 expression responding to CCL8 expressed around the blood vessels of the thymus (148), and pDC expressing CCR9 and migrating to CCL25 expression in the thymus (147). Interestingly, following TLR signalling pDC were shown to downregulate CCR9, aborting their ability to migrate to the thymus (147). This represents a mechanism that restricts peripheral DC to only present self-antigen they have attained in the periphery, ensuring developing thymocytes are not tolerised to foreign antigen they are designed to target.

1.3 T-CELL DEVELOPMENT IN THE THYMUS

1.3.1 Progenitor Recruitment and $\alpha\beta$ T-Cell Lineage Commitment within the Thymus

Although the thymus is responsible for the development and production of T-cells it does not have the ability to produce its own pool of haematopoietic stem-cells (HSC) from which to generate these T-cells, and therefore requires constant seeding of HSC from the bone marrow (150). The earliest well-defined population of progenitor cells within the thymus are referred to as early T-cell progenitors (ETP), however a progenitor cell that seeds the thymus must exist upstream of these cells. These thymus settling progenitors (TSP) exist in very small numbers within the adult thymus, whilst a number of different lymphoid progenitor cells from the bone marrow further complicate a comprehensive phenotypic definition of these cells (150–152).

Stem-cells within the bone marrow are comprised of a number of different blood-cell lineage progenitors, with the most immature of these being phenotyped as Lineage$^-$ sca1$^+$ c-kit$^+$ (LSK) (153). Within the LSK population lie the self-renewing Flt-3$^-$ HSC

population, and downstream Flt-3^{+} multipotential progenitor cells (MPP) (154). Further, lymphoid restricted progenitors within the bone marrow include Flt-3^{HI} IL-7Rα^{HI} common lymphoid progenitors (CLP) that can give rise to both T and B-cells (155,156). For such cells to be considered progenitors that seed the thymus they must be identifiable in transit within the peripheral blood. Of these progenitors, LSK phenotype cells were the first to be identified in low numbers within the blood and were shown to be heterogenous for Flt-3 expression, indicating this population consisted of both HSC and MPP (157). Despite this identification of circulating HSC within LSK cells, these HSC are known to not be capable of thymus colonisation (158). CLPs have later been defined within peripheral blood (159,160), and subsequent fate-mapping experiments showed that the majority of ETP had previously expressed IL-7Rα (142), characteristic of the CLP population and therefore suggesting progenitors downstream of the previously considered HSC/MPP cells are responsible for seeding.

Despite the difficulty involved with defining a distinct population that supplies the thymus directly from the pool of bone marrow progenitors, the factors controlling their recruitment to, and subsequent colonisation of the thymus are better understood. Progenitors are thought to enter the adult thymus through vessels at the cortico-medullary junction (161). Common adhesion molecule CD44 on progenitor cells was first described to have a role in colonisation through antibody blockade resulting in reduced reconstitution by progenitor cells when introduced I.V., but not intrathymically (I.T.) (162). Similarly, P-selectin glycoprotein ligand 1 (PSLG-1) on progenitors upstream of ETP and its interaction with P-selectin expressed by thymic endothelium have been shown to be crucial for colonisation, with both blockade and total loss of PSLG-1 expression separately causing a loss in progenitor recruitment and resultant

ETP numbers (108,163). LTβR, known to be a key regulator in the development of TEC, was also shown to be directly linked to T-cell progenitor recruitment with LTβR deficient mice showing reduced numbers of ETP (164,165). An LTβR-dependant population of endothelial cells found within the thymus; thymic portal endothelial cells (TPEC) have been shown to regulate entry of progenitor cells to the thymus. This population was shown to be associated with progenitor cells entering the thymus in short-term homing assay experiments, and is also reduced in LTβR KO mice (164), more recently attributed to specific loss of LTβR expression on endothelial cells (98). Provision of LTβR ligands required for these TPEC is thought to come from thymocytes via thymic cross-talk, with TCR$\alpha^{-/-}$ mice lacking such mature thymocytes displaying a reduction in TPEC and subsequently ETP numbers (164). Furthermore, LTβR KO mice also show reduced intracellular adhesion molecule 1 (ICAM-1) and vascular cellular adhesion molecule 1 (VCAM-1) expression (165), both of which have previously been linked with progenitor recruitment with antibody blockade (108). This clearly suggests a role for LTβR in the regulation of specialised endothelial cells involved in recruiting progenitors via cell-adhesion molecules.

Chemokine receptors CCR7, CCR9, and CXCR4 are also required for this process. These chemokine receptors are expressed on progenitors downstream of HSC such as MPP and CLP, being upregulated through these more mature populations (106), and fittingly their respective chemokines, CCL19/21, CCL25, and CXCL12 are known to be expressed within the thymus, particularly the stroma and endothelium (107,166). As such, inhibition of CCR7 (108) and CCR9 (106,158) interaction with these ligands via both knockout and blockade exhibit reduced ETP in mixed bone marrow chimera

models, with double-knockout models resulting in a great loss of thymic seeding and ETP (106). Interestingly, when looking within the embryonic thymus, CCR7, CCR9, CXCR4 triple KO models show a considerably larger loss of ETP than any single knockout, or combination of double knockouts, suggesting a significant amount of redundancy in each chemokine-receptors role in progenitor recruitment (166). Together these studies outline several different molecules and processes involved in progenitor colonisation, and importantly that a combination of these factors is required for efficiency in the earliest stages of T-cell development.

1.3.2 Cortical Thymocyte Development

1.3.2.1 Transition to Double-Positive Thymocytes

ETP are phenotyped within the thymus as $CD4^{-}CD8^{-}$ double-negative (DN) cells. Thymocytes then progress through separately defined DN populations characterised phenotypically by varying CD25 and CD44 expression, but key to this progression are changes in the localisation and functional potential of these cells (167). ETP fall within the earliest $CD25^{-}CD44^{+}$ DN1 population, localised around the corticomedullary junction (167,168), fitting with this being the thymic entry site of T-cell progenitors (161). Interestingly, at this stage of their development the ETP/DN1 population are not restricted to the T-cell lineage, and have the potential to become B-cells, DC, and natural killer (NK) cells (167). Commitment to the DN2 stage is characterised by upregulation of CD25 and involves migration of these cells towards the subcapsular zone (SCZ) of the thymus.

This process was initially thought to be driven by expression of CXCR4 on developing thymocytes interacting with CXCL12 expressed on cTEC owing to a block in

development at the DN1 stage when these interactions were inhibited (105). Subsequent studies have suggested a role for CXCR4 further downstream in early thymocyte development (116,169), however the migration of these early thymocytes and subsequent interactions with cTEC around them remain crucial to their development. The differentiation and proliferation of these cells as they progress are controlled by a number of these interactions, including Notch – DLL4 signalling, IL-7Rα on the surface of thymocytes responding to cTEC-produced IL-7 (113,115), and cTEC membrane bound cKit-ligand SCF interacting with thymocyte cKit (CD117) (114). The latter of these is in keeping with characterisation of further subpopulations within the DN1 population based on CD24 and CD117 expression, with upregulation of CD117 linked to T-cell lineage commitment (170). Similarly, DN2 can be subdivided into DN2a and DN2b, defining the stage at which DC lineage potential is lost (171).

The transition from the DN2 to DN3 stage is shown through downregulation of CD44, but more importantly defines a key process in thymocyte development in TCRβ chain rearrangement (172). Initiated at the DN2 stage, RAG1 and RAG2 promote TCRβ-chain rearrangement through recombination of the VDJ genes, a process which involves random cutting and joining of gene fragments resulting in the generation of a random and unique TCRβ chain (173). This rearrangement and production of the TCRβ chain can be seen as a final commitment step, restricting these cells to exclusively the T-cell lineage. These cells will then undergo β selection whereby the rearranged TCRβ chain forms a 'pre-TCR' with an invariant pre-Tα chain and CD3 signalling components (174). Successful rearrangement of the β chain and hence formation of the pre-TCR results in ligand independent cell signalling (175,176). In addition to pre-TCR complex signalling, the importance of CXCR4 and notch are

reemphasised at this stage, with both further contributing to positive signalling during β-selection, leading to the survival and proliferation of these cells (116,169). Interestingly, it was shown that loss of CXCR4-CXCL12 interaction led to a blockade at the DN3 stage rather than the previously reported DN1 stage (105,169), emphasising the requirement for CXCR4 as a costimulatory molecule allowing progression through β-selection. Failure to successfully rearrange the TCRβ chain will lead to failure to receive such signals, and result in death by apoptosis (177). Furthermore, similar to the DN populations that precede them, DN3 can be phenotypically separated into sequential DN3a and DN3b populations based on upregulation of CD27, with $CD27^{HI}$ DN3b cells showing greater progression to more mature DP thymocyte populations than $CD27^{LO}$ DN3a cells, indicating CD27 as a marker of cells that have entered β-selection (178). DN3b cells will then downregulate CD25 to progress to the final DN4 phenotype, before upregulating both CD4 and CD8 and beginning TCRα rearrangement to become DP thymocytes via an intermediate immature single positive CD8 population, termed iSP8 (167,179).

1.3.2.2 Positive Selection

Thymocytes that pass-through β selection rearrange and upregulate their TCRα chain to form a complete αβTCR expressed on their surface. As discussed previously in part 1.1.2.3, a functional TCR able to recognise self-MHC/peptide complexes is key to the function of mature T-cells in the periphery. As such, positive selection acts as a checkpoint ensuring that only thymocytes with a functional TCR are able to progress further through maturation (180). Key to this process is thymocyte interactions with cTEC and their unique ability to express a variety of self-MHC/peptide complexes as

discussed previously in 1.2.3. To induce such interactions, DP thymocytes translocate back towards the cortex away from the SCZ, where they are highly motile until such interactions with cTEC occur, arresting their movement within the cortex (181,182). When thymocytes successfully interact with self-MHC/peptide complexes via their rearranged TCR, TCR signalling is triggered leading to a downregulation of RAG1/2 genes, stopping further rearrangement (183). This signalling also promotes survival through anti apoptotic factors such as RORγT, T-cell factor-1, and B-cell lymphoma extra-large (Bcl-xL), with a loss of these leading to spontaneous death of DP thymocytes, emphasising their role in maintaining survival and maximising the time allowed for DP thymocytes to be positively selected (184,185). Survival of thymocytes is only induced in those cells that successfully recognise the self-MHC/peptide complexes presented on cTEC. Those that cannot do not have a functional use in the periphery and therefore undergo death by neglect, where a lack of survival signals leaves cells to persist into programmed cell death (180,184). Thymocytes that pass through this checkpoint progress to the next stages of development, downregulating either the CD4 or CD8 coreceptor to become single positive CD4 thymocytes (SP4), or single positive CD8 thymocytes (SP8). Key to the decision are the respective MHC complexes presented by cTEC that DP thymocytes interact with during positive selection, with MHC class I complex favouring SP8, and MHC class II biasing towards SP4, however, this decision is more complex and thought to encompass several different factors.

1.3.3 Commitment to Single Positive CD4 and CD8 Lineages

Multiple mechanisms by which thymocytes commit to the SP4 or SP8 lineage have been proposed, including a number of 'classical' models, and the differential 'co-receptor reversal' model (186). One classical model, termed 'instructional', suggests that during positive selection, interaction with MHC via TCR determines downregulation of mismatched coreceptors. That is MHC class I-interacting thymocytes downregulated CD4 and commit to SP8, and class II-interacting thymocytes downregulated CD8 and commit to SP4. Initially this proposed that the signals given from the CD4 and CD8 coreceptors are specific and different from one another upon interaction with respective MHC molecules. This differential signalling was therefore thought to instruct mismatched co-receptor downregulation and commitment to the SP4 or SP8 lineage (187). Further work elaborated on this, suggesting instead that differing signal strength instructed lineage commitment, with stronger TCR signals leading to commitment to the SP4 lineage and weaker signals causing SP8 commitment, explained by the increased $p56^{Lck}$ binding by the cytosolic tail of the CD4 coreceptor when compared to CD8 (188,189). Further studies implicated the duration of these signals, with longer lasting TCR signals favouring SP4 lineage commitment (190), however the shorted TCR signalling associated with SP8 commitment was later described further using the kinetic signalling model (191,192), a differential model discussed further later. The stochastic model is a classical model with different key assumptions to the instructional models described above. Rather than coreceptor downregulation being a result of TCR-MHC engagement, this model suggests that downregulation is random during positive selection, and those cells that have maintained expression of the correct coreceptor corresponding to the MHC they

interact with survive through TCR mediated ‘rescue signalling’, whilst those which no longer express the coreceptor that matches their TCR do not receive such TCR mediated survival signals and die (186,193,194).

The ‘kinetic signalling’ model offers an explanation for lineage commitment very different from the classical models already discussed. This model is based on the observation that CD8 gene transcription was downregulated in uncommitted cells still undergoing positive selection. As such, this model suggests that all thymocytes terminate CD8 transcription and subsequently downregulate surface CD8 expression to have a $CD4^{+}CD8^{LOW}$ phenotype that remain in an uncommitted state (191). The duration of TCR signals in response to this downregulation of CD8 then determines commitment to the SP4 and SP8 lineages; if TCR signalling is maintained following the downregulation of CD8 then the TCR expressed is MHC II restricted and therefore the cells will persist with CD8 downregulation and commit to the SP4 lineage. MHC class-I restricted TCRs require CD8 to transduce such signals, hence signalling in these thymocytes would not continue following CD8 downregulation. A lack of these signals results these undergoing ‘co-receptor reversal’, reinitiating CD8 transcription and terminating CD4, committing these cells to the SP8 lineage. Key to this is responsiveness common cytokine receptor γ chain (γc) family members such as IL-7 (191,192,195). Cessation of TCR signalling results in the intermediate $CD4^{+}CD8^{LOW}$ population becoming responsive to these cytokines, with a lack of these signals specifically limiting SP8 production (186,191).

Although the mechanisms of lineage commitment remain debated, there are a number of transcription factors known to be involved in this process. ThPOK and RUNX1 and 3 represent the key transcription factors in commitment to the SP4 and SP8 lineages

respectively (186). ThPOK has been shown to be expressed exclusively by SP4 thymocytes (196,197), and mice deficient in a functional version of this transcription factor resulted in MHC II restricted cells becoming SP8 T-cells (197). In accordance, overexpression of ThPOK leads to all thymocytes, including those with MHC I restricted TCR, to become SP4 (196,197). The RUNX proteins are shown to have a similar importance within SP8 commitment, with overexpression leading to increased downregulation of CD4, and lack of expression leading to further commitment to the SP4 lineage (198). RUNX3 is shown to both actively downregulate CD4 expression through binding of silencers, and actively upregulate CD8 transcription by binding to CD8 gene enhancers (198,199). Interestingly, whilst RUNX appears to have active roles in upregulating CD8 gene transcription, it appears ThPOK does not have a reciprocal role in CD4 upregulation, rather in the binding of RUNX3 to silence it's activity (198), and downregulate CD8 gene enhancers (200).

Recognition of either MHC class I or MHC class II complexes by TCR therefore drives transition to either SP8 or SP4 thymocytes through the initiation of different transcription factors. Accordingly, the dynamics of DP to SP transition is different between the two lineages. Studies using inducible Zap70 mice, where thymocyte selection can be 'switched on' following introduction of doxycycline antibiotic, show that SP4 appear around 2-3 days earlier than SP8 following commencing of positive selection (201). Interestingly this relationship fitted with the emergence of different DP subsets based on CD5 and TCRβ expression, with SP4 emergence being preceded by $CD5^{HI}TCR\beta^{INT}$ DP2, whilst SP8 only emerge following $CD5^{INT}TCR\beta^{HI}$ DP3 cells being seen. This SP8 precursor population with DP was further confirmed using I.T. injection, with DP2 giving rise to SP4 and SP8, but DP3 exclusively giving rise to SP8

(201). As well as differences in the populations class I and class II restricted thymocytes pass though during lineage commitment, differences in the requirement for the key chemokine receptor CCR7 have been described, with a higher proportion of thymocytes selected on MHC class I expressing CCR7 than those selected on class II (202,203). Interestingly this requirement for CCR7 expression is thought to be involved in the lineage decision programme, with forced CCR7 expression on thymocytes in a class II restricted TCR transgenic model increasing the number of SP8 thymocytes produced (202).

Beyond the complex role in lineage decision, CCR7 is known to have a clear role in the commencement of the following stages of T-cell development in their translocation to the thymus medulla. Following TCR engagement and positive selection, DP and SP thymocytes upregulate CCR7, migrating towards CCR7-ligands CCL19/21 expressed by mTEC (100,204). Of these, CCL21 has been more recently shown to be the main CCR7 ligand involved in this process, with specific CCL21ser KO mice lacking medullary accumulation of thymocytes (127). Involved in a converse manner is expression of CCR9 by these post-selection thymocytes. Whilst expression of this receptor drives migration towards CCL25-expressing cTEC, following selection expression of PlexinD1 inhibits this migration, promoting CCR7-CCL21 mediated translocation towards the medulla (205,206). This movement of thymocytes into the medulla promotes two key processes in their further development; both the post-selection maturation of these cells to reach functionally maturity prior to their egress into the periphery, and the induction of tolerance to ensure these cells are not self-reactive to the body's own endogenously expressed antigen (180,204). Interestingly, the former is shown be possible without access to the medulla, with cells undergoing

cortical maturation in RelB KO thymuses that lack mTEC (207). However, despite this these thymocytes have not undergone tolerance induction (207), a process that exemplifies the importance of the thymic medulla to T-cell development.

1.3.4 Induction of Tolerance in the Medulla

The random rearrangement of TCRα and TCRβ chains allow for a diverse T-cell repertoire to maximise the chances of generating a TCR that can recognise foreign antigen presented by self-MHC complexes; however, this process will also generate TCRs that recognise self-peptides. Cells that are specific for self-peptide would target the body's own tissue and lead to autoimmunity. As such, a key role of the thymus in the development of T-cells is ensuring these self-reactive thymocytes are removed from the thymic T-cell pool in a process termed central tolerance. The induction of tolerance can be separated into two key aspects: negative selection, where these autoreactive cells are targeted for clonal deletion in the thymus, and the generation of nTreg which circulate in the periphery and actively suppress autoreactive peripheral T-cell responses.

For negative selection to occur thymocytes must be screened against self-peptide that they may encounter in the periphery. This process is possible through the specialised ectopic expression of these TRAs by mTEC (56), discussed in more detail *1.2.3.* Following their translocation from the cortex to the medulla, thymocytes are exposed to TRAs expressed either directly by mTEC, or by medullary APC such as DC and interact with them via their rearranged TCR. Interaction with these self-peptides leads to rapid calcium-flux and subsequent arrest in migration (208) allowing for TCR signalling and ultimately decision over the cells' fate. The basis for this decision is the

affinity with which the thymocytes' TCR interacts with self-antigen. A high affinity interaction with the MHC presented self-peptide results in clonal deletion, whereas low affinity for the self-peptide allows for thymocyte survival and positive selection (209,210). The intracellular signalling through the mitogen activated protein kinase (MAPK) pathway, specifically through the member extracellular signal regulated kinase (ERK), is shown to be key to the choice between positive and negative selection (211,212). Upon high affinity TCR interactions strong and immediate ERK activation is triggered, which is linked to cell death. Conversely, following low affinity TCR binding, ERK activation is of a lower intensity and occurs over a prolonged period (210,211). Differential dynamics in ERK signalling as a result of either high or low affinity TCR interactions therefore determine whether thymocytes survive or undergo clonal deletion.

Despite the narrow window of TCR affinity that determines whether cells are positively or negatively selected (210), a third fate exists specifically for MHC class II restricted thymocytes with intermediate affinity for self-peptide MHC complexes: lineage divergence to nTreg (209). Use of Nur77GFP mouse models, where strength of TCR signal correlates to the level of GFP expressed, has shown that Treg's affinity for self-antigen is higher than conventional SP4, and only slightly lower than cells that are negatively selected (35,213). The dynamics by which this lineage divergence occurs can be debated. One model proposes that following TCR signalling the IL-2 receptor α-chain CD25 is upregulated giving responsiveness to IL-2, and subsequently upregulation of Treg master transcription factor Foxp3 (214,215). This gives a two-step differentiation, first to $CD25^{+}Foxp3^{-}$ precursor Treg, and then to $CD25^{+}Foxp3^{+}$ Treg (215). Interestingly, another population of $CD25^{-}Foxp3^{+}$ Treg exist within the thymus,

which have been alternatively suggested as precursors to Treg (216). This model suggests that following high affinity TCR interactions, Foxp3 is first upregulated and leads to upregulation of pro-apoptotic proteins and downregulation of anti-apoptotic proteins. CD25 upregulation then rescues these cells from apoptosis through responsiveness to γc cytokines such as IL-2 (216). Evidence for both models exists, with both progenitor candidates giving rise to mature $CD25^{+}Foxp3^{+}$ Treg in vivo (215,216). Despite their recognition for self-peptide at a higher affinity than conventional SP4, these cells act to suppress self-reactive immune responses in the periphery and are therefore a major part of the thymus' role in tolerance induction.

The generation of these nTreg represents another key aspect of tolerance induction, and furthermore the key role of the thymus medulla in this process. RelB knockout mice, which lack development of mTEC and therefore any medulla formation, suffer from severe autoimmunity owing to a loss of Treg and adequate clonal deletion of self-reactive thymocytes (86,207,217). Although this shows the importance of the thymus medulla for the induction of tolerance, negative selection has been shown to also occur within the cortex. Use of the HY^{CD4} model, where DP thymocytes undergo negative selection, showed that thymocytes with high affinity for self-peptide undergo clonal deletion in the cortex (218), with later use of the Nurr77GFP model suggesting that as many as 75% of the cells undergoing negative selection are localised in the cortex rather than the medulla (213). Interestingly, although cTEC possess the ability to present specific antigen to self-reactive cells in the cortex, they were not efficient inducers of clonal deletion. Instead, it was shown that a rare but distinct population of $CD11c^{+}$ DC within the cortex underpin negative selection in the cortex. Capable of both

presentation of self-antigen and induction of apoptosis, cortical clonal deletion was greatly reduced upon loss of these cells (218).

Following the processes of positive and negative selection, the thymus is left with a pool of self-tolerant thymocytes, capable of specifically recognising either MHC class I or MHC class II -presented antigens. The final role of the thymus in the development of these cells is controlling their final maturation ready for egress into the periphery.

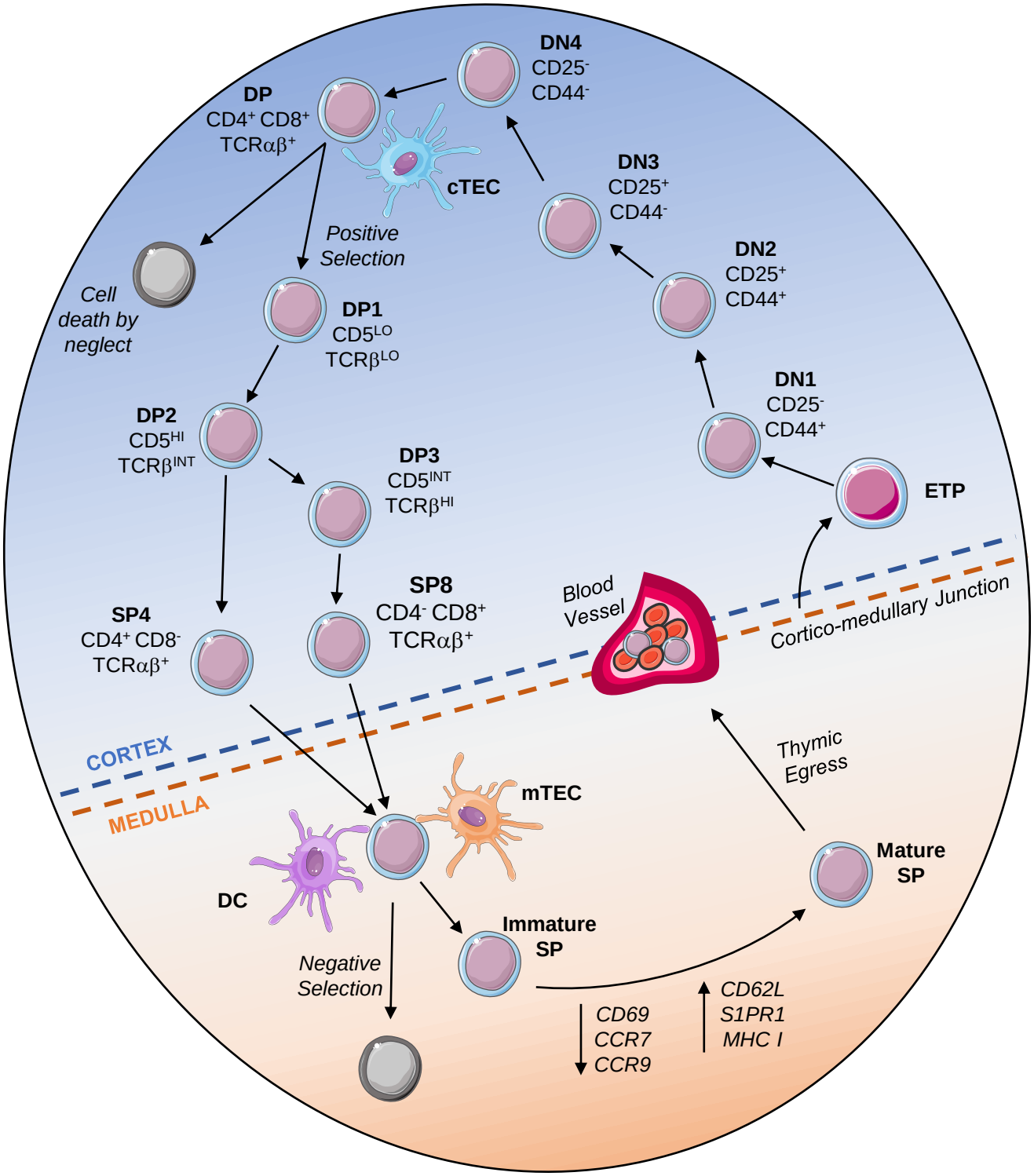
DN4
CD25-
CD44-
DP
CD4+ CD8+
TCRαβ+
cTEC
DN3
CD25+
CD44-
Positive
Selection
DN2
CD25+
CD44+
Cell
death by
neglect
DP1
CD5LO
TCRβLO
DN1
CD25-
CD44+
DP2
CD5HI
TCRβINT
DP3
CD5INT
TCRβHI
ETP
Blood
Vessel
Cortico-medullary Junction
SP8
CD4- CD8+
TCRαβ+
SP4
CD4+ CD8-
TCRαβ+
CORTEX
MEDULLA
Thymic
Egress
mTEC
DC
Mature
SP
Immature
SP
Negative
Selection
CD69
CCR7
CCR9
CD62L
S1PR1
MHC I

Figure 1.1. Thymic T-cell Development

T-cell development begins with recruitment of progenitor cells to the cortico-medullary junction (CMJ). Early thymic progenitors (ETP) begin their differentiation into T-cells in the cortex, progressing through sequential double negative (DN) populations defined by CD25 and CD44 expression. The end of this progression is marked with the upregulation of T-cell receptor (TCR) β and subsequently TCRα chains followed by CD4 and CD8 to give double positive (DP) thymocytes. Thymocytes then interact with self-MHC/peptide complexes on cortical thymic epithelial cells (cTEC) via their TCR, where cells that recognise these complexes are positively selected, and those that do not undergo death by neglect. DP thymocytes will progress through a series of subpopulations identified by CD5 and TCRβ expression. DP1 and DP2 represent cells that are uncommitted, whilst DP3 are committed to the CD8 lineage. Following positive selection, DP thymocytes downregulate either CD4 or CD8 to become single positive (SP) -8 or SP4 respectively, before progressing to the medulla. Medullary SP thymocytes then interact with APC such as mTEC and DC that express self-peptide. Thymocytes interact with this self-peptide via their TCR, and those that bind with high affinity are negatively selected and undergo apoptosis induction, whilst those that bind with lower affinity progress through negative selection and continue to mature within the thymic medulla. This post selection maturation prepares these cells for their exit into the periphery, and once thymocytes are deemed egress competent they leave the thymus via vessels at the CMJ.

1.3.5 Post-selection Maturation

Before they can exit the thymus and enter the peripheral T-cell pool, thymocytes must continue their thymic development to acquire a mature phenotype suited for their role in the periphery in a process known as post-selection maturation. This maturation can be tracked through a series of alterations in surface marker expression. These markers have been used in multiple different combinations so as to give sequential populations that SP thymocytes progress through before their egress (219). Initial candidates for these markers acted to separate SP thymocytes into distinct immature and mature populations. Expression of CD24 and CD69 defined the immature population of SP thymocytes most similar to the DP population, and incapable of producing anti-TCR responses similar to peripheral T-cells. Mature thymocytes lack expression of CD69 and CD24, but unlike immature cells express Qa-2 and CD62L, with these cells appearing later in development whilst also being capable of responding to TCR triggers with signalling comparable to peripheral T-cells (220–224). In keeping with this, CD69 is linked to thymic retention, whilst CD62L expression is required for entry into secondary lymphoid tissues (221,223,224), supplying functional evidence that immature thymocytes are not competent for thymic egress, whilst mature cells are.

Whilst phenotypic and functional markers alone allowed for subdivision into immature and mature populations of developing thymocytes, use of the Rag2GFP reporter mouse model (referred to herein as RagGFP) has been essential to further understanding thymocyte development following selection and transition to SP thymocytes. These mice express GFP under the control of the Rag2 promoter which is activated at the DN stage of thymocyte development. Following TCR rearrangement Rag2 transcription is switched off and GFP fluorescence diminishes over time, giving

a read-out of cell age (225,226). Importantly, RagGFP expression also allows the separation of those cells within the thymus that are newly generated and those that have recirculated from the periphery that have lost expression of GFP (93,227). Although the relevance of recirculating T-cells to the thymus is not yet clear, failure to isolate and remove them from analysis of thymocytes would be to include functionally mature cells from the periphery in analysis of newly generated cells. Use of RagGFP mice in conjunction with the developmental markers defined previously showed that loss of GFP correlated with a loss of CD69 and CD24 and an upregulation of CD62L and Qa-2, further confirming $CD69^{+}$ $CD24^{+}$ cells as immature and $CD62L^{+}$ $QA\text{-}2^{+}$ cells as mature (227).

More recent work has used surface expression of CD69 and MHC class I to define sequential developmental populations, whilst also identifying functional characteristics that distinctly separate each population (228). Cells progress from $CD69^{+}MHCI^{-}$ semi-mature (SM), through $CD69^{+}MHCI^{+}$ mature 1 (M1), and finally $CD69^{-}MHCI^{+}$ mature 2 (M2), confirmed with a progressive loss RagGFP between these stages. Transition from the SM to the M1 stage is characterised by developing the ability to proliferate in response to TCR signalling within the thymus, before cells become cytokine licensed following the transition from M1 to M2, acquiring the ability to respond to type 1 interferon within the medulla (228). Interestingly, this study also showed that Qa-2 expression, a marker previously used to define mature thymocytes, was actually dependant on type-1 interferon signalling as opposed to cells gaining a mature phenotype, questioning its relevance as a developmental marker (228). Importantly, the most mature M2 population were shown to be egress competent, expressing

Sphingosine-1-Phosphate Receptor 1 (S1PR1) (228) which is crucial for exit from the thymus (229), discussed further in *1.3.6.*

The requirement for different chemokines and therefore expression of different chemokine receptors, specifically CCR4, CCR7, and CCR9, has also been shown to differ through SP thymocyte development. CCR7 is upregulated as SP4 thymocytes progress through maturation fitting with its key role in cortico-medullary translocation (100,230). CCR9 and CCR4 is shown to be upregulated on pre and post-selection DP thymocytes respectively, before both are progressively downregulated as SP4 thymocytes mature. (207,230). Immature SP4 thymocytes are therefore $CCR4^{+}CCR7^{-}CCR9^{+}$, whilst mature SP4 are $CCR4^{-}CCR7^{+}CCR9^{-}$ (207,230). Interestingly, differences can be seen between SP4 and SP8 in their thymic expression of chemokine receptors. Whilst immature SP4 thymocytes still express CCR4 following upregulation post-selection, it was reported that immature SP8 lack CCR4 expression (230). Conversely, whilst CCR9 is lost on mature SP4 thymocytes, its expression on mature SP8 is more complicated as CCR9 expression is required for SP8 to home towards the gut following their thymic development (231). The requirement for CCR7 is also suggested to be complex and differ between SP4 and SP8. As discussed previously, CCR7 is thought to be linked to the decision between commitment to the SP4 or SP8 lineage, with CCR7 expression favouring MHC I restricted DP over MHC II restricted (202).

Despite a wide range of surface markers, both phenotypic and functional, being used to define post selection maturation in SP thymocytes, clear unexplored discrepancies between SP4 and SP8 still exist, perhaps hinting at differential maturation programmes between the two lineages.

1.3.6 Thymic Egress

The most well-defined marker required for thymocyte egress is the G protein-coupled receptor S1PR1 and its key role in controlling the migration of thymocytes towards the high concentration of sphingosine-1-phosphate (S1P) expressed in the blood (229). Expression of S1PR1 is restricted to mature thymocytes, shown to only be expressed by the M2 population (228), fitting with its role in thymocyte egress. S1PR1 upregulation through maturation can be linked to its relationship with two previously mentioned maturational markers. S1PR1 expression is regulated by transcription factors Forkhead box protein O1 (Foxo1), and Krüpple-like factor 2 (Klf-2), both of which are upregulated during thymocyte maturation (223,232). Importantly, CD62L is also under the transcriptional control of Klf2, linking both maturational markers (233). CD69 can internalise surface S1PR1 expression, and as such as CD69 is downregulated through thymocyte maturation, this inhibition of S1PR1 is lifted, allowing surface expression to be upregulated (234).

S1PR1 acts to allow thymocyte egress by following a gradient of low S1P expression within the thymus towards high expression within the peripheral blood and thymus vasculature (229,235). Such interaction is shown to be essential for thymic egress with the use of FTY720, an agonist of S1PR1 that causes its downregulation that inhibits interaction with S1P and subsequently causes intrathymic accumulations of mature thymocytes, indicative of a failure to exit the thymus (236–238). As such, maintenance of this S1P gradient is key to the regulation of thymus egress. Pericytes found at the thymic blood vessels by which thymocytes exit are shown to express sphingosine kinases (Sphk) 1 and 2, enzymes that generate S1P through phosphorylation of sphingosine (235). Specific loss of Sphk1/2 from thymic pericytes again causes

accumulation of mature thymocytes as a result in a failure of egress (235). Whilst this exemplifies the importance of high levels of S1P at the point of thymic egress, equally important is the maintenance of low S1P concentration within the thymus. Lipid phosphate phosphatase 3 (Lpp3) acts opposingly to Sphk1/2 by dephosphorylating S1P and keep thymic S1P levels low (239). Specific deletion from both TEC and endothelial cells leads to mature thymocyte accumulations similar to loss of Sphk1/2, showing that both stromal populations act to maintain this gradient (239). As well as thymus stroma, haematopoietic cells within the thymus also maintain the low levels of S1P, with loss of S1P lyase (SPL), an enzyme that breaks down S1P, specifically on bone-marrow derived cells such as DC leading to intrathymic accumulations (240).

Acquisition of S1PR1 and the responsiveness to S1P that it brings is clearly key to thymocytes attaining egress competence, however different models exist to explain the dynamics involved in which cells are selected for thymic egress: the ‘lucky dip’ stochastic model, and the ordered ‘conveyor belt’ model (241,242). The lucky dip model proposes that once cells reach a certain level of maturity and are capable of thymic egress they can undergo such egress at any point, regardless of how long they have spent at this maturational state, whilst the conveyor belt model suggests that the process is more systematic, with the most mature cells being preferentially selected for thymic egress and entry into the periphery (241,242). Recent work provides clear evidence for the latter model by separating the most mature M2 SP4 thymocytes into three sequential populations M2a, M2b, and M2c based on increasing levels of CD62L. Using RagGFP it was shown that progressive upregulation of both CD62L and S1PR1 occurs as these cells age, showing that thymocytes continue to further mature towards peak egress-competence within the most mature population (98). Furthermore, this

study utilises the anti-CD4-PE i.v. injection experimental model, isolating cells located between the pericytes and endothelial cells of the blood vessels, in the perivascular space (PVS) and therefore in the process of thymic egress (235). The egressing SP4 isolated in the PVS as well as recent thymic emigrants (RTE), identified as RagGFP^{+} cells within the spleen, were shown to be enriched for the most mature M2c population, suggesting that the most mature thymocytes are preferentially selected for egress ahead of other cells that are also deemed egress competent (98).

The study discussed above also looked to elucidate how thymic microenvironments interact with thymocytes to promote their translocation across multiple membranes and ultimately their thymic egress. LTβR is known to have a key role in thymus medullary organisation whilst also being implicated in thymic egress with thymocyte accumulations occurring with its loss (94). Accumulations occurring as a result of LTβR loss was attributed to its expression on endothelium within the thymus as opposed to TEC. Subsequently its role in egress was linked directly to entry of cells from the thymus into the PVS, shown through SP4 M2c accumulations occurring within the whole thymus but not within the PVS (98). IL-4Rα has also been shown to be implicated in thymocyte egress, with IL-4Rα KO mice showing accumulation of mature SP4 thymocytes, as well as reduced RTE. Interestingly however, IL-4Rα's role appears to be linked to thymocyte entry into the blood vessels from the PVS, with accumulations of cells clearly occurring within the PVS (243) rather than the whole thymus as seen with loss of LTβR (98). Importantly, FTY720 blockage in IL-4Rα KO mice significantly increases mature SP4 thymocyte numbers, showing that the S1PR1 – S1P axis is still functioning despite the interruption to thymic egress (243) Taken together this suggests a two-stepped approach for egress, with endothelial LTβR controlling PVS

entry, and IL-4Rα controlling egress from the PVS into the blood vessels, with S1PR1 guiding cells towards the high concentration of S1P in the blood throughout.

Whilst the importance of S1PR1 throughout thymic egress is clear in adult mice, this does not appear to be the case in neonatal models, rather the chemokine CCR7 and its ligands have been reported to play a key role. CCR7 KO mice show increased thymocytes and decreased splenic T-cells in neonates (244), with this study linking this effect to CCR7's interaction with CCL19 and not CCL21, with CCL19-mediated egress from foetal thymic organ cultures, and a decrease in splenic T-cells with CCL19-neutralisation (244). A more recent study, however, has emphasised CCL21's role in egress from the neonatal thymus, with CCL21 KO but not CCL19 KO mice showing evidence of thymic accumulations (245). Furthermore, this study proposed that multiple thymic stromal cell subsets are implicated in the process of neonatal thymic egress. Whilst the production of CCL21 was shown to be limited to mTEC, CCL21 was shown to be captured and presented by mesenchymal stroma found at vessels responsible for thymocyte egress (245). A possible explanation for the role of CCL21 and not CCL19 in this process comes from the mechanism of presentation in a heparan sulfate-dependant manner via CCL21's C-terminus extension, a domain which CCL19 is shown to lack (245). Interestingly CCR7 has been shown to be dispensable for egress in adults (246), suggesting that the factors controlling egress differ throughout development from neonates to adults. In fitting with this it was shown that the S1PR1-S1P axis was functional in neonatal Aire KO mice where thymic CCR7 is reduced. Despite this, thymic accumulations were still seen suggesting the function of S1PR1 alone did not allow for thymic egress. Subsequently at three weeks these mice upregulated S1PR1 expression on thymocytes to a degree capable of compensating

for the loss of CCR7 and allowing thymic egress (247). This further complicates the factors involved in thymic egress, with differential requirements at both different steps in leaving the thymus in adults, as well as at different ages through development.

The study of SP thymocyte maturation and progression towards thymic egress has identified a number of different markers that have subsequently been used to define progressive maturational populations with differing functional properties. Despite this, a clear understanding of this process relies on consensus on the phenotypic markers used, a point that is not only complicated by the volume of these markers made available through previous study, but also through discrepancies between the two SP thymocyte lineages that exist within the thymus in SP4 and SP8. Further to the latter point, the majority of work to previously define post-selection maturation has focussed solely on SP4 thymocytes, perhaps due to both their higher quantity within the thymus compared to SP8, and also the fact that a number of experimental models used only allow for SP4 thymocyte analysis such as the CD4 I.V. injections. Drawing such a consensus that will allow for a complete understanding of the events that occur between thymic selection and egress and the factors that control these processes requires the study of the SP4 and SP8 thymocytes congruently.

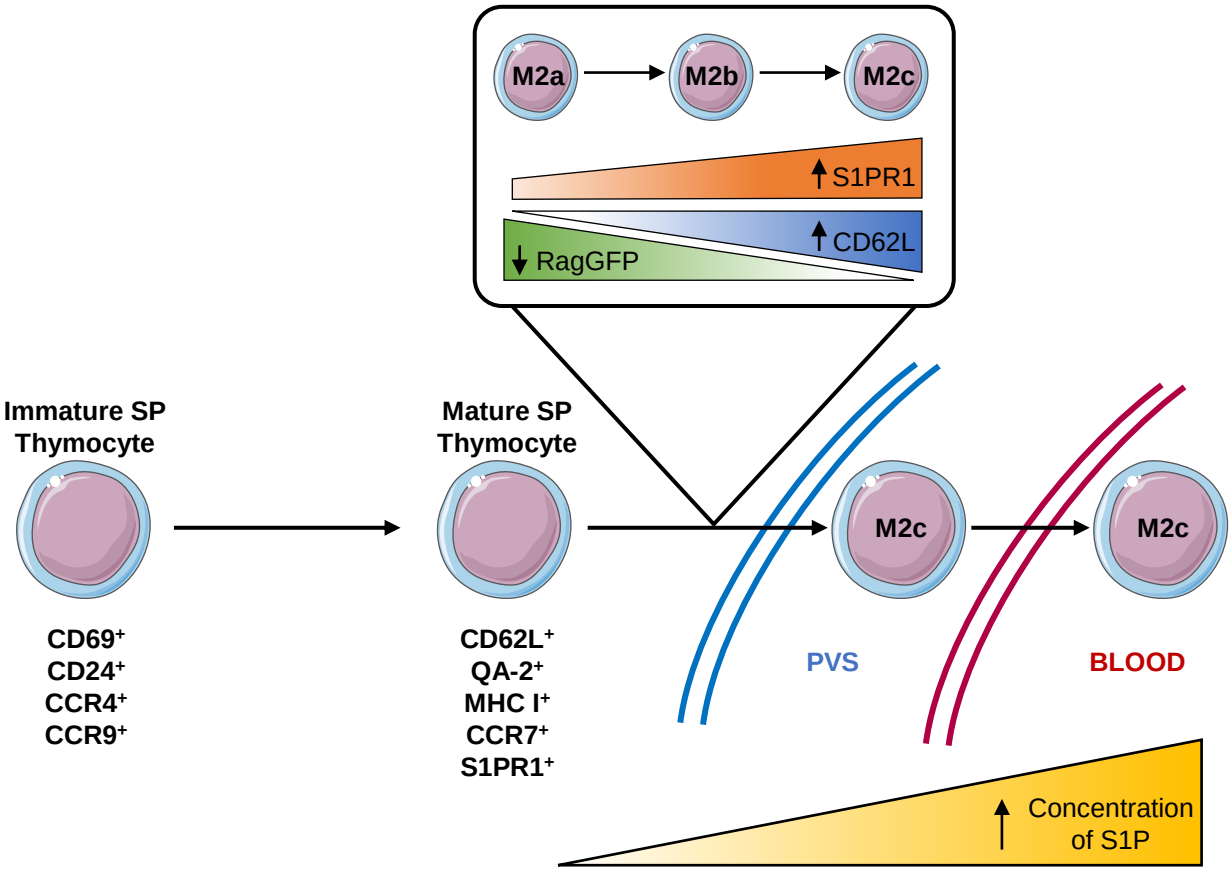
M2a
M2b
M2c
S1PR1
CD62L
RagGFP
Immature SP Thymocyte
Mature SP Thymocyte
M2c
M2c
CD69+
CD24+
CCR4+
CCR9+
CD62L+
QA-2+
MHC I+
CCR7+
S1PR1+
PVS
BLOOD
Concentration of S1P

Figure 1.2 Summary of Post-selection Maturation and Thymic Egress in Adult Mice

Following their selection and transition from DP thymocytes, SP thymocytes undergo maturation to the point of egress competence where they have completed their thymic development and are suitable for entry into the periphery. This maturation is defined by differential expression of certain markers as these cells progress through post-selection maturation as summarised above. The most mature thymocytes, termed M2c are preferentially selected for thymic egress in what is described as a conveyor belt mechanism of egress. This egress is guided by the expression of S1PR1 on mature thymocytes responding to a gradient of S1P, with a higher concentration in the blood compared to the thymus. Thymic egress into the periphery first requires thymocytes to enter the PVS, before crossing the endothelium into the peripheral blood.

1.4 PROJECT AIMS

The thymus controls the selection of SP thymocytes to ensure that T-cells in the periphery recognise self-MHC/peptide complexes and are tolerant to self-antigen. Following this, the thymus has a key role in controlling the maturation of these thymocytes to ensure cells that enter the periphery are functionally competent, as well as regulating their egress from the thymus into associated blood vessels to enter the periphery. This maturation has been defined using a number of different markers, with a progressive change in the phenotype as the cells get closer the thymic egress. Despite this, much of this work has focussed on SP4 thymocytes and failed to address the differences seen between SP4 and SP8 and the implications this may have in a differential control of the post-selection maturation of each of these SP thymocytes by the thymus medulla. As such, we have used a range of approaches to compare SP4 and SP8 thymocyte development to answer the following questions:

1. How does the post-selection maturation and thymic egress of conventional SP4 and conventional SP8 thymocytes compare with one another?
2. How is the maturation and egress of cSP4 and cSP8 within the thymus affected following changes in the thymus stroma as a result of BMT?
3. How does the thymus control the development of non-conventional SP8 thymocyte populations?

CHAPTER 2: MATERIALS AND METHODS

2.1 MICE

All mice were bred, housed, and maintained within the University of Birmingham Biomedical Services Unit (BMSU). All animal work was carried out following regulation in accordance with the UK Home Office regulations. Mixed sex adult mice were sacrificed for tissue harvest aged 8-12 weeks and culled using schedule one cervical dislocation.

Both wildtype (WT) and genetically manipulated mice were used, listed in full in Table 2.1. WT mice allowed the characterisation of normal, unmanipulated thymic T-cell development, whilst genetically manipulated mice allowed for the assessment of roles of specific genes, cell types, and mechanisms in this process. Alongside manipulated mice, age matched WT C57BL/6 or Balb/c mice were used as unmanipulated controls depending on the background of the transgenic strain.

2.2 CELL PREPERATION MEDIA

RF10 media (Table 2.2) was used for storage of tissues following dissection, as well as preparation by mechanical disaggregation and storage of subsequent single-cell suspensions. Following generation of single-cell suspensions, cells were handled in either FACS (Table 2.3) or MACS (Table 2.4) buffer in preparation for flow cytometric analysis.

Table 2.1 Mouse Strains

Mouse Strain	***Phenotype***	***Supplier***
C57BL/6	Wildtype (CD45.2).	BMSU / External (Charles River)
BoyJ	Congenic C57BL/6 wildtype (CD45.1)	BMSU
Balb/c	Wildtype.	BMSU / External (Charles River)
WT RagGFP	Transgenic mouse with bacterial artificial chromosome encoding for green fluorescent protein reporter under the control of the Rag-2 gene (226).	BMSU
Tnfrsf11b$^{-/-}$ x RagGFP	Mice lack RANK-L soluble decoy receptor OPG and exhibit uninhibited RANK - RANK-L interactions resulting in larger medulla with more mTEC (93). OPG$^{-/-}$ crossed to RagGFP reporter mice.	BMSU
CCR7$^{-/-}$ x RagGFP	Mice lack CCR7 expression important in migration of T-cells within the thymus and peripheral lymphoid organs, with migration within the periphery being severely reduced (100). CCR7$^{-/-}$ crossed to RagGFP reporter mice.	BMSU
IL-4R$\alpha^{-/-}$	Mice have complete loss of IL-4Rα, resulting in loss of IL-4 signalling	BMSU
CD1d$^{-/-}$	Mice lack CD1d1/CD1d2 loci and lack iNKT in the thymus and periphery.	BMSU
dblGATA	Mice have a deletion of the double GATA binding site from the GATA-1 allele causing a loss ability to generate eosinophils	BMSU
Balb/c RagGFP	RagGFP mice were bred in house with wildtype Balb/c mice to allow analysis of relative cell age in unmanipulated Balb/c mice, with the potential to breed RagGFP into genetically manipulated strains on a Balb/c background	Generated at BMSU

Table 2.2 RPMI-1640 Hepes Medium (RF10) Components

Medium and Additives	***Volume***	***Final Concentration***	***Source***
RPMI-1640 +20Mm Hepes, with L-glutamine, without bicarbonate	500ml	-	Sigma, Poole, UK
200mM L-Glutamine	5ml	2mM	Sigma, Poole, UK
5000 IU/ml Penicillin and Streptomycin	10ml	100IU/ml	Sigma, Poole, UK
Fetal Calf Serum (FCS) – Heat inactivated	50ml	10%	Sigma, Poole, UK

Table 2.3 Components of FACS Buffer

Medium and Additives	***Volume***	***Final Concentration***	***Source***
Dulbecco's phosphate buffered saline with calcium and magnesium	500ml	-	Sigma, Poole, UK
FCS – Heat Inactivated	15ml	3%	Sigma, Poole, UK

Table 2.4 Components of MACS buffer

Medium and Additives	***Volume***	***Final Concentration***	***Source***
Dulbecco's phosphate buffered saline with calcium and magnesium	500ml	-	Sigma, Poole, UK
FCS – Heat Inactivated	2.5ml	5%	Sigma, Poole, UK
EDTA 0.05M	2ml	0.02M	Sigma, Poole, UK

2.3 PREPERATION OF TISSUE

2.3.1 Tissue Dissection

The thymus and spleen were dissected immediately following sacrifice of mice at the BMSU, with tissues being placed in RF10 media and stored on ice. If necessary, excess blood and fatty deposits were removed from the tissues before processing into single cell suspensions.

2.3.2 Generation of Single-cell Thymocyte and Splenocyte Suspensions

For thymocyte analysis both thymus and spleen were mechanically disaggregated between two frosted glass slides (Thermo Scientific) into a dish of RF10. The slides were then washed with a further 2ml of RF10 following disaggregation, before the single-cell suspension was transferred to 15ml Falcon tubes (Corning Centistar) and filtered through a mesh-membrane filter to remove coagulated tissue. The cell suspensions were then centrifuged for 4 minutes at 4 °C at 1400 RPM. Thymocytes were then resuspended in 2ml of RF10, whilst splenocytes were resuspended in 2ml of red blood cell lysis buffer (Sigma Aldrich) and left at room temperature for 5 minutes to remove erythrocytes from the samples. After incubation, equal amounts of RF10 media were added as to neutralize the reaction, before the sample was centrifuged as previously and resuspended in 2ml of RF10 ready to carry out cell counts.

For analysis of stromal populations, thymuses were cut into small pieces using scissors in a 1.5ml Eppendorf tube in enzyme digest solution, of which the components are outlined in table 2.5. This was then transferred to a 5ml polyptopylene round bottom digestion tubes (Falcon, Thermo Fisher Scientific) and placed on a thermoblock (Eppendorf Thermomixer C) at 37^{o}C rotating at 650rpm for 60 minutes. The samples

were removed from the thermoblock and neutralised with 0.5M EDTA (Sigma Aldrich). Samples were then washed in MACS buffer and centrifuged under the same conditions asfollowing mechanical disaggregation, supernatant removed and resuspended in 1ml of MACS buffer. 25μl was then removed from each sample for counts, and 25μl for a pre-depletion control. The remaining cells were then stained with 20ml of anti-CD45 beads (Miltenyi Biotech) and incubated in the fridge for 20 minutes at 4^{o}C. Following incubation, cells were passed through LS MACS separation columns (Miltenyi Biotec) on a QuadroMACS separator magnet, holding $CD45^{+}$ cells within the column, with desired $CD45^{-}$ cells passing through and being collected in a 15ml Falcon (Corning Centristar). These cells were centrifuged and resuspended in 200μl with the whole sample to be stained.

Spherotech AccuCount cell count beads were used to obtain accurate cell counts of the thymocyte and splenocyte suspensions. 5μl of the bead solution, known to contain 5000 beads, were added to 100μl of phosphate buffered saline (PBS), with the mixture then added to a FACs tube along with 50μl from the 2ml resuspended thymocyte and splenocyte suspensions. The samples were then run on a BD LSR Fortessa flow cytometer to record the number of cells and count beads. Knowing the ratio of cells in the tube to that in the 2ml tube is 1:40, we can use the following formula to determine the total cell numbers;

$$Total\ Cell\ Count = \left(\left(\frac{Number\ of\ Cells}{Number\ of\ beads}\right) \times 5000\right) \times 40$$

Table 2.5 Components of Enzyme Digest Solution

Medium and Additives	***Volume***	***Final Concentration***	***Source***
RF10 (Table 2.2)	1ml	-	Sigma, Poole, UK
Deoxyribonuclease 1	25μl	2.5mg/ml	Sigma, Poole, UK
Collagenase Dispase	40μl	0.4mg/ml	Sigma, Poole, UK

2.4 FLOW CYTOMETRY

2.4.1 Surface Antibody Staining

To identify target cell populations by flow cytometry, antibodies to a variety of cell surface markers were used, largely directly conjugated primary antibodies, but also biotinylated antibodies with subsequent fluorochrome-tagged secondary antibodies. Both primary and secondary antibodies are listed in Table 2.5. $5x10^6$ cells were removed from the thymocyte and splenocyte suspensions and aliquoted into different wells in a 96-well plate (Costar) before being centrifuged for 2 minutes 4 °C at 1400 RPM. If the cell preparation required specific depletion steps, for example PE-depletion following CD45-PE I.V. injections (described in section 2.5), leaving less than $5x10^6$ cells, then all remaining cells were aliquoted and stained. Following centrifugation the supernatant was discarded, and cells resuspended in 50μl of the antibody mixture, made up in either MACS or FACS staining buffer depending on whether samples would undergo magnetic-activated cell sorting or not respectively. All antibodies were titrated for optimal staining, with the concentrations used outlined in Table 2.5. As well as staining with antibody mixtures containing all antibodies, single-colour samples were set up and used to determine the compensation parameters on the flow cytometer. To

accurately define ‘real’ antibody staining isotype or ‘fluorescence minus one’ staining controls were also set up within the 96-well plate and stained with these mixtures accordingly. Samples were left to incubate on ice at ~4 °C for 30 minutes in the dark. 150μl of the relevant staining buffer was then added to wash the cells, and the samples centrifuged again as above before the supernatant was removed. If necessary, secondary antibody mixtures were added at this point following the same protocol as described for primary surface antibodies. Once all antibody staining steps were complete, cells were finally washed and resuspended in 200μl of FACS staining buffer and added to 5ml polystyrene FACS tubes (BD), and either run on the flow cytometer immediately, or stored at 4 °C in the short term before being run.

2.4.2 Intracellular Antibody Staining

In order to characterise expression of transcription factors such as Eomes and nuclear proteins such as Ki67, additional fixation and permeabilization of cells was required. Cells were stained for surface markers as described in Section 2.4.1 but following the addition of all surface antibody steps and subsequent washes, rather than being resuspended in staining buffer the samples were fixed and permeabilized. Different fixation methods were used dependant on whether RagGFP reporter fluorescence retention was required.

2.4.2.1 Fixation and Permeabilization without Reporter Retention

For fixation/permeabilization without fluorescent reporter retention, the eBioscience Foxp3/Transcription Factor Staining Buffer Set (ThermoFisher) was used, following manufacturers protocol. Following the final wash after complete surface antibody staining, all samples were resuspended and incubated for 45 minutes with 150μl of

Fixation/Permeabilization solution, composed of fixative concentrate and diluent at a 1:3 ratio. The cells were then washed and centrifuged twice with 100μl of 1X permeabilization buffer, made from stock 10X permeabilization buffer diluted 10% in distilled water. Following this permeabilization of cells, they were then stained for Eomes and/or Ki67. These antibodies were made up in 1X permeabilization buffer using concentrations outlined in Table 2.5 and were incubated for 30 minutes before being washed and centrifuged, again in 1X permeabilization buffer. The samples were then resuspended in FACS buffer and transferred into FACS tubes, ready to be treated and run of the flow cytometer or stored until ready to do so.

2.4.2.2 Fixation and Permeabilization with Fluorescent Reporter Retention

Mice such as the RagGFP model express endogenous green fluorescent protein, acting as a reporter for relative cell age. Normal fixation methods are shown to be incapable of retaining fluorescent proteins within cells prior to permeabilization, and therefore an adapted fixation method capable of retaining fluorescent reporter expression was required to analyse expression of RagGFP alongside staining for intracellular proteins. Following methods outlined by Heinen *et al.* (248), following surface staining samples were resuspended 2% formaldehyde, diluted from 10% neutral-buffered formalin (Sigma), which is 4% formaldehyde, 1:1 in PBS. Cells were then left at room temperature to fix for 60 minutes before being washed with 1X permeabilization buffer, made as above from the eBioscience fixation kit. The cells were then stained for Eomes, again using concentrations outlined in Table 2.5 made up in 100μl of 1X permeabilization buffer. The samples were then left to incubate in the antibody mixture overnight (16 hours), before being washed and centrifuged twice

using 1X permeabilization buffer. After washing, samples were resuspended in FACS buffer and transferred to FACS tubes ready to run on the flow cytometer.

2.4.3 Flow Cytometric Analysis

All stained samples were run on an LSR Fortessa (BD) the FACS Diva software (BD), before data was exported and analysed using FlowJo software (version 10.7.1). Single colour samples were initially run on the fortessa to set voltages for each channel being used as well as compensation against each fluorochrome. Exclusively viable cells were analysed by pre-gating on FSC and SSC, also removing doublets from analysis. Isotype and 'fluorescence minus one' samples were used to determine positive staining and set gates for given populations. 1 million events were collected for each sample, unless analysis was focussed on a rarer population, where instead the sample would be run until completion to improve the number of events collected within these rare populations.

Table 2.6 List of Immunolabelling Antibody Reagents

Marker	***Conjugate***	***Clone***	***Dilution***	***Stock Concentration***	***Manufacturer***
CD4	Brilliant Violet 711 Brilliant Violet 605	RM4-5	1:200 1:800	100 μg/ml 0.2 μg/ml	Biolegend
CD8α	Brilliant Violet 786 Brilliant Violet 711	53-6.7	1:200 1:100	60 μg/ml	Biolegend
TCRβ	APC Cyanide 7	H57597	1:200	0.2 μg/ml	Invitrogen
CD69	PerCP Cyanide 5.5	H1.2F3	1:200	0.2 μg/ml	Invitrogen
CD62L	APC	MEL-14	1:1500	0.2 μg/ml	eBioscience
MHC I	eFlour 450 Biotin	28-14-8	1:50 1:400	0.2 μg/ml 0.5 μg/ml	Invitrogen

IgG2α κ	APC	eBR2a	1:1500	0.2 μg/ml	eBioscience
Eomes	PE Cyanide 7	Dan11 Mag	1:100	0.2 μg/ml	Biolegend
CD44	A700	IM7	1:50	0.2 μg/ml	Invitrogen
CD122	PE	5H4	1:100	0.2 μg/ml	Biolegend
CCR7	PE	4B12	1:100	0.2 μg/ml	Invitrogen
Live/Dead Viability Dye	Brilliant Violet 510	-	1:1000	-	Biolegend
CD5	PE	53.7.3	1:100	0.2 μg/ml	Invitrogen
Streptavidin	Brilliant Violet 786	-	1:200/1500	0.1 μg/ml	BD Bioscience
CD8β	PE Texas Red	YTS 156.7.7	1:2000	0.2 μg/ml	Biolegend
CD45	PE	30.5.11	1:200	0.2 μg/ml	eBioscience
CD45.1	PE Cy7	A20	1:400	0.2 μg/ml	Invitrogen
CD45.2	A700	104	1:100	0.2 μg/ml	Invitrogen
Ki67	PE Cy7	SolA15	1:1000	0.2 μg/ml	Invitrogen
CD25	Brilliant Violet 650	PC61	1:800	0.2 μg/ml	Biolegend
CD1d Tetramer (PBS-57)	Brilliant Violet 421	-	1:100	1.2 mg/ml	NIH Tetramer Facility
Ter119	A700	TER-119	1:200		
EpCAM	Brilliant Violet 711	G8.8	1:400	0.2 mg/ml	BD Bioscience
CD31	APC	390	1:400	0.2 mg/ml	Invitrogen
P-selectin	FITC	RB 40.34	1:100	0.5 mg/ml	eBioscience
BST-1	PE	BP-3	1:400	0.2 mg/ml	BioLegend
CD45	Brilliant Violet 605	30-F11	1:2000	100 μg/ml	BioLegend
Ly6c	PE Cy7	HK1.4	1:4000	0.2 mg/ml	BioLegend
VCAM-1	Biotin	429	1:200	0.5 mg/ml	eBioscience
Sca-1	PE	D7	1:5000	0.2 mg/ml	Invitrogen
Ter119	FITC	TER-119	1:100	0.5 mg/ml	BD Bioscience
ITGa7	A700	334908	1:100	-	R&D Sytems
ICAM-1	Brilliant Violet 421	YN1/1.7.4	1:200	0.5 mg/ml	BioLegend

2.5 ANTI-CD45 INTRAVENOUS LABELLING

To analyse cells currently in the process of thymic egress we used I.V. injection of anti-CD45 PE antibody, isolating cells in the perivascular space, adapted from protocols used in previous studies (98,235). Using a 25-gauge needle, mice were injected I.V. with 1mg of anti-CD45 PE antibody (clone 30.5.11) in 200μl of PBS. Mice were sacrificed 3 minutes after injection, allowing for the antibody to enter the vasculature of the thymus, before the thymus was immediately dissected and mechanically disaggregated in 20ml of RF10 as to dilute excess unbound anti-CD45 antibody. Samples were then placed on ice until ready for further processing where they were centrifuged for 4 minutes at 4 °C at 1400 RPM, resuspended in 2ml and counted using Spherotech AccuCount beads as described before, with the addition of the PE channel on the fortessa allowing for an accurate count of PE-labelled PVS cells.

Following counts, $5x10^6$ cells were removed from each sample and added to separate wells for staining. The remaining samples were further centrifuged and resuspended in 1ml of MACS staining buffer. To enrich the relatively small number of PE-labelled PVS cells, magnetic-activated cell sorting was used to isolate PE labelled cells for staining using anti-PE microbeads (Miltenyi Biotec). 10μl of beads was used for every 10^7 cells in the sample and left to incubate at 4 °C for 15 minutes. Samples were then washed twice with MACS staining buffer and passed through already primed MACS separation columns (Miltenyi Biotec) attached to QuadroMACS separator magnets. PE labelled cells were retained within the columns and washed-out forcing MACS through the column with the syringe supplied with the kit, collected, and stored on ice. The enriched sample was then centrifuged and the whole sample aliquoted into separate

wells in a 96-well plate. Cells were then stained with surface and intracellular antibodies and run on the flow cytometer as described in Section 2.4.

2.6 BONE MARROW CHIMERAS

Bone marrow chimeras (BMC) were used to determine how thymus recovery after damage impacts the development of thymocytes. To do this we used a combination of congenically marked bone marrow and fluorescent reporter mice to determine between host and donor cells. WT RagGFP mice on a C57/B6 express CD45.2, whilst BoyJ WT mice express CD45.1. WT RagGFP mice were therefore used as donor cells, and BoyJ mice are hosts, with donor derived cells isolated through expression of CD45.2.

2.6.1 Mouse Irradiations

To generate bone marrow chimeras, mice deemed healthy (over 18g weight) were lethal irradiated before reconstitution. Before irradiation began, mice were given antibiotic Baytrill in their drinking water for 7 days leading up to the first irradiation. These host mice were then given dosage of 500 rads of irradiation initially on day one of the protocol, before being given the same dose the following day amounting to a lethal dose. Following the second dose, mice were reconstituted with donor bone marrow in the afternoon of the same day. $5x10^6$ donor bone marrow cells, prepared as in Section 2.6.2, were injected intravenously into each host mouse, before being sacrificed at varying timepoints to assess how different cell populations recover.

2.6.2 Bone Marrow Preparation

Bone marrow was isolated in sterile conditions from tibia and femur bones of donor mice. Excess blood and tissue were removed, and the femur and tibia separated by cutting above the knee joint of the leg. A sterile needle was inserted through the centre

of the bone, and sterile RF10 used to flush through the bone marrow into a petri dish containing further sterile RF10. Bones were flushed through until clear, indicating all bone marrow had been harvested. Bone marrow within the petri dish was further passed through the needle to disaggregate any clumps that had formed during the process, generating a single-cell suspension. The bone marrow suspension was then filtered through a sterile mesh membrane into a 50ml Falcon tube (Corning Centristar) before being centrifuged for 10 minutes at 4 C at 1400 RPM. The supernatant was then discarded, and cells resuspended in 2ml of red blood cell lysis buffer (Sigma-Aldrich) at room temperature for 10 minutes, before being neutralized with equal volumes of RF10, and centrifuged again as before. The bone marrow cells were then resuspended in MACS staining buffer, and cells were removed to count as previously described in Section 2.3.2.

The samples were then depleted of mature T-cells using a CD3 depletion. This first required staining with anti-CD3 PE antibody, with samples being centrifuged and resuspended in 50μl antibody mixture for every 5 $x10^6$ cells (made up in MACS) and left to incubate for 30 minutes in the dark on ice. After incubation, a small portion of the sample was removed and run on the flow cytometer to determine the proportion of CD3 PE^+ cells pre-depletion, whilst the rest of the sample had antibody washed off using MACS staining buffer and were centrifuged, before being resuspended in 10μl anti-PE microbeads per 10^7 cells and left to incubate at 4^oC for 20 minutes. The samples were then added to primed LS columns attached to QuadroMACS magnets, depleting CD3 PE labelled cells. The depleted sample then had a portion of cells removed and run on the flow cytometer to compare for the proportions of CD3 PE^+ cells, assessing the efficacy of the depletion. This post-depletion sample was the counted as previously

and resuspended in sterile PBS without magnesium and calcium (Sigma Aldrich) in Eppendorf's ready for I.V. injection into host mice. $5x10^6$ cells were injected into host mice in 200μl of PBS.

2.7 STATISTICAL ANALYSIS

To produce graphical representation of proportions and numbers of cell populations, GraphPad Prism 9.0 software was used. Statistical analysis was also carried out using this software, with unpaired student two-tailed T tests was used for normally distributed data, and non-parametric equivalent Mann Whitney U test for skewed data. If statistical analysis was carried out between more than on population, a one-way ANOVA with multiple comparisons. Specific tests used are clarified in figure legends. Statistical significance was confirmed in P values were below 0.05, and are denoted as follows: *<0.05, **<0.01, ***<0.001, ****<0.0001.

CHAPTER 3: CHARACTERISATION OF THE INTRATHYMIC DEVELOPMENT OF CONVENTIONAL $CD8^+$ T-CELLS

3.1 INTRODUCTION

The thymus is responsible not just for the selection of SP thymocytes, but also supporting their maturation through to their egress into the periphery. This post selection maturation has been defined using a series of different markers, namely CD69 expression identifying immature cells, and upregulation of MHC I and CD62L being linked to more mature populations (221,224,228). Use of RagGFP reporter mice in conjunction with these markers further indicates that cells progress through these maturational populations as they age (225,226). Furthermore, these progressive populations are shown to have functional relevance within SP thymocyte egress. Expression of S1PR1 on thymocytes is required for their exit from the thymus (229), and as such is restricted to the most mature populations (98,228), with blocking of S1PR1-S1P interactions through use of FTY720 leading to selective intrathymic accumulation of mature thymocytes (237,238). Further within this mature thymocyte population that is capable of thymic egress, the most mature cells are shown to be preferentially selected to leave the thymus. Cells isolated in the PVS, and therefore in the process of leaving the thymus, are shown to have a higher expression of both CD62L and S1PR1 compared to intrathymic populations (98), supporting a conveyor belt mechanism of egress.

Despite the process of post selection maturation in the thymus being well-defined as above, characterisation of this process has been almost exclusively within the SP4 lineage, with the stages in thymic SP8 development less understood. Additionally, the characterisation of these stages in SP4 development looks to comprehensively define conventional SP4 by removing non-conventional lineages such as $\gamma\delta$ T-cells, iNKT, and $CD25^+$ regulatory T-cells (228). Despite this, no such isolation and removal of non-

conventional SP8 lineages has been reported (228), ignoring the heterogeneity seen within the SP8 compartment. Subsequently these populations such as Eomes^{+} SP8 and CD8$\alpha\alpha^{+}$ intraepithelial lymphocytes (IEL) may disrupt the analysis of truly conventional SP8.

Within the thymus, the selection of SP4 and SP8 T-cells is proposed to differ beyond their recognition of MHC I or MHC II. Different models suggest that during selection SP8 receive either weaker (188,189), or shorter signals (190) following TCR stimulation, deciding lineage fate. The kinetic signalling model proposes that both CD4 and CD8 committed thymocytes transition to a CD4^{+}CD8^{low} population, before CD8 committed cells respond to IL-7 and transition back towards a classic CD8 phenotype (186,191). The dynamics involved in the selection of each of these lineages are clearly different to one another. Combined with the clear phenotypic and functional differences of the SP4 and SP8 lineages in the periphery, it could be expected that these populations behave differently within the thymus through their post selection maturation and subsequent egress from the thymus.

In this chapter, we have therefore looked to comprehensively define conventional SP8 thymocytes and characterise their post selection maturation and thymic egress alongside that previously defined in conventional SP4 thymocytes.

3.2 RESULTS

3.2.1 Characterisation of Classical Maturational Populations in cSP8 Thymocytes

In order to bring the understanding of post selection maturation in SP8s alongside that of SP4s, we first needed to define conventional SP8 thymocytes by flow cytometric analysis. Following mechanical disaggregation of the thymus, cells were stained with an extensive antibody panel that was capable of identifying and isolating subpopulations of thymocytes, enabling us to focus our analysis solely on conventional SP4 and SP8 thymocytes. Firstly, a viability dye was used to ensure analysis was focussed on live cells, and CD1d tetramer staining to remove non-conventional iNKT. The resulting population was then separated into $CD4^+CD8\alpha^-$ SP4, $CD4^-CD8\alpha^+$ SP8, and $CD4^+CD8\alpha^+$ DP. SP4 were then further gated on $TCR\beta^+$ and separated into $CD25^+$ Treg, and $CD25^-$ conventional cells. SP8 were gated on $TCR\beta$ in conjunction with Eomes, identifying three populations of SP8: $TCR\beta^-$ $Eomes^-$ iSP8, $TCR\beta^+$ $Eomes^+$ Eomes SP8, and $TCR\beta^+$ $Eomes^-$ SP8. The latter of these were further separated on $CD8\beta$, isolating $CD8\alpha^+CD8\beta^-$ $CD8\alpha\alpha$ IEL, leaving the remaining conventional population identified as $TCR\beta^+$ $Eomes^-$ $CD8\alpha\beta^+$ SP8 (Figure 3.1A).

The definition of newly produced conventional thymic populations was further aided through the use of WT RagGFP mice (225). As described previously, this model allows for the identification of newly produced cells that are GFP^+, with GFP^- cells representing those that either recirculated from the periphery or have remained resident in the thymus following their production. $TCR\beta^+$ $CD25^-$ SP4 and $TCR\beta^+$ $Eomes^-$ $CD8\alpha\beta^+$ SP8 were gated on $RagGFP^+$ newly produced cells using a WT GFP^-

mouse as a control (Figure 3.1B), with the vast majority of both populations being GFP^+ (Figure 3.1C). This gating strategy therefore shows our definition of conventional SP4 (cSP4) as CD1d $Tetramer^-$ $CD4^+$ $CD8\alpha^-$ $TCR\beta^+$ $CD25^-$ $RagGFP^+$ cells, and conventional SP8 (cSP8) as CD1d $Tetramer^-$ $CD4^-$ $CD8\alpha\beta^+$ $TCR\beta^+$ $Eomes^-$ $RagGFP^+$.

To further characterise the progression through maturational populations of cSP8, the panel also included markers previously used to define maturation in SP4 populations CD69 and CD62L (221,224). The expression pattern of these markers on cSP4 and cSP8 allow for separation into $CD69^+CD62L^-$ immature, and $CD69^-CD62L^+$ mature cells (Figure 3.2A). Interestingly, when comparing the distribution amongst these two populations between cSP4 and cSP8, cSP8 show a significantly higher proportion of mature cells than cSP4 (Figure 3.2B). This is further reinforced by the total numbers of these populations, with an average of 7.8 fold more cSP4 immature cells, but only 2 fold more cSP4 mature cells when compared with cSP8 populations (Figure 3.2C).

Use of the WT RagGFP model again aided analysis of the maturation of these populations, using a loss of RagGFP as a readout of cell-aging (225,226). Comparing RagGFP levels on immature and mature cells in the cSP4 and cSP8 populations indicated that both lineages progress through these maturational populations (Figure 3.3A). The more mature phenotype seen with proportions and numbers of cSP8 compared with cSP4 was further seen when comparing RagGFP levels on both immature and mature populations between the two lineages, with a lower RagGFP mean fluorescence intensity (MFI) in both immature and mature cSP8 compared with the equivalent cSP4 populations (Figure 3.3B).

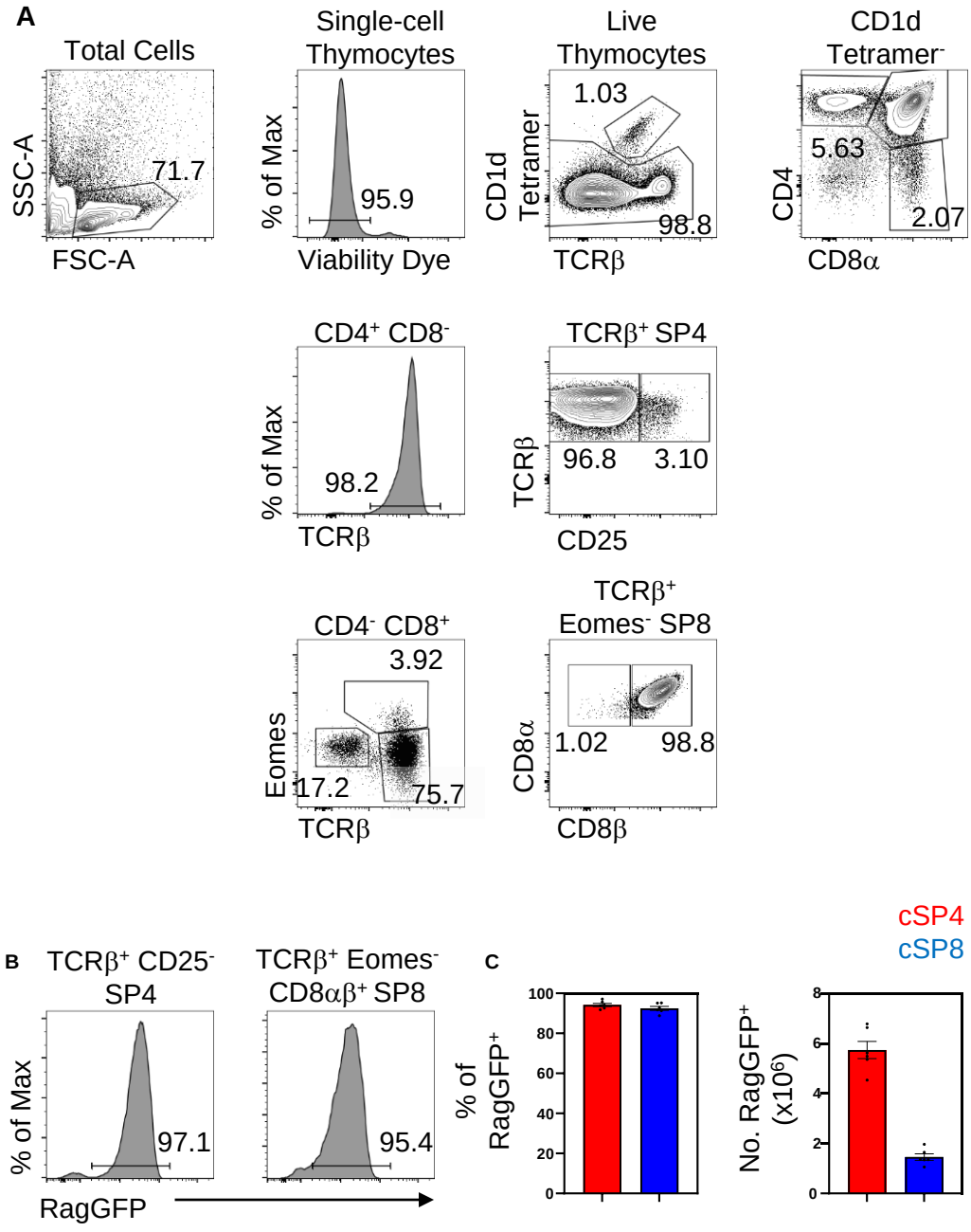
A
Total Cells
SSC-A
FSC-A
71.7
Single-cell Thymocytes
% of Max
Viability Dye
95.9
Live Thymocytes
CD1d Tetramer
TCRβ
1.03
98.8
CD1d Tetramer-
CD4
CD8α
5.63
2.07
CD4+ CD8-
% of Max
TCRβ
98.2
TCRβ+ SP4
TCRβ
CD25
96.8
3.10
CD4- CD8+
Eomes
TCRβ
3.92
17.2
75.7
TCRβ+ Eomes- SP8
CD8α
CD8β
1.02
98.8
B
TCRβ+ CD25- SP4
TCRβ+ Eomes- CD8αβ+ SP8
% of Max
RagGFP
97.1
95.4
C
cSP4
cSP8
% of RagGFP+
100
80
60
40
20
0
No. RagGFP+ (x10^6)
8
6
4
2
0

Figure 3.1. Characterisation of Subsets within SP4 and SP8 Thymocyte Populations

Thymuses were harvested from WT RagGFP mice and mechanically disaggregated for FACS analysis of thymocyte subpopulations.

(A) Gating strategy of total thymocyte populations to identify iNKT and bulk $CD4^+$ and $CD8^+$ thymocytes (top row), Treg and conventional SP4 (middle row), and Eomes SP8, iSP, $CD8\alpha\alpha$ SP8, and conventional SP8 (bottom row).

(B) Gating strategy to identify $RagGFP^+$ conventional SP4 (left) and conventional SP8 (right).

(C) Graphical representation of percentages (left) and total number (right) of $RagGFP^+$ conventional SP4 (red) and conventional SP8 (blue).

Data is taken from 3 separate experiments with n=6. Each data point represents an individual mouse, with bars plotting the mean and error bars representing the SEM.

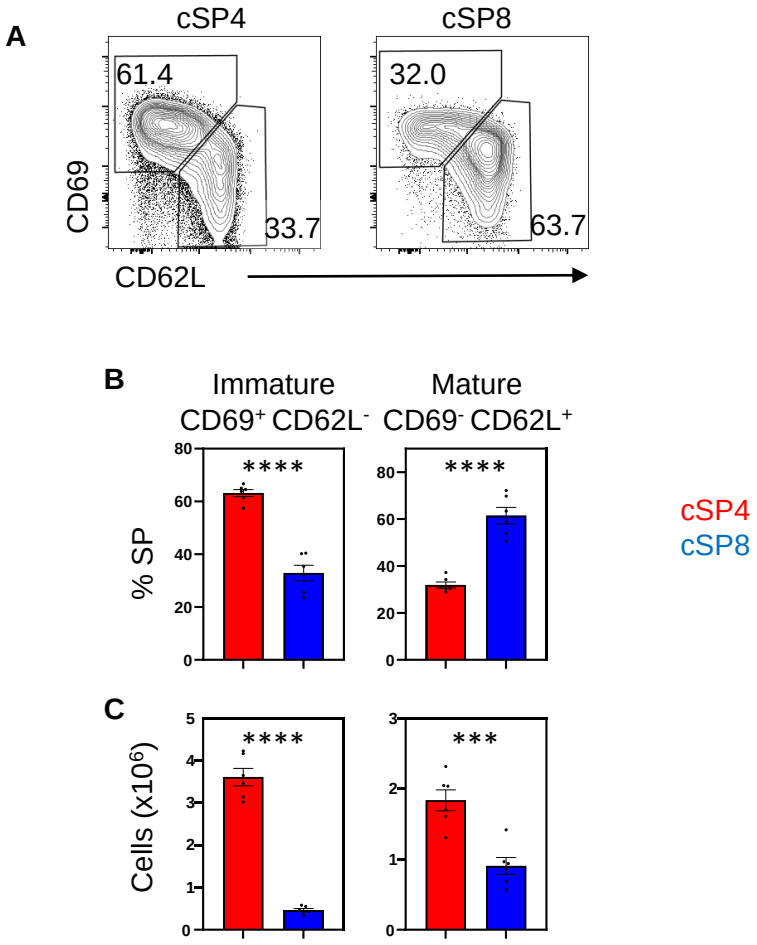
A
cSP4
cSP8
61.4
33.7
32.0
63.7
CD69
CD62L
B
Immature
CD69+ CD62L-
Mature
CD69- CD62L+
% SP
****
****
cSP4
cSP8
C
Cells (x10^6)
****
***

Figure 3.2. Conventional SP8 Represent More Mature Cells than SP4

Thymuses were harvested from WT RagGFP mice and mechanically disaggregated for FACS analysis of thymocyte subpopulations.

(A) Representative FACS plots to identify $CD69^{+}$ $CD62L^{-}$ Immature and $CD69^{-}$ $CD62L^{+}$ Mature cSP4 (left) and cSP8 (right)

(B) Comparison of percentages of immature and mature populations between cSP4 (red), and cSP8 (blue).

(C) Comparison of total numbers of immature and mature populations between cSP4 (red), and cSP8 (blue).

Data is taken from 3 separate experiments with n=6. Each data point represents an individual mouse, with bars plotting the mean and error bars representing the SEM. Statistical significance was determined using Independent Student's T-test, with (***) representing $P<0.001$, and (****) representing $P<0.0001$.

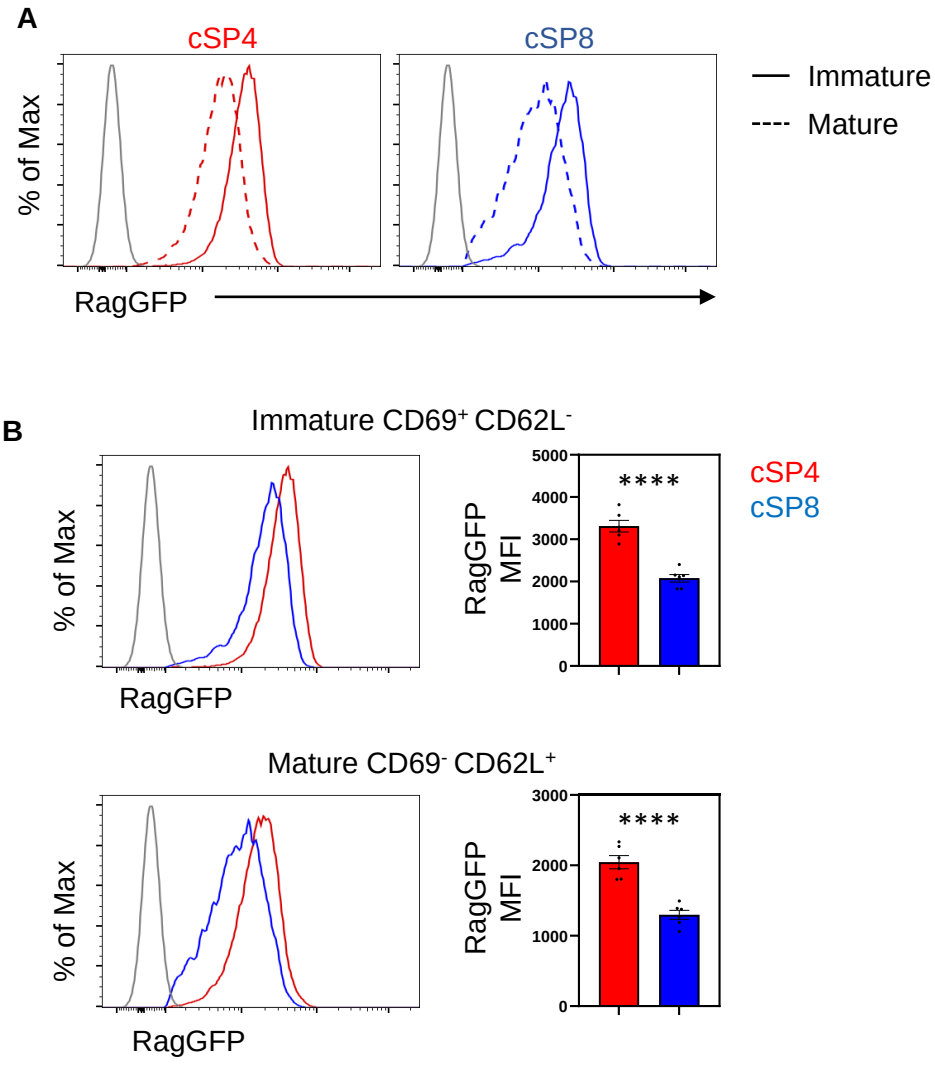
A
cSP4
cSP8
% of Max
RagGFP
Immature
Mature
B
Immature CD69+ CD62L-
% of Max
RagGFP
RagGFP MFI
5000
4000
3000
2000
1000
0
****
cSP4
cSP8
Mature CD69- CD62L+
% of Max
RagGFP
RagGFP MFI
3000
2000
1000
0
****

Figure 3.3. Both Immature and Mature cSP8 Populations are Older than Equivalent cSP4 Populations

Thymuses were harvested from WT RagGFP mice and mechanically disaggregated for FACS analysis of thymocyte subpopulations.

(A) RagGFP expression by immature (solid line) and mature (dashed line) populations within cSP4 (red) and cSP8 (blue).

(B) Comparison of RagGFP expression on immature (top) and mature (bottom) between cSP4 (red) and cSP8 (blue). Graphs represent calculated MFI of RagGFP for cSP4 and cSP8.

Data is taken from 3 separate experiments with n=6. Each data point represents an individual mouse, with bars plotting the mean and error bars representing the SEM. Statistical significance was determined using Independent Student's T-test, with (****) representing $P<0.0001$. Grey histogram plots represent $RagGFP^-$ control mice.

Grey histogram plots represent $RagGFP^-$ control mice.

Rather than CD62L, a more recent definition of maturational stages in thymocyte development has utilised MHC I expression alongside CD69, separating SP thymocytes into $CD69^+$ MHC I^- SM, $CD69^+$ MHC I^+ M1, and $CD69^-$ MHC I^+ M2 (228). We identified these populations in our own hands within the cSP4 lineage, however when applying the same gating method to cSP8 the SM population was clearly missing (Figure 3.4A). As seen with the mature populations in Figure 3.2B, the proportion of M2 cSP8 was significantly higher than cSP4. However, presumably as the immature cSP4 population is split between the SM and M1 when using this gating method, the proportion of M1 shows no difference between cSP4 and cSP8 (Figure 3.4B). Again, mimicking the total numbers of immature and mature populations of cSP4 and cSP8, there are around 4.2 fold more cSP4 M1 than cSP8, but only 2.4 fold more cSP4 M2 (Figure 3.4C).

Using RagGFP to compare the ages of these populations, we focussed on the M1 and M2 populations as the cSP8 population appeared to lack any discernible SM cells. Again, both cSP4 and cSP8 progressed through the M1 and M2 populations sequentially (Figure 3.5A). Further replicating the comparison between cSP4 and cSP8 in the immature and mature populations, both cSP8 M1 and M2 have a lower RagGFP MFI than the same populations in the cSP4 lineage (Figure 3.5B).

Following the observation of a more mature phenotype within the cSP8 population using multiple gating strategies, we next looked to further investigate the mature cells by separating this population in M2 a/b/c (242). Firstly, the vast majority of $CD62L^+$ mature cells lay within the M2 populations, showing a clear overlap between the populations (Figure 3.6A), allowing gating on these $CD69^-$ $CD62L^+$ cells with confidence that they represent the M2 population.

When M2a/b/c gates were applied to our cSP4 population, we saw even separation based on CD62L expression, with a progressive loss of RagGFP between these populations, confirming what has been reported in the sequential upregulation of CD62L through further maturation of the most mature population of cells (98) (Figure 3.6B). We next carried out the same of cSP8 M2, separating this populations into equal M2a, M2b, and M2c populations, we saw a trend towards a progressive loss of RagGFP between these populations (Figure 3.6C), showing cSP8 progress through the same sequential populations as cSP4 during thymic development. Furthermore, in keeping with the older phenotype seen in cSP8, all three M2a, M2b, and M2c populations showed a lower level of RagGFP in cSP8 than cSP4 (Figure 3.7A), further confirmed by significantly lower RagGFP MFIs (Figure 3.7B).

Given that the older phenotype of cSP8 compared with cSP4 persisted through the most mature populations of thymocytes, we then looked to see how this increased thymic dwell time affected the expression of CD62L. Here, we applied the M2a/b/c gates that separated cSP4 M2 into equal populations (Figure 3.6A) to the cSP8 M2 population. In keeping with a more mature phenotype, the cSP8 M2 showed a higher proportion of the most mature M2c, indicative of a higher level of CD62L, and increased maturation in the cSP8 (Figure 3.8A). Again, even when changing the gating of cSP8 M2a/b/c to this method, the significantly lower RagGFP in cSP8 compared with cSP4 is maintained throughout all of these populations (Figure 3.8B,C)

Taken together, these data indicate that whilst cSP8 populations progress through similar sequential maturational populations to cSP4, there are key differences. A more mature phenotype in cSP8 is seen when separating into these populations which is underpinned by a significantly lower RagGFP expression throughout these stages.

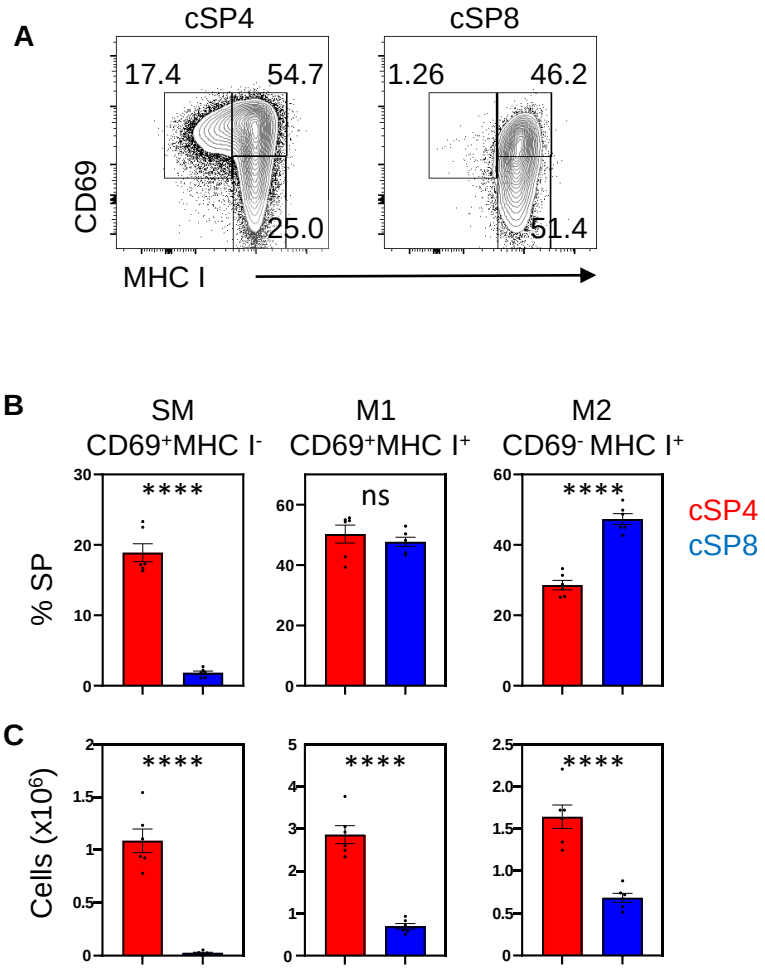
A
cSP4
cSP8
17.4
54.7
25.0
1.26
46.2
51.4
CD69
MHC I
B
SM
CD69+MHC I-
M1
CD69+MHC I+
M2
CD69- MHC I+
% SP
****
ns
****
cSP4
cSP8
C
Cells (x10^6)
****
****
****

Figure 3.4. Conventional SP8 lack the Semi-mature Population and Represent more Mature Cells than SP4

Thymuses were harvested from WT RagGFP mice and mechanically disaggregated for FACS analysis of thymocyte subpopulations.

(A) Representative FACS plots to identify $CD69^{+}$ MHC I^{-} (SM), $CD69^{+}$ MHC I^{+} (M1), and $CD69^{-}$ MHC I^{+} (M2) in cSP4 (left) and cSP8 (right).

(B) Comparison of percentages of SM, M1, and M2 populations between cSP4 (red), and cSP8 (blue).

(C) Comparison of total numbers of SM, M1, and M2 populations between cSP4 (red), and cSP8 (blue).

Data is taken from 3 separate experiments with n=6. Each data point represents an individual mouse, with bars plotting the mean and error bars representing the SEM. Statistical significance was determined using Independent Student's T-test, with (****) representing $P<0.0001$, and (ns) no significance.

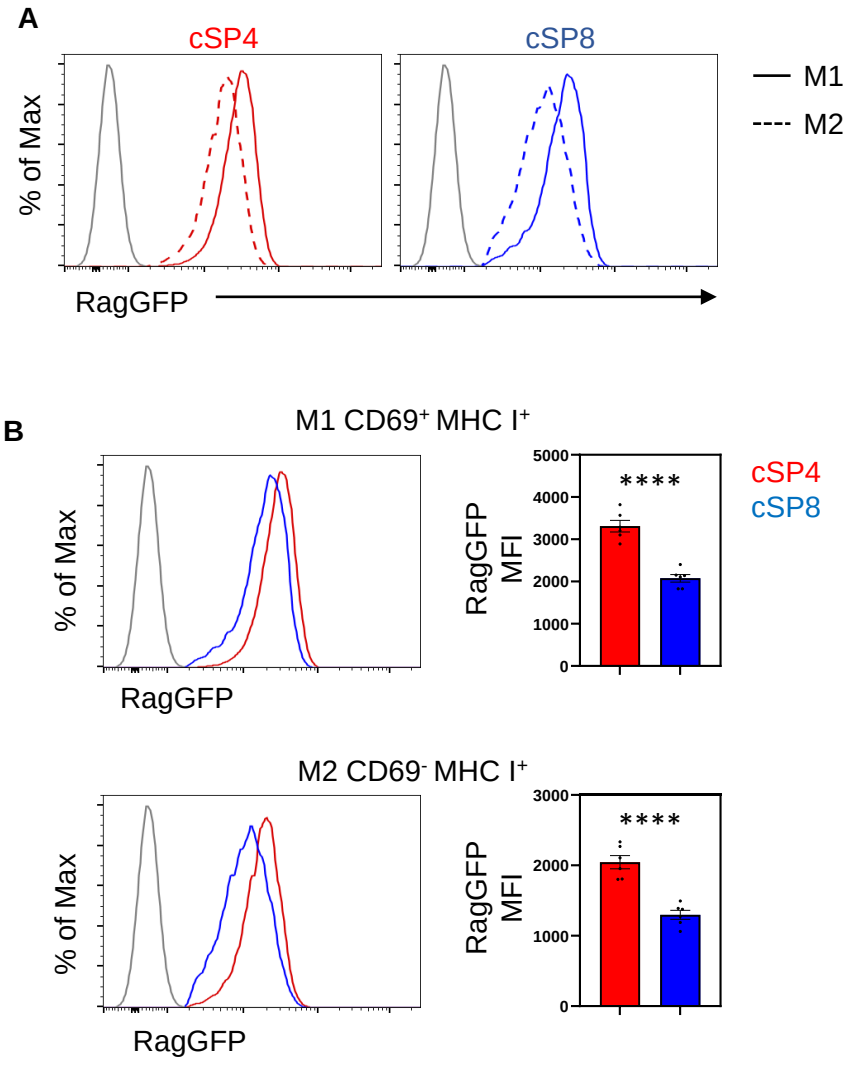
A
cSP4
cSP8
M1
M2
% of Max
RagGFP
B
M1 CD69+ MHC I+
% of Max
RagGFP
RagGFP MFI
5000
4000
3000
2000
1000
0
****
cSP4
cSP8
M2 CD69- MHC I+
% of Max
RagGFP
RagGFP MFI
3000
2000
1000
0
****

Figure 3.5. cSP8 M1 and M2 Populations are Older than Equivalent cSP4 Populations

Thymuses were harvested from WT RagGFP mice and mechanically disaggregated for FACS analysis of thymocyte subpopulations.

(A) RagGFP expression by M1 (solid line) and M2 (dashed line) populations within cSP4 (red) and cSP8 (blue).

(B) Comparison of RagGFP expression on M1 (top) and M2 (bottom) between cSP4 (red) and cSP8 (blue). Graphs represent calculated MFI of RagGFP for cSP4 and cSP8.

Data is taken from 3 separate experiments with n=6. Each data point represents an individual mouse, with bars plotting the mean and error bars representing the SEM. Statistical significance was determined using Independent Student's T-test, with (****) representing $P<0.0001$. Grey histogram plots represent $RagGFP^-$ control mice.

Grey histogram plots represent $RagGFP^-$ control mice.

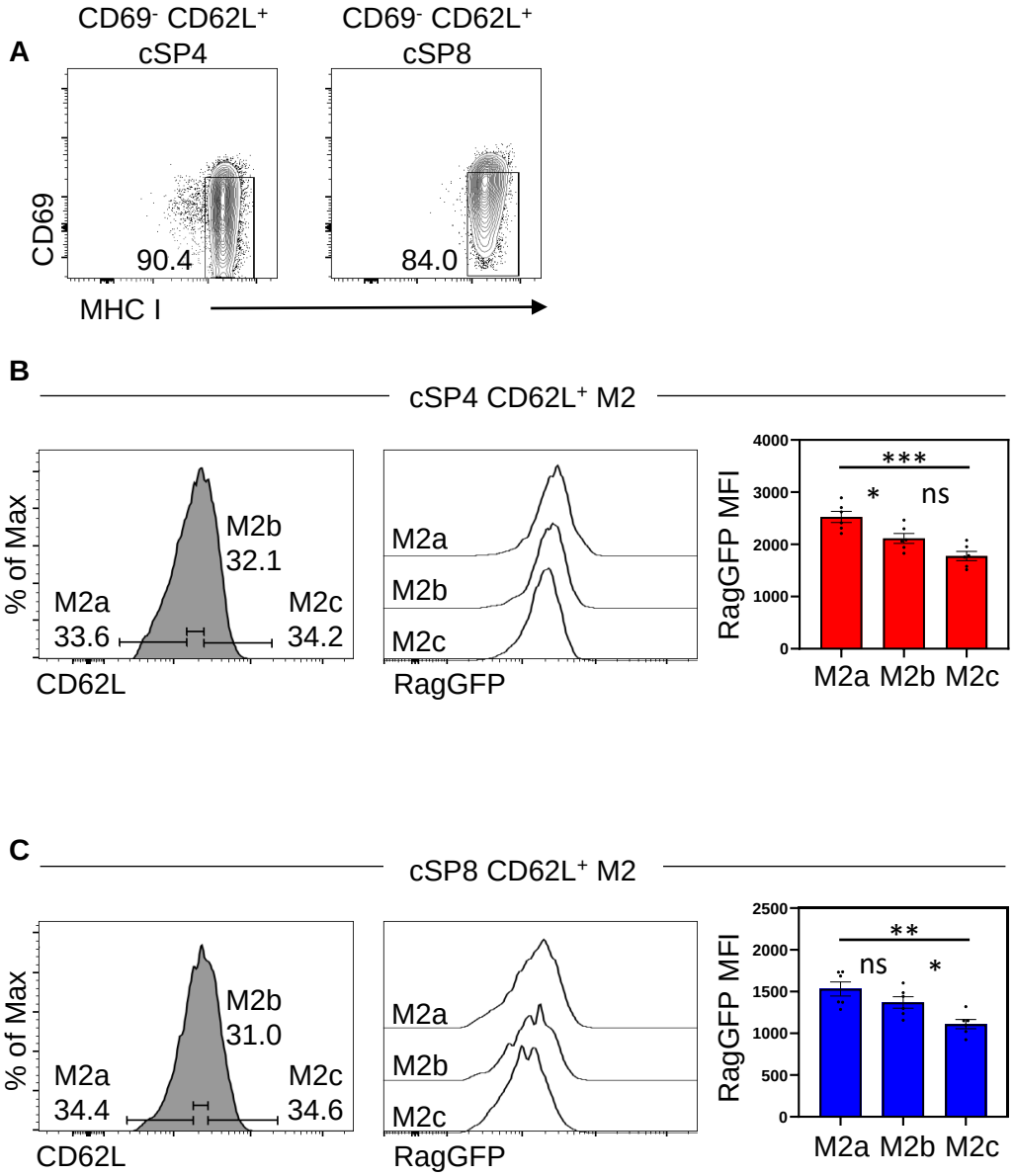
A
CD69- CD62L+
cSP4
CD69- CD62L+
cSP8
CD69
90.4
84.0
MHC I
B
cSP4 CD62L+ M2
% of Max
M2b
32.1
M2a
33.6
M2c
34.2
CD62L
M2a
M2b
M2c
RagGFP
RagGFP MFI
4000
3000
2000
1000
0
***
*
ns
M2a M2b M2c
C
cSP8 CD62L+ M2
% of Max
M2b
31.0
M2a
34.4
M2c
34.6
CD62L
M2a
M2b
M2c
RagGFP
RagGFP MFI
2500
2000
1500
1000
500
0
**
ns
*
M2a M2b M2c

Figure 3.6. cSP8 M2 can be Separated into Progressive M2a/b/c Populations as in cSP4 M2

Thymuses were harvested from WT RagGFP mice and mechanically disaggregated for FACS analysis of thymocyte subpopulations.

(A) $CD69^{-}$ MHC I^{+} M2 gates applied to mature cSP4 (left) and cSP8 (right)

(B) Separation of cSP4 M2 into equal proportions of M2a/b/c populations based on increasing CD62L expression (left), with histogram plots of RagGFP expression on all three of these populations (middle), and graphical representation of calculated RagGFP MFI (right).

(C) Separation of cSP8 M2 into equal proportions of M2a/b/c populations based on increasing CD62L expression (left), with histogram plots of RagGFP expression on all three of these populations (middle), and graphical representation of calculated RagGFP MFI (right).

Data is taken from 3 separate experiments with n=6. Each data point represents an individual mouse, with bars plotting the mean and error bars representing the SEM. Statistical significance was determined using Ordinary One-way ANOVA with Tukey's multiple comparisons, with (*) representing $P<0.05$, (**) representing $P<0.01$, (***) representing $P<0.001$, and (ns) representing no significance.

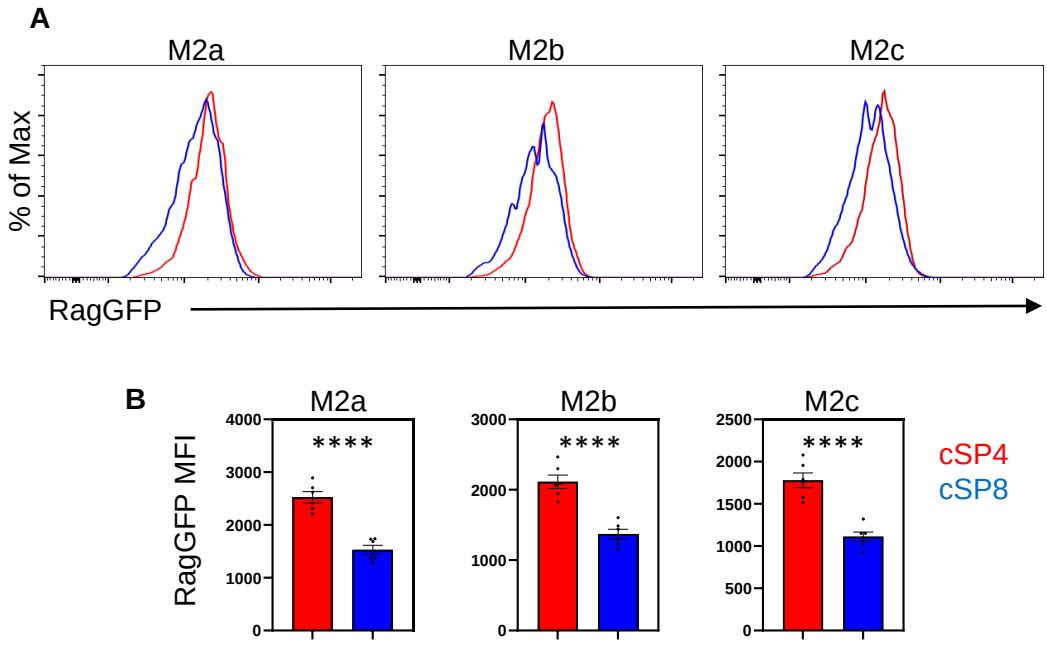
A
M2a
M2b
M2c
% of Max
RagGFP
B
M2a
M2b
M2c
RagGFP MFI
****
****
****
4000
3000
2000
1000
0
3000
2000
1000
0
2500
2000
1500
1000
500
0
cSP4
cSP8

Figure 3.7. cSP8 M2a/b/c populations are all older than cSP4 counterparts

Thymuses were harvested from WT RagGFP mice and mechanically disaggregated for FACS analysis of thymocyte subpopulations.

(A) Histograms of RagGFP expression by M2a (left), M2b (middle), and M2c (right) populations comparing cSP4 (red) and cSP8 (blue).

(B) Graphs comparing the calculated MFI of RagGFP between cSP4 (red) and cSP8 (blue) in M2a (left), M2b (middle), and M2c (right)

Data is taken from 3 separate experiments with n=6. Each data point represents an individual mouse, with bars plotting the mean and error bars representing the SEM. Statistical significance was determined using Independent Student's T-test, with (****) representing $P<0.0001$.

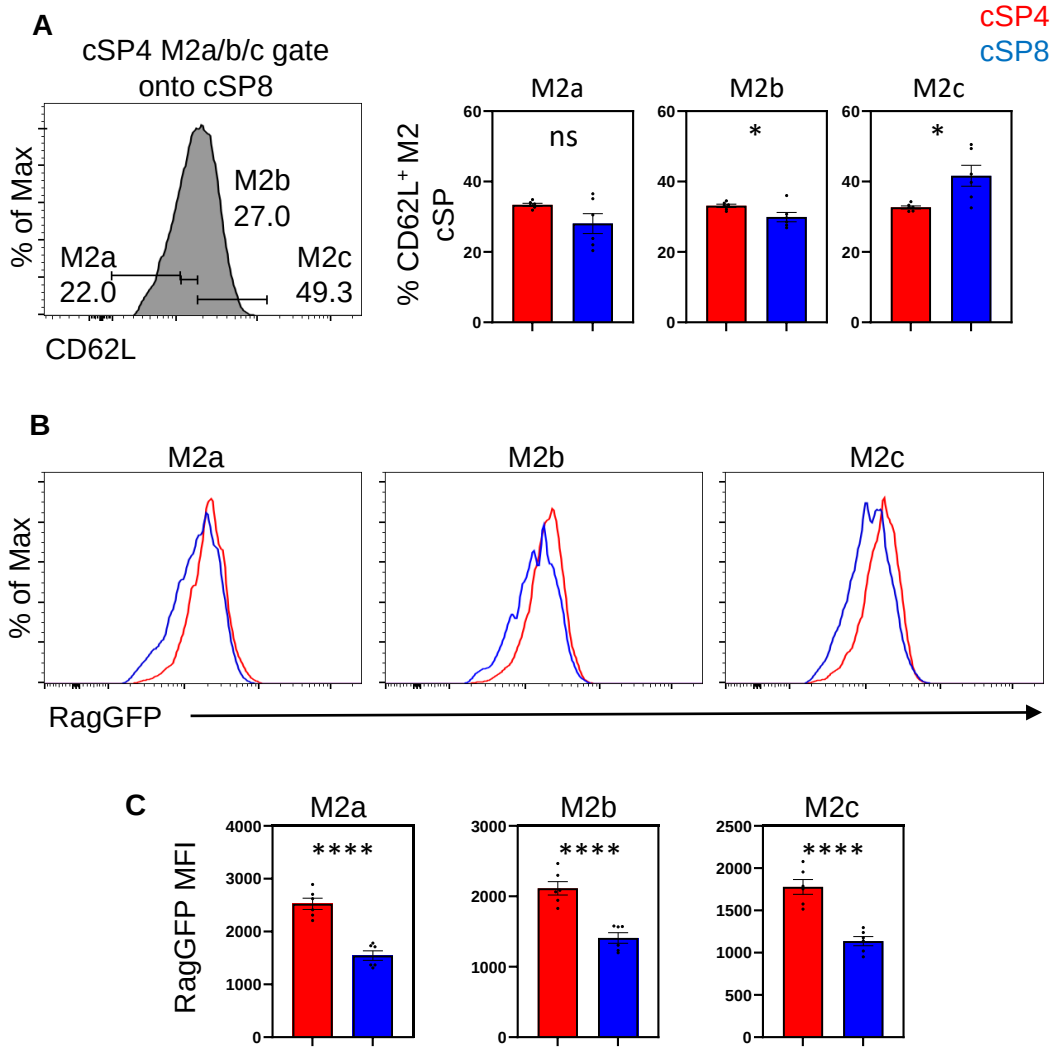
A
cSP4
cSP8
cSP4 M2a/b/c gate
onto cSP8
% of Max
M2a
22.0
M2b
27.0
M2c
49.3
CD62L
% CD62L+ M2
cSP
M2a
M2b
M2c
ns
*
*
B
M2a
M2b
M2c
% of Max
RagGFP
C
RagGFP MFI
M2a
M2b
M2c
****
****
****

Figure 3.8. M2 cSP8 have higher Expression of CD62L than cSP4 M2

Thymuses were harvested from WT RagGFP mice and mechanically disaggregated for FACS analysis of thymocyte subpopulations.

(A) Separation of cSP8 into M2a/b/c populations using the same gates previously used to separate cSP4 into equal populations based on CD62L expression shown in figure 3.7A. Graphs summarise the percentages of M2a/b/c between cSP4 and cSP8 using this gating strategy.

(B) Histogram plots of the RagGFP expression on cSP4 (red) and cSP8 (blue) M2a/b/c using the above gating strategy.

(C) Summary of calculated RagGFP MFI between cSP4 (red) and cSP8 (blue) M2a/b/c populations.

Data is taken from 3 separate experiments with n=6. Each data point represents an individual mouse, with bars plotting the mean and error bars representing the SEM. Statistical significance was determined using Independent Student's T-test, with (*) representing $P<0.05$, (****) representing $P<0.0001$, and (ns) representing no significance.

3.2.2 Conventional SP8 Emigrate the Thymus using the same Conveyor Belt Mechanism as Conventional SP4

Analysis of the intrathymic maturation of cSP4 and cSP8 suggested that cSP8 represent a more mature population that is older than its cSP4 counterparts. Previous work has suggested that thymic egress works in a 'conveyor belt' model, whereby the most mature cSP4 are preferentially selected to leave the thymus (98). As such, we thought that the altered maturational status of cSP8 compared to cSP4 could mean the dynamics of thymic egress differ between the two lineages. We investigated this by adapting a model previously used to define this conveyor belt egress in cSP4 cells. I.V. injection of anti-CD4 PE antibody enters the vasculature, but not the thymus, labelling cells in the PVS in the process of thymic egress. In order to label both cSP4 and cSP8, we injected anti-CD45 PE antibody, and followed the same protocol as previously described (98,235). Thymuses were harvested, and PE-labelled PVS cells were enriched, stained with our extensive panel, and isolated using flow cytometry (Figure 3.9). As this model enables us to isolate all $CD45^+$ cells within the PVS, we could apply our gating strategy outlined in Figure 3.1A to identify cSP4 and cSP8 populations, and further evaluate their maturational status in the PVS compared to the thymus.

We first sought to confirm the CD45 I.V. experiment provides the same results as previously seen within the cSP4 lineage. We identified CD45-PE^- thymic cells and CD45-PE^+ PVS cells and compared their maturational status. Firstly, using the SM-M1-M2 gating strategy we saw that the majority of cSP4 in the PVS are M2, entirely lacking an SM population, with a significantly higher proportion of M2 (Figure 3.10A). These PVS cSP4 M2 also show a significantly lower expression of RagGFP compared

with thymic cSP4 M2, suggesting that the cells in the PVS are older and further along their maturation (Figure 3.10B). We then further separated the cSP4 M2 that were shown to be enriched within the PVS into our M2a/b/c populations. We separated thymic cSP4 M2 into equal proportions based on CD62L expression and applied this to the cSP4 M2 within the PVS. This showed a significant increase in the proportion of M2c within the PVS compared with cells still in the thymus (Figure 3.10C). This enrichment for the most mature cSP4 M2c fits with what has been previously reported using the anti-CD4 PE I.V. injection, suggesting use of the anti-CD45 antibody I.V. is identifying the same egressing population (98) (Figure 3.10C). Furthermore, the RagGFP MFI of the PVS isolated cSP4 M2c is significantly lower than that of the most mature thymic cSP4 M2c (Figure 3.10D). This further suggests that even within the most mature fraction of cSP4, the oldest, most mature of these are preferentially selected for thymic egress by the thymic conveyor belt.

Having confirmed the effectiveness of the anti-CD45 PE I.V. injection model for isolating PVS cells and setting a baseline in our analysis of cSP4, we next looked to see how cSP8 that are present in the PVS compare with their intrathymic counterparts. Similar to what was seen for cSP4, cSP8 have a significantly higher proportion of M2, with a nominal proportion of M1 (Figure 3.11A). The increased proportion of M2 in the PVS cSP8 is not as dramatic as that seen in the cSP4, however this is likely due to the increased M2 in thymic cSP8 when compared to cSP4 (Figure 3.4). Again, replicating what we see in the cSP4 isolated in the PVS, the RagGFP MFI of the PVS cSP8 M2 was significantly lower than that of the thymic cSP8 M2, suggesting the enriched mature population is also older in the PVS (Figure 3.11B). Separation of thymic cSP8 M2 into equal M2a, M2b, and M2c populations and applying this to PVS cSP8 M2

showed that the most mature M2c are enriched within the PVS as seen within the cSP4 population (Figure 3.11C). The M2c population within the cSP8 PVS also had a significantly lower RagGFP than thymic cSP8 M2c (Figure 3.11D).

We then looked to see whether the observation of an older, more mature cSP8 compartment within the thymus was carried through into the PVS during the egress of these cells, or whether the cells egressing the thymus were at the same level of maturity in both lineages. Initially comparing the RagGFP levels between cSP4 and cSP8 M2 isolated in the PVS showed that cSP8 maintained a lower level of RagGFP expression in the PVS compared to cSP4 (Figure 3.12A), with this also translating to the most mature M2c within the PVS (Figure 3.12B). This suggested that the cSP8 selected for thymic egress are older than cSP4 undergoing the same process. By applying the gates used to determine the distribution of M2a, M2b, and M2c in PVS cSP4 M2 to cSP8 M2 in the PVS, cSP8 M2 in the PVS were shown to be more biased towards M2c than cSP4 (Figure 3.12C), as seen within the whole thymus (Figure 3.8A).

Taken together, this data suggests that cSP8 follow the same conveyor belt maturation programme as cSP4, whereby the most mature M2c cells are preferentially selected for entry to the PVS and thymic egress. The older, more mature phenotype seen within cSP8 in the thymus is conserved within these cells specifically in the process of egress, suggesting that the more mature phenotype does not alter egress for cSP8 compared to cSP4.

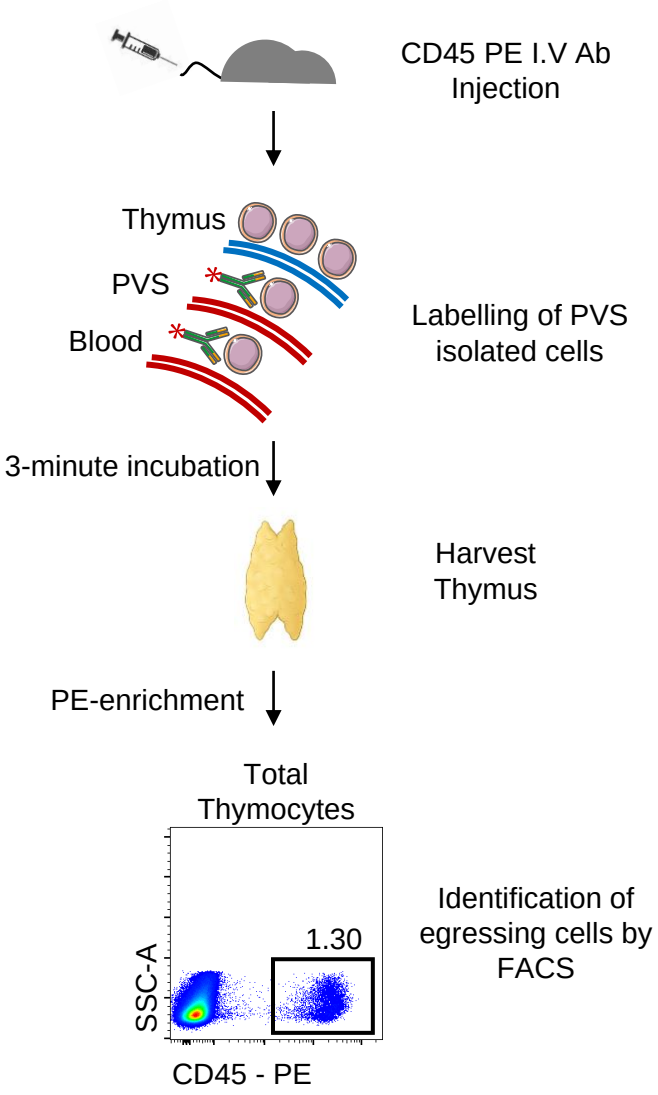
CD45 PE I.V Ab
Injection
Thymus
PVS
Blood
Labelling of PVS
isolated cells
3-minute incubation
Harvest
Thymus
PE-enrichment
Total
Thymocytes
1.30
SSC-A
CD45 - PE
Identification of
egressing cells by
FACS

Figure 3.9. Model of Isolation of Egressing Thymocytes in the PVS by CD45-PE I.V. injection

Mice are I.V. injected with PE-conjugated CD45 antibody, entering the circulation and subsequently thymic vasculature. The size of the PE conjugate prohibits entry into the thymus, and so only cells in contact with the blood in the PVS, therefore egressing the thymus, are labelled. Following a 3-minute incubation following injection, the mouse is sacrifice, and thymus harvested and mechanically disaggregated. Thymocytes are then enriched for PE-labelled cells using magnetic cell-sorting and, stained for thymocyte analysis.

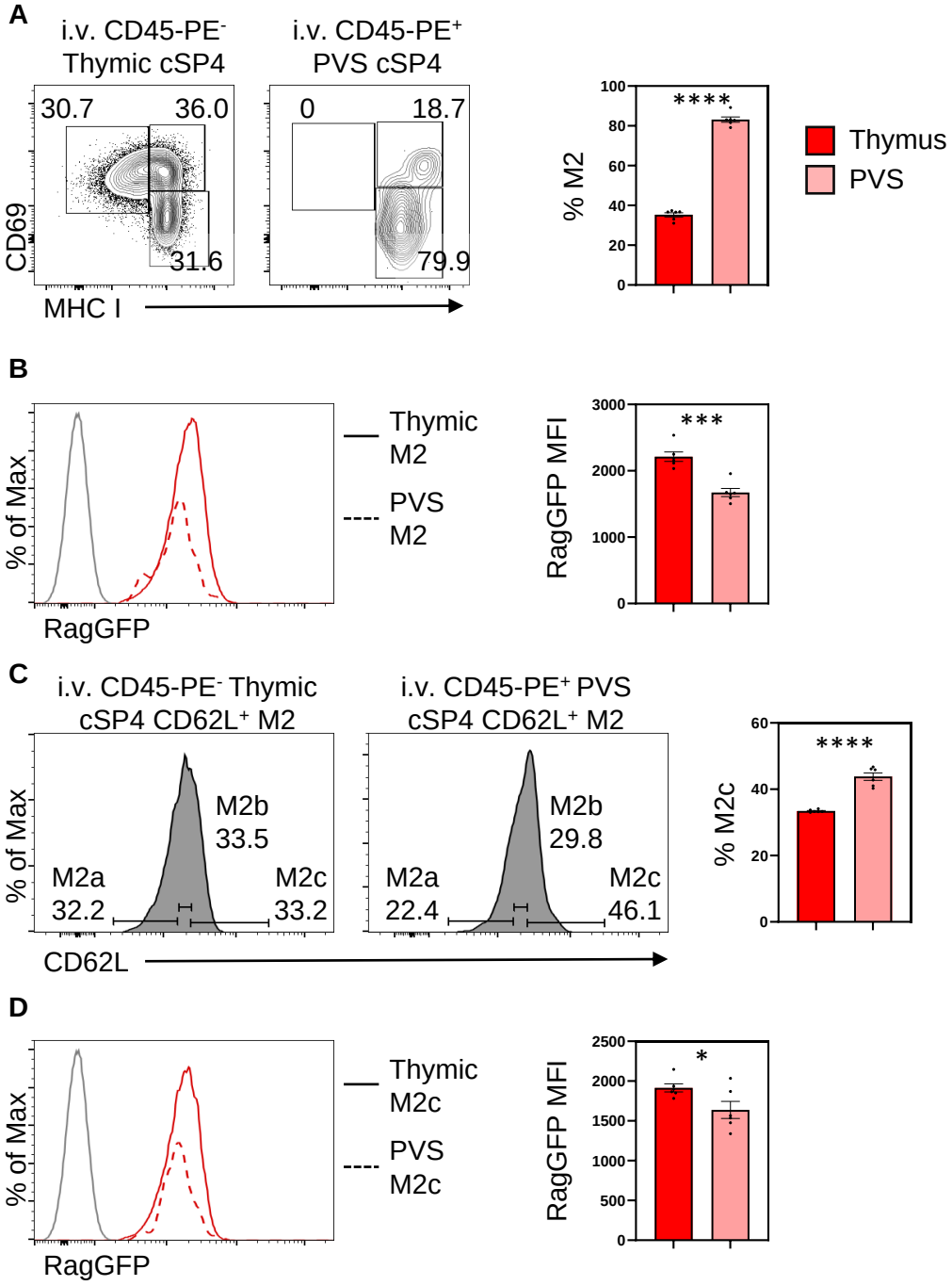
A
i.v. CD45-PE-
Thymic cSP4
i.v. CD45-PE+
PVS cSP4
30.7
36.0
31.6
0
18.7
79.9
CD69
MHC I
% M2
****
Thymus
PVS
B
% of Max
RagGFP
Thymic M2
PVS M2
RagGFP MFI
***
C
i.v. CD45-PE- Thymic cSP4 CD62L+ M2
i.v. CD45-PE+ PVS cSP4 CD62L+ M2
M2a 32.2
M2b 33.5
M2c 33.2
M2a 22.4
M2b 29.8
M2c 46.1
CD62L
% M2c
****
D
% of Max
RagGFP
Thymic M2c
PVS M2c
RagGFP MFI
*

Figure 3.10. CD45-PE I.V. Isolates cSP4 in the PVS, Enriched for the Most Mature Cells

Mice were I.V. injected with anti CD45-PE and sacrificed 3 minutes later for thymuses to be harvested from WT RagGFP mice and mechanically disaggregated for FACS analysis of thymocyte subpopulations. Samples were enriched for PE-labelled cells, with a pre-enrichment sample taken as a control.

(A) Gating of $CD69^+$ MHC I^- (SM), $CD69^+$ MHC I^+ (M1), and $CD69^-$ MHC I^+ (M2) in cSP4 from pre- PE enrichment CD45-PE^- thymic (left), and post- PE enrichment CD45-PE^+ PVS cSP4 (right). Graph to summarise percentages of M2 in thymic cSP4 (solid red) and PVS cSP4 (light red).

(B) Histogram plots of the RagGFP expression on thymic cSP4 M2 (solid line) and I.V. CD45-PE labelled PVS cSP4 M2 (dashed line). Graph summarises calculated MFI of RagGFP in thymic cSP4 M2 (solid red) and PVS cSP4 M2 (light red).

(C) Separation of M2a/b/c populations based on equal separation of thymic cSP4 M2 (left) and applied to I.V. CD45-PE labelled PVS cSP4 M2 (right). Graph summarises percentages of M2c in thymic cSP4 (solid red) and PVS cSP4 (light red).

(D) Histogram plots of the RagGFP expression on thymic cSP4 M2c (solid line) and I.V. CD45-PE labelled PVS cSP4 M2c (dashed line). Graph summarises calculated MFI of RagGFP in thymic cSP4 M2c (solid red) and PVS cSP4 M2c (light red).

Data is taken from 2 separate experiments with n=6. Each data point represents an individual mouse, with bars plotting the mean and error bars representing the SEM. Statistical significance was determined using Independent Student's T-test, with (*) representing $P<0.05$, (***) representing $P<0.001$, and (****) representing $P<0.0001$. Grey histogram plots represent $RagGFP^-$ control mice.

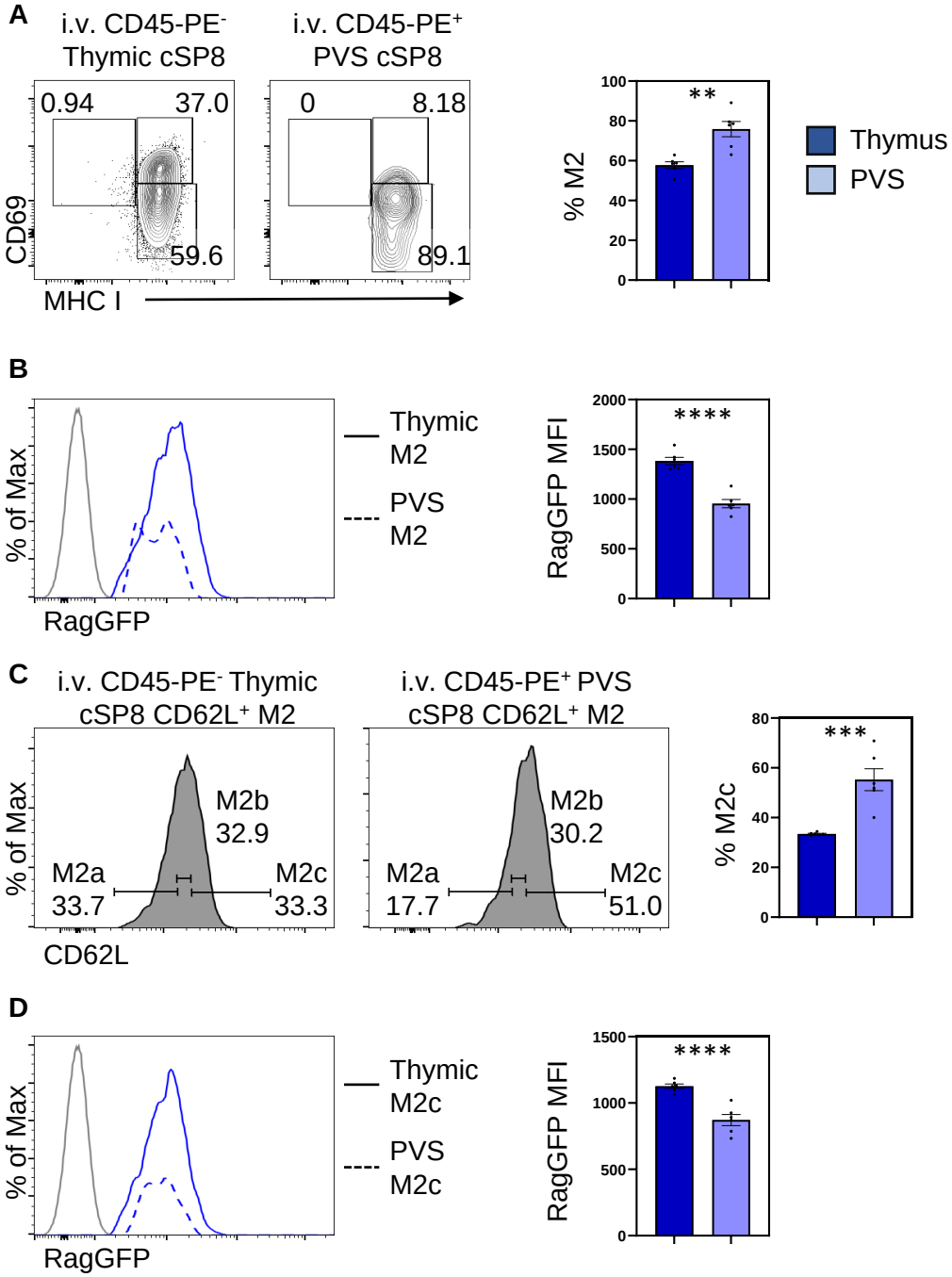
A
i.v. CD45-PE-
Thymic cSP8
i.v. CD45-PE+
PVS cSP8
0.94
37.0
59.6
0
8.18
89.1
CD69
MHC I
% M2
**
Thymus
PVS
B
% of Max
RagGFP
Thymic M2
PVS M2
RagGFP MFI
****
C
i.v. CD45-PE- Thymic cSP8 CD62L+ M2
i.v. CD45-PE+ PVS cSP8 CD62L+ M2
M2a 33.7
M2b 32.9
M2c 33.3
M2a 17.7
M2b 30.2
M2c 51.0
CD62L
% M2c
***
D
Thymic M2c
PVS M2c

Figure 3.11. CD45-PE I.V. Labelled PVS cSP8 are Enriched for the Most Mature Cells

Mice were I.V. injected with anti CD45-PE and sacrificed 3 minutes later for thymuses to be harvested from WT RagGFP mice and mechanically disaggregated for FACS analysis of thymocyte subpopulations. Samples were enriched for PE-labelled cells, with a pre-enrichment sample taken as a control.

(A) Gating of $CD69^+$ MHC I^- (SM), $CD69^+$ MHC I^+ (M1), and $CD69^-$ MHC I^+ (M2) in cSP8 from pre- PE enrichment CD45-PE^- thymic (left), and post- PE enrichment CD45-PE^+ PVS cSP8 (right). Graph to summarise percentages of M2 in thymic cSP8 (solid blue) and PVS cSP4 (light blue).

(B) Histogram plots of the RagGFP expression on thymic cSP8 M2 (solid line) and I.V. CD45-PE labelled PVS cSP8 M2 (dashed line). Graph summarises calculated MFI of RagGFP in thymic cSP8 M2 (solid blue) and PVS cSP8 M2 (light blue).

(C) Separation of M2a/b/c populations based on equal separation of thymic cSP8 M2 (left) and applied to I.V. CD45-PE labelled PVS cSP8 M2 (right). Graph summarises percentages of M2c in thymic cSP8 (solid blue) and PVS cSP8 (light blue).

(D) Histogram plots of the RagGFP expression on thymic cSP8 M2c (solid line) and I.V. CD45-PE labelled PVS cSP8 M2c (dashed line). Graph summarises calculated MFI of RagGFP in thymic cSP8 M2c (solid blue and PVS cSP8 M2c (light blue).

Data is taken from 2 separate experiments with n=6. Each data point represents an individual mouse, with bars plotting the mean and error bars representing the SEM. Statistical significance was determined using Independent Student's T-test, with (**) representing $P<0.01$, (***) representing $P<0.001$, and (****) representing $P<0.0001$. Grey histogram plots represent $RagGFP^-$ control mice.

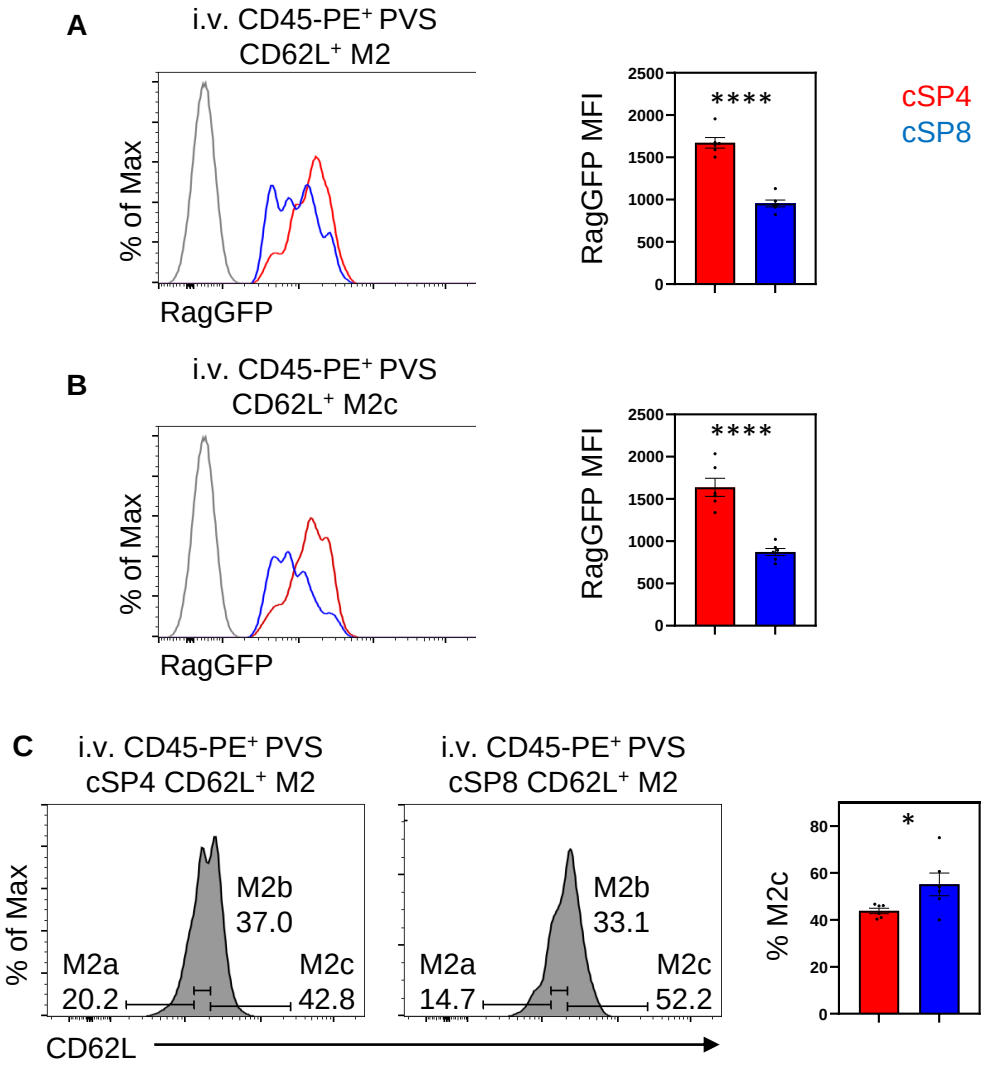
A
i.v. CD45-PE+ PVS
CD62L+ M2
% of Max
RagGFP
RagGFP MFI
2500
2000
1500
1000
500
0
****
cSP4
cSP8
B
i.v. CD45-PE+ PVS
CD62L+ M2c
% of Max
RagGFP
RagGFP MFI
2500
2000
1500
1000
500
0
****
C
i.v. CD45-PE+ PVS
cSP4 CD62L+ M2
i.v. CD45-PE+ PVS
cSP8 CD62L+ M2
% of Max
M2a
20.2
M2b
37.0
M2c
42.8
M2a
14.7
M2b
33.1
M2c
52.2
CD62L
% M2c
80
60
40
20
0
*

Figure 3.12. CD45-PE I.V. Labelled PVS cSP8 more Mature than cSP4 within the PVS

Mice were I.V. injected with anti CD45-PE and sacrificed 3 minutes later for thymuses to be harvested from WT RagGFP mice and mechanically disaggregated for FACS analysis of thymocyte subpopulations. Samples were enriched for PE-labelled cells, with a pre-enrichment sample taken as a control.

(A) Histogram plots of the RagGFP expression on I.V. CD45-PE labelled PVS cSP4 M2 (red) and cSP8 M2 (blue). Graph summarises calculated MFI of RagGFP in PVS cSP4 M2 (red), and cSP8 M2 (blue).

(B) Histogram plots of the RagGFP expression on I.V. CD45-PE labelled PVS cSP4 M2c (red) and cSP8 M2c (blue). Graph summarises calculated MFI of RagGFP in PVS cSP4 M2c (red), and cSP8 M2c (blue).

(C) Separation of M2a/b/c populations in I.V. CD45-PE labelled PVS cSP4 M2 based on equal separation of M2a/b/c populations in thymic cSP4 M2 (left). These gates were then applied to PVS cSP8 M2 (right). Graph summarises percentages of M2c in PVS cSP4 M2 (red) and cSP8 M2 (blue) using this gating strategy.

Data is taken from 2 separate experiments with n=6. Each data point represents an individual mouse, with bars plotting the mean and error bars representing the SEM. Statistical significance was determined using Independent Student's T-test, with (*) representing $P<0.05$, and (****) representing $P<0.0001$. Grey histogram plots represent $RagGFP^-$ control mice.

3.2.3 The CD5^{INT} TCRβ^{HI} DP3 Population Contains The Missing Immature cSP8 Thymocyte Populations

Throughout our analysis of the maturation and egress of cSP8 in comparison to cSP4, it is clear that cSP8 represent older cells, with a lower level of RagGFP expressed at each stage in development. We therefore sought to determine the cause of this delay in the maturation of cSP8 thymocytes. As a lower RagGFP MFI was seen at each stage in development, it was not clear from this alone at what stage this delay was occurring. To study this further, we calculate the ratio of RagGFP MFI between each transition in cSP4 and cSP8 development and compared the two lineages. The relative loss of RagGFP between M1-M2a, M2a-M2b, and M2b-M2c was the same in both cSP4 and cSP8. However, the DP-M1 transition showed a significantly greater relative loss of RagGFP in the cSP8 compared to the cSP4 (Figure 3.13A). We also looked to make this comparison by converting the loss of RagGFP into real-time (Figure 3.13B). Using the rearranged formula for exponential decay shown in Figure 3.13C, and assuming that the half-life of RagGFP *in vivo* is a reported 54 hours (227), we calculated that the transition between DP and cSP4 M1 took an average of 50 hours, whereas the same transition to cSP8 took on average 90 hours, almost double that of cSP4s (Figure 3.13B).

Both approaches clearly suggest that the transition from DP to SP is delayed in the cSP8 lineage compared to the cSP4 lineage. This led us to investigate the DP population further to identify an intermediate population to explain this lag. Subpopulations based on expression of CD5 and TCRβ have previously been identified within DP thymocytes, importantly including a population that represent cells committed exclusively to the SP8 lineage (201). Gating on RagGFP^{+} newly produced

DP thymocytes identified using the gating strategy previously described (Figure 3.1A), we identified $CD5^{LO}TCR\beta^{LO}$ DP1, $CD5^{HI}TCR\beta^{INT}$ DP2, and $CD5^{INT}TCR\beta^{HI}$ DP3 populations (Figure 3.14A). Whilst DP1 and DP2 cells represent populations that contain cells yet uncommitted to the SP4 or SP8 lineage, DP3 are exclusively cells committed to SP8 (201), suggesting they are older than the preceding DP1 and DP2 populations. Accordingly, DP3 have a significantly lower level of RagGFP compared to DP1 and DP2 populations (Figure 3.14B). As these cells represent committed SP8, we looked to see whether they expressed the maturational markers CD69 and MHC I. Applying gates used to identify these populations in cSP4 and cSP8, DP3 displayed a similar expression pattern to that in cSP populations, albeit with a significantly higher proportion of SM, and a less obvious M2 population (Figure 3.14C). Furthermore, when comparing expression of RagGFP between these populations, a significant progressive loss of RagGFP from SM through to M1 and M2 was seen, suggesting that these are sequential populations that the DP3 pass through with maturation (Figure 3.14D). Given this sequential relationship between the DP3 SM and M1 population, we looked to see how this fitted with the progression between the M1 and M2 population in the cSP8 lineage. Fitting with their role as SP8 precursors, the DP3 population showed progressive downregulation of RagGFP from the DP3 SM stage through to the cSP8 M2 stage (Figure 3.15A), mirroring the same progressive loss seen from the cSP4 SM through to the cSP4 M2 (Figure 3.15B).

As the separation of CD8-committed DP3 into SM and M1 appeared to represent the early SM and M1 populations preceding the M1 and M2 populations within cSP8 according to both phenotype and RagGFP expression, we aimed to combine the two populations, therefore allowing analysis of total committed SP8s. Applying the CD5

and TCRβ gates used to identify DP1, DP2, and DP3 populations to total RagGFP^{+} SP8 showed that the majority of cells are CD5^{INT}TCRβ^{HI}, with the remaining significant proportion being the TCRβ^{-} iSP8 populations (Figure 3.16A). We then devised a gating strategy to utilise this, gating on total CD8αβ^{+} Eomes^{-} RagGFP^{+} conventional thymocytes to incorporate both the DP and the cSP8 populations, before applying the CD5 and TCRβ gates to identify CD5^{INT}TCRβ^{HI} total committed SP8 (Figure 3.16B). Separation of these total committed SP8s into our maturational populations based on CD69 and MHC I expression showed a comparable expression profile to that of the cSP4 cells (Figure 3.16C). Importantly, the total committed SP8 contained a significant population of CD69^{-} M2, missing from the DP3 population, and likewise a clear SM population previously unseen in the cSP8 population (Figure 3.16C). The proportion of SM, M1, and M2 were the same when compared between cSP4 and total committed SP8, correcting the difference seen previously. Accordingly, the fold difference between total numbers of cSP4 and total committed SP8 at each stage remained much more consistent, ranging from 1.5 fold more cSP4 SM, to 2.1 fold more cSP4 M2 (Figure 3.16D). As this new gating strategy appeared to bring cSP8 maturation further in line with that of cSP4, we looked to see how the RagGFP MFI compared between the two lineages. Importantly, a progressive loss of RagGFP between the SM, M1, and M2 populations was still seen in both the cSP4 and the total committed SP8 lineages (Figure 3.17A). Comparing the two lineages, the RagGFP MFI of the SM populations was shown to be moderately higher in the total committed SP8 lineage (Figure 3.17B), however there was no such difference seen at the M1 (Figure 3.17C) or M2 (Figure 3.17D) stages, suggesting the progression through these populations is occurring at the same rate with the inclusion of the DP3 population.

Together, this data elucidates the earliest populations of cSP8 thymocytes, which is still yet to downregulate the CD4 coreceptor but is found specifically within a $CD5^{INT}TCR\beta^{HI}$ subset of DP thymocytes. The presence of this population may be responsible for the lag in transition to cSP8 when compared with cSP4, and this delay is lost when the DP3 population is included into analysis.

A

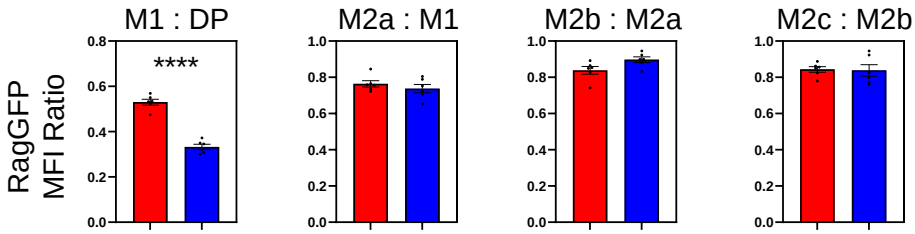

B

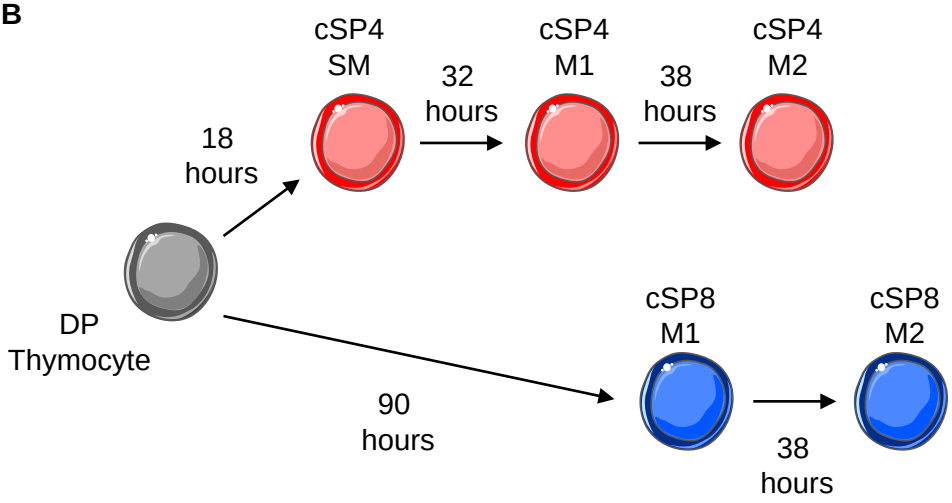

C

$$t = \ln\left(\frac{N_t}{N_0}\right) \div -\left(\frac{\ln 2}{t_{\frac{1}{2}}}\right)$$

Figure 3.13. Older Phenotype of cSP8 comes from a Delay at the DP to SP Transition

(A) Graphs summarising the ratio of calculated RagGFP MFI between sequential developmental populations, displaying the relative loss of RagGFP between each of these stages; M1:DP, M2a:M1, M2b:M2a, M2c:M2b, in cSP4 (red), and cSP8 (blue).

(B) Diagram showing the progression through maturation populations of cSP4 (red) and cSP8 (blue) in terms of hours between each stage. Time was calculated using RagGFP MFI and the formula shown in (C)

(C) Equation used to convert changes in RagGFP MFI between each maturational population into hours where the decay of RagGFP is assumed to be exponential. N_t is RagGFP at a given point, N_0 is the starting RagGFP MFI, and $t_{1/2}$ is the half life of RagGFP, reported to be 54 hours in vivo (227).

Data is taken from 3 separate experiments with n=6. Each data point represents an individual mouse, with bars plotting the mean and error bars representing the SEM. Statistical significance was determined using Independent Student's T-test, (****) representing P<0.0001.

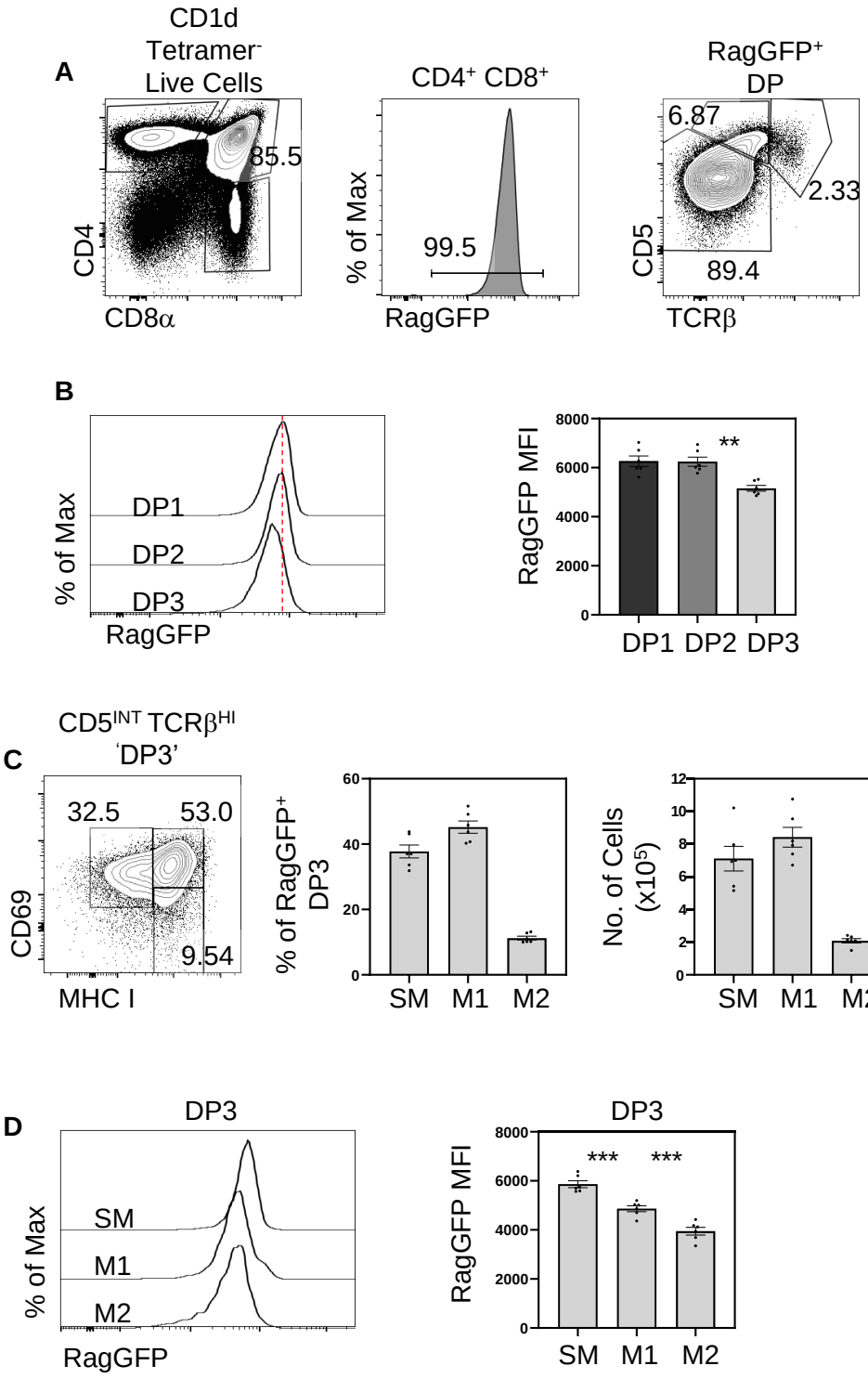
A
CD1d Tetramer- Live Cells
85.5
CD4
CD8α
CD4+ CD8+
99.5
% of Max
RagGFP
RagGFP+ DP
6.87
2.33
89.4
CD5
TCRβ
B
DP1
DP2
DP3
% of Max
RagGFP
RagGFP MFI
8000
6000
4000
2000
0
**
DP1 DP2 DP3
C
CD5INT TCRβHI 'DP3'
32.5
53.0
9.54
CD69
MHC I
% of RagGFP+ DP3
60
40
20
0
SM M1 M2
No. of Cells (x10^5)
12
10
8
6
4
2
0
SM M1 M2
D
DP3
SM
M1
M2
% of Max
RagGFP
DP3
RagGFP MFI
8000
6000
4000
2000
0
***
***
SM M1 M2

Figure 3.14. Heterogeneity within the DP Population Identifies the Earliest SP8 Populations

Thymuses were harvested from WT RagGFP mice and mechanically disaggregated for FACS analysis of thymocyte subpopulations.

(A) Representative gating to identify $CD5^{LO}$ $TCR\beta^{LO}$ DP1, $CD5^{HI}$ $TCR\beta^{INT}$ DP2, and$CD5^{INT}$ $TCR\beta^{HI}$ DP3 within $RagGFP^{+}$ DP thymocytes.

(B) Histograms of RagGFP expression by DP1 (top), DP2 (middle), and DP3 (bottom) populations. The red dotted line highlights the peak of RagGFP histogram in DP1. Graph summarises the calculate RagGFP MFI of the DP1, DP2, and DP3 populations.

(C) Representative FACS plot to identify $CD69^{+}$ MHC I^{-} (SM), $CD69^{+}$ MHC I^{+} (M1), and $CD69^{-}$ MHC I^{+} (M2) in DP3. Graphs summarise the percentages (left) and total numbers (right) of SM, M1, and M2 in DP3.

(D) Histograms of RagGFP expression by DP3 SM, M1, and M2 populations. Graph summarises calculated RagGFP MFI of DP3 SM, M1, and M2.

Data is taken from 3 separate experiments with n=6. Each data point represents an individual mouse, with bars plotting the mean and error bars representing the SEM. Statistical significance was determined using Ordinary One-way ANOVA with Tukey's multiple comparisons, (**) representing $P<0.01$, and (***) representing $P<0.001$.

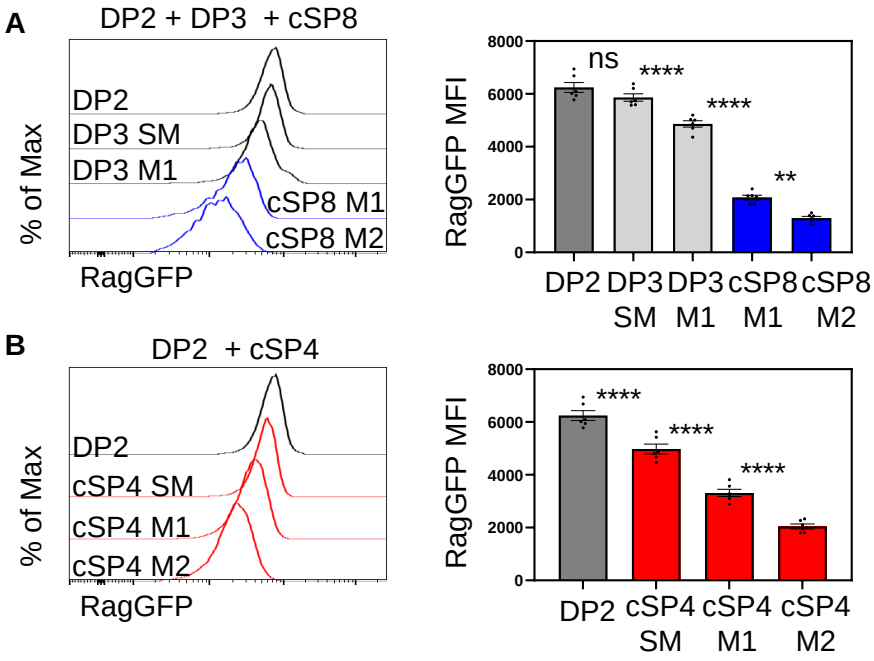
A
DP2 + DP3 + cSP8
% of Max
DP2
DP3 SM
DP3 M1
cSP8 M1
cSP8 M2
RagGFP
RagGFP MFI
8000
6000
4000
2000
0
ns
****
****
**
DP2
DP3 SM
DP3 M1
cSP8 M1
cSP8 M2
B
DP2 + cSP4
% of Max
DP2
cSP4 SM
cSP4 M1
cSP4 M2
RagGFP
RagGFP MFI
8000
6000
4000
2000
0
****
****
****
DP2
cSP4 SM
cSP4 M1
cSP4 M2

Figure 3.15. Thymocytes Transition through DP3 SM and M1 Populations into cSP8 M1 and M2 Populations, Replicating cSP4 Populations

Thymuses were harvested from WT RagGFP mice and mechanically disaggregated for FACS analysis of thymocyte subpopulations.

(A) Histogram plots of RagGFP expression by (from top to bottom) DP2, DP3 SM, DP3 M1, cSP8 M1, and cSP8 M2. Graph summarises calculated RagGFP MFI on these populations.

(B) Histogram plots of RagGFP expression by (from top to bottom) DP2, cSP4 SM, cSP4 M1, and cSP4 M2. Graph summarises calculated RagGFP MFI on these populations.

Data is taken from 3 separate experiments with n=6. Each data point represents an individual mouse, with bars plotting the mean and error bars representing the SEM. Statistical significance was determined using Ordinary One-way ANOVA with Tukey's multiple comparisons, with (**) representing $P<0.01$, (****) representing $P<0.0001$, and (ns) representing no significance.

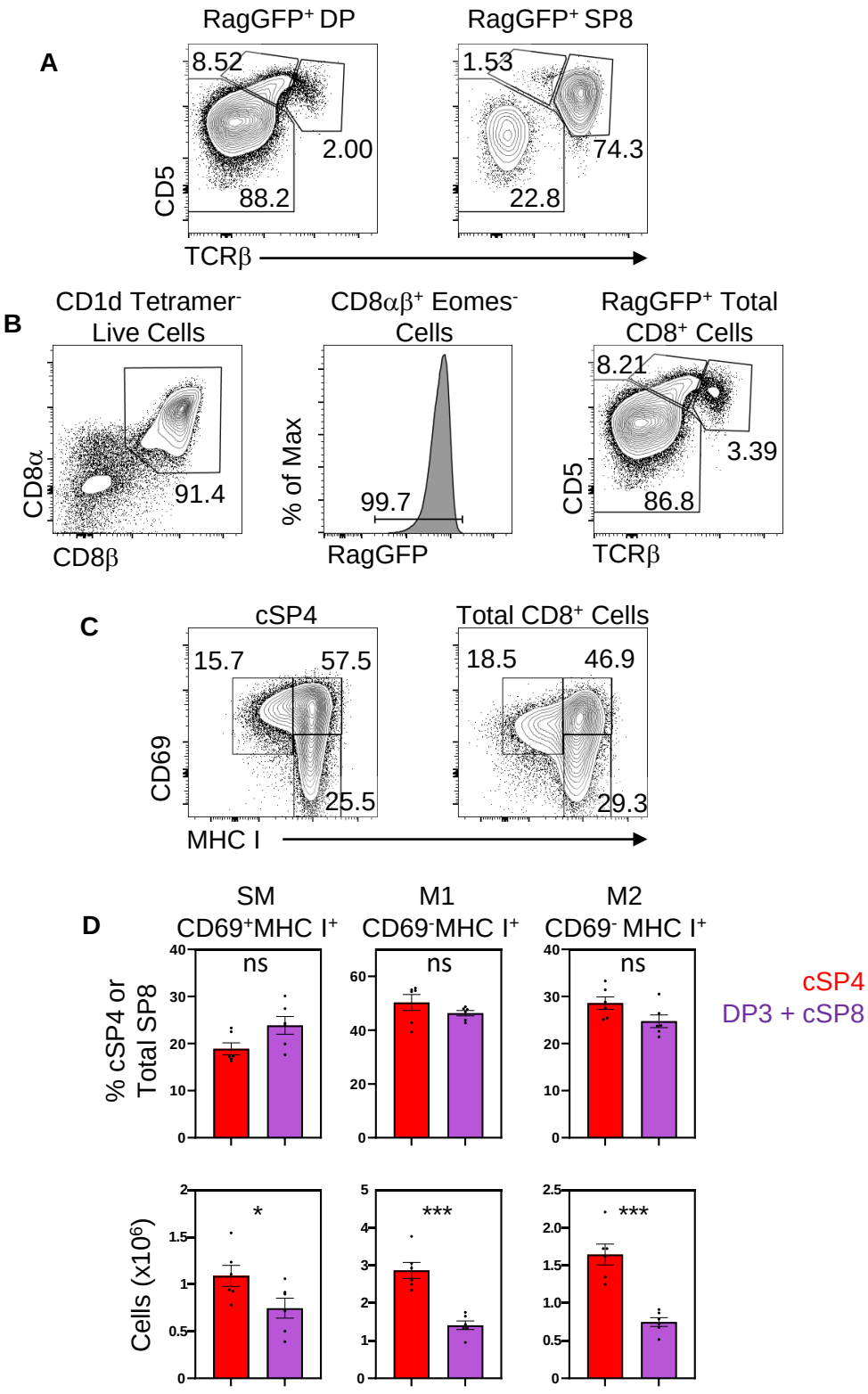
A
RagGFP+ DP
RagGFP+ SP8
8.52
2.00
88.2
1.53
74.3
22.8
CD5
TCRβ
B
CD1d Tetramer-
Live Cells
CD8αβ+ Eomes-
Cells
RagGFP+ Total
CD8+ Cells
91.4
CD8α
CD8β
99.7
% of Max
RagGFP
8.21
3.39
86.8
CD5
TCRβ
C
cSP4
Total CD8+ Cells
15.7
57.5
25.5
18.5
46.9
29.3
CD69
MHC I
D
SM
CD69+MHC I+
M1
CD69-MHC I+
M2
CD69- MHC I+
% cSP4 or
Total SP8
ns
ns
ns
Cells (x10^6)
*
***
***
cSP4
DP3 + cSP8

Figure 3.16. cSP8 can be Combined with DP3 to Analyse Total Committed Cells and Directly Compare to cSP4 Populations

Thymuses were harvested from WT RagGFP mice and mechanically disaggregated for FACS analysis of thymocyte subpopulations.

(A) Representative gating of $CD5^{LO}$ $TCR\beta^{LO}$ DP1, $CD5^{HI}$ $TCR\beta^{INT}$ DP2, and $CD5^{INT}$ $TCR\beta^{HI}$ DP3 within $RagGFP^{+}$ DP thymocytes (left) and applied to $CD4^{-}$ $CD8^{+}$ $RagGFP^{+}$ SP8 (right)

(B) Representative gating to identify total committed $CD8^{+}$ cells within the $CD5^{INT}$ $TCR\beta^{HI}$ DP3 gate, having pregated on CD1d $Tetramer^{-}$ $CD8\alpha\beta^{+}$ $Eomes^{-}$ $RagGFP^{+}$ live thymocytes.

(C) Representative gating to identify $CD69^{+}$ MHC I^{-} (SM), $CD69^{+}$ MHC I^{+} (M1), and $CD69^{-}$ MHC I^{+} (M2) within cSP4 (right) and total $CD8^{+}$ cells including DP3 and cSP8 populations (right).

(D) Graphs summarise the percentages (top row) and total numbers (bottom row) of SM (left), M1 (middle), and M2 (right) in cSP4 (right) and total $CD8^{+}$ cells including DP3 and cSP8 populations (right).

Data is taken from 3 separate experiments with n=6. Each data point represents an individual mouse, with bars plotting the mean and error bars representing the SEM. Statistical significance was determined using Independent Student's T-test, with (*) representing $P<0.05$, (***) representing $P<0.001$, and (ns) representing no significance.

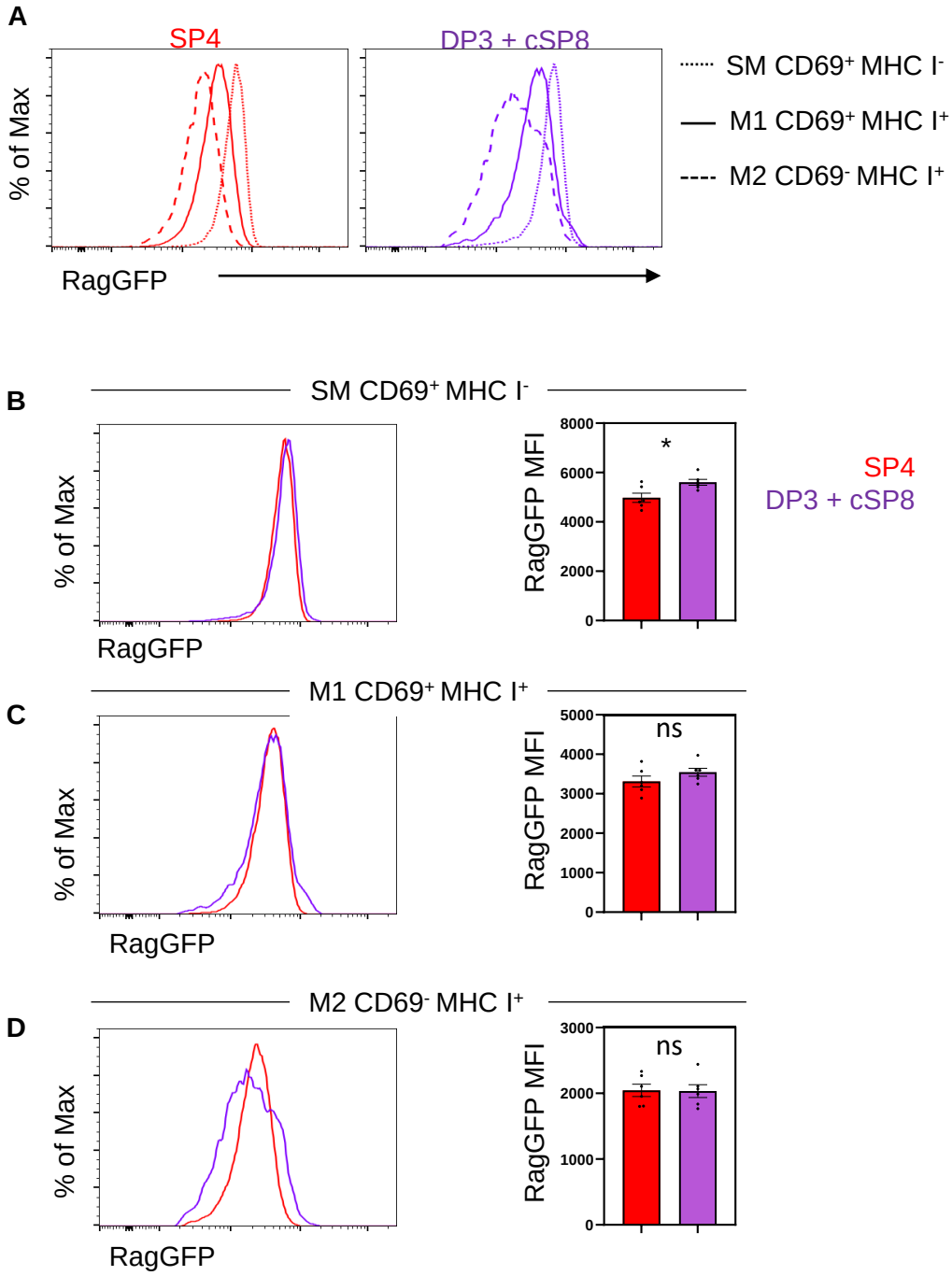
A
SP4
DP3 + cSP8
% of Max
RagGFP
SM CD69+ MHC I-
M1 CD69+ MHC I+
M2 CD69- MHC I+
B
SM CD69+ MHC I-
% of Max
RagGFP
RagGFP MFI
8000
6000
4000
2000
0
*
SP4
DP3 + cSP8
C
M1 CD69+ MHC I+
% of Max
RagGFP
RagGFP MFI
5000
4000
3000
2000
1000
0
ns
D
M2 CD69- MHC I+
% of Max
RagGFP
RagGFP MFI
3000
2000
1000
0
ns

Figure 3.17. Inclusion of the DP3 Population Corrects the RagGFP Expression of cSP8 to replicate that of cSP4 through Development

Thymuses were harvested from WT RagGFP mice and mechanically disaggregated for FACS analysis of thymocyte subpopulations.

(A) Histogram plots showing expression of RagGFP by SM (dotted line), M1 (solid line), and M2 (dashed line) by cSP4 (left) and total $CD8^+$ cells including DP3 and cSP8 populations (right).

(B) Histogram plots to show RagGFP expression by cSP4 (red) and total $CD8^+$ cells including DP3 and cSP8 populations (purple) SM populations. Graph summarised calculated RagGFP MFI between cSP4 (red) and total $CD8^+$ cells including DP3 and cSP8 populations (purple).

(C) Histogram plots to show RagGFP expression by cSP4 (red) and total $CD8^+$ cells including DP3 and cSP8 populations (purple) M1 populations. Graph summarised calculated RagGFP MFI between cSP4 (red) and total $CD8^+$ cells including DP3 and cSP8 populations (purple).

(D) Histogram plots to show RagGFP expression by cSP4 (red) and total $CD8^+$ cells including DP3 and cSP8 populations (purple) M2 populations. Graph summarised calculated RagGFP MFI between cSP4 (red) and total $CD8^+$ cells including DP3 and cSP8 populations (purple).

Data is taken from 3 separate experiments with n=6. Each data point represents an individual mouse, with bars plotting the mean and error bars representing the SEM. Statistical significance was determined using Independent Student's T-test, (*) representing $P<0.05$.

3.2.4 The Peripheral Ratio of SP4:SP8 is Established During Thymocyte Commitment to the CD4 or CD8 Lineage

Following our identification of the most immature subsets of SP8 within the DP3 population, and the impact this had on our analysis of the development and maturation cSP8 lineage, we wondered what implications this may have on the analysis of further comparisons between the SP4 and SP8 lineages, namely the ratio of SP4 to SP8 thymocytes and peripheral T-cells. To study this, RTE cSP T-cells were analysed in the spleen. Our gating strategy removed dead cells and CD1d Tetramer^{+} iNKT as in the thymus, before gating on TCRβ^{+} cells to identify T-cells. These were then separated into SP4 and SP8, before SP4 were gated on CD25^{-} RagGFP^{+} cells to identify cSP4 RTE, and SP8 were gated on CD8$\alpha\beta^{+}$ Eomes^{-} RagGFP^{+} cells to identify cSP8 RTE (Figure 3.18A). After identifying these populations, we then analysed the ratio of cSP4 RTE:cSP8 RTE, which showed to be an average of just over 2:1 (Figure 3.18B), fitting with the reported of the 2:1-1:1 CD4:CD8 ratio in the periphery (249).

We then looked to see how this compared to the thymic ratio of cSP4:cSP8, reported previously to differ from the peripheral ratio at around 4:1 (250,251). Interestingly, when using our classical definition of cSP4 and cSP8, the ratio between the two remained at roughly 2:1 through the mature M2a, M2b, and M2c stages, however the ratio at the M1 stage was shown to be significantly higher at 4:1 (Figure 3.19A). Using our new gating strategy to identify the total committed SP8 allowed inclusion of the SM population provided from the DP3 population, as well as a large proportion of DP3 M1. As such, the ratio of cSP4:cSP8 when including total committed SP8 was consistent throughout all developmental stages, from the earliest SM through the most mature M2c in the thymus, and ultimately RTE within the periphery (Figure 3.19B).

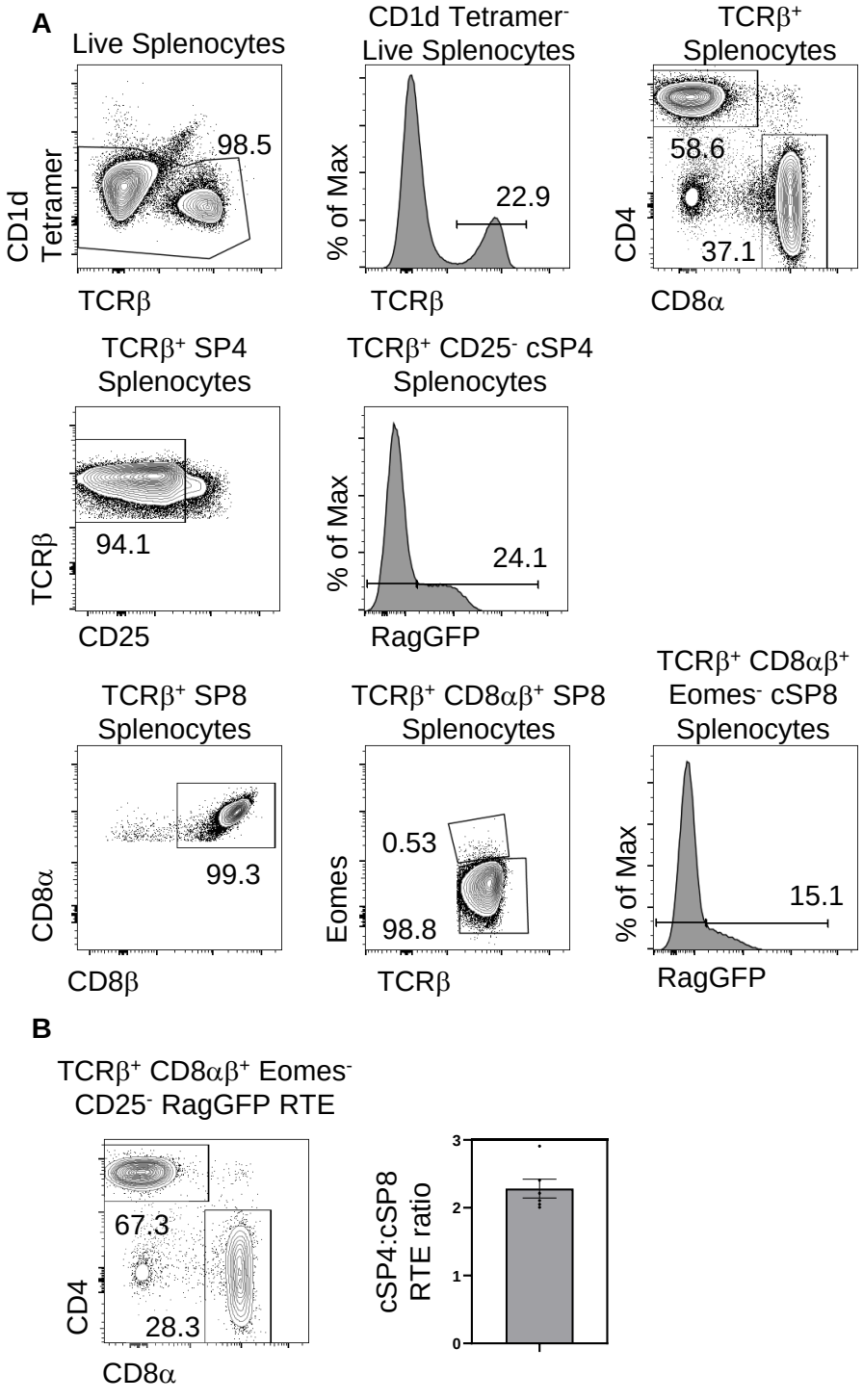
A
Live Splenocytes
CD1d Tetramer
98.5
TCRβ
CD1d Tetramer- Live Splenocytes
% of Max
22.9
TCRβ
TCRβ+ Splenocytes
58.6
37.1
CD4
CD8α
TCRβ+ SP4 Splenocytes
TCRβ
94.1
CD25
TCRβ+ CD25- cSP4 Splenocytes
% of Max
24.1
RagGFP
TCRβ+ SP8 Splenocytes
CD8α
99.3
CD8β
TCRβ+ CD8αβ+ SP8 Splenocytes
Eomes
0.53
98.8
TCRβ
TCRβ+ CD8αβ+ Eomes- cSP8 Splenocytes
% of Max
15.1
RagGFP
B
TCRβ+ CD8αβ+ Eomes- CD25- RagGFP RTE
CD4
67.3
28.3
CD8α
cSP4:cSP8 RTE ratio
3
2
1
0

Figure 3.18. Identification of Recent Thymic Emigrants within the Spleen

Spleens were harvested from WT RagGFP mice, mechanically disaggregated, and red cell lysed for FACS analysis of thymocyte subpopulations.

(A) Representative gating to identify splenic total SP4 and SP8 (total), cSP4 RTE (middle), and cSP8 RTE (bottom).

(B) Representative FACS plot identifying cSP4 and cSP8 RTE, having pregated on CD1d Tetramer^{-} CD25^{-} Eomes^{-} TCRβ^{+} RagGFP^{+} cells. Graph summarised the ratio of the total number of splenic cSP4:cSP8 RTE.

Data is taken from 3 separate experiments with n=6. Each data point represents an individual mouse, with bars plotting the mean and error bars representing the SEM.

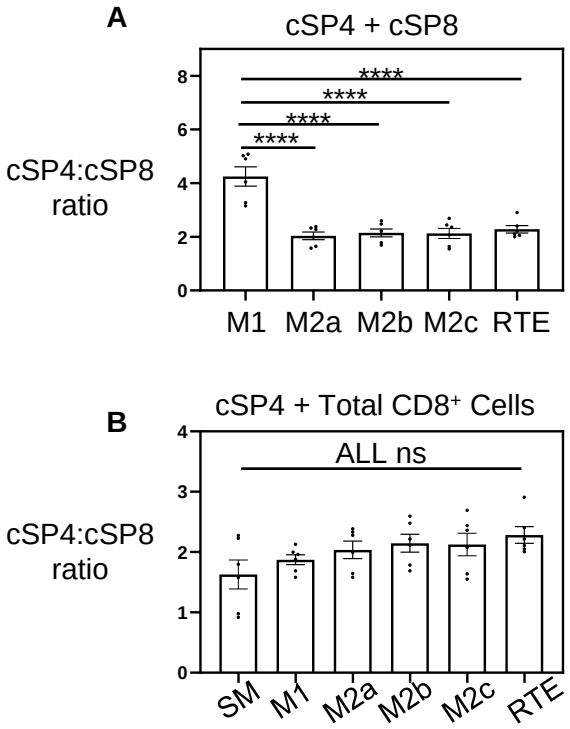
A
cSP4 + cSP8
cSP4:cSP8 ratio
8
6
4
2
0
****
****
****
****
M1
M2a
M2b
M2c
RTE
B
cSP4 + Total CD8⁺ Cells
cSP4:cSP8 ratio
4
3
2
1
0
ALL ns
SM
M1
M2a
M2b
M2c
RTE

Figure 3.19. cSP4:cSP8 Peripheral Ratio is Established Early in Thymic T-cell Development

Thymuses and spleens were harvested from WT RagGFP mice, mechanically disaggregated, and red cell lysed for FACS analysis of thymocyte subpopulations.

(A) Graph summarising the ratio of total numbers of cSP4:cSP8 at each stage of development from M1 through to RTE.

(B) Graph summarising the ratio of total numbers of cSP4:cSP8+DP3 at each stage of development from SM through to RTE

Data is taken from 3 separate experiments with n=6. Each data point represents an individual mouse, with bars plotting the mean and error bars representing the SEM. Statistical significance was determined using Ordinary One-way ANOVA with Tukey's multiple comparisons, with (****) representing $P<0.0001$, and (ns) representing no significance.

3.3 DISCUSSION

Previous studies characterising the steps involved in the post-selection maturation of SP thymocytes have used a number of markers to define sequential maturational populations that these cells pass through before their thymic egress (221,224,228). However, whilst these studies provide a comprehensive analysis how cSP4 thymocytes undergo this process, less is known about how cSP8 mature in the thymus, either through a lack of analysis completely, or a failure to appreciate the heterogeneity within SP8 and the impact non-conventional lineages may have on interpretation of data. As such we looked to define truly conventional SP8 within the thymus before carrying out this analysis of their post-selection maturation. Eomes^{+} 'memory-like' SP8 and CD8$\alpha\alpha^{+}$ IEL represent non-conventional populations within the SP8 lineage that are distinct from cSP8 (51,252), hence their isolation and removal from our analysis, alongside TCRβ^{-} iSP8 and RagGFP^{-} cells, allowed us to confidently define newly generated cSP8 within the thymus.

The maturation of SP thymocytes is often assessed using the expression of surface markers CD69, MHC I, and CD62L, with one study using the two former markers to define CD69^{+} MHC I^{-} (SM), CD69^{+} MHC I^{+} (M1), and CD69^{-} MHC I^{+} (M2) populations with cSP4 and SP8, with the most mature cells also upregulating CD62L (228). Our cSP8 population was shown to follow a similar sequential transition through previously described maturational populations, confirmed with a progressive loss of RagGFP throughout this maturation. Our comparison with cSP4 however showed a key difference within the cSP8, with the latter displaying a clearly more mature phenotype than the cSP4 lineage. This observation was evident in both the lineages' distribution amongst the maturational populations and their expression of RagGFP, with a

significantly higher proportion of cells having a mature phenotype, and a lower level of RagGFP throughout all stages of maturation. Such a difference was indicative of cSP8 being older cells with a longer thymic dwell time than cSP4 and subsequently acquiring a more mature phenotype.

With this is mind, we looked to see whether these differences in maturation affected the final stages thymic development and ultimately thymic egress. The process by which cSP4 egress the thymus has been well described, proposed to follow a 'conveyor belt' mechanism of egress whereby amongst those cells that are egress competent, the most mature cells are preferentially selected for thymic egress. Cells are then thought to egress the thymus in multi-stepped process, first entering the PVS thought to be controlled by specialised portal endothelial cells (98), and then entering the peripheral blood via an IL-4Rα-dependant mechanism (243). Adapting a pre-existing method to isolate both cSP4 and cSP8 within the PVS, we showed that cSP8 follow the same conveyor belt mechanism of egress, with the most mature populations enriched within the PVS. Further confirming this, our PVS isolated cells showed a lower level of RagGFP to their equivalent thymic populations, showing that the oldest cells within the most mature populations are preferentially selected for entry to the PVS. Within the PVS, cSP8 maintained their more mature phenotype when compared to cSP4, suggesting that their more mature status did not result in any preference of these cells to leave the thymus, and that the cause of this difference in maturational status must be determined early in thymocyte development following the selection of SP thymocytes.

The cause of the delay in development of cSP8 as a lineage compared with cSP4 has previously been suggested to emanate from the early stages post selection. Through

the use of inducible Zap70 mice, where introduction of doxycycline activates thymocyte selection, SP4 were shown to emerge 2 days following doxycycline treatment, whilst SP8 did not emerge until around day 4 (201). Significantly, a subpopulation of $CD5^{INT}TCR\beta^{HI}$ DP thymocytes, termed DP3, shown to exclusively give rise to SP8 and not SP4, preceded the emergence of SP8 (201), identifying these cells as a precursor to SP8 yet to downregulate the CD4 coreceptor. In keeping with this, the initial description of SM, M1, and M2 populations within cSP4 and SP8 lineages define 'SP8' SM as a population clearly still expressing the CD4 coreceptor (228), explaining why our definition of these populations could not identify cSP8 SM, having pre-gated on $CD4^{-}CD8^{+}$ SP8. This combined with our own analysis of relative RagGFP loss pointed towards the DP to SP transition as cause for an older cSP8 phenotype. Investigation of the DP3 population in our own hands with the maturational markers used to define cSP maturation showed that these cells display the same SM to M1 progression seen in cSP4 but lacking in our cSP8. Furthermore, these cells were shown to progress into the M1 and M2 populations within cSP8, with a combination of the DP3 and cSP8 population replicating a similar progression through SM-M1-M2 as the cSP4 lineage, compensating for the older, more mature phenotype previously seen. This would suggest that more than just a transitional population, DP3 thymocytes are SP8 committed cells that already begun their maturation before their downregulation of the CD4 coreceptor, and therefore an important population to consider when analysing cSP8 development. Failure to include such populations ignores the earliest cells of the SP8 lineage following their selection.

The importance of all CD8-committed cells being included during the analysis of cSP8 was emphasised when we considered the ratio of CD4:CD8 T-cells through

development and in the periphery. That the thymus has a bias for CD4 over CD8 T-cell production has long been seen, with the ratio of SP4:SP8 within the thymus consistently reported as around 4:1 (250,251). Despite this, the peripheral ratio, although generally still favour CD4 T-cells, differs from that in the thymus, ranging from 1:1 to around 2:1 between both different studies and different strains of mice (249). Whilst the establishment of this CD4 biased selection in the thymus has been linked to an increased susceptibility to apoptosis in MHC I restricted thymocytes at the DP2 stage (250), the reason for difference between the thymus and the periphery is less clear. In fact, our data suggests that no such difference exists, with the inclusion of the DP3 population and subsequent breakdown into developmental stages showing that the cSP4:DP3+cSP8 ratio is established at 2:1 at the earliest SM stage post-selection and is maintained at such a ratio throughout thymic development and into the periphery. Whilst relevance of the bias for CD4 over CD8 T-cells remains unclear, this data shows that it is not as a result of peripheral expansion or survival, nor from preferential export of SP4 over SP8 from the thymus. Instead, it appears the thymus sets up the conserved 2:1 ratio of CD4:CD8 T-cells during the selection of both lineages, exemplifying another role for the thymus in establishing immune homeostasis.

This chapter characterises truly conventional SP8 thymocytes allowing for the comprehensive analysis of cSP8 side-by-side with the more well-defined cSP4 lineage, whilst also exemplifying the importance of $CD5^{INT}TCR\beta^{HI}$ DP3 thymocytes as SP8-committed cells that have not downregulated the CD4 coreceptor. Taken together, this data suggests that whilst typically defined cSP8 represent older cells than cSP4, the youngest of the SP8 lineage are contained within the DP3 population, and inclusion of

such cells draws the maturation of cSP8 equivalent to that of cSP4. This equivalent progression through post-selection maturation of the two lineages is replicated in thymic egress, with cSP8 appearing to follow a conveyor belt mechanism of entry into the PVS and subsequently exit the thymus. Such analysis underlines the conserved role of the thymus in controlling the development of both of these lineages, despite their phenotypic and functional differences.

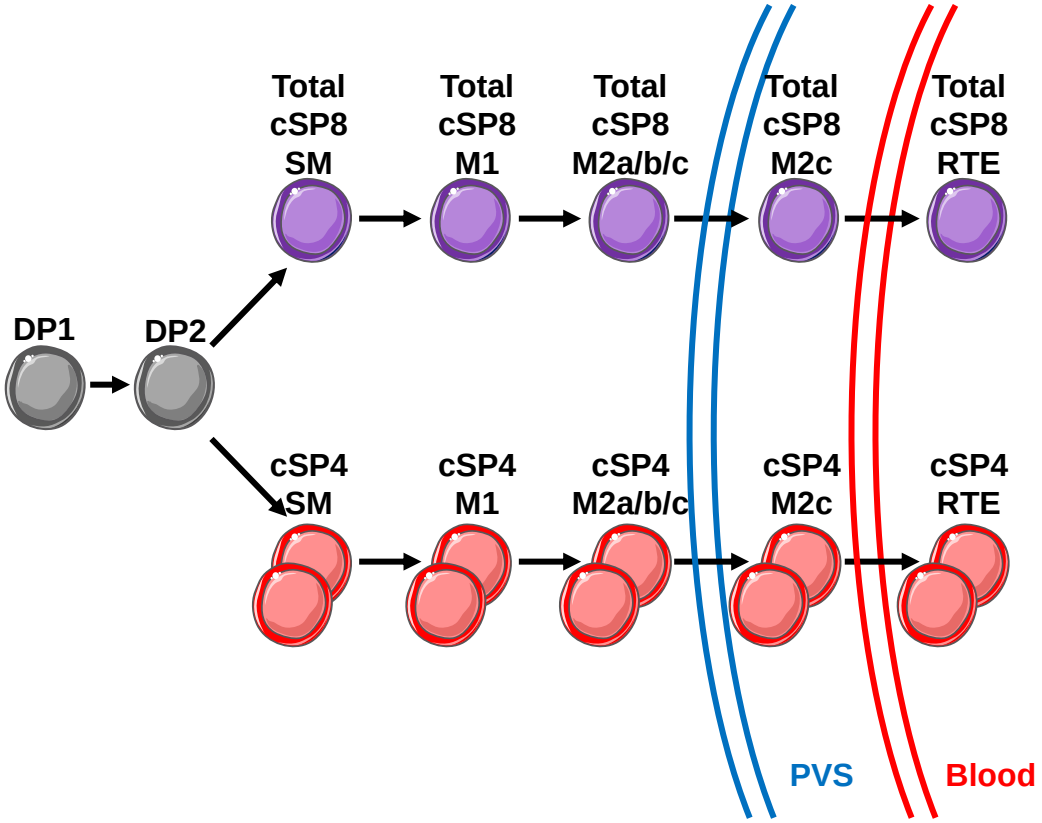
Total
cSP8
SM
Total
cSP8
M1
Total
cSP8
M2a/b/c
Total
cSP8
M2c
Total
cSP8
RTE
DP1
DP2
cSP4
SM
cSP4
M1
cSP4
M2a/b/c
cSP4
M2c
cSP4
RTE
PVS
Blood

Figure 3.20. Summary of the Post-Selection Maturation of cSP4 and cSP8 Thymocytes.

Analysing the cSP4 and cSP8 populations side by side with the inclusion of the most immature cSP8 population, defined as $CD5^{INT}$ $TCR\beta^{HI}$ DP3, shows that both pass through the same sequential populations through post-selection maturation and egress into the PVS and periphery. Throughout this progression, there is a 2:1 ratio of cSP4:cSP8, suggesting the ratio is established during selection and maintained into the periphery.

CHAPTER 4: THE IMPACT OF BONE MARROW TRANSPLANTATION ON THE MATURATION AND EGRESS OF THYMOCYTES

4.1 INTRODUCTION

The thymus has a key role in establishing and subsequently maintaining the generation of a mature, competent, self-tolerant peripheral T-cell pool. In addition to this role in the steady state, the thymus is also shown to be key to the recovery and reestablishment of the T-cell compartment following the use of therapeutic bone marrow transplantation (BMT). BMT is a clinical therapy that has long been used for the treatment of a number of blood disorders, including haematological cancers (253). Both clinical human and experimental mouse BMT involves the transplantation of haematopoietic stem cells derived from bone marrow but is first preceded by ablative therapy given to the recipient, depleting the haematopoietic compartment to provide niche availability for successful engraftment (253,254). Subsequent reconstitution of the haematopoietic system is first seen in innate immune cells, which show a relatively quick recovery following BMT (255). T-cell recovery is however shown to be more complex. Whilst initial expansion of peripheral T-cells supplied from the donor provide a level of T-cell mediated immunity within recipients, this process is thymic-independent and results in a restricted TCR repertoire, as well as a bias towards CD8-memory T-cells (255–257). For the T-cell compartment to return to the capacity of that prior to ablative therapy and maintained long-term, thymopoiesis of donor-derived stem cells must first occur, generating a new pool of T-cells from within the thymus of the transplant recipient, with this process taking considerably longer (258,259).

Despite the requirement for the thymus in complete reconstitution following BMT, the ablative therapies involved are shown to damage the thymus, causing a reduction in the TEC that dictate thymic development, and therefore reducing the capacity for thymic output immediately following BMT. Thymus capability to recover and regenerate

from such insult is thought to coincide with increased T-cell output from the thymus and subsequently the recovery of the T-cell pool (258–260). Recent work, however, has suggested that the thymus fails to fully recover from ablative therapies such as irradiation (261,262). Specifically, mTEC within the thymus medulla are significantly reduced even 56 days following BMT in mice, whilst cTEC within the cortex show no difference throughout the time course. Furthermore, cDC1, the population of DC generated within the thymus and localised to the medulla, are also significantly reduced in BMT mice (261). Importantly, this failure of recovery within the thymus medulla translates to medullary-specific defects in thymus function post-BMT. Following selection in the cortex SP thymocytes undergo tolerance induction through the removal of self-reactive thymocytes by induced cell death, and the generation of nTreg, diverging as non-conventional cells within the SP4 lineage, processes shown to be reliant on the medulla (207,217). Following BMT, mice show a reduction in negative selection, and reduced generation of nTreg, with subsequent signs of autoimmunity within the periphery (261). This clearly suggests that ablative therapies used in BMT cause long-term damage to the medulla which limits the thymus' capability to effectively control thymopoeisis, resulting in failed negative selection within the medulla.

As well as inducing tolerance, the thymus medulla is also where the post-selection maturation of single positive thymocytes that was described in the previous chapter occurs, as these cells gain functional maturity and egress competence (219,228). As such, it is these mature cells within the medulla that subsequently undergo thymic egress, using the conveyor belt mechanism previously described (98,228). The thymus medulla therefore harbours SP thymocytes as they undergo the crucial final stages of

T-cell development that ensures mature, self-tolerant T-cells are exported from the thymus into the periphery. As recent work shows the inability of the thymus to effectively impose tolerance mechanisms within the medulla following BMT, it is possible that the maturation and egress of thymocytes, normally controlled by the medulla, is also hampered post-BMT.

We have therefore looked to use our comprehensive definition of post-selection maturation and egress within cSP4 and cSP8 thymocytes outlined in the previous chapter to determine if these processes are affected by the lack of mTEC recovery post-BMT.

4.2 RESULTS

4.2.1 Changes in Conventional and Non-Conventional Thymocyte Populations Following Bone Marrow Transplantation

In order to assess how previously described changes in the thymic microenvironment post-BMT might affect the maturation and egress of SP thymocytes following their selection, we generated bone marrow chimeras using WT RagGFP T-cell depleted bone marrow and congenially mismatched WT hosts. Host adult BoyJ mice expressing CD45.1 were subject to two doses of total body irradiation on consecutive days, before being reconstituted with T-cell depleted bone marrow harvested from WT RagGFP CD45.2 expressing mice to distinguish donor-derived cells. Following reconstitution, mice were left for 28 days (d28) before thymus and spleen were harvested and mechanically disaggregated for FACS analysis. The d28 timepoint was chosen as recent work has identified this as a stage at which both cTEC and total thymocyte numbers have recovered, but a failure in mTEC recovery is present (261).

We first looked to identify how bulk thymic populations are affected in d28 BMT mice compared with age-matched WT control mice. Firstly. the total thymus cellularity was unchanged in d28 BMT mice (Figure 4.1A). From herein, thymic analysis was pregated CD45.2$^+$ donor cells to analyse how these cells reconstitute the thymus in d28 BMT mice. These CD45.2$^+$ donor cells make up essentially all thymocytes present within the thymus in d28 BMT mice. Within the CD45.2$^+$ donor population both the proportions and numbers of TCRβ^+ CD25$^-$ SP4 and TCRβ^+ Eomes$^-$ CD8$\alpha\beta^+$ SP8 were significantly higher when compared with control mice. Despite this, although d28 BMT mice showed a significantly lower proportion of DP thymocytes, the total numbers were unchanged (Figure 4.1B). Using RagGFP expression to separate TCRβ^+ CD25$^-$ SP4 into RagGFP$^+$ and RagGFP$^-$ populations showed that the increase in this population in d28 BMT mice was a result of increased RagGFP$^+$ cSP4, whilst there were fewer RagGFP$^-$ recirculating SP4 (Figure 4.1C). Similarly, when separating TCRβ^+ Eomes$^-$ CD8$\alpha\beta^+$ SP8 into RagGFP$^+$ and RagGFP$^-$ cells there was a significant increase in the number of RagGFP$^+$ cSP8 at d28 BMT, showing that the increase in both cSP4 and cSP8 populations is a result of more newly generated cells as opposed to recirculating or resident populations. Interestingly, however RagGFP$^-$ TCRβ^+ Eomes$^-$ CD8$\alpha\beta^+$ SP8 were unchanged at d28 BMT unlike the RagGFP$^-$ TCRβ^+ CD25$^-$ SP4 (Figure 4.1D).

Within SP8 thymocytes, Eomes-expressing cells represent a non-conventional, memory-like population that are generated within the thymus. Eomes$^+$ SP8 have been shown to be dependant on IL-4 provision by PLZF$^+$ thymic iNKT2, with the population being reduced in models lacking iNKT2, and increased in models of increased iNKT2 availability (51,52). iNKT themselves represent another non-conventional lineage within the thymus that have been shown to be dependent on the thymus medulla for

their generation (104). As such, we looked to see how the relationship between these non-conventional populations is affected in d28 BMT where the thymus medulla is shown to not recover (261). iNKT were identified as CD1d Tetramer^{+} cells within bulk live thymocytes. Thymic iNKT are significantly reduced in d28 BMT in both proportion and total numbers (Figure 4.2A), further emphasising the reliance on the medulla for these cells to develop. Interestingly, Eomes^{+} TCRβ^{+} Eomes SP8 were unchanged in d28 BMT mice (Figure 4.2B) despite the significant loss of the iNKT population they are dependent upon. This would suggest a more complex relationship between the two populations, with the generation Eomes SP8 within the thymus being dependant on more than just IL-4 provision by iNKT2.

This analysis shows that the development of different thymocyte populations within the thymus is altered following BMT. Whilst GFP^{-} cells and iNKT appear to be at reduced levels within the thymus, newly generated GFP^{+} cSP thymocyte populations appear to be increased.

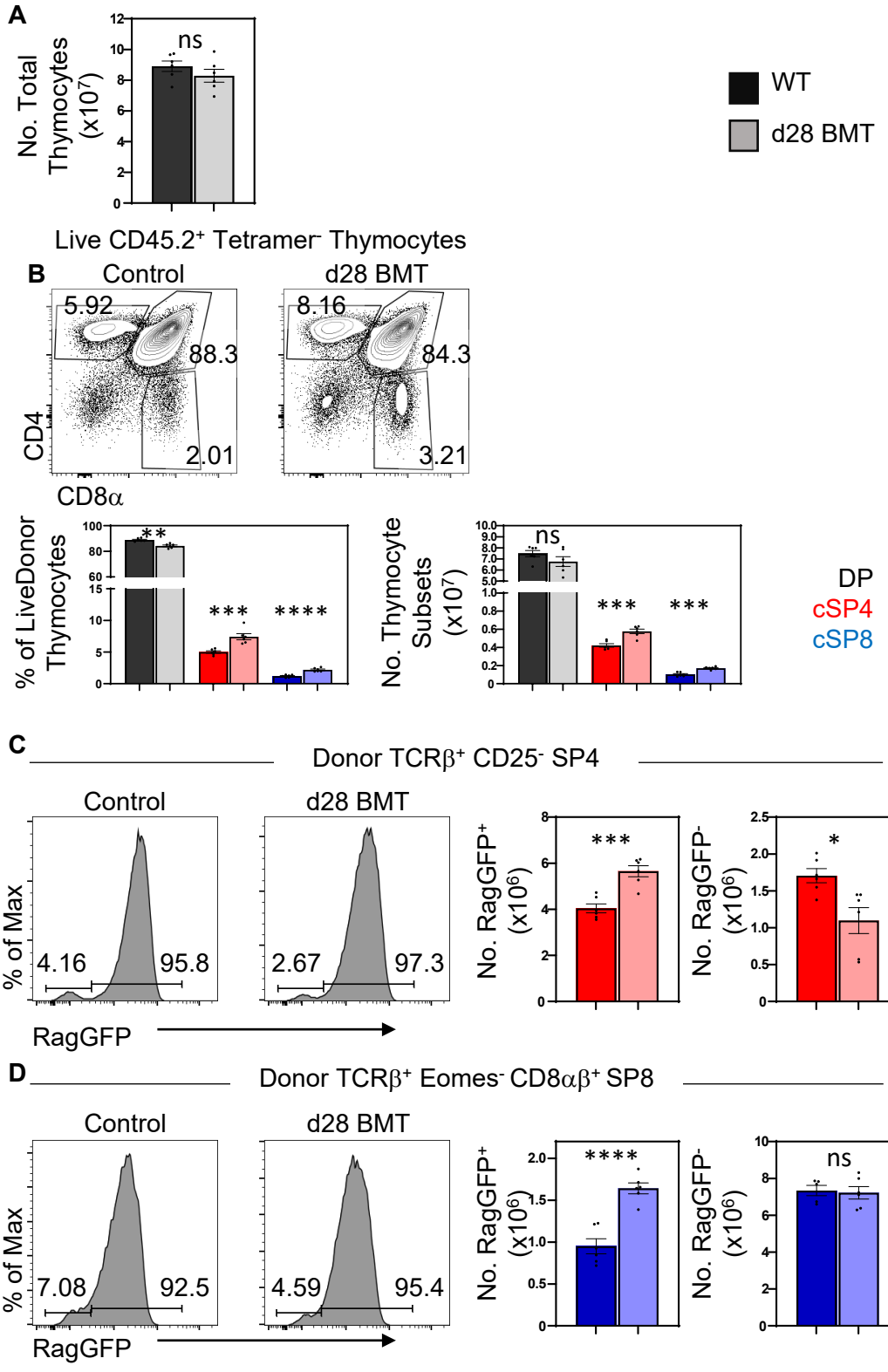
A
No. Total Thymocytes (x10⁷)
ns
WT
d28 BMT
Live CD45.2⁺ Tetramer⁻ Thymocytes
B
Control
d28 BMT
5.92
88.3
2.01
8.16
84.3
3.21
CD4
CD8α
% of LiveDonor Thymocytes
**
***
****
No. Thymocyte Subsets (x10⁷)
ns
***
***
DP
cSP4
cSP8
C
Donor TCRβ⁺ CD25⁻ SP4
Control
d28 BMT
% of Max
4.16
95.8
2.67
97.3
RagGFP
No. RagGFP⁺ (x10⁶)
***
No. RagGFP⁻ (x10⁶)
*
D
Donor TCRβ⁺ Eomes⁻ CD8αβ⁺ SP8
Control
d28 BMT
% of Max
7.08
92.5
4.59
95.4
RagGFP
No. RagGFP⁺ (x10⁶)
****
No. RagGFP⁻ (x10⁶)
ns

Figure 4.1. Conventional SP4 and SP8 are increased in mice 28 days post-BMT

Thymuses were harvested from CD45.1 WT mice 28 days following a lethal dose of irradiation and reconstitution with T-cell depleted CD45.2 WT RagGFP bone marrow. Age matched WT RagGFP mice were taken alongside as controls. The tissues were mechanically disaggregated and stained for FACS analysis. Analysis was pregated on CD45.2$^+$ donor cells.

(A) Summary of total thymus cellularity in WT control (dark grey bar) and d28 post-BMT mice (light grey bar).

(B) Representative FACS plots of SP4, SP8, and DP thymocyte subpopulations in WT control (left) and d28 BMT (right) mice pregated on live CD1d Tetramer$^-$ CD45.2$^+$ donor cells. Graphs summarise percentages (left) and numbers (right) of DP thymocytes (black), TCRβ^+ CD25$^-$ SP4 (red), TCRβ^+ Eomes$^-$ CD8$\alpha\beta^+$ SP8 (blue) in WT control (dark bars) and d28 BMT (light bars) mice.

(C) Representative gating of RagGFP$^+$ and RagGFP$^-$ populations in TCRβ^+ CD25$^-$ SP4 in WT control (left) and d28 BMT (right) mice, with graphical representation of numbers of RagGFP$^+$ (left) and RagGFP$^-$ (right) cells in WT control (dark red bar) and d28 BMT (light red bar) mice.

(D) Representative gating of RagGFP$^+$ and RagGFP$^-$ populations in TCRβ^+ Eomes$^-$ CD8$\alpha\beta^+$ SP8 in WT control (left) and d28 BMT (right) mice, with graphical representation of numbers of RagGFP$^+$ (left) and RagGFP$^-$ (right) cells in WT control (dark blue bar) and d28 BMT (light blue bar) mice.

Data is taken from 3 separate experiments with n=6 WT control and d28 BMT mice. Each data point represents an individual mouse, with bars plotting the mean and error bars representing the SEM. Statistical significance was determined using Independent Student's T-test, with (*) representing P<0.05, (**) representing P<0.01, (***) representing P<0.001, and (****) representing P<0.0001, and (ns) representing no significance.

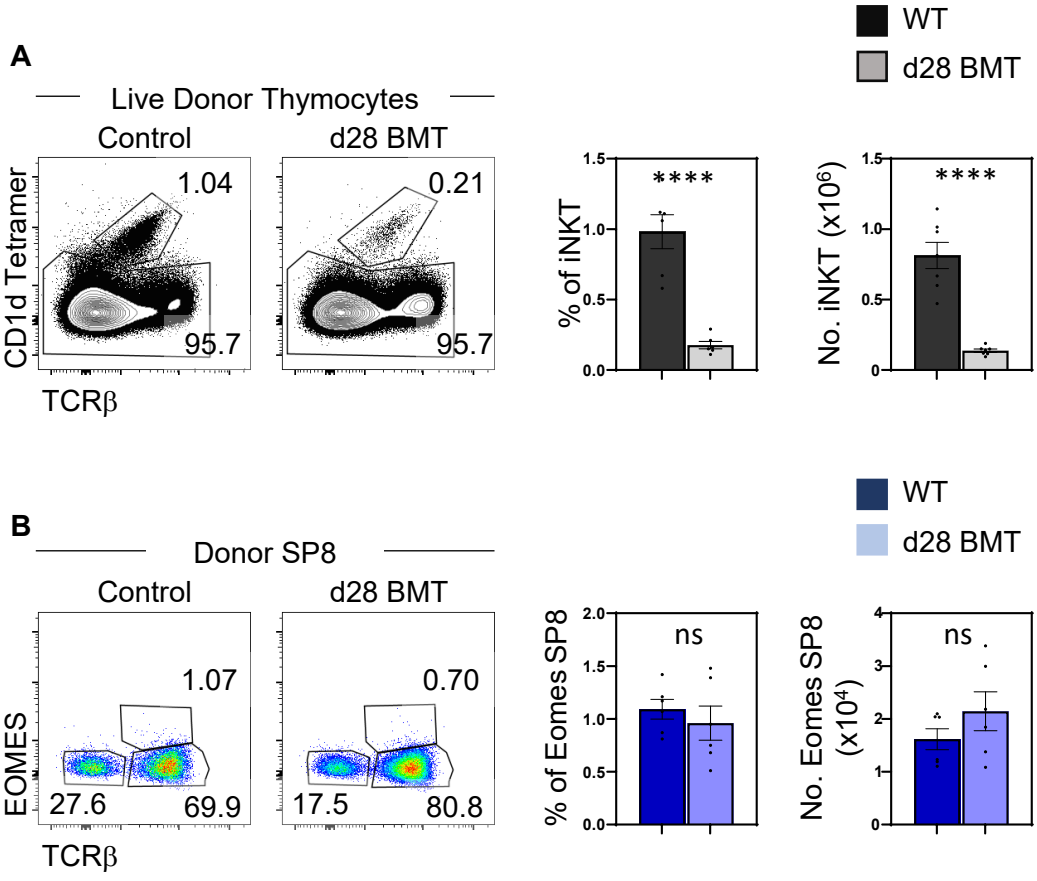
A
Live Donor Thymocytes
Control
d28 BMT
CD1d Tetramer
TCRβ
1.04
95.7
0.21
95.7
WT
d28 BMT
% of iNKT
****
No. iNKT (x10^6)
****
B
Donor SP8
Control
d28 BMT
EOMES
TCRβ
1.07
27.6
69.9
0.70
17.5
80.8
WT
d28 BMT
% of Eomes SP8
ns
No. Eomes SP8 (x10^4)
ns

Figure 4.2. Significant Loss of iNKT but no Change in Eomes SP8 in day 28 BMT mice

Thymuses were harvested from CD45.1 WT mice 28 days following a lethal dose of irradiation and reconstitution with T-cell depleted CD45.2 WT RagGFP bone marrow. Age matched WT RagGFP mice were taken alongside as controls. The tissues were mechanically disaggregated and stained for FACS analysis. Analysis was pregated on CD45.2^{+} donor cells.

(A) Representative FACS plots to identify CD1d Tetramer^{+} iNKT in WT control (left) and d28 BMT (right) mice. Graphical representation of percentages (left) and numbers (right) of iNKT in WT control (dark grey bar) and d28 BMT (light grey bar) mice.

(B) Representative FACS plots to identify subpopulations of SP8 based on TCRβ and Eomes in WT control (left) and d28 BMT (right) mice. Graphical representation of percentages (left) and numbers (right) of Eomes^{+} SP8 in WT control (dark blue bar) and d28 BMT (light blue bar) mice.

Data is taken from 3 separate experiments with n=6 WT control and d28 BMT mice. Each data point represents an individual mouse, with bars plotting the mean and error bars representing the SEM. Statistical significance was determined using Independent Student's T-test, with (****) representing P<0.0001, and (ns) representing no significance.

4.2.2 Mature Conventional Thymocytes Accumulate Post-BMT

Following the observation of significantly more donor-derived cSP4 and cSP8 at d28 following BMT, we look to further investigate the cause of this by analysing the maturational status of these populations. Gating on SM, M1, and M2 cSP4 in both age-matched control and d28 BMT mice (Figure 4.3A) showed a significant decrease in the proportions of SM and M1 populations, but a significant increase in the proportion of M2 in d28 BMT mice (Figure 4.3B). Importantly, whilst the numbers of SM and M1 cSP4 are unchanged at d28 post-BMT, the M2 population is significantly different, with an over 2-fold increase compared with age-matched control mice (Figure 4.3C). This specific increase in the most mature M2 population is indicative of restricted egress from the thymus and subsequent accumulation of the most mature cSP4 population of cells. Comparing levels of RagGFP in SM, M1, and M2 between d28 BMT and age-matched controls we looked to see how the ages of these populations differ, as such an accumulation in the BMT mice would suggest the mature population retained within the thymus would represent older cells (Figure 4.4). Whilst the RagGFP MFI of SM and M1 was unchanged between d28 BMT and control mice, d28 BMT mice have a lower level of RagGFP than control mice. However, although significant the RagGFP level is only moderately lower in d28 BMT (Figure 4.4), suggesting there is not a dramatic increase in medullary dwell time of cSP4 following BMT, with the cells not accumulating within the thymus for much longer than in control mice.

Similar to cSP4, the cSP8 population was significantly increased in d28 BMT mice. We therefore looked to see whether the cSP8s were affected by the same accumulation of mature cells as seen in the cSP4 cells. Analysing the M1 and M2 populations identifiable in cSP8 (Figure 4.5A) showed a similar trend in the distribution of cells

amongst immature and mature populations, with a significantly higher proportion of M2, and lower proportion of M1 in d28 BMT mice (Figure 4.5B). Again, replicating what is seen in cSP4, there is a significant increase in the numbers of cSP8 M2, with an over 2-fold change in d28 BMT mice. Unlike in cSP4, M1 cSP8 were significantly increased in d28 BMT mice, although this is a more moderate increase than that seen in cSP8 M2 (Figure 4.5C). By calculating the ratio of M2:M1 cSP8 cells in both WT control and d28 BMT mice it was clear that although both populations are increased in d28 BMT mice, the cSP8 M2 population is increased to a greater degree, with a significantly higher M2:M1 ratio in d28 BMT mice when compared to WT control mice (Figure 4.5D). Although the increase in cSP8 was not exclusive to the M2 population as in cSP4, the greater degree of increase in the M2 population again suggested an accumulation and appeared to be similar to the effect seen in cSP4. However, when comparing RagGFP levels between control and d28 BMT mice, there is no change in either the cSP8 M1 or M2 populations (Figure 4.6). Whilst this shows that the cSP8 M2 that have accumulated in the d28 BMT mice are no older than the M2 within age-matched control mice, this observation is not dissimilar from that seen in cSP4, as the difference seen in cSP4 M2 is only minor, although significantly different.

Given the observation of an increased M1 population in the cSP8 but not the cSP4 in d28 BMT mice, we looked to include the SM and early M1 cells contained within the DP3 population in our analysis of the recovery of cSP8 following BMT. By gating on total CD8$\alpha\beta^{+}$ Eomes^{-} RagGFP^{+} cells we could identify CD5^{INT} TCRβ^{HI} cells that include both the DP3 and cSP8 populations. Using this gating strategy, we see that d28 BMT mice showing a higher proportion of these total committed-SP8 cells than control mice (Figure 4.7A), likely due to the increased number of cSP8 previously outlined. When

we gated on the SM, M1, and M2 populations within these total-committed SP8 we could identify all three populations in both control and d28 BMT mice (Figure 4.7B). Comparing proportions of SM, M1, and M2 within the total-committed SP8 population in both control and BMT mice showed a significantly lower SM population, an unchanged M1, and increased M2 population (Figure 4.7C). Comparing the total numbers of these maturational populations showed that the total-committed SP8 population mirrored the cSP4 population, showing no significant change in the SM and M1 populations, but significantly more M2 (Figure 4.7D) This emphasises the specific accumulation of M2 cells in the cSP8 of d28 BMT mice, with the inclusion of the total M1 population removing the previous increase in this population that was seen. Comparing the RagGFP levels between control and d28 BMT mice in the SM, M1, and M2 populations it is clear that there was no significant difference amongst any of the populations (Figure 4.8). This further suggests that whilst there is a specific increase in the most mature cSP8, the thymic dwell time of this population is unaffected, similar to the minimal affect seen within the cSP4 cells.

Whilst both cSP4 and cSP8 phenotypes have increased proportions of M2 cells in d28 BMT mice, both lineages also don't appear to have dramatically increased medullary dwell time as a result of the accumulation. We therefore looked to investigate this accumulation further by breaking down the M2 population into sequential M2a, M2b, and M2c populations to determine whether the increased M2 populations in d28 BMT represented more mature cells than in control mice. By applying the evenly distributed M2a/b/c gates from cSP4 M2 in control mice to cSP4 M2 from BMT mice, we saw an increase in the proportion of the most mature M2c population within d28 BMT mice (Figure 4.9A,B). Similarly, whilst the total numbers of M2a, M2b, and M2c populations

all showed some degree of increase, only M2b and M2c were significantly increased in BMT mice. Furthermore, there was a dramatically higher increase in the number of M2c, showing a 2.6-fold increase compared to only a 1.7-fold increase in M2b (Figure 4.9B). This showed that within the increased population of cSP4 M2, specifically the most mature M2c, identified with the highest level of expression of CD62L, are increased 28 days following BMT. When we applied the same comparison of the M2a, M2b, and M2c population between control and BMT mice to the cSP8 M2 population, we see a similar trend. The most mature of these populations, the M2c, had significantly higher proportions in BMT mice (Figure 4.9C,D). Despite this, the total number of the M2a, M2b, and M2c populations in cSP8 does not show such an obvious specific increase in the M2c within BMT mice as seen in cSP4. Whilst the greatest increase was still seen the M2c population at around 2.4-fold, the increase in both the M2a and M2b populations was around 1.9-fold (Figure 4.9D), higher than that seen in cSP4 between control and BMT mice. This would suggest that whilst donor-derived populations of both cSP4 and cSP8 show an accumulation of the most mature populations of cells at day 28 post-BMT, it is both more apparent and more specific to the most mature populations in cSP4 than cSP8.

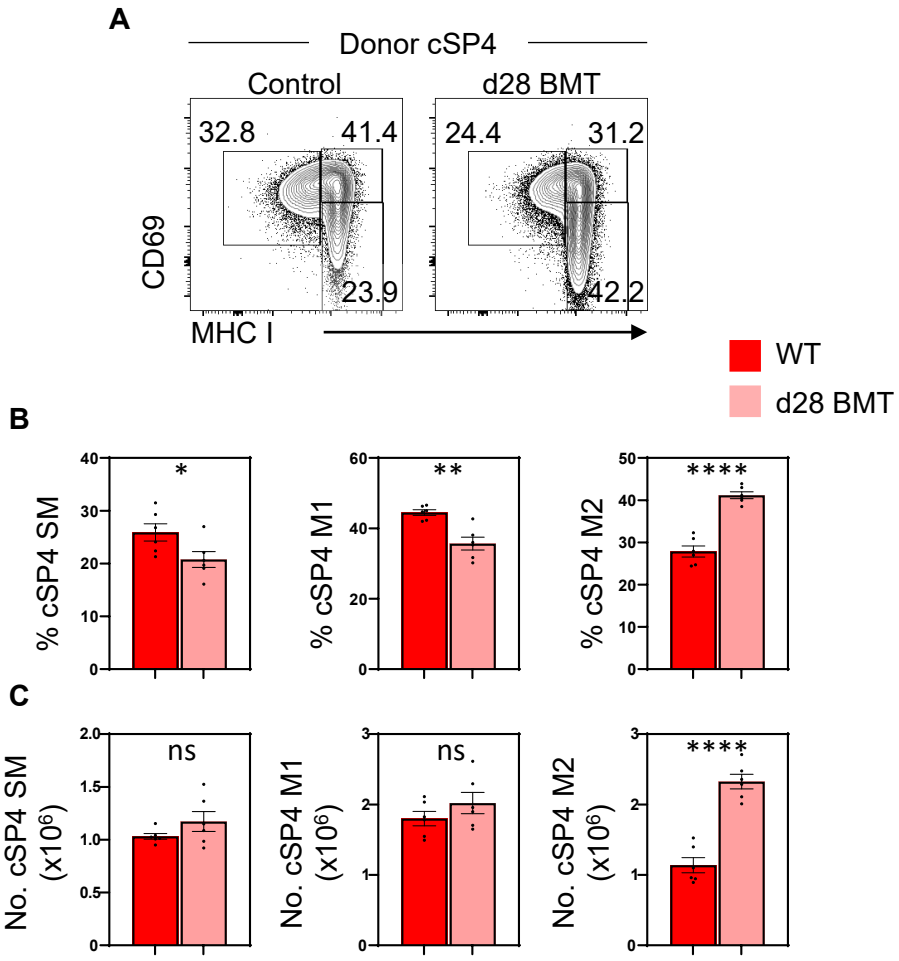
A
Donor cSP4
Control
d28 BMT
32.8
41.4
23.9
24.4
31.2
42.2
CD69
MHC I
WT
d28 BMT
B
% cSP4 SM
% cSP4 M1
% cSP4 M2
*
**
****
C
No. cSP4 SM (x10^6)
No. cSP4 M1 (x10^6)
No. cSP4 M2 (x10^6)
ns
ns
****

Figure 4.3. Increase in cSP4 M2 population in day 28 post-BMT mice

Thymuses were harvested from CD45.1 WT mice 28 days following a lethal dose of irradiation and reconstitution with T-cell depleted CD45.2 WT RagGFP bone marrow. Age matched WT RagGFP mice were taken alongside as controls. The tissues were mechanically disaggregated and stained for FACS analysis. Analysis was pregated on $CD45.2^{+}$ donor cells.

(A) Representative FACS plots to identify $CD69^{+}$ MHC I^{-} (SM), $CD69^{+}$ MHC I^{+} (M1), and $CD69^{-}$ MHC I^{+} (M2) cSP4 in WT control (left) and d28 BMT (right) mice.

(B) Graphical representation of percentages of SM (left), M1 (middle), and M2 (right) cSP4 in WT control (dark red bar) and d28 BMT (light red bar) mice.

(C) Graphical representation of numbers of SM (left), M1 (middle), and M2 (right) cSP4 in WT control (dark red bar) and d28 BMT (light red bar) mice.

Data is taken from 3 separate experiments with n=6 WT control and d28 BMT mice. Each data point represents an individual mouse, with bars plotting the mean and error bars representing the SEM. Statistical significance was determined using Independent Student's T-test, with (*) representing $P<0.05$, (**) representing $P<0.01$, (****) representing $P<0.0001$, and (ns) representing no significance.

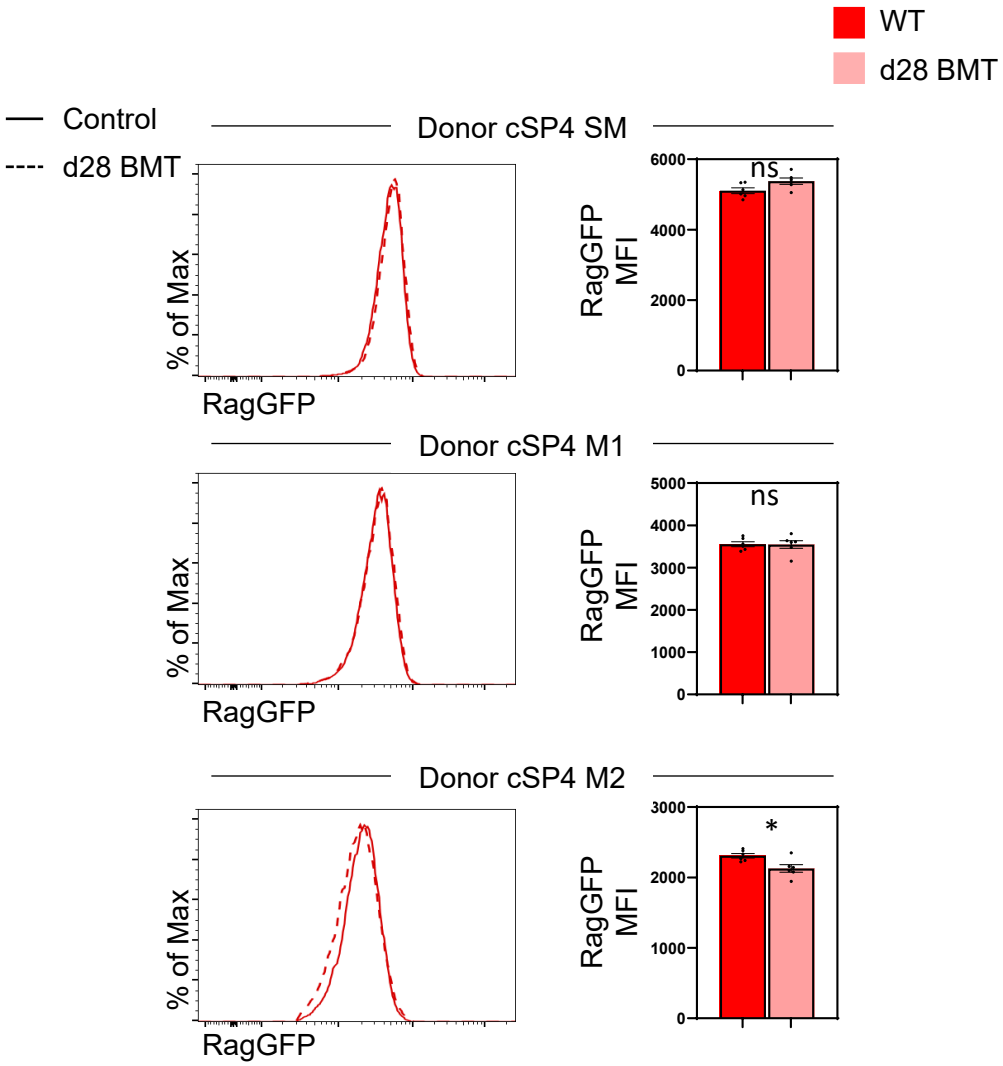
WT
d28 BMT
Control
d28 BMT
Donor cSP4 SM
% of Max
RagGFP
RagGFP MFI
ns
6000
4000
2000
0
Donor cSP4 M1
% of Max
RagGFP
RagGFP MFI
ns
5000
4000
3000
2000
1000
0
Donor cSP4 M2
% of Max
RagGFP
RagGFP MFI
*
3000
2000
1000
0

Figure 4.4. RagGFP Levels are only Moderately Lower in d28 BMT cSP4 M2 Compared with WT Controls

Thymuses were harvested from CD45.1 WT mice 28 days following a lethal dose of irradiation and reconstitution with T-cell depleted CD45.2 WT RagGFP bone marrow. Age matched WT RagGFP mice were taken alongside as controls. The tissues were mechanically disaggregated and stained for FACS analysis. Analysis was pregated on $CD45.2^{+}$ donor cells.

Summary of RagGFP expression by cSP4 SM (top), M1 (middle), and M2 (bottom) in WT control (solid line, dark red bar) and d28 BMT (dashed line, light red bar) mice.

Data is taken from 3 separate experiments with n=6 WT control and d28 BMT mice. Each data point represents an individual mouse, with bars plotting the mean and error bars representing the SEM. Statistical significance was determined using Independent Student's T-test, with (*) representing $P<0.05$, and (ns) representing no significance.

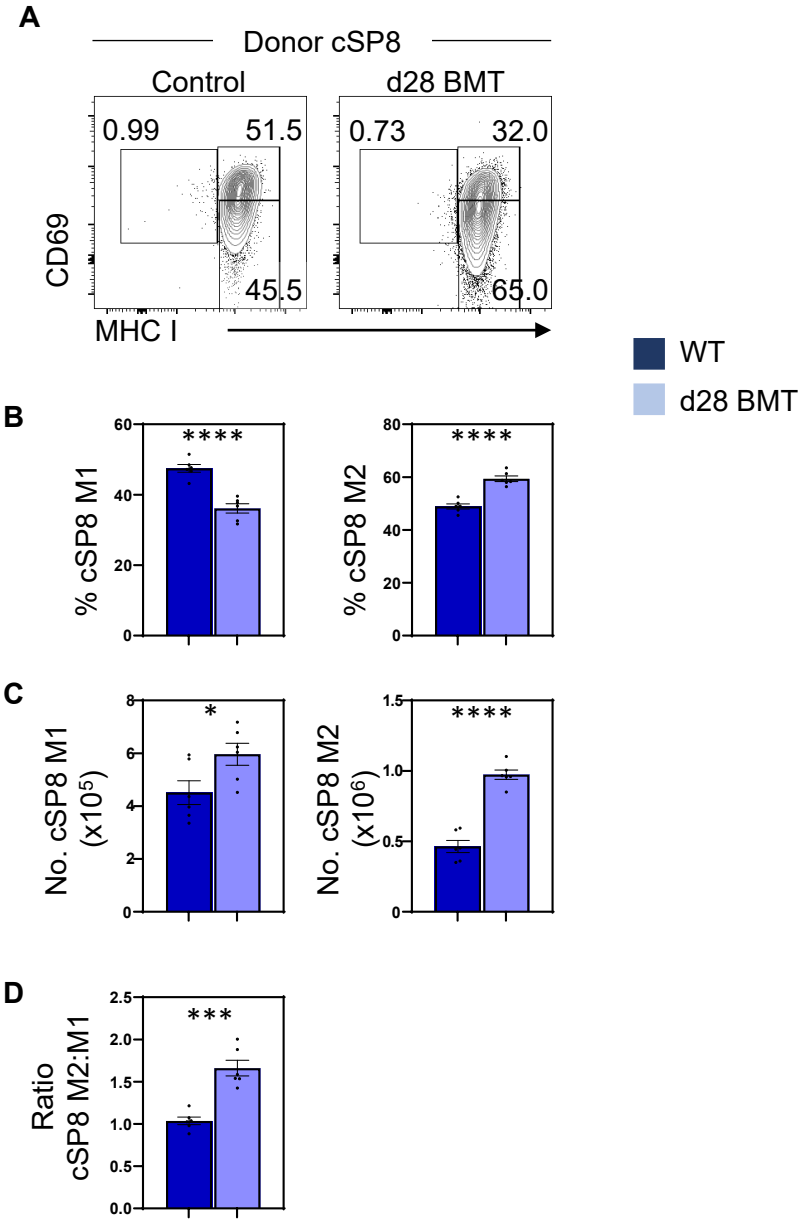
A
Donor cSP8
Control
d28 BMT
0.99
51.5
45.5
0.73
32.0
65.0
CD69
MHC I
WT
d28 BMT
B
% cSP8 M1
% cSP8 M2
****
****
C
No. cSP8 M1 (x10^5)
No. cSP8 M2 (x10^6)
*
****
D
Ratio cSP8 M2:M1
***

Figure 4.5. Increase in cSP8 at Day 28 post-BMT is not specific to, but is Enriched within the M2

Thymuses were harvested from CD45.1 WT mice 28 days following a lethal dose of irradiation and reconstitution with T-cell depleted CD45.2 WT RagGFP bone marrow. Age matched WT RagGFP mice were taken alongside as controls. The tissues were mechanically disaggregated and stained for FACS analysis. Analysis was pregated on $CD45.2^+$ donor cells.

(A) Representative FACS plots to identify $CD69^+$ MHC I^- (SM), $CD69^+$ MHC I^+ (M1), and $CD69^-$ MHC I^+ (M2) cSP8 in WT control (left) and d28 BMT (right) mice.

(B) Graphical representation of percentages of M1 (left), and M2 (right) cSP8 in WT control (dark blue bar) and d28 BMT (light blue bar) mice.

(C) Graphical representation of numbers of M1 (left), and M2 (right) cSP8 in WT control (dark blue bar) and d28 BMT (light blue bar) mice.

(D) Graphical representation of the ratio of cSP8 M2:cSP8 M1 in WT control (dark blue bar) and d28 BMT (light blue bar) mice.

Data is taken from 3 separate experiments with n=6 WT control and d28 BMT mice. Each data point represents an individual mouse, with bars plotting the mean and error bars representing the SEM. Statistical significance was determined using Independent Student's T-test, with (*) representing $P<0.05$, (***) representing $P<0.001$, and (****) representing $P<0.0001$.

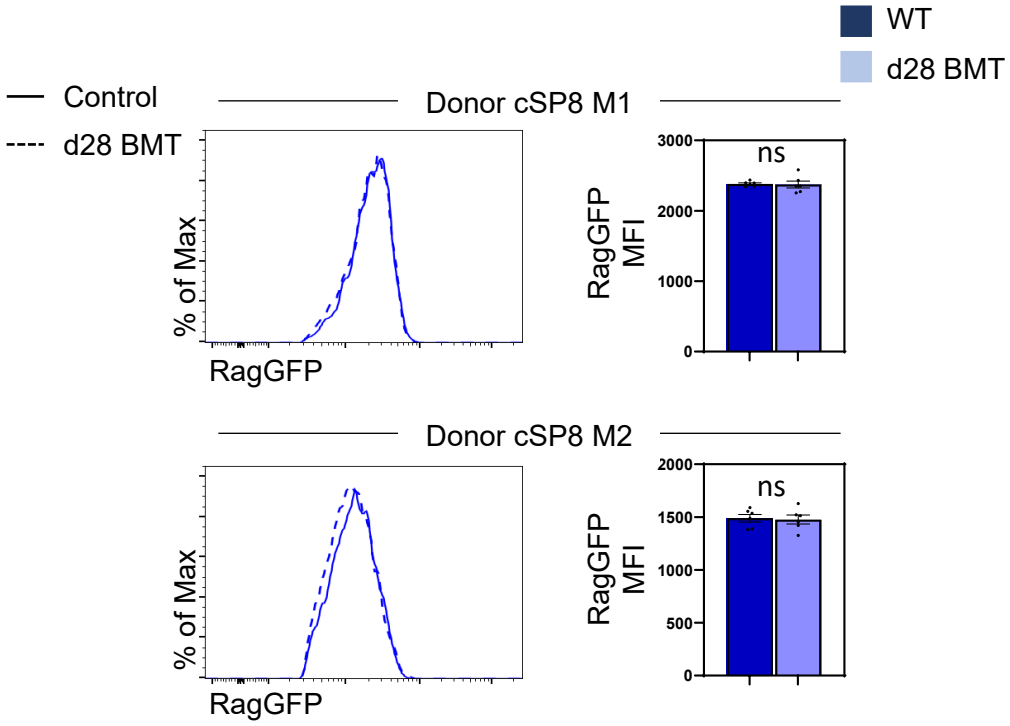
WT
d28 BMT
Control
d28 BMT
Donor cSP8 M1
% of Max
RagGFP
RagGFP MFI
3000
2000
1000
0
ns
Donor cSP8 M2
% of Max
RagGFP
RagGFP MFI
2000
1500
1000
500
0
ns

Figure 4.6. RagGFP Levels are Unchanged in cSP8 populations of d28 BMT mice

Thymuses were harvested from CD45.1 WT mice 28 days following a lethal dose of irradiation and reconstitution with T-cell depleted CD45.2 WT RagGFP bone marrow. Age matched WT RagGFP mice were taken alongside as controls. The tissues were mechanically disaggregated and stained for FACS analysis. Analysis was pregated on $CD45.2^{+}$ donor cells.

Summary of RagGFP expression by cSP8 M1 (top), and M2 (bottom) in WT control (solid line, dark blue bar) and d28 BMT (dashed line, light blue bar) mice.

Data is taken from 3 separate experiments with n=6 WT control and d28 BMT mice. Each data point represents an individual mouse, with bars plotting the mean and error bars representing the SEM. Statistical significance was determined using Independent Student's T-test, with (ns) representing no significance.

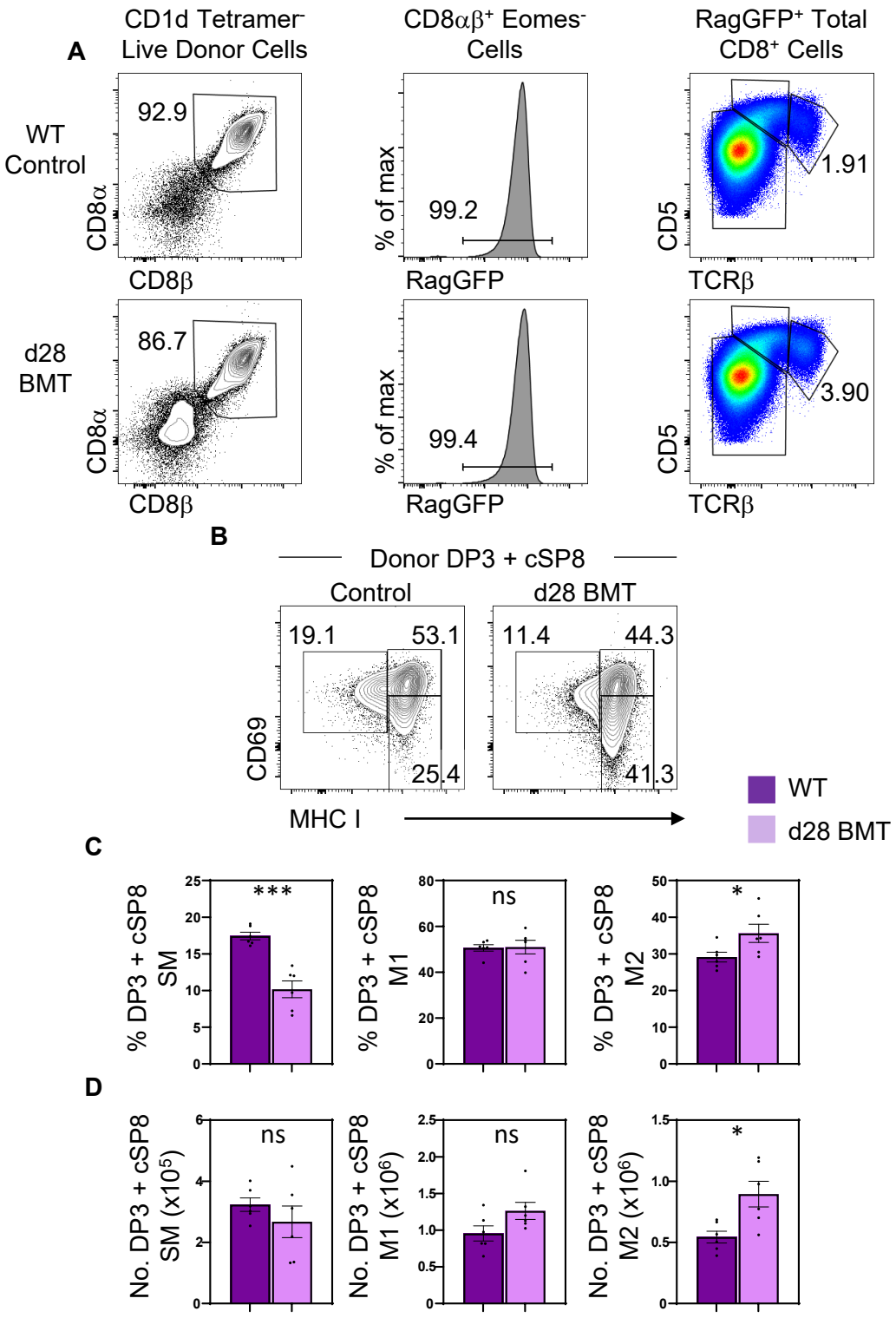
A
CD1d Tetramer⁻ Live Donor Cells
CD8αβ⁺ Eomes⁻ Cells
RagGFP⁺ Total CD8⁺ Cells
WT Control
d28 BMT
92.9
86.7
CD8α
CD8β
99.2
99.4
% of max
RagGFP
1.91
3.90
CD5
TCRβ
B
Donor DP3 + cSP8
Control
d28 BMT
19.1
53.1
25.4
11.4
44.3
41.3
CD69
MHC I
WT
d28 BMT
C
% DP3 + cSP8 SM
% DP3 + cSP8 M1
% DP3 + cSP8 M2
***
ns
*
D
No. DP3 + cSP8 SM (x10⁵)
No. DP3 + cSP8 M1 (x10⁶)
No. DP3 + cSP8 M2 (x10⁶)
ns
ns
*

Figure 4.7. Inclusion of the DP3 Population shows M2-specific increase in cSP8

Thymuses were harvested from CD45.1 WT mice 28 days following a lethal dose of irradiation and reconstitution with T-cell depleted CD45.2 WT RagGFP bone marrow. Age matched WT RagGFP mice were taken alongside as controls. The tissues were mechanically disaggregated and stained for FACS analysis. Analysis was pregated on $CD45.2^+$ donor cells.

(A) Representative FACS plots to identify total committed $CD8^+$ cells, identified as CD1d $Tetramer^-$ $CD8\alpha\beta^+$ $Eomes^-$ $RagGFP^+$ live $CD5^{INT}$ $TCR\beta^{HI}$ thymocytes in WT control (top row) and d28 BMT (bottom row) mice.

(B) Representative FACS plots to identify $CD69^+$ MHC I^- (SM), $CD69^+$ MHC I^+ (M1), and $CD69^-$ MHC I^+ (M2) total committed $CD8^+$ cells in WT control (left) and d28 BMT (right) mice.

(C) Graphical representation of percentages of SM (left), M1 (middle), and M2 (right) total committed $CD8^+$ cells in WT control (dark purple bar) and d28 BMT (light purple bar) mice.

(D) Graphical representation of numbers of SM (left), M1 (middle), and M2 (right) total committed $CD8^+$ cells in WT control (dark purple bar) and d28 BMT (light purple bar) mice.

Data is taken from 3 separate experiments with n=6 WT control and d28 BMT mice. Each data point represents an individual mouse, with bars plotting the mean and error bars representing the SEM. Statistical significance was determined using Independent Student's T-test, with (*) representing $P<0.05$, (***) representing $P<0.001$, and (ns) representing no significance.

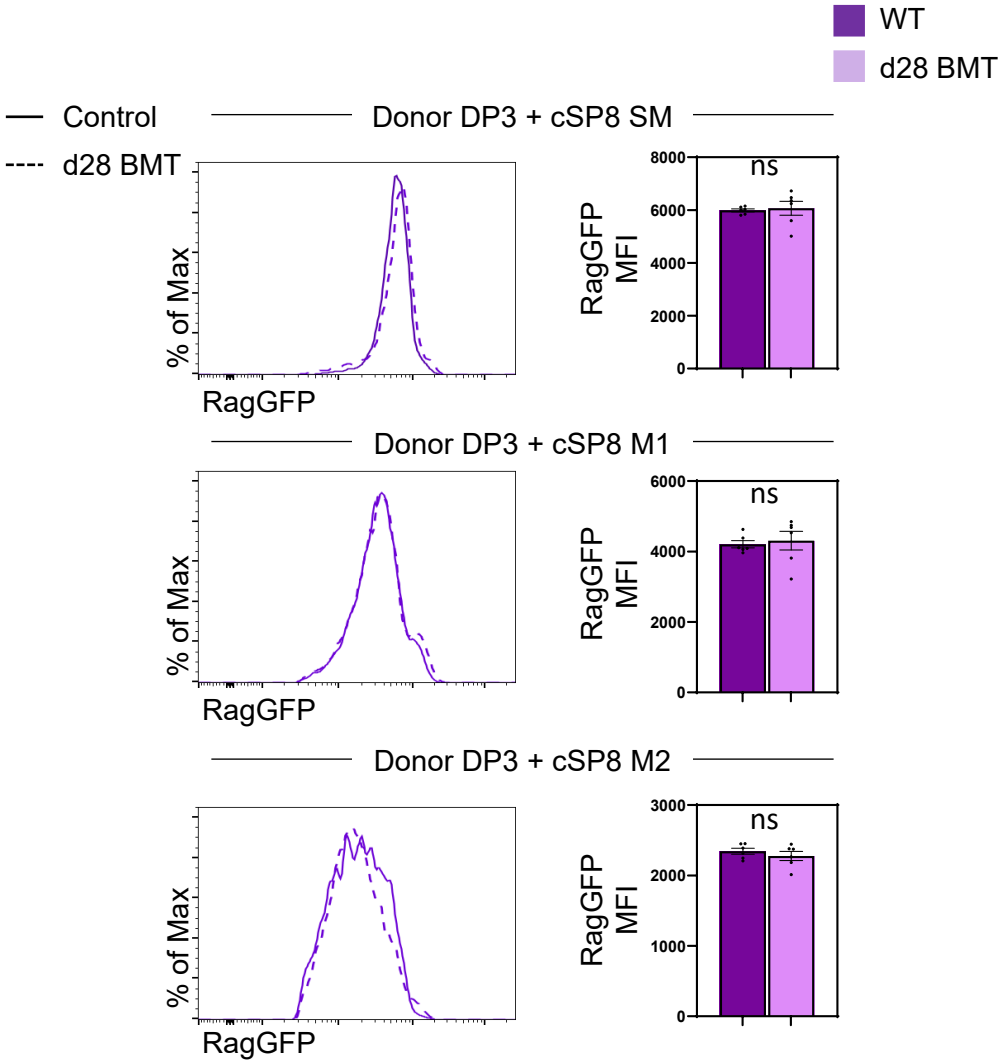
WT
d28 BMT
Control
d28 BMT
Donor DP3 + cSP8 SM
% of Max
RagGFP
RagGFP MFI
ns
8000
6000
4000
2000
0
Donor DP3 + cSP8 M1
% of Max
RagGFP
RagGFP MFI
ns
6000
4000
2000
0
Donor DP3 + cSP8 M2
% of Max
RagGFP
RagGFP MFI
ns
3000
2000
1000
0

Figure 4.8. RagGFP Levels Remain Unchanged in cSP8 Populations 28 days post-BMT Despite Inclusion of the DP3 Population

Thymuses were harvested from CD45.1 WT mice 28 days following a lethal dose of irradiation and reconstitution with T-cell depleted CD45.2 WT RagGFP bone marrow. Age matched WT RagGFP mice were taken alongside as controls. The tissues were mechanically disaggregated and stained for FACS analysis. Analysis was pregated on $CD45.2^+$ donor cells.

Summary of RagGFP expression by total committed $CD8^+$ cells SM (top), M1 (middle), and M2 (bottom) in WT control (dark purple line, solid bar) and d28 BMT (dashed line, light purple bar) mice.

Data is taken from 3 separate experiments with n=6 WT control and d28 BMT mice. Each data point represents an individual mouse, with bars plotting the mean and error bars representing the SEM. Statistical significance was determined using Independent Student's T-test, with (ns) representing no significance.

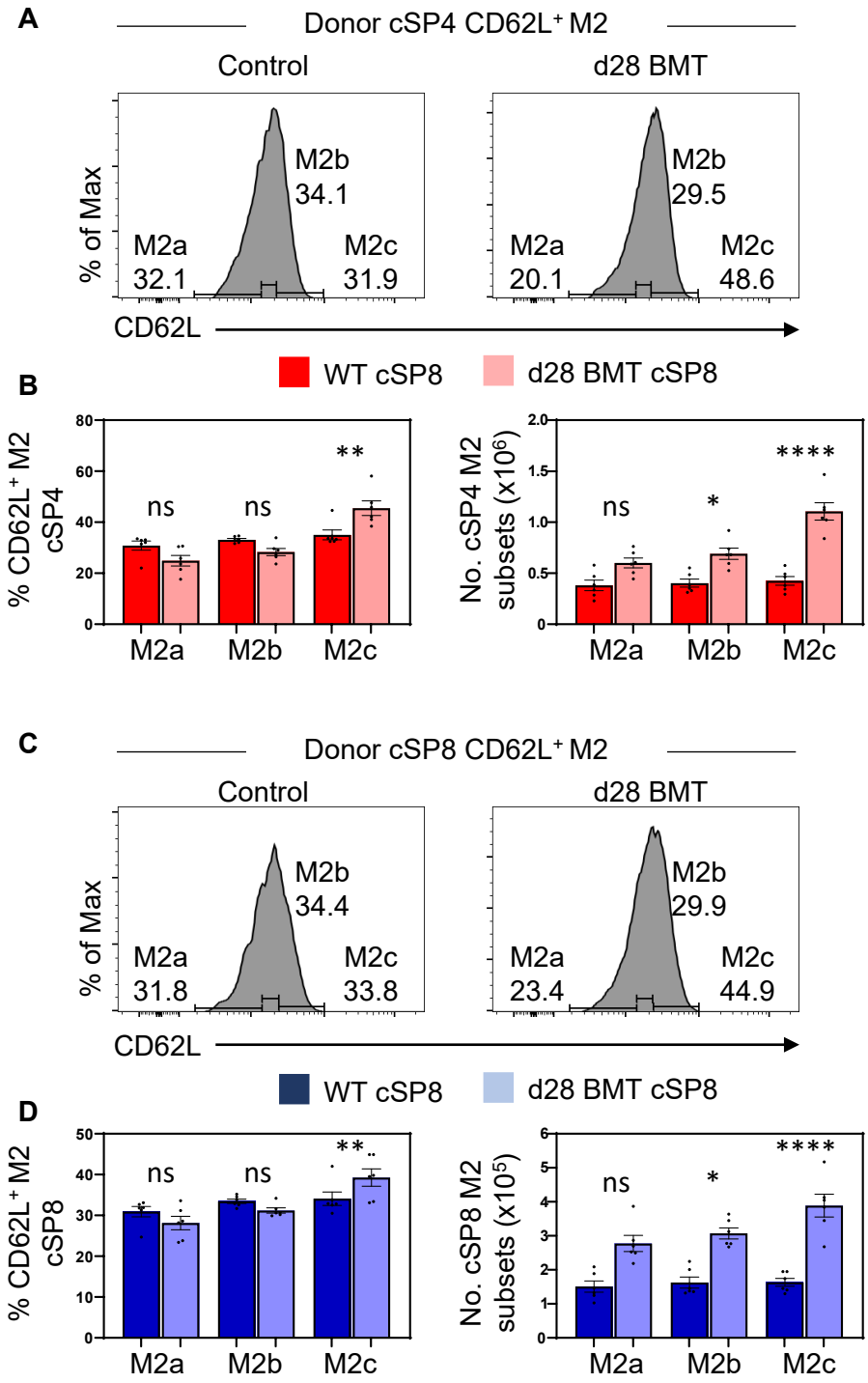
A
Donor cSP4 CD62L+ M2
Control
d28 BMT
% of Max
M2b
34.1
M2a
32.1
M2c
31.9
M2b
29.5
M2a
20.1
M2c
48.6
CD62L
WT cSP8
d28 BMT cSP8
B
% CD62L+ M2 cSP4
ns
ns
**
No. cSP4 M2 subsets (x10^6)
ns
*
****
M2a
M2b
M2c
C
Donor cSP8 CD62L+ M2
Control
d28 BMT
% of Max
M2b
34.4
M2a
31.8
M2c
33.8
M2b
29.9
M2a
23.4
M2c
44.9
CD62L
WT cSP8
d28 BMT cSP8
D
% CD62L+ M2 cSP8
ns
ns
**
No. cSP8 M2 subsets (x10^5)
ns
*
****
M2a
M2b
M2c

Figure 4.9. cSP4, and to a lesser extent cSP8 are Enriched for the Most Mature M2c in d28 BMT mice

Thymuses were harvested from CD45.1 WT mice 28 days following a lethal dose of irradiation and reconstitution with T-cell depleted CD45.2 WT RagGFP bone marrow. Age matched WT RagGFP mice were taken alongside as controls. The tissues were mechanically disaggregated and stained for FACS analysis. Analysis was pregated on $CD45.2^{+}$ donor cells.

(A) Separation of M2a/b/c populations based on equal separation of cSP4 M2 from WT control mice (left) and applied to d28 BMT cSP4 M2 (right).

(B) Graphical representation of percentages (left) and numbers (right) of cSP4 M2a, M2b, and M2c in WT control (dark red bar) and d28 BMT (light red bar) mice.

(C) Separation of M2a/b/c populations based on equal separation of cSP8 M2 from WT control mice (left) and applied to d28 BMT cSP8 M2 (right).

(D) Graphical representation of percentages (left) and numbers (right) of cSP8 M2a, M2b, and M2c in WT control (dark blue bar) and d28 BMT (light blue bar) mice.

Data is taken from 3 separate experiments with n=6 WT control and d28 BMT mice. Each data point represents an individual mouse, with bars plotting the mean and error bars representing the SEM. Statistical significance was determined using Independent Student's T-test, with (*) representing $P<0.05$, (**) representing $P<0.01$, (****) representing $P<0.0001$ and (ns) representing no significance.

4.2.3 Egress 28 Days Post-Bone Marrow Transplant

Our observation that both cSP4 and cSP8 show accumulations of the most mature populations in the thymuses of d28 BMT implied a limited ability of these cells to undergo thymic egress. We therefore looked to further investigate egress of donor-derived thymocytes within mice recovering from BMT. To do this, we again used the anti-CD45 PE antibody I.V. injection model. This allowed us to isolate cells in the PVS of both control and d28 BMT, and subsequently determine whether thymic egress via the ordered conveyor belt is hampered in BMT mice, leading to the observed accumulation. In order to make this comparison, we first looked to determine whether the proportion of egressing cells in BMT mice was the same in control mice. Whilst we could not calculate the total number of egressing cells in the control and BMT mice, we could still compare the proportion of egressing cells by pregating on total GFP^+ $CD45.2^+$ CD1d $Tetramer^-$ cells. The percentage of $TCR\beta^+$ $CD45\text{-}PE^+$ cells therefore represent the proportion of newly generated, donor T-cells in the PVS of control and BMT thymuses (Figure 4.10). In doing this, we see that a greater proportion of the newly generated donor T-cells are found in the PVS of d28 BMT mice compared to control mice. This suggests that there is a greater volume of egressing cells contained within the PVS in d28 BMT mice compared to control mice, implying that the accumulation seen within the thymus is also present within the PVS, and entry into the PVS is not hampered following recovering from BMT.

To further investigate this, we looked to determine whether the ‘conveyor belt’, previously described in cSP4 and now in cSP8 was still functional following BMT. In order to do this we compared the maturational status of cells isolated within the PVS between control and d28 BMT mice to determine whether the most mature cells were

still being preferentially selected for egress following recovery from BMT. By applying our SM, M1, and M2 gates to CD45.2^{+} donor cells isolated in the PVS as CD45-PE^{+} in both control and d28 BMT mice. This showed that the vast majority of cSP4 within the PVS are M2 in both control and d28 BMT mice, with no significant difference between the two (Figure 4.11A). Comparing the levels of RagGFP on cSP4 M2 in the PVS between control and BMT mice showed no significance between the two (Figure 4.11B), suggesting the cSP4 M2 found in the PVS of d28 BMT are of the same age as in control mice. We then looked further within the M2 population isolated within the PVS to the sequential M2a, M2b, and M2c populations. The CD45-PE^{-} portion of thymic cSP4 M2 in control mice were separated into evenly distributed M2a, M2b, and M2c populations, before being applied to CD45.2^{+} CD45-PE^{+} PVS isolated donor cells in both control mice and d28 BMT mice. This shows that both control mice and d28 BMT mice are enriched for the most mature M2c population, with no significant difference between the proportions of each of these populations found within the PVS (Figure 4.11C). The enriched M2c population within the PVS of both control and BMT mice shows that, again, these cells egressing via the PVS are no older in d28 BMT mice than in age matched controls, with no significant difference in the levels of RagGFP (Figure 4.11D). We can then make this same comparison within the cSP8 populations isolated in the PVS's of age matched control and d28 BMT mice. Mirroring what was seen within cSP4 cells isolated in the PVS, cSP8 in the PVS are primarily M2 in BMT mice to the same extent to that seen in age matched control mice (Figure 4.12A), again with the same level of RagGFP suggesting that these cells are the same age in BMT mice as in control mice (Figure 4.12B). We then used the same method to determine the distribution of cSP8 M2a, M2b, and M2c populations within the PVS of

control and BMT thymuses as in cSP4, applying the evenly distributed gates from CD45-PE^{-} thymic M2 to CD45-PE^{+} PVS-isolated M2 from both control and BMT mice. This again showed the cSP8 egress is unaffected in d28 BMT mice, with the same level of enrichment of the most mature M2c cells (Figure 4.12C) and having the same level of RagGFP expression (Figure 3.12D). Together, this shows that the conveyor belt mechanism in both cSP4 and cSP8 populations is unaffected in d28 BMT mice, with the most mature populations being preferentially selected from the thymus for egress via the PVS, even despite the accumulation seen within the bulk thymus. Combined with the moderate increase in the total proportion of cells within the PVS in BMT mice compared to control mice, this may suggest that the accumulation seen is not caused by limited entry into the PVS, with the process still occurring in the standard ordered manner.

Whilst the conveyor belt mechanism of egress is unperturbed in d28 BMT mice, following BMT there is still clear evidence of an accumulation of the most mature populations of cSP4 and cSP8 within the thymus, and of bulk cells within the PVS. We have therefore looked to the periphery to determine whether this accumulation is apparent within cells that have left the thymus, expecting to see a reduction in our recent thymic emigrant population of donor cells. We analysed peripheral T-cell populations by looking within the spleens of both age-matched control mice and d28 BMT mice. The total number of splenocytes was unaffected in d28 BMT mice compared to controls (Figure 4.13A), and importantly so was the number of CD45.2^{+} donor cells, indicating that the haematopoietic compartment as a whole had recovered their numbers within the 28 days following BMT (Figure 4.13B). We then specifically looked to analyse the recovery of the T-cell compartment 28 days following BMT by

gating on CD45.2$^+$ donor splenocytes and removing CD1d tetramer$^+$ iNKT, before gating on TCRβ^+ cells. In doing this we saw that donor T-cells are dramatically reduced following BMT, both in terms of proportions and numbers of cells, with roughly a 3.6-fold reduced number of peripheral T-cells (Figure 4.13C). This suggests that whilst total CD45.2$^+$ cells reach normal levels following BMT, the T-cell compartment has failed to return to normal numbers.

We next looked further within the donor T-cell compartment to determine which subpopulations were the cause of this significantly lower cell number. First, by separating the donor T-cell compartment into bulk CD4 and CD8 T-cells (Figure 3.14A) it is clear that both lineages are significantly reduced in BMT mice, with a 3.3-fold and 4.4-fold decrease respectively (Figure 3.14B). Whilst both are similar to the 3.6-fold decrease seen in total T-cells, there is a greater loss within the CD8 T-cell compartment, further exemplified by the significantly lower proportions of CD8's (Figure 3.14B). The donor CD4 and CD8 T-cell populations within the spleen can then be further separated into circulating T-cells and cells that have recently left the thymus, RTE, using expression of RagGFP. In doing this we could determine whether the loss in number of T-cells was due to a specific reduction in either newly generated or circulating T-cells. Separating cSP4 within the spleen into RagGFP$^+$ and RagGFP$^-$ populations, we saw that there is a significantly higher proportion of RagGFP$^+$ RTE within the spleens of d28 BMT mice compared to age-matched control mice. This increased proportion was proven to be a result of a significantly reduced number of RagGFP$^-$ circulating donor cSP4 T-cells, with the number of RTE being the same control and BMT mice (Figure 4.14C). Similarly, separating splenic cSP8 T-cells based on RagGFP showed the same observation, with a higher proportion of RTE

resulting from the same number of RTE, and therefore a significant loss of RagGFP^{-} circulating donor cells (Figure 3.14D). This suggests that the reduced donor T-cell population seen in BMT mice is not due to a reduced thymic output as a result of an accumulation, and instead that 28 days following lethal irradiation is not enough time for the production of new, donor T-cells to match that from control mice.

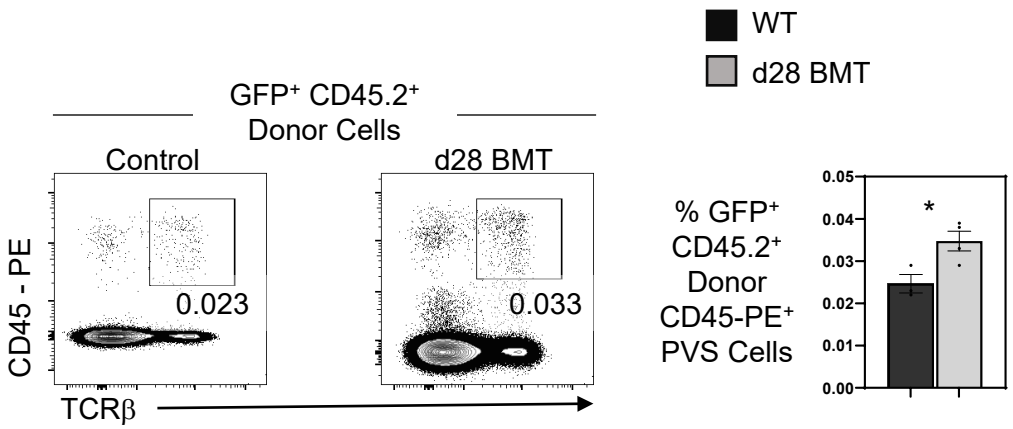
WT
d28 BMT
GFP+ CD45.2+
Donor Cells
Control
d28 BMT
CD45 - PE
TCRβ
0.023
0.033
% GFP+
CD45.2+
Donor
CD45-PE+
PVS Cells
0.05
0.04
0.03
0.02
0.01
0.00
*

Figure 4.10. Increased Proportion of Newly Generated Thymic Donor T-cells Isolated in the PVS of BMT Mice

28 days following a lethal dose of irradiation and reconstitution with T-cell depleted CD45.2 WT RagGFP bone marrow, mice were I.V. injected with anti CD45-PE and sacrificed 3 minutes later. Thymuses were harvested and mechanically disaggregated for FACS analysis of thymocyte subpopulations. Samples were enriched for PE-labelled cells, with a pre-enrichment sample taken as a control. Age matched WT RagGFP mice were injected under the same procedure as controls. Analysis was pregated on $CD45.2^{+}$ donor cells.

Pre-gating on $CD45.2^{+}$ $RagGFP^{+}$ $Tetramer^{-}$ Live cells to show the make-up of newly generated donor T-cells in d28 BMT and age-matched BMT control mice. Subsequent gating on $TCR\beta^{+}$ $CD45\text{-}PE^{+}$ cells identifies T-cells isolated in the PVS of control and BMT thymuses labelled with I.V. injected CD45-PE antibody. Graph summarises the proportion of newly generated donor T-cells that are isolated within the PVS of control (dark grey bar) and BMT mice (light grey bar).

Data is taken from 1 experiment with n=4. Each data point represents an individual mouse, with bars plotting the mean and error bars representing the SEM. Statistical significance was determined using Independent Student's T-test, with (*) representing $P<0.05$.

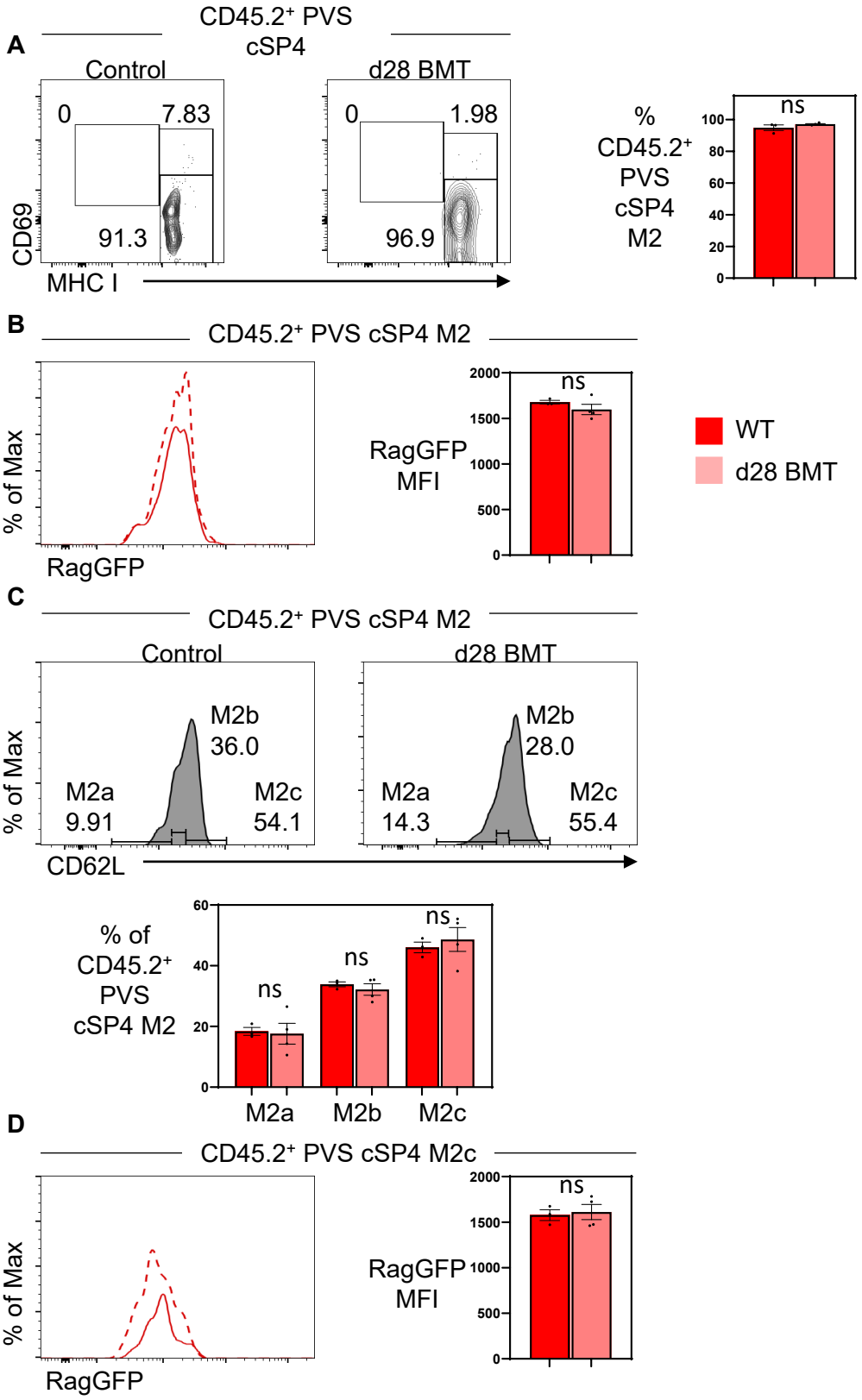
A
CD45.2+ PVS cSP4
Control
d28 BMT
0
7.83
91.3
0
1.98
96.9
CD69
MHC I
% CD45.2+ PVS cSP4 M2
ns
100
80
60
40
20
0
B
CD45.2+ PVS cSP4 M2
% of Max
RagGFP
RagGFP MFI
2000
1500
1000
500
0
ns
WT
d28 BMT
C
CD45.2+ PVS cSP4 M2
Control
d28 BMT
% of Max
M2b 36.0
M2a 9.91
M2c 54.1
M2b 28.0
M2a 14.3
M2c 55.4
CD62L
% of CD45.2+ PVS cSP4 M2
60
40
20
0
ns
ns
ns
M2a
M2b
M2c
D
CD45.2+ PVS cSP4 M2c
% of Max
RagGFP
RagGFP MFI
2000
1500
1000
500
0
ns

Figure 4.11. The cSP4 Conveyor Belt is Still Functional in Mice Recovering from BMT

28 days following a lethal dose of irradiation and reconstitution with T-cell depleted CD45.2 WT RagGFP bone marrow, mice were I.V. injected with anti CD45-PE and sacrificed 3 minutes later. Thymuses were harvested and mechanically disaggregated for FACS analysis of thymocyte subpopulations. Samples were enriched for PE-labelled cells, with a pre-enrichment sample taken as a control. Age matched WT RagGFP mice were injected under the same procedure as controls. Analysis was pregated on CD45.2$^+$ donor cells.

(A) Gating of CD69$^+$ MHC I$^-$ (SM), CD69$^+$ MHC I$^+$ (M1), and CD69$^-$ MHC I$^+$ (M2) in post- PE enrichment CD45-PE$^+$ PVS cSP4 from aged matched control (left), and d28 BMT (right) mice. Graph to summarise percentages of M2 in PVS cSP4 from control (dark red bar) and d28 BMT mice (light red bar).

(B) Histogram plots of the RagGFP expression of I.V. CD45-PE labelled PVS cSP4 M2 from age-matched control (solid line) and d28 BMT mice (dashed line). Graph summarises calculated MFI of RagGFP in I.V. CD45-PE labelled PVS cSP4 M2 from control (dark red bar) and BMT mice (light red bar).

(C) Separation of M2a/b/c populations based on equal separation of thymic cSP4 M2 from control mice, and applied to I.V. CD45-PE labelled PVS cSP4 M2 from control mice (left) and d28 BMT mice (right). Graph summarises percentages of I.V. CD45-PE labelled PVS cSP4 in control (dark red bar) BMT mice (light red bar).

(D) Histogram plots of the RagGFP expression of I.V. CD45-PE labelled PVS cSP4 M2c from age-matched control (solid line) and d28 BMT mice (dashed line). Graph summarises calculated MFI of RagGFP in I.V. CD45-PE labelled PVS cSP4 M2c from control (dark red bar) and BMT mice (light red bar).

Data is taken from 1 experiment with n=4. Each data point represents an individual mouse, with bars plotting the mean and error bars representing the SEM. Statistical significance was determined using Independent Student's T-test, with (ns) representing no significance.

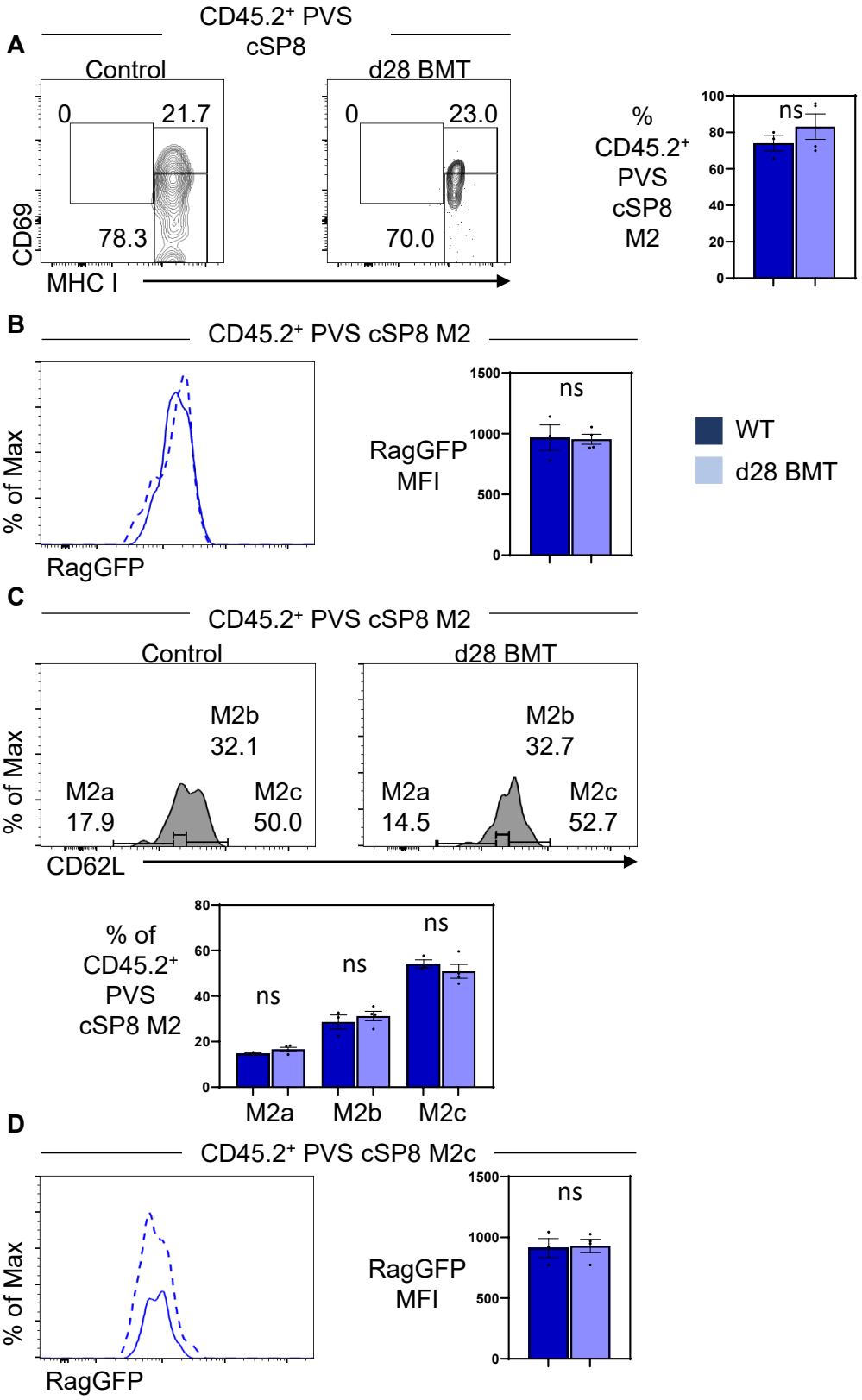
A
CD45.2⁺ PVS cSP8
Control
d28 BMT
0
21.7
78.3
0
23.0
70.0
CD69
MHC I
% CD45.2⁺ PVS cSP8 M2
ns
B
CD45.2⁺ PVS cSP8 M2
% of Max
RagGFP
RagGFP MFI
ns
WT
d28 BMT
C
CD45.2⁺ PVS cSP8 M2
Control
d28 BMT
M2b 32.1
M2a 17.9
M2c 50.0
M2b 32.7
M2a 14.5
M2c 52.7
% of Max
CD62L
% of CD45.2⁺ PVS cSP8 M2
ns
M2a
M2b
M2c
D
CD45.2⁺ PVS cSP8 M2c
% of Max
RagGFP
RagGFP MFI
ns

Figure 4.12. The cSP8 Conveyor Belt is Still Functional in Mice Recovering from BMT

28 days following a lethal dose of irradiation and reconstitution with T-cell depleted CD45.2 WT RagGFP bone marrow, mice were I.V. injected with anti CD45-PE and sacrificed 3 minutes later. Thymuses were harvested and mechanically disaggregated for FACS analysis of thymocyte subpopulations. Samples were enriched for PE-labelled cells, with a pre-enrichment sample taken as a control. Age matched WT RagGFP mice were injected under the same procedure as controls. Analysis was pregated on CD45.2$^+$ donor cells.

(A) Gating of CD69$^+$ MHC I$^-$ (SM), CD69$^+$ MHC I$^+$ (M1), and CD69$^-$ MHC I$^+$ (M2) in post- PE enrichment CD45-PE$^+$ PVS cSP8 from aged matched control (left), and d28 BMT (right) mice. Graph to summarise percentages of M2 in PVS cSP8 from control (dark blue bar) and d28 BMT mice (light blue bar).

(B) Histogram plots of the RagGFP expression of I.V. CD45-PE labelled PVS cSP8 M2 from age-matched control (solid line) and d28 BMT mice (dashed line). Graph summarises calculated MFI of RagGFP in I.V. CD45-PE labelled PVS cSP8 M2 from control (dark blue bar) and BMT mice (light blue bar).

(C) Separation of M2a/b/c populations based on equal separation of thymic cSP8 M2 from control mice, and applied to I.V. CD45-PE labelled PVS cSP8 M2 from control mice (left) and d28 BMT mice (right). Graph summarises percentages of I.V. CD45-PE labelled PVS cSP8 in control (dark blue bar) BMT mice (light blue bar).

(D) Histogram plots of the RagGFP expression of I.V. CD45-PE labelled PVS cSP8 M2c from age-matched control (solid line) and d28 BMT mice (dashed line). Graph summarises calculated MFI of RagGFP in I.V. CD45-PE labelled PVS cSP8 M2c from control (dark blue bar) and BMT mice (light blue bar).

Data is taken from 1 experiment with n=4. Each data point represents an individual mouse, with bars plotting the mean and error bars representing the SEM. Statistical significance was determined using Independent Student's T-test, with (ns) representing no significance.

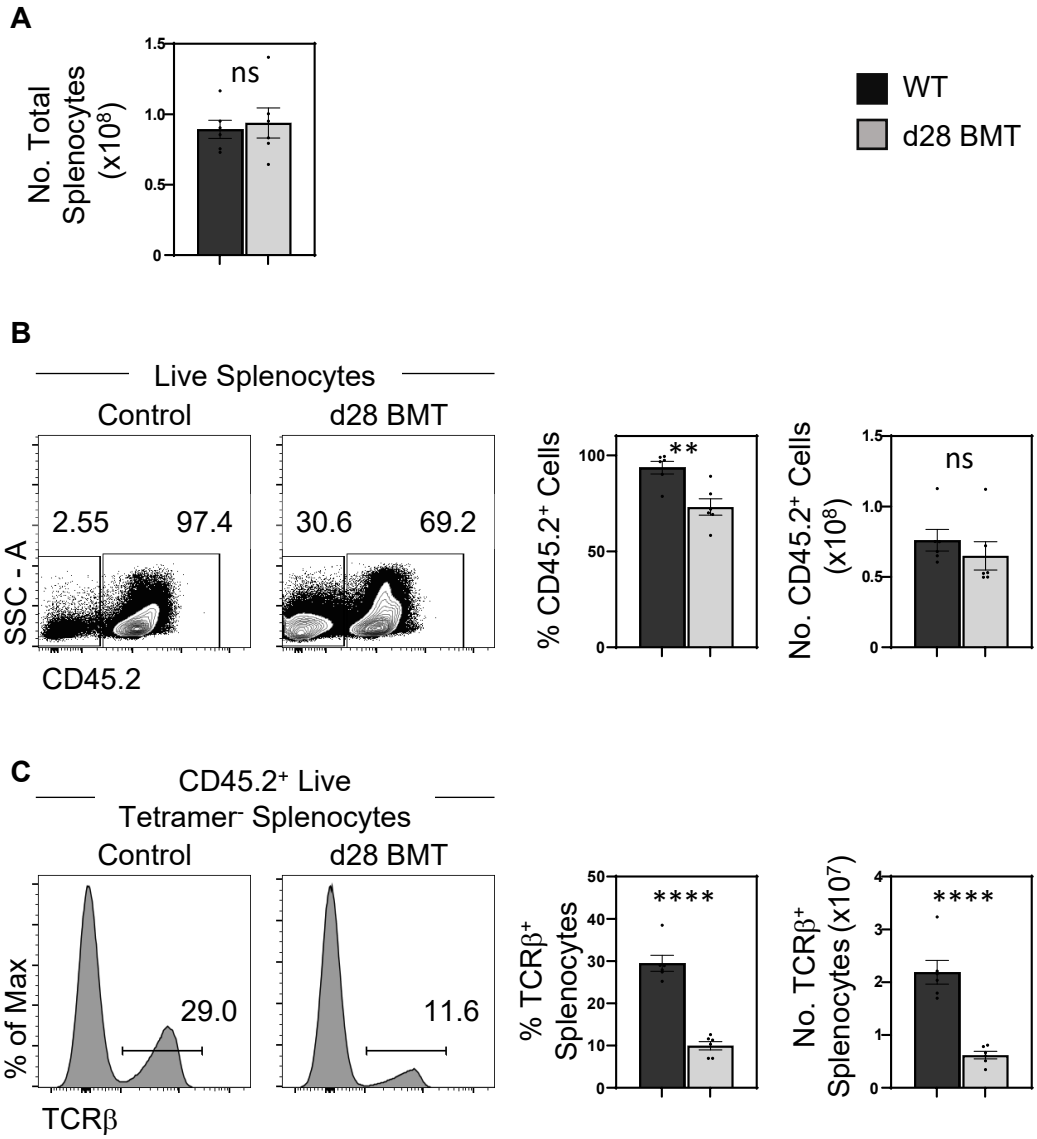
A
No. Total Splenocytes (x10^8)
ns
WT
d28 BMT
B
Live Splenocytes
Control
d28 BMT
2.55
97.4
30.6
69.2
SSC - A
CD45.2
% CD45.2+ Cells
**
No. CD45.2+ Cells (x10^8)
ns
C
CD45.2+ Live Tetramer- Splenocytes
Control
d28 BMT
% of Max
29.0
11.6
TCRβ
% TCRβ+ Splenocytes
****
No. TCRβ+ Splenocytes (x10^7)
****

Figure 4.13. Reduced Donor T-cells at day 28 post-BMT

Spleens were harvested from CD45.1 WT mice 28 days following a lethal dose of irradiation and reconstitution with T-cell depleted CD45.2 WT RagGFP bone marrow. Age matched WT RagGFP mice were taken alongside as controls. The tissues were mechanically disaggregated and stained for FACS analysis.

(A) Summary of total splenic cellularity in WT control (dark grey bar) and d28 post-BMT mice (light grey bar).

(B) Representative FACS plots to identify $CD45.2^+$ donor cells in WT control (left) and d28 BMT (right) mice. Graphical representation of percentages (left) and numbers (right) of $CD45.2^+$ donor cells in WT control (dark grey bar) and d28 BMT (light grey bar) mice.

(C) Representative FACS plots to identify $TCR\beta^+$ T-cells in WT control (left) and d28 BMT (right) mice. Graphical representation of percentages (left) and numbers (right) of $TCR\beta^+$ T-cells in WT control (dark grey bar) and d28 BMT (light grey bar) mice.

Data is taken from 3 separate experiments with n=6 WT control and d28 BMT mice. Each data point represents an individual mouse, with bars plotting the mean and error bars representing the SEM. Statistical significance was determined using Independent Student's T-test, with (**) representing $P<0.01$, and (****) representing $P<0.0001$, and (ns) representing no significance.

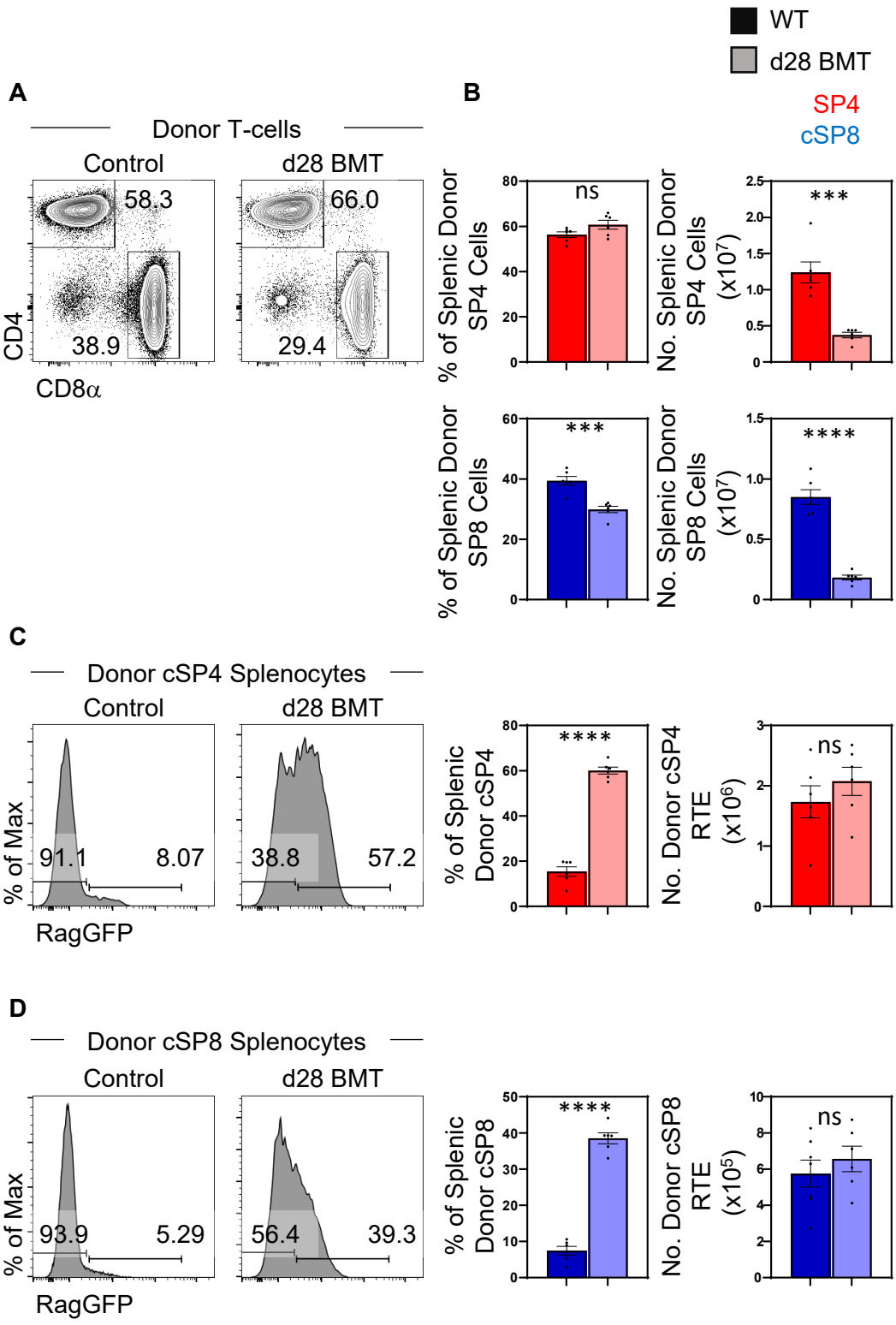
WT
d28 BMT
A
Donor T-cells
Control
d28 BMT
58.3
66.0
38.9
29.4
CD4
CD8α
B
SP4
cSP8
% of Splenic Donor SP4 Cells
ns
No. Splenic Donor SP4 Cells (x10^7)
***
% of Splenic Donor SP8 Cells
***
No. Splenic Donor SP8 Cells (x10^7)
****
C
Donor cSP4 Splenocytes
Control
d28 BMT
% of Max
91.1
8.07
38.8
57.2
RagGFP
% of Splenic Donor cSP4
****
No. Donor cSP4 RTE (x10^6)
ns
D
Donor cSP8 Splenocytes
Control
d28 BMT
% of Max
93.9
5.29
56.4
39.3
RagGFP
% of Splenic Donor cSP8
****
No. Donor cSP8 RTE (x10^5)
ns

Figure 4.14. Reduced Circulating T-cells, but No Change in RTE within d28 BMT Mice

Spleens were harvested from CD45.1 WT mice 28 days following a lethal dose of irradiation and reconstitution with T-cell depleted CD45.2 WT RagGFP bone marrow. Age matched WT RagGFP mice were taken alongside as controls. The tissues were mechanically disaggregated and stained for FACS analysis.

(A) Representative histogram plots of SP4 and SP8 donor splenic T-cells in WT control (left) and d28 BMT (right) mice.

(B) Graphical representation of percentages (left) and numbers (right) of SP4 (top row) and SP8 (bottom row) donor splenic T-cells in WT control (dark bars) and d28 BMT (light bars) mice.

(C) Representative FACS plots to identify RagGFP^{+} donor splenic cSP4 RTE in WT control (left) and d28 BMT (right) mice. Graphical representation of percentages (left) and numbers (right) of donor splenic cSP4 RTE in WT control (dark red bar) and d28 BMT (light red bar) mice.

(D) Representative FACS plots to identify RagGFP^{+} donor splenic cSP8 RTE in WT control (left) and d28 BMT (right) mice. Graphical representation of percentages (left) and numbers (right) of donor splenic cSP8 RTE in WT control (dark blue bar) and d28 BMT (light blue bar) mice.

Data is taken from 3 separate experiments with n=6 WT control and d28 BMT mice. Each data point represents an individual mouse, with bars plotting the mean and error bars representing the SEM. Statistical significance was determined using Independent Student's T-test, with (***) representing $P<0.001$, and (****) representing $P<0.0001$, and (ns) representing no significance.

4.2.4 Specific Endothelial Cells Involved in Thymocyte Egress are Reduced Following Bone Marrow Transplantation

Whilst any effect of an egress defect seen within the peripheral tissues is unclear within d28 BMT mice, both an accumulation of the most mature donor populations within the thymus and a higher frequency of donor cells within the PVS is apparent. We therefore looked to determine what may be the cause of this intrathymic accumulation following BMT. LTβR KO mice have been shown to have a loss in the number of mTEC, similar to the failure in mTEC recovery post-BMT that results in the lower mTEC numbers seen at d28 (94,261). Whilst LTβR KO mice show thymic accumulations similar to that we have seen in d28 BMT mice, this accumulation was shown to not be specifically caused by this loss of mTEC. Instead, accumulations were attributed to the specific loss of a specialised endothelial population involved in thymic ingress and egress, TPEC (98). TPEC were shown to be the population of endothelial cells that both ETP homing to the thymus (164) and CD45-PE labelled cells leaving the thymus (263) are most closely associated with, with specific loss of TPEC resulting in both failure to recruit thymic progenitors and accumulations of mature thymocytes (164,165,263). This led us to question the status of these cells within d28 BMT mice, and whether the failure of mTEC recovery reported following BMT extends to these endothelial cells within the thymus and may subsequently be the cause of our observed thymic accumulation.

In order to do this, we first looked to identify endothelial populations within the thymus that have previously been defined and implicated with thymic egress. Figure 4.15 shows this gating strategy, pre-gating on live Ter119^{-} cells to remove dead cells and red blood cells, we then gated on CD45^{-} EpCAM1^{-} non-epithelial stromal cells. We then

gated on $CD31^+$ cells, representing the total endothelial population. Further subsets of endothelial cells have been identified within this $CD31^+$ population using expression of Ly6c and P-selectin. Importantly, TPEC are defined as P-$selectin^+$ $Ly6c^-$ endothelial cells (164), a population we can clearly identify using this gating strategy (Figure 4.15A). Within the TPEC population, more recent work has identified BST-1 as a marker to further subdivide the population based on specific roles. Whilst TPEC are involved in both key processes involving the thymic vasculature in the recruitment of progenitors and the egress of mature thymocytes, BST-1 expression is proposed to separate TPEC into each defined role. BST-1^{LO} vessels are associated with homing of progenitor cells, and BST-1^{HI} vessels' role lies in thymic egress (263). Importantly, both P-$selectin^+$ $Ly6c^-$ and the P-$selectin^+$ $Ly6c^+$ endothelial population were shown to express BST-1 at much higher levels than the P-$selectin^-$ $Ly6c^+$ population (263), which we confirm with our gating strategy (Figure 4.15B). Looking specifically within the TPEC population, we can identify BST-1^{LO} and BST-1^{HI} populations, again with the TPEC population proving to be wholly positive for BST-1 expression (Figure 4.15C).

Having identified the key populations of endothelial cells that are implicated in thymic egress within WT mice, we looked to see how they may be affected in d28 BMT mice. First, there showed to be no difference in the numbers of overall endothelial cells, suggesting that as a bulk population they are either unaffected by BMT, or are able to recover within 28 days (Figure 4.16A). When separating $CD31^+$ endothelial cells into subpopulations based on expression of P-selectin and Ly6c all three populations are clearly identifiable within d28 BMT mice. However, whilst the numbers of P-$selectin^-$ $Ly6c^+$ and P-$selectin^+$ $Ly6c^+$ populations are unaffected, P-$selectin^+$ $Ly6c^-$ TPEC are significantly reduced in the d28 BMT mice (Figure 4.16B), indicating a specific loss of

TPEC following BMT. This loss is further outlined when comparing the d28 BMT mice to age-matched control mice as a percentage of the average control mice from each experiment, with TPEC numbers in d28 BMT mice on average being 38% that of control mice (Figure 4.16C). As this clearly shows a specific loss of TPEC in d28 BMT mice, we next looked to see whether this specifically affected the BST-1^{HI} TPEC population associated with egress, or whether both TPEC subsets were affected. In doing this we saw that there is a significant loss of both BST-1^{LO} and BST-1^{HI} populations, suggesting that both ingress and egress-associated TPEC fail to recover in d28 BMT mice (Figure 3.17). The specific reduction in TPEC seen within d28 BMT mice, and furthermore the reduction in BST-1^{HI} TPEC, therefore provides a cause for the thymic accumulation we observe within these mice.

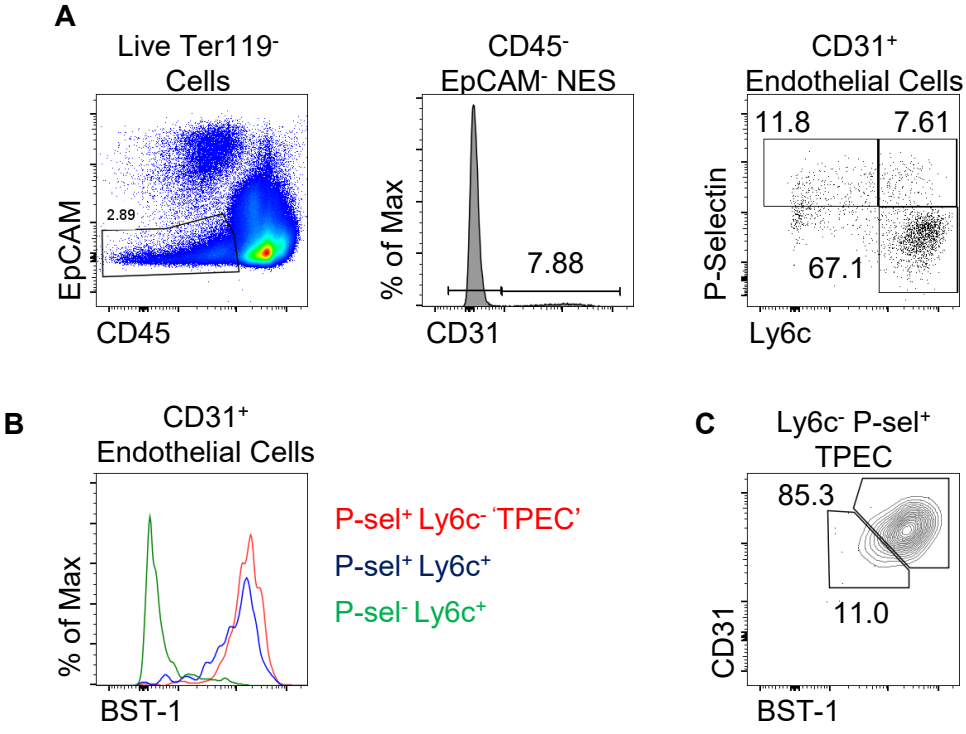
A
Live Ter119- Cells
EpCAM
2.89
CD45
CD45- EpCAM- NES
% of Max
7.88
CD31
CD31+ Endothelial Cells
11.8
7.61
P-Selectin
67.1
Ly6c
B
CD31+ Endothelial Cells
% of Max
BST-1
P-sel+ Ly6c- 'TPEC'
P-sel+ Ly6c+
P-sel- Ly6c+
C
Ly6c- P-sel+ TPEC
85.3
11.0
CD31
BST-1

Figure 4.15. Identification of Endothelial Populations in the Thymus by FACS

Thymuses were harvested from WT B6 mice and enzymatically digested, CD45 depleted, and stained for FACS analysis.

(A) Gating strategy used to identify Live Ter119$^-$ CD45$^-$ EpCAM$^-$ non-epithelial stromal cells (NES), CD31$^+$ endothelial subset of NES, and Ly6c$^-$ P-sel$^+$ thymic portal endothelial cells (TPEC) within these endothelial cells.

(B) Representative histogram plot of BST-1 expression on the three subsets of endothelial cells based on Ly6c and P-selectin expression, Ly6c$^+$ P-sel$^-$ (green), Ly6c$^+$ P-sel$^+$ (blue), and Ly6c$^-$ P-sel$^+$ TPEC (red).

(C) Representative gating of BST-1^{LO} and BST-1^{HI} populations of Ly6c$^-$ P-sel$^+$ TPEC

Data is taken from 3 separate experiments with n=7

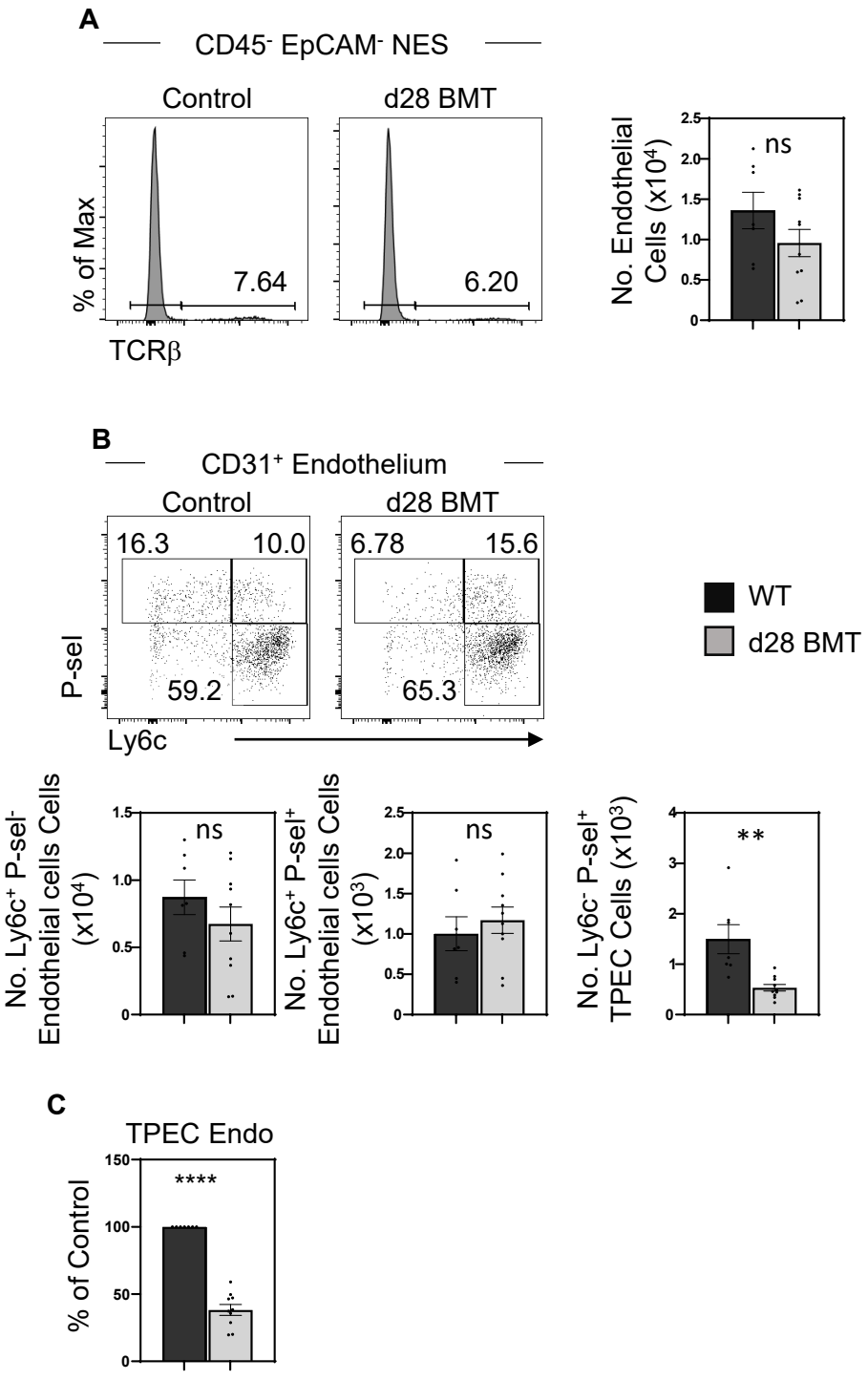
A
CD45- EpCAM- NES
Control
d28 BMT
% of Max
7.64
6.20
TCRβ
No. Endothelial Cells (x10^4)
ns
B
CD31+ Endothelium
Control
d28 BMT
16.3
10.0
59.2
6.78
15.6
65.3
P-sel
Ly6c
WT
d28 BMT
No. Ly6c+ P-sel- Endothelial cells Cells (x10^4)
ns
No. Ly6c+ P-sel+ Endothelial cells Cells (x10^3)
ns
No. Ly6c- P-sel+ TPEC Cells (x10^3)
**
C
TPEC Endo
% of Control
****

Figure 4.16. Specific Loss of TPEC in d28 BMT mice

Thymuses were harvested from WT mice 28 days following a lethal dose of irradiation and reconstitution with T-cell depleted WT bone marrow. Age matched WT mice were taken alongside as controls. The tissues were enzymatically digested, CD45 depleted, and stained for FACS analysis.

(A) Representative histogram plots to identify $CD31^+$ endothelial cells within non-epithelial stroma in WT control (left) and d28 BMT (right) mice. Graphical representation of numbers of $CD31^+$ endothelial cells in WT control (dark grey bar) and d28 BMT (light grey bar) mice.

(B) Representative FACS plots to identify subpopulations of endothelial cells based on Ly6c and P-sel expression, including $Ly6c^-$ $P\text{-}sel^+$ TPEC in WT control (left) and d28 BMT (right) mice. Graphical representation of numbers of $Ly6c^+$ $P\text{-}sel^-$ (left), $Ly6c^+$ $P\text{-}sel^+$ (middle), and $Ly6c^-$ $P\text{-}sel^+$ TPEC (right) in WT control (dark grey bar) and d28 BMT (light grey bar) mice.

(C) Graphical representation of the number of $Ly6c^-$ $P\text{-}sel^+$ TPEC as a percentage of age-matched WT control mice (dark grey bar) in d28 BMT mice (light grey bar).

Data is taken from 3 separate experiments with n=7 WT control and n=10 d28 BMT mice. Each data point represents an individual mouse, with bars plotting the mean and error bars representing the SEM. Statistical significance was determined using Independent Student's T-test, with (**) representing $P<0.01$, and (****) representing $P<0.0001$, and (ns) representing no significance.

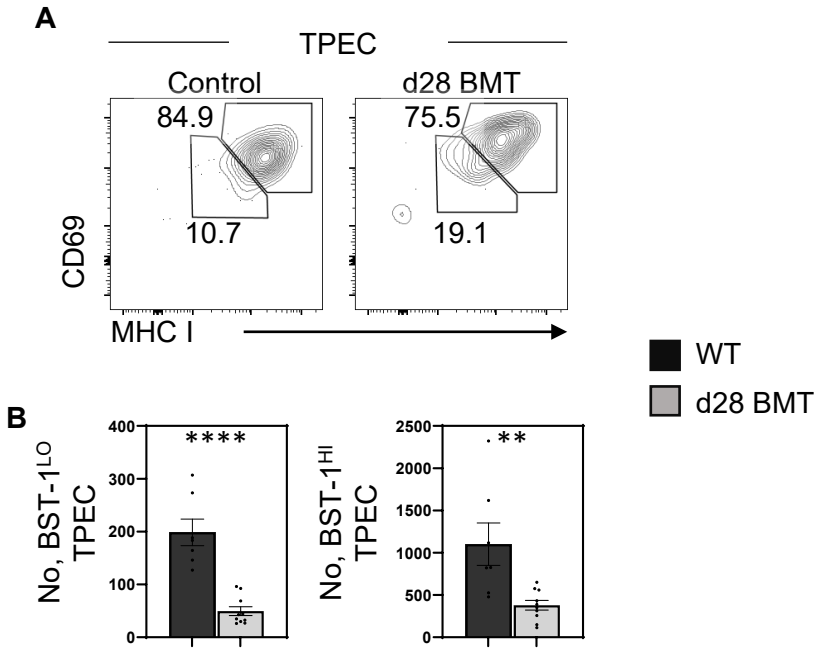
A
TPEC
Control
d28 BMT
84.9
10.7
75.5
19.1
CD69
MHC I
WT
d28 BMT
B
No, BST-1LO TPEC
No, BST-1HI TPEC
****
**
400
300
200
100
0
2500
2000
1500
1000
500
0

Figure 4.17. Both BST-1^{LO} and BST-1^{HI} TPEC Populations are Reduced at day 28 post-BMT

Thymuses were harvested from WT mice 28 days following a lethal dose of irradiation and reconstitution with T-cell depleted WT bone marrow. Age matched WT mice were taken alongside as controls. The tissues were enzymatically digested, CD45 depleted, and stained for FACS analysis.

(A) Representative FACS plots to identify BST-1^{LO} and BST-1^{HI} TPEC in WT control (left) and d28 BMT (right) mice.

(B) Graphical representation of numbers of BST-1^{LO} (left) and BST-1^{HI} (right) TPEC in WT control (dark grey bar) and d28 BMT (light grey bar) mice.

Data is taken from 3 separate experiments with n=7 WT control and n=10 d28 BMT mice. Each data point represents an individual mouse, with bars plotting the mean and error bars representing the SEM. Statistical significance was determined using Independent Student's T-test, with (**) representing P<0.01, and (****) representing P<0.0001.

4.3 DISCUSSION

Following BMT, recent studies have shown that mTEC fail to recover following damage from the ablative therapies involved in the procedure (261,262). It was subsequently shown that such a loss of mTEC results in medullary-specific thymic defects, with a reduction in both negative selection and Treg generation leading to signs of autoimmunity within the periphery (261). Given that these processes known to take place within the medulla were impacted by the lack of medullary recovery, we looked to investigate how other medullary processes such as post-selection maturation and thymic egress are affected in the BMT model. To assess this, we chose the d28 timepoint as the previous study has shown that whilst the mTEC compartment was still severely reduced at this point, the thymus cellularity and furthermore the DP, SP4 and SP8 populations had all recovered to comparable numbers to control mice (261). Using our definition of thymocyte populations, we we observe this same recovery in the DP, cSP4, and cSP8 populations, however there is a clear significant increase in both donor derived cSP populations on top of this recovery.

We assessed how post-selection maturation may be affected by the failure in medullary recovery at d28 post-BMT using the sequential SM-M1-M2 (228) maturational populations in conjunction with RagGFP expression (226), defined in both cSP4 and cSP8 in the last chapter. In doing this we found that both the cSP4 and cSP8 populations progress through these maturational populations, with all present and showing a progressive loss of RagGFP moving through the sequential populations. This would suggest that in order to mature within the thymus from their selection to the point of egress, cSP thymocytes do not require a complete mTEC compartment. That post-selection maturation occurs independently of interaction with mTEC has

previously been shown using other experimental models that inhibit these interactions. Firstly, grafting thymuses of Relb$^{-/-}$ mice, known to lack a thymus medulla due to a block in mTEC development (85,86), into WT hosts showed that thymocytes had similar expression of maturational markers CD69 and Qa-2 (207). CCR7$^{-/-}$ and CCR7-ligand deficient *plt/plt* mice show a failure of SP thymocytes to translocate to the medulla following their selection, therefore inhibiting interactions with mTEC (100,204). Despite this lack of mTEC-contact, mature thymocytes are still present in these mice to the same degree as control mice, shown using the expression of a number of maturational markers (100,204). The limited access to mTEC that is present in d28 BMT therefore does not limit the maturation of donor-derived cSP thymocytes owing to a lack of requirement for thymocyte-mTEC interactions in this process.

Whilst cSP4 and cSP8 both progress through the SM-M1-M2 populations, we do see clear signs of an accumulation in our d28 BMT mice. Both cSP4 and cSP8 show specific increases in the number of M2 cells, shown clearly using the gating strategy to include DP3 to analyse total-committed SP8. Furthermore, this followed through to the M2a/b/c populations, again with increases in both the cSP4 and cSP8 disproportionately affecting the most mature M2c population in d28 BMT mice. Such an increase specifically within the most mature cells hints at an egress defect following BMT causing this accumulation. Whilst the failure of recovery within the thymus medulla is clearly present following BMT, that this may be the cause of a failure in thymic egress is perhaps unlikely. The previously mentioned studies in both Relb$^{-/-}$ grafted thymuses and CCR7/CCR7-ligand deficient mice show no thymic accumulation or egress defect despite the lack of medulla to support this process (100,204,207). Furthermore, whilst LTβR KO mice show severe loss of mTEC and medullary

disorganisation alongside an accumulation of mature thymocytes (94), this was shown to not be attributed to the loss of mTEC, and rather to a loss in a specific population of endothelial cells within the thymus: TPEC (98). TPEC have been identified as specialised endothelial cells that are important in controlling the entry and egress of cells into and from the thymus (164,263). Specific loss of LTβR on endothelial cells resulted in reduced TPEC and accumulation of the most mature populations within the thymus (98,263) showing that a loss of this population leads to an egress defect. Investigating this population within our d28 BMT mice as a potential candidate for the accumulation within the thymus that we see showed a significant reduction in the numbers of TPEC within BMT mice, with no significant effect on any other endothelial population. Such radio-resistance of endothelial populations has previously been reported (264), suggesting that only this specialised thymic TPEC population is susceptible to irradiation and subsequently fails to recover following BMT. A specific loss of TPEC and subsequent thymic accumulation therefore mirrors what has previously been shown in studies identifying the role of TPEC in thymic egress (98,263), and therefore implicates a specific loss of these cells in d28 BMT mice and the accumulation seen within them.

Studies describing the thymic egress defects seen with a reduced TPEC population show intrathymic accumulations with a lack of access to the PVS's subsequently hindering egress (98,263). Although we show a significant loss of TPEC in d28 BMT mice, our pilot experiment isolating cells within the PVS suggested that there are in fact a higher proportion of newly generated donor cells found within the PVS of d28 BMT mice compared to age-matched controls. This would suggest that cells are able to gain access to the PVS as they undergo thymic egress, but the next step in egress,

entry into the blood vessel, is limited, thus causing the accumulation. Whilst previous work has suggested TPEC regulate PVS entry, both studies used endothelial cell specific LTβR deletion as a model for reduced TPEC and hence suggest that LTβR expression by TPEC controls this process (98,263). Whilst TPEC are reduced in d28 BMT mice, there is a small population that survives, with this population still likely to express LTβR, unlike those in the conditional LTβR KO studies. The LTβR still expressed by remaining TPEC could therefore be licencing entry to the PVS that is still seen following BMT. The fact that the accumulation in d28 BMT mice appears to occur in the PVS with a limited entry into the blood vessels may still be attributed to the loss in TPEC. Cells undergoing thymic egress, labelled in the PVS, are shown to associate closely to vessels containing TPEC (263). A reduction in these TPEC may therefore leave d28 BMT thymuses with less exit-points within the thymic vasculature, leaving cells to accumulate in the steps preceding this egress in the PVS and the thymus.

Interestingly, despite signs of an accumulation in the thymus and PVS, and a strong candidate for the cause of this in the loss of TPEC in d28 BMT mice, some of our data appears to contradict such an egress defect. Whilst we see a specific increase in the most mature donor derived populations of both cSP4 and cSP8 in BMT mice, levels of RagGFP are comparable to what is seen in age-matched control mice where we may expect to see lower levels indicative of an increased thymic dwell time. Similarly, when looking within the periphery of d28 BMT mice, whilst we see that total T-cells are reduced, both cSP4 and cSP8 RTE are no different to control mice where we would likely expect reduced RTE owing to a reduction in egress. In fact, it could be possible that such observations come from the timings involved in our model. The fact that peripheral T-cell numbers have not returned to that of a control mouse at d28 post-

BMT both in our own study and reported in previous work (261), suggests that the thymus has not been producing newly generated, donor-derived T-cells for enough time to match that of control mice. Similarly, the number of DP and SP thymocytes only returns to a level comparable with controls around d21 (261), suggesting at d28 'normal' thymopoiesis of these donor cells has only been occurring for around 7 days. It is therefore possible that the cells accumulating within the thymus have not been doing so long enough to show significant reductions in RagGFP as the accumulation is not as substantial as one that seen in adult mouse models, such as the conditional LTβR KO mice, that have undergone normal thymopoesis for 8-12 weeks to build up the observed accumulation. As such, it is also likely that all donor cells within the spleens of d28 BMT mice have recently left the thymus, as the thymus has only been producing cells for around 7 days. It is also likely that these cells undergo peripheral expansion in response to the lymphopenic periphery caused by the ablative therapy preceding transplantation, an observation seen within peripheral T-cells following BMT (255,257). As such, whilst there are some clear signs of accumulation following BMT, the d28 timepoint may be too early to detect all signs commonly associated with an egress defect in mice.

Together this data shows that a failure in mTEC recovery does not appear to directly affect the post -selection maturation and thymic egress of cSP thymocytes. Instead, we have identified the impact of BMT on another specialised stromal population, TPEC, with these cells being significantly reduced in d28 BMT mice despite bulk thymic endothelium being unaffected. Loss of these cells leads to a defect in thymic egress within BMT mice at d28 despite normal generation of cSP thymocytes. In conjunction with previous studies, this analysis outlines the importance of a full recovery of the

thymic microenvironments following BMT to ensure normal T-cell development and reestablishment of the peripheral T-cell pool.

CHAPTER 5: INVESTIGATION OF THE NON-CONVENTIONAL EOMES^{+} SP8 POPULATION WITHIN THE THYMUS

5.1 INTRODUCTION

Following their positive-selection from DP thymocytes, SP thymocytes upregulate expression of CCR7 and translocate to the thymus medulla, guided by CCL21-expression by mTEC (100,204). In the medulla they continue their development and maturation to become functional T-cells ready to enter the periphery, interacting with medullary populations such as mTEC and DC. This development includes a number of key processes, including the induction of negative selection to remove self-reactive thymocytes, post-selection maturation as cells gain functional maturity, and ordered thymic egress where the most mature cells are preferentially selected to leave the thymus into the periphery (180,219,242). Another crucial process in T-cell development is supported by the thymus medulla, the lineage divergence of non-conventional thymocyte populations. Two key examples of this include $CD4^+$ nTreg, and innate-like CD1d-restricted iNKT. nTreg represent a non-conventional lineage within SP4 thymocytes that act to maintain immune tolerance by supressing peripheral responses (34), whilst iNKT are a non-conventional thymocyte lineage with innate-like properties, capable of rapid cytokine production following stimulation and selected within the cortex through CD1d-presented peptides via their invariant TCR (265,266) The requirement for the medulla in the emergence of both of these lineages is outlined in $Relb^{-/-}$ mice that lack mTEC, with both iNKT (91) and nTreg (207) being significantly reduced as a result. Furthermore, different subsets of mTEC control the differentiation of iNKT precursor cells into the different iNKT1, iNKT2, and iNKT17 subsets (104).

Alongside these cells, another non-conventional T-cell population exists with the phenotype of memory T-cells. Whilst conventional memory T-cells emerge and persist within the periphery following naïve T-cell recognition and response to antigen, a

population of memory-phenotype cells have also been shown to circulate in the periphery without foreign antigen recognition via their TCR. Identified with a memory phenotype, expressing surface markers CD44 and CD122, and the transcription factor Eomes, these cells can emerge in different ways without the requirement of antigen-stimulation, and hence are often referred to as 'innate memory' cells (51). One instance in which these innate-memory T-cells emerge is in response to lymphopenia, whereby naïve T-cells will proliferate to fill the space available within the peripheral T-cell compartment. Importantly, alongside expansion, these naïve cells also differentiate to develop the memory-like phenotype described (267–269). Such expansion and differentiation can be triggered as a result of ablative therapies to deplete the peripheral T-cell compartment, but also through the comparatively 'empty' periphery of neonates before T-cell production by the thymus has reached levels seen within the adult, providing an evidence of these lymphopenia-derived innate-memory T-cells in the steady-state (270,271). As well as in response to lymphopenia, innate memory cells can also be induced by IL-4. Increased availability of IL-4, namely through production by $PZLF^+$ iNKT2, is shown to cause an increase in the size of the $CD8^+$ innate memory T-cell population (272–274). A number of gene-KO mice display dramatically elevated levels of $Eomes^+$ innate memory CD8 T-cells, with the common feature of these mice being an increase in either $PZLF^+$ iNKT2, or IL-4 availability by other means, reviewed in greater detail by Jameson*. et al.* (51). This link is also clearly seen in different WT mouse strains. Balb/c mice have a much larger population of IL-4-producing $PZLF^+$ iNKT2 than C57/B6 mice, and as such have a much larger $Eomes^+$ innate memory CD8 population. Similarly, in CD1d and IL-4Rα KO mice which lack iNKT and the ability to respond to IL-4 respectively, the $Eomes^+$ innate-memory population SP8 is

significantly reduced (272–274). Whilst lymphopenia-induced innate memory cells appear within the periphery, IL-4-induced innate memory T-cells largely emerge within the thymus, likely due to the increased availability of iNKT2 within the thymuses of both Balb/c mice and KO mice that display increased innate memory CD8 populations (51,274).

The role of the thymus in the development and production of Eomes^{+} innate-memory SP8 beyond the site of large numbers of iNKT2 has more recently been studied further. Work by Miller *et al.* showed that specific TCRs that recognise self-antigen with moderate affinity give rise to innate-memory CD8 T-cells in the periphery (52), implicating thymic selection in generation of these cells. Furthermore, whilst complete establishment of the innate memory phenotype through expression of CD44 and CD122 was not completed until cells had entered the periphery, thymocytes yet to undergo egress expressing TCRs of innate-memory cells had high levels of Eomes expression, with a portion of these being newly generated RagGFP^{+} cells (52).

Eomes innate memory CD8 T-cells therefore represent a non-conventional T-cell population that are generated within the thymus, similar to the other non-conventional lineages previously described. Whilst both TCR-specificity and IL-4 availability from PZLF^{+} iNKT2 play a role in the development of innate-memory CD8 T-cells, how the thymus controls the development of these cells via both requirements remains unclear. We've therefore looked to further understand the role of the thymus in the development of innate memory CD8 T-cells.

5.2 RESULTS

5.2.1 Defining Eomes$^+$ SP8 within the Thymus

To help define the development and role of innate memory SP8 within the thymus, we first looked to define them using flow cytometric analysis, slightly adapting this from our definition of thymocyte populations previously used in Chapter 3. Given the recent report that suggests innate-memory SP8 express Eomes within the thymus before their full maturation to express CD44 and CD122 in the periphery, we defined thymic innate-memory SP8 as CD4$^-$CD8$^+$ TCRβ^+ Eomes$^+$ and have looked to compare them with CD4$^-$CD8$^+$ TCRβ^+ Eomes$^-$ SP8, represented in the large part by the conventional SP8 population. Importantly, whilst this gating strategy differs from that previously used, it still separates the three key SP8 populations previously identified; TCRβ^- iSP, Eomes$^+$ SP8, and TCRβ^+ Eomes$^-$ SP8 (Figure 5.1A). In the WT RagGFP mice on a C57/B6 background used to define this population, Eomes$^+$ SP8 represent a relatively small population within the SP8 compartment, around 1.9% of total SP8, and around 2.8x10^4 cells compared to the 1.3x10^6 TCRβ^+ Eomes$^-$ population (Figure 5.1A). Utilising the WT RagGFP mouse model, we then looked to define the RagGFP status of our Eomes$^+$ SP8 within the thymus compared to TCRβ^+ Eomes$^-$ SP8. In doing this it is clear that a larger proportion of the Eomes$^+$ SP8 within the thymus are comprised of RagGFP$^-$ cells compared to TCRβ^+ Eomes$^-$ SP8, however the majority of Eomes$^+$ SP8 are RagGFP$^+$ cells, indicating they are newly generated cells within the thymus (Figure 5.1B). This larger RagGFP$^-$ population likely represents either recirculating cells from the periphery, or resident cells retained within the thymus, however the extent to which each of these contribute to the RagGFP$^-$ population is unclear. Due to the complex

nature of RagGFP$^-$ populations within the thymus, we looked to further define the RagGFP$^+$ newly generated population using the maturational populations used in previous chapters. Using expression of CD69 and MHC I, we separated RagGFP$^+$ Eomes$^+$ SP8 into M1 and M2 maturational population, using gates previously applied to RagGFP$^+$ TCRβ^+ Eomes$^-$ SP8 to determine the maturational status of Eomes$^+$ SP8 generated within the thymus. Whilst Eomes$^+$ SP8 have clear M1 and M2 populations as seen in TCRβ^+ Eomes$^-$ SP8, Eomes$^+$ SP8 have a higher proportion of more mature M2 cells (Figure 5.2A). Furthermore, comparing levels of RagGFP between TCRβ^+ Eomes$^-$ SP8 and Eomes$^+$ SP8, Eomes$^+$ SP8 showed significantly lower RagGFP expression at both the M1 and M2 stages, indicating an older and more mature population than TCRβ^+ Eomes$^-$ SP8 (Figure 5.2B). Combining the higher proportion of M2 with the lower level of RagGFP seen at both the M1 and M2 stages, this may suggest that Eomes$^+$ SP8 diverge within the SP8 lineage late within the M1 stage of development, before continuing their maturation through the late M1 and M2 stages within the thymus.

An interesting characteristic of Eomes$^+$ SP8 is the dramatic variation in the size of the population between different mouse strains. The clearest example of this is seen within Balb/c WT mice compared with C57/B6 WT mice. An increased availability of IL-4 from the larger iNKT2 population in Balb/c background mice has been shown to be the cause of this increased Eomes$^+$ population, dictating the size of the population (273,274). From our own comparison of C57/B6 and Balb/c strains, the significant increase in both the proportion and the number of Eomes$^+$ SP8 is clear, with the majority of SP8 in a WT Balb/c mouse expressing Eomes (Figure 5.3A,C). Interestingly, whilst there are less TCRβ^+ Eomes$^-$ SP8 in a Balb/c mouse compared to

a B6, this loss is not relative to the significant increase seen in the Eomes$^+$ SP8 (Figure 5.3B,C). The 48-fold larger Eomes$^+$ SP8 populations compared to the minor 1.3-fold smaller TCRβ^+ Eomes$^-$ population would suggest that the expanded Eomes$^+$ SP8 population is not solely a result of increased divergence towards this non-conventional lineage over conventional SP8, and instead largely supplements that cSP8 population that already exists.

If not an increased divergence of SP8 from a more conventional route of development, the large Eomes$^+$ SP8 population within Balb/c mice compared to C57/B6 may be attributed to an increase in proliferation of the population within Balb/c. In order to measure levels of proliferation we used intracellular staining of Ki67, a marker commonly used to identify proliferating populations of cells entering the growth stages of the cell cycle (275). Analysing the proportion of Ki67$^+$ Eomes$^+$ SP8 in Balb/c mice showed that the majority of the population are in fact Ki67$^-$, and therefore likely not proliferating. Furthermore, the proportion of Ki67$^+$ cells in C57/B6 mice was significantly higher than a Balb/c mouse (Figure 5.4). This would suggest that the significantly larger Eomes$^+$ SP8 population seen within Balb/c compared to C57/B6 mice is not a result of increased proliferation, and actually that Eomes$^+$ SP8 in C57/B6 mice represent a more proliferative population than in Balb/c, despite their lower numbers.

With the size difference of the Eomes$^+$ SP8 population between different WT mouse strains not being dictated by proliferation, we next looked to determine whether this expanded population consisted of newly generated Eomes$^+$ SP8, or a recirculated or resident population within the thymus given that both were identifiable in WT RagGFP C57/B6 mice (Figure 5.1B). In order to assess this, we required the WT RagGFP mice

on a C57/B6 background to be crossed to WT Balb/c mice to utilise the RagGFP transgene in this strain. Whilst the goal of this process was to assess RagGFP expression within WT Balb/c mice, it provided us with an interesting opportunity to analyse the effect of the C57/B6 x Balb/c cross on the size of the Eomes^{+} SP8 population through each generation of the crossbreeding. Moving through the generations there was a clear increased in the proportion of Eomes^{+} SP8, shown with example plots from F1, F3, and F5 mice (Figure 5.5A,B). Importantly, when comparing the proportion of Eomes^{+} SP8 across these generations with that of the Balb/c WT mouse, only at F5 was there no significant difference seen. This was true both when comparing base proportions of Eomes^{+} SP8, and when comparing each generation as a percentage of the control Balb/c mice, where WT Balb/c represent 100% (Figure 5.5B). We therefore identified WT RagGFP C57/B6 x Balb/c cross F5 generation mice as the earliest generation with no significant difference to WT Balb/c mice, and so decided upon this as the point at which to assess the RagGFP expression by Eomes^{+} SP8 in a Balb/c background. Whilst some variation in the proportions of Eomes^{+} SP8 was still present within the F5 mice, it was clear that at this generation the mice would represent a WT model where a large proportion of SP8 were Eomes^{+} cells. Looking within Eomes^{+} SP8 in the Balb RagGFP F5 mice, it is clear that whilst there are both GFP^{+} and GFP^{-} cells, the vast majority, around 82%, of Eomes^{+} SP8 are RagGFP^{-} (Figure 3.5D). This would suggest that the increased Eomes^{+} SP8 that is seen in WT Balb/c mice is not through an increase in the generation of new thymocytes. Instead, the fact that the majority of the expanded Eomes^{+} SP8 population in WT RagGFP Balb/c F5 mice were RagGFP^{-} would imply that there is an increase in recirculated Eomes^{+} SP8 from the periphery, or an increased retention of Eomes^{+} SP8 that are

generated within the thymus, both of which would represent RagGFP^{-} thymic populations.

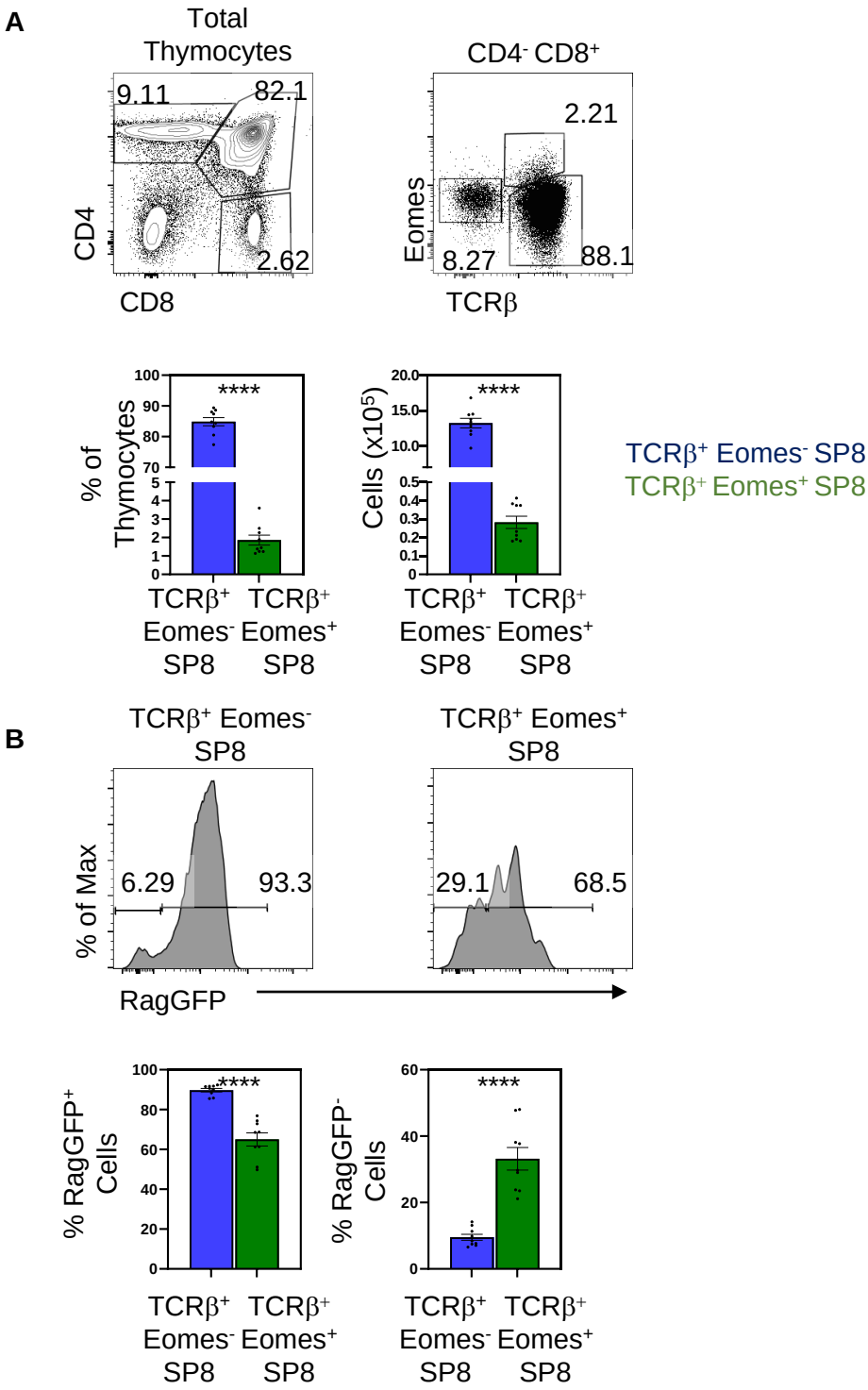
A
Total Thymocytes
9.11
82.1
2.62
CD4
CD8
CD4- CD8+
2.21
8.27
88.1
Eomes
TCRβ
% of Thymocytes
Cells (x10^5)
****
TCRβ+ Eomes- SP8
TCRβ+ Eomes+ SP8
B
TCRβ+ Eomes- SP8
TCRβ+ Eomes+ SP8
% of Max
6.29
93.3
29.1
68.5
RagGFP
% RagGFP+ Cells
% RagGFP- Cells

Figure 5.1. Defining Eomes$^+$ SP8 in WT RagGFP Mice

Thymuses were harvested from WT RagGFP mice and mechanically disaggregated for FACS analysis of thymocyte subpopulations.

(A) Representative gating strategy to identify SP8 subpopulations using expression of TCRβ and Eomes, with graphs representing summaries of percentages and numbers of TCRβ$^+$ Eomes$^-$ SP8 (blue) and TCRβ$^+$ Eomes$^+$ SP8 (green).

(B) Representative histograms of RagGFP expression and graphical representation of percentages of RagGFP$^+$ and RagGFP$^-$ cells in TCRβ$^+$ Eomes$^-$ SP8 (blue) and TCRβ$^+$ Eomes$^+$ SP8 (green).

Data is taken from 4 separate experiments with n=9. Each data point represents an individual mouse, with bars plotting the mean and error bars representing the SEM. Statistical significance was determined using Independent Student's T-test, with (****) representing $P<0.0001$.

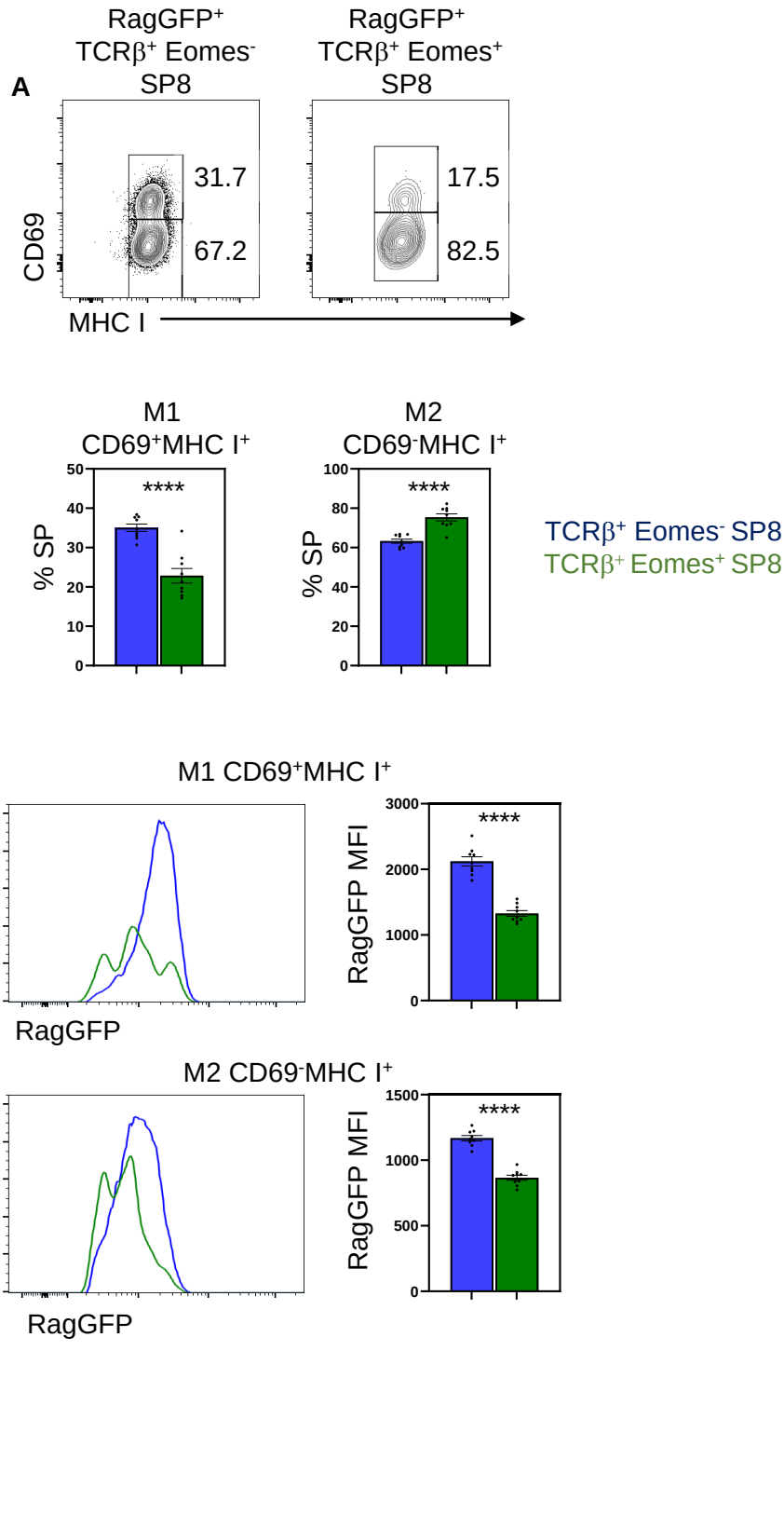
A
RagGFP+ TCRβ+ Eomes- SP8
RagGFP+ TCRβ+ Eomes+ SP8
31.7
67.2
17.5
82.5
CD69
MHC I
M1 CD69+MHC I+
M2 CD69-MHC I+
% SP
****
TCRβ+ Eomes- SP8
TCRβ+ Eomes+ SP8
B
M1 CD69+MHC I+
% of Max
RagGFP
RagGFP MFI
M2 CD69-MHC I+

Figure 5.2. Eomes$^+$ SP8 Represent more Mature Cells than Eomes$^-$ SP8

Thymuses were harvested from WT RagGFP mice and mechanically disaggregated for FACS analysis of thymocyte subpopulations.

(A) Representative FACS plots identifying CD69$^+$ MHC I$^+$ (M1) and CD69$^-$ MHC I$^+$ (M2) in RagGFP$^+$ TCRβ^+ Eomes$^-$ SP8 (left) and RagGFP$^+$ TCRβ^+ Eomes$^+$ SP8 (right). Graphs represent comparison of percentages of M1 (left) and M2 (right) populations between RagGFP$^+$ TCRβ^+ Eomes$^-$ SP8 (blue) and RagGFP$^+$ TCRβ^+ Eomes$^+$ SP8 (green).

(B) Representative histograms comparing expression of RagGFP by M1 cells (top) and M2 (bottom) from RagGFP$^+$ TCRβ^+ Eomes$^-$ SP8 (blue) and RagGFP$^+$ TCRβ^+ Eomes$^+$ SP8 (green).

Data is taken from 4 separate experiments with n=9. Each data point represents an individual mouse, with bars plotting the mean and error bars representing the SEM. Statistical significance was determined using Independent Student's T-test, with (****) representing P<0.0001.

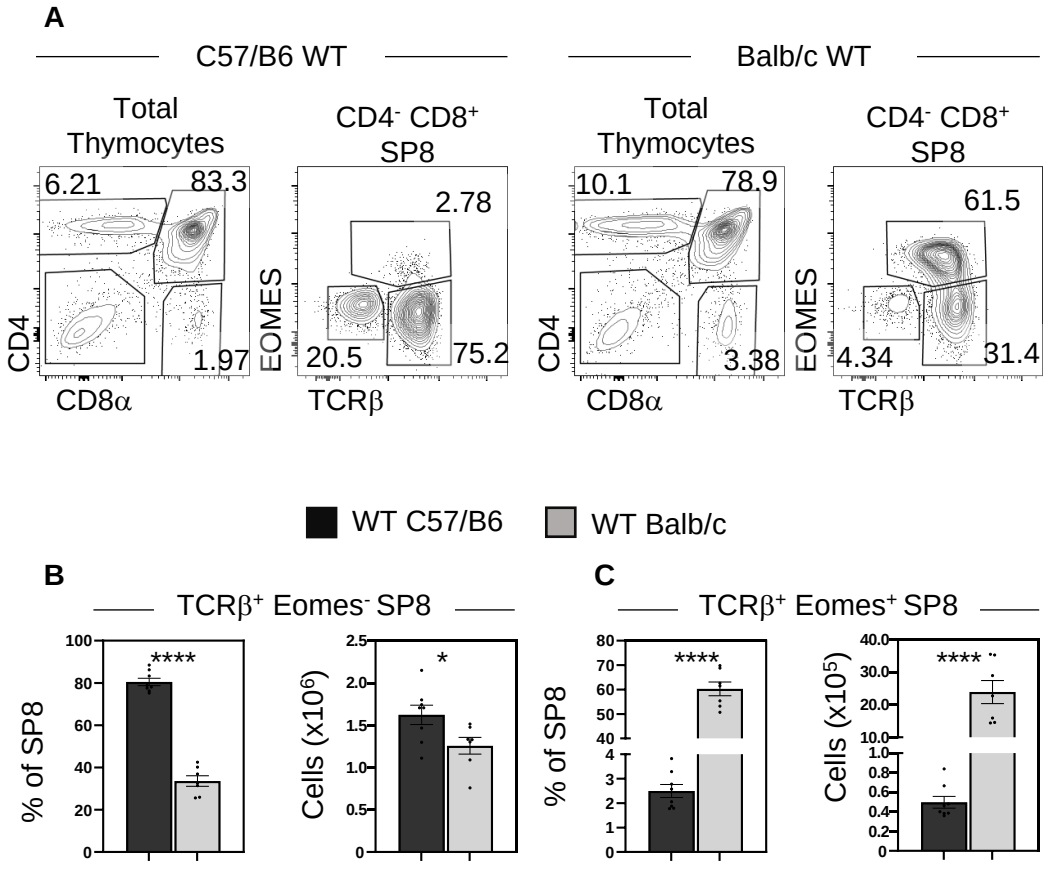
A
C57/B6 WT
Balb/c WT
Total Thymocytes
CD4- CD8+ SP8
6.21
83.3
1.97
2.78
20.5
75.2
10.1
78.9
3.38
61.5
4.34
31.4
CD4
CD8α
EOMES
TCRβ
WT C57/B6
WT Balb/c
B
TCRβ+ Eomes- SP8
C
TCRβ+ Eomes+ SP8
% of SP8
Cells (x10^6)
Cells (x10^5)
****
*

Figure 5.3. WT Balb/c Mice have a Significantly Expanded Eomes^{+} SP8 Population

Thymuses were harvested from WT C57/B6 and Balb/c mice and mechanically disaggregated for FACS analysis of thymocyte subpopulations.

(A) Representative FACS plots identifying SP8 subpopulations in WT C57/B6 (left) and WT Balb/c (right) mice.

(B) Comparison of percentages (left) and numbers (right) of TCRβ^{+} Eomes^{-} SP8 between WT C57/B6 (dark grey) and WT Balb/c (light grey) mice.

(C) Comparison of percentages (left) and numbers (right) of TCRβ^{+} Eomes^{+} SP8 between WT C57/B6 (dark grey) and WT Balb/c (light grey) mice.

Data is taken from 3 separate experiments with n=8 C57/B6 and n=7 Balb/c mice. Each data point represents an individual mouse, with bars plotting the mean and error bars representing the SEM. Statistical significance was determined using Independent Student's T-test, with (*) representing $P<0.05$, and (****) representing $P<0.0001$.

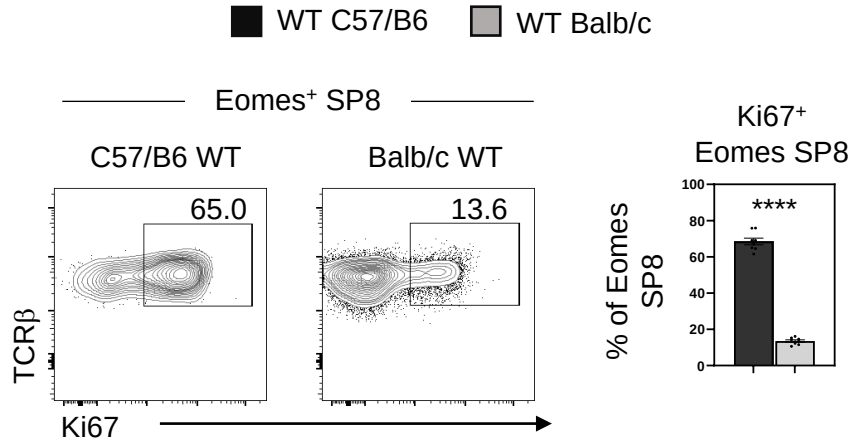
WT C57/B6
WT Balb/c
Eomes+ SP8
C57/B6 WT
Balb/c WT
65.0
13.6
TCRβ
Ki67
Ki67+
Eomes SP8
% of Eomes
SP8
****
100
80
60
40
20
0

Figure 5.4. Eomes$^+$ SP8 in Balb/c Mice are less Proliferative than in C57/B6 Mice

Thymuses were harvested from WT C57/B6 and Balb/c mice and mechanically disaggregated for FACS analysis of thymocyte subpopulations.

Representative FACS plots of Ki67 expression in TCRβ^+ Eomes$^+$ SP8 from WT C57/B6 (left) and WT Balb/c (right) mice, with graphical representation of percentages of Ki67$^+$ TCRβ^+ Eomes$^+$ SP8.

Data is taken from 3 separate experiments with n=8 C57/B6 and Balb/c mice. Each data point represents an individual mouse, with bars plotting the mean and error bars representing the SEM. Statistical significance was determined using Independent Student's T-test, with (****) representing P<0.0001.

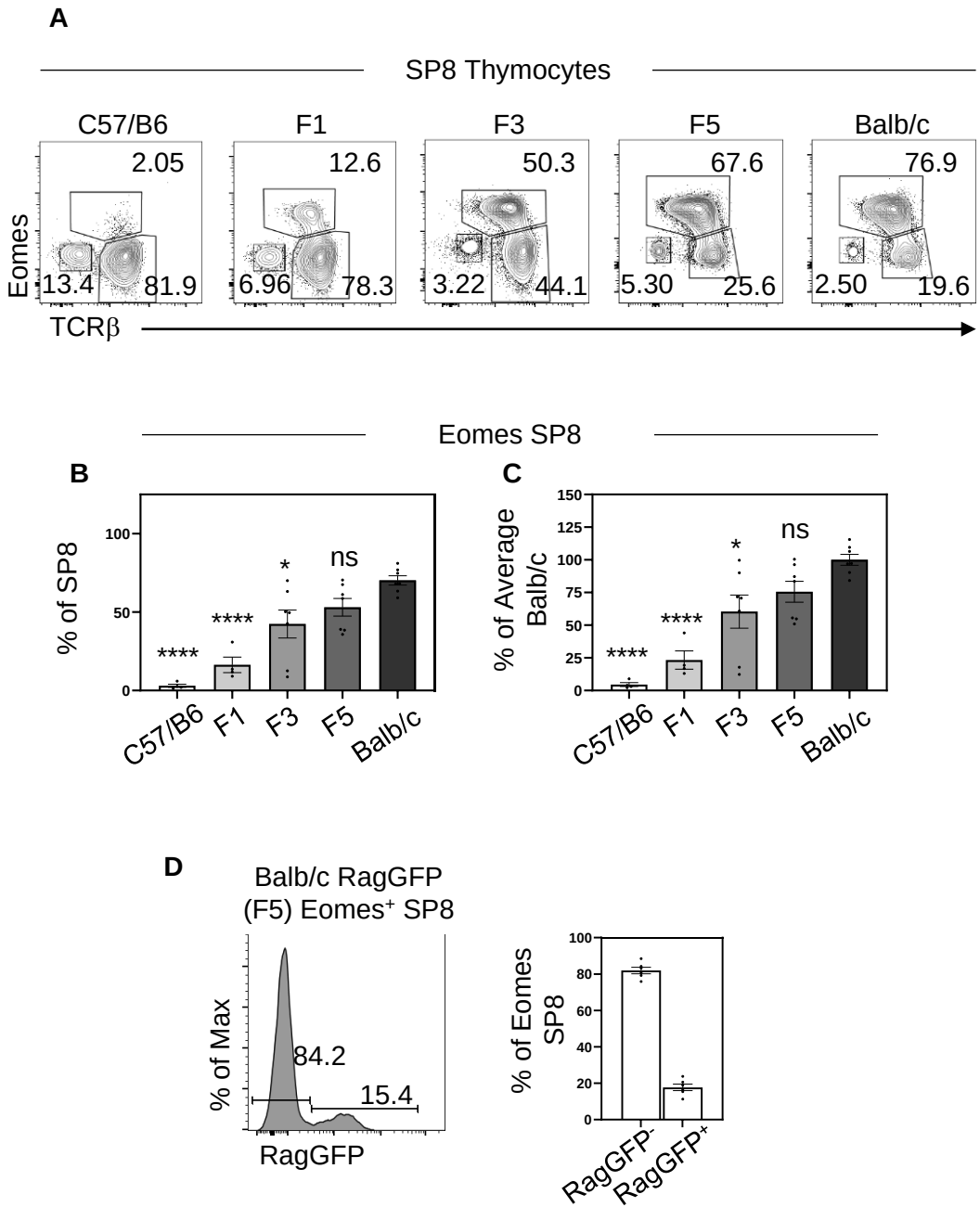
A
SP8 Thymocytes
C57/B6
F1
F3
F5
Balb/c
2.05
12.6
50.3
67.6
76.9
Eomes
13.4
81.9
6.96
78.3
3.22
44.1
5.30
25.6
2.50
19.6
TCRβ
Eomes SP8
B
% of SP8
100
50
0
****
****
*
ns
C57/B6
F1
F3
F5
Balb/c
C
% of Average Balb/c
150
125
100
75
50
25
0
****
****
*
ns
C57/B6
F1
F3
F5
Balb/c
D
Balb/c RagGFP
(F5) Eomes+ SP8
% of Max
84.2
15.4
RagGFP
% of Eomes SP8
100
80
60
40
20
0
RagGFP-
RagGFP+

Figure 5.5. Size of the Eomes$^+$ SP8 Population Increases through Generations of C57/B6 x Balb/c Crossbreeding

Thymuses were harvested from WT C57/B6, Balb/c, and C57/B6 x Balb/c mice and mechanically disaggregated for FACS analysis of thymocyte subpopulations.

(A) Representative FACS plots of SP8 subpopulations in C57/B6 (outer left), Balb/c (outer right), and C57/B6 x Balb/c F1 (centre left), F3 (centre), and F5 (centre right) generation mice.

(B) Graphical representation of percentages of TCRβ^+ Eomes$^+$ SP8 in C57/B6 (outer left), Balb/c (outer right), and C57/B6 x Balb/c F1 (centre left), F3 (centre), and F5 (centre right) generation mice.

(C) Graphical representation of percentages of TCRβ^+ Eomes$^+$ SP8 relative to control WT Balb/c mice in C57/B6 (outer left), Balb/c (outer right), and C57/B6 x Balb/c F1 (centre left), F3 (centre), and F5 (centre right) generation mice.

(D) Representative histogram plot of RagGFP expression in TCRβ^+ Eomes$^+$ SP8 from Balb/c RagGFP F5 mice. Graphical representation of percentages RagGFP$^+$ and RagGFP$^-$ TCRβ^+ Eomes$^+$ SP8 in Balb/c RagGFP F5 mice

Data is taken from 5 separate experiments with n=5-7 mice in C57/B6 x Balb/c crosses, and 1 experiment with n=6 in Balb/c RagGFP F5 mice. Each data point represents an individual mouse, with bars plotting the mean and error bars representing the SEM. Ordinary One-way ANOVA with Tukey's multiple comparisons, with (*) representing $P<0.05$, (****) representing $P<0.0001$, and (ns) representing no significance as compared to WT Balb/c mice as a control.

5.2.2 The Requirement for the Thymic Medulla by Eomes$^+$ SP8

Our data would suggest that the varying size of the Eomes$^+$ SP8 population looks to not be determined by increased proliferation, nor from increased production of newly generated cells in the WT Balb/c model. We therefore looked to further investigate the factors that may control Eomes$^+$ SP8 within the thymus with a view to further understanding the dynamics of this non-conventional thymic population. To do this we have looked to the thymus medulla, as Eomes$^+$ SP8 are reported to be a medullary-dependant population. Firstly, recent work is in alignment with our characterisation of Eomes$^+$ SP8 being largely of M2 phenotype (52), with M2 cells known to be a medullary thymocyte population (228). Furthermore, as previously mentioned the size of the thymic Eomes$^+$ SP8 population is directly controlled by the availability of IL-4 within the thymus, largely provided by iNKT2, (272–274). Thymic iNKT are another population of cells that require the thymus medulla for their development, whilst also being resident within the medulla (91,276), therefore providing another medullary requirement for Eomes$^+$ SP8 via iNKT2. We looked to confirm this direct relationship between medullary iNKT provision of IL-4 and Eomes$^+$ SP8 using multiple mouse models on a Balb/c background. As expected, IL-4Rα KO mice that lack the ability to respond to IL-4 have a dramatically reduced Eomes$^+$ SP8 population (Figure 5.6A). Importantly, whilst the Eomes$^+$ SP8 population showed a significant 135-fold decrease in numbers, the TCRβ^+ Eomes$^-$ SP8 popuation was not significantly changed (Figure 5.6B), exemplifying the specific role that IL-4 availability plays in controlling the size of the Eomes$^+$ SP8 population in the thymus. We next looked in CD1d KO mice known to have a significant reduction in iNKT (277). In keeping with the key role of iNKT in the provision of IL-4 for Eomes$^+$ SP8, CD1d KO mice mirrored IL-4Rα KO mice, showing

similar proportions and numbers of Eomes$^+$ SP8 that were significantly reduced compared to control mice, again with no effect on the TCRβ^+ Eomes$^-$ SP8 population (Figure 3.6C,D). Whilst we had previously determined that the increased size of the Eomes$^+$ SP8 population in WT Balb/c compared to C57/B6 mice was not due to an increase in proliferation in the former, this does not necessarily rule out a role for proliferation in IL-4's control of the Eomes$^+$ SP8. We therefore looked to determine whether the loss of Eomes$^+$ SP8 in the IL-4Rα KO and CD1d KO mice may be caused by a decrease in proliferation resulting from a lack of IL-4-provision. We again used Ki67 staining in both IL-4Rα KO and CD1d KO mice to determine the level of expression within the Eomes$^+$ SP8 population. Interestingly, the proportion of Ki67$^+$ Eomes$^+$ SP8 remained the same between WT Balb/c mice and both KO models (Figure 5.7A,B), suggesting that the loss of IL-4-provision within these mice does not result in reduced proliferation of the Eomes$^+$ SP8 population.

The loss of Eomes$^+$ SP8 in Balb/c IL-4Rα KO and CD1d KO models clearly show the control of iNKT-supplied IL-4 has on the size of the Eomes$^+$ SP8 population within the thymus. As these iNKT represent a medullary population, we next looked to see how altered access to the medulla, and therefore medullary populations including iNKT and mTEC, affects the development of Eomes$^+$ SP8. To do this, we analysed the Eomes$^+$ SP8 population in CCR7 KO RagGFP mice. CCR7 is crucial for the translocation of positively selected thymocytes into the medulla via CCL21 expression by mTEC, with mice deficient for either CCR7 or it's ligands showing accumulation of SP thymocytes in cortical regions (100,204). Surprisingly, we observed a significant increase in the size of the Eomes$^+$ SP8 population within CCR7 KO mice compared to WT C57/B6 mice (as CCR7 KO mice come from a C57/B6 background) (Figure 5.8A). Whilst

TCRβ$^+$ Eomes$^-$ SP8 were unaffected in CCR7 KO mice, the Eomes$^+$ SP8 populaiton showed a significant 15-fold increase in the numbers of cells (Figure 5.8B). Utilising the RagGFP expression in both WT and CCR7 KO mice we next looked to determine whether this increase was due to new production of Eomes$^+$ SP8, or like in the Balb/c model a result of an increase in RagGFP$^-$ cells. Interestingly we found the latter to be true, with a significant and specific increase in the number of RagGFP$^-$ Eomes$^+$ SP8 in CCR7 KO mice, with no significant change in RagGFP$^+$ numbers (Figure 5.8C). This would suggest that when SP thymocytes are denied access to the medulla there is an increase in either recirculated or long-term resident Eomes$^+$ SP8 within the thymus. Given that such a dramatic effect on the Eomes$^+$ SP8 population was observed when access to the medulla is impaired in CCR7 KO mice, we looked to see how an increased availability of mTEC may affect this population by using OPG KO mice. These mice lack OPG, a soluble decoy receptor of RANK (89), therefore resulting in an expanded mTEC population within the thymus, shown by a roughly 3-fold increase in all mTEC populations (93). Interestingly, within OPG RagGFP mice, we observe a similar phenotype to that seen in the CCR7 KO mice, in an increase in the proportion of Eomes$^+$ SP8 (Figure 5.9A). This was specific to this population, with no increase in the number of TCRβ$^+$ Eomes$^-$ SP8, but a significant increase the numbers of Eomes$^+$ SP8 (Figure 5.9B). Again, by separating the Eomes$^+$ SP8 population based on RagGFP expression we see a similar phenotype in the OPG KO mice as seen in the CCR7 KO mice, with a specific increase to the numbers of RagGFP$^-$ cells, and no significant difference within the RagGFP$^+$ population (Figure 5.9C). This data therefore shows that despite CCR7 KO mice having limited access to mTEC, and OPG KO mice

having increased availability of mTEC, the two have the same effect on Eomes^{+} SP8, showing dramatic increases in the size of the RagGFP^{-} population of Eomes^{+} SP8.

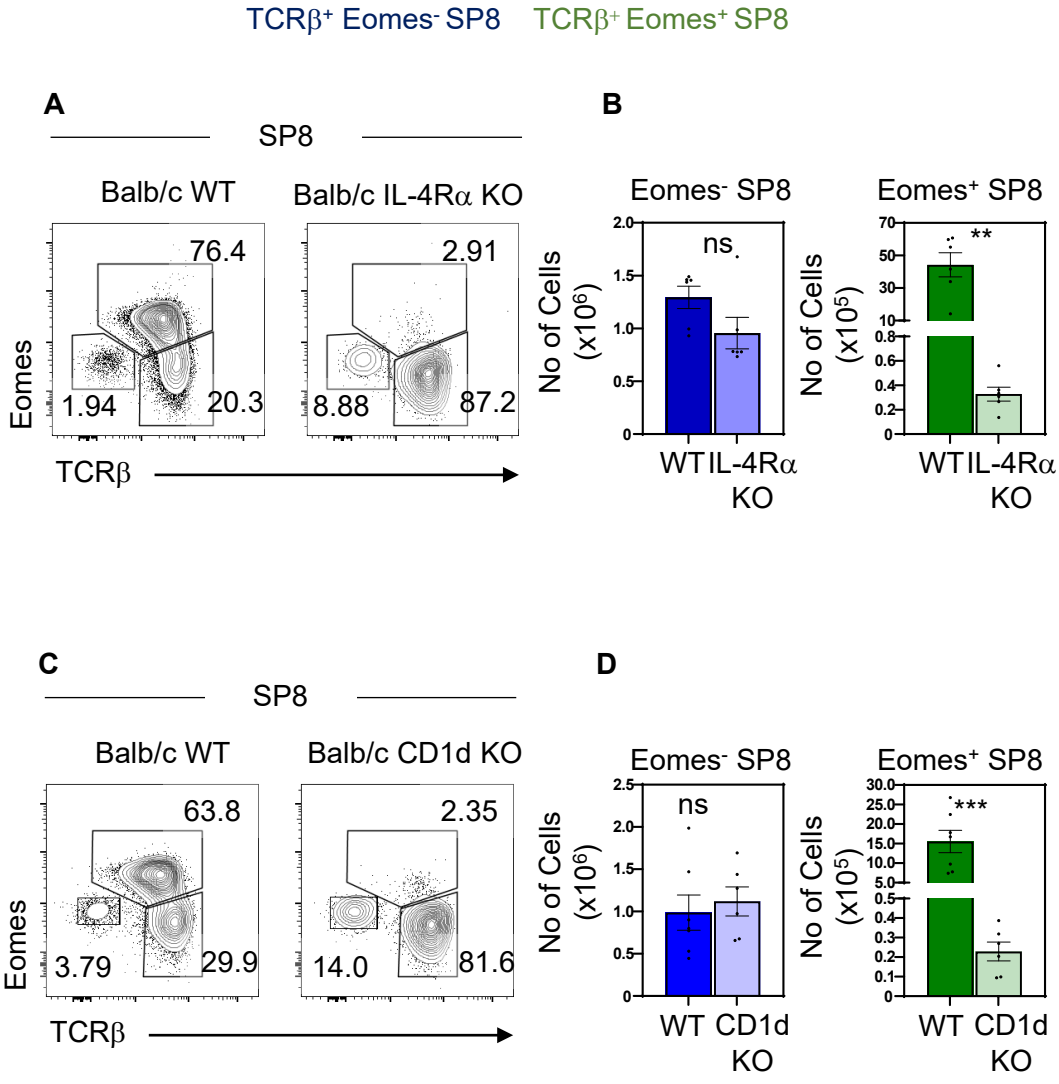
TCRβ+ Eomes- SP8
TCRβ+ Eomes+ SP8
A
SP8
Balb/c WT
Balb/c IL-4Rα KO
76.4
1.94
20.3
2.91
8.88
87.2
Eomes
TCRβ
B
Eomes- SP8
Eomes+ SP8
No of Cells (x10^6)
No of Cells (x10^5)
ns.
**
WT
IL-4Rα KO
C
SP8
Balb/c WT
Balb/c CD1d KO
63.8
3.79
29.9
2.35
14.0
81.6
Eomes
TCRβ
D
Eomes- SP8
Eomes+ SP8
No of Cells (x10^6)
No of Cells (x10^5)
ns
***
WT
CD1d KO

Figure 5.6. IL-4Rα KO and CD1d KO mice have a Dramatically Reduced Eomes$^+$ SP8 Population

Thymuses were harvested from WT Balb/c, IL-4Rα KO Balb/c, and CD1d KO Balb/c mice and mechanically disaggregated for FACS analysis of thymocyte subpopulations.

(A) Representative FACS plots identifying SP8 subpopulations in WT Balb/c (left) and IL-4Rα KO Balb/c (right) mice.

(B) Graphical representation of TCRβ$^+$ Eomes$^-$ SP8 (left) and TCRβ$^+$ Eomes$^+$ SP8 (right), in WT Balb/c (dark bars) and IL-4Rα KO Balb/c (light bars) mice.

(C) Representative FACS plots identifying SP8 subpopulations in WT Balb/c (left) and CD1d KO Balb/c (right) mice.

(D) Graphical representation of TCRβ$^+$ Eomes$^-$ SP8 (left) and TCRβ$^+$ Eomes$^+$ SP8 (right), in WT Balb/c (dark bars) and CD1d KO Balb/c (light bars) mice.

Data is taken from 3 separate experiments with n=6 mice (A,B) and 3 separate experiments with n=7 mice (C,D). Each data point represents an individual mouse, with bars plotting the mean and error bars representing the SEM. Statistical significance was determined using Independent Student's T-test, with (**) representing $P<0.01$, (***) representing $P<0.001$, and (ns) representing no significance.

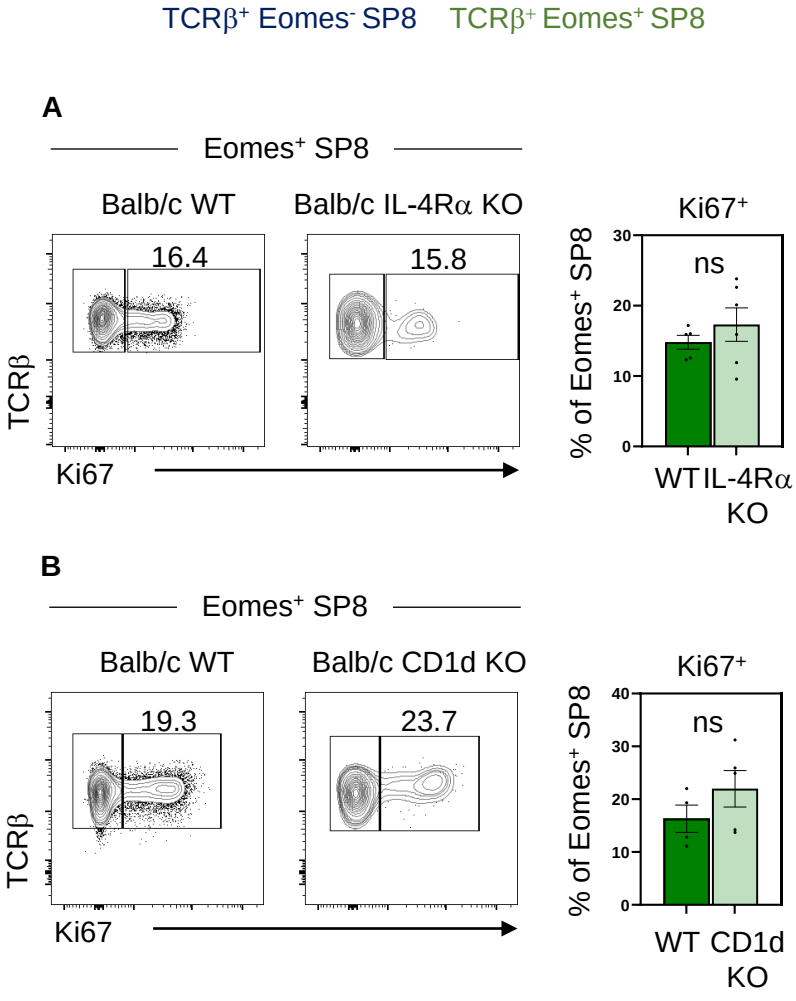
TCRβ+ Eomes- SP8
TCRβ+ Eomes+ SP8
A
Eomes+ SP8
Balb/c WT
Balb/c IL-4Rα KO
16.4
15.8
TCRβ
Ki67
Ki67+
% of Eomes+ SP8
ns
30
20
10
0
WT
IL-4Rα KO
B
Eomes+ SP8
Balb/c WT
Balb/c CD1d KO
19.3
23.7
TCRβ
Ki67
Ki67+
% of Eomes+ SP8
ns
40
30
20
10
0
WT
CD1d KO

Figure 5.7. Reduction in Eomes$^+$ SP8 through loss of IL-4 Provision is not caused by Loss of Proliferation

Thymuses were harvested from WT Balb/c, IL-4Rα KO Balb/c, and CD1d KO Balb/c mice and mechanically disaggregated for FACS analysis of thymocyte subpopulations.

(A) Representative FACS plots of Ki67 expression in TCRβ$^+$ Eomes$^+$ SP8 from WT Balb/c (left) and IL-4Rα KO Balb/c (right) mice, with graphical representation of Ki67$^+$ TCRβ$^+$ Eomes$^+$ SP8 in WT Balb/c (dark green bar) and IL-4Rα KO Balb/c (light green bar) mice.

(B) Representative FACS plots of Ki67 expression in TCRβ$^+$ Eomes$^+$ SP8 from WT Balb/c (left) and CD1d KO Balb/c (right) mice, with graphical representation of Ki67$^+$ TCRb$^+$ Eomes$^+$ SP8 in WT Balb/c (dark green bar) and CD1d KO Balb/c (light green bar) mice.

Data is taken from 2 separate experiments with n=5 WT Balb/c and n=6 IL-4Rα KO mice (A) and 2 separate experiments with n=4 WT Balb/c and n=5 CD1d KO mice (B). Each data point represents an individual mouse, with bars plotting the mean and error bars representing the SEM. Statistical significance was determined using Independent Student's T-test, with (ns) representing no significance.

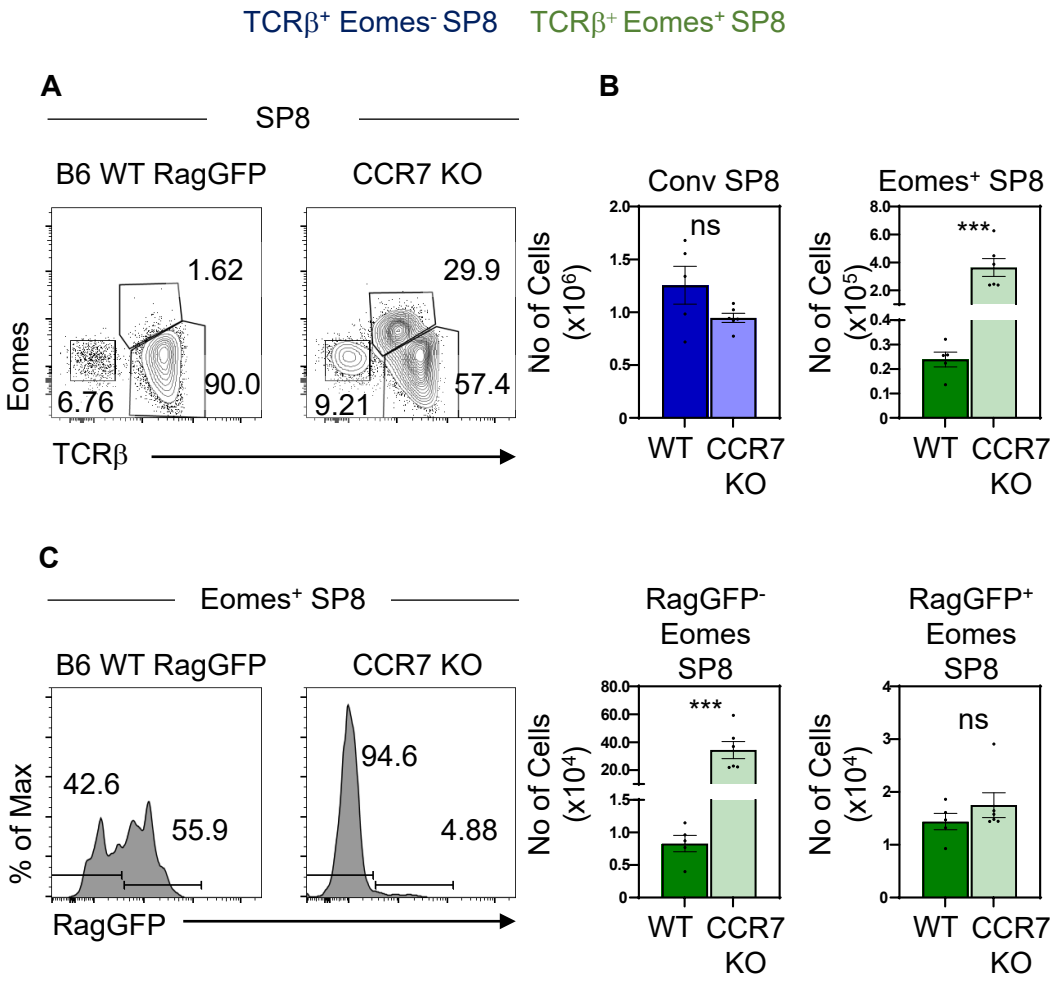
TCRβ+ Eomes- SP8
TCRβ+ Eomes+ SP8
A
SP8
B6 WT RagGFP
CCR7 KO
1.62
90.0
6.76
29.9
57.4
9.21
Eomes
TCRβ
B
Conv SP8
Eomes+ SP8
No of Cells (x10^6)
No of Cells (x10^5)
ns
***.
WT
CCR7 KO
C
Eomes+ SP8
B6 WT RagGFP
CCR7 KO
42.6
55.9
94.6
4.88
% of Max
RagGFP
RagGFP- Eomes SP8
RagGFP+ Eomes SP8
No of Cells (x10^4)
***
ns
WT
CCR7 KO

Figure 5.8. CCR7 KO mice show Increase in RagGFP$^-$ Eomes$^+$ SP8

Thymuses were harvested from WT RagGFP C57/B6 and CCR7 KO x RagGFP C57/B6 mice and mechanically disaggregated for FACS analysis of thymocyte subpopulations.

(A) Representative FACS plots identifying SP8 subpopulations in C57/B6 WT RagGFP (left) and CCR7 KO x RagGFP C57/B6 (right) mice.

(B) Graphical representation of numbers of TCRβ^+ Eomes$^-$ SP8 (left) and TCRβ^+ Eomes$^+$ SP8 (right), in C57/B6 WT RagGFP (dark bars) and CCR7 KO x RagGFP C57/B6 (light bars) mice.

(C) Representative histogram plots of RagGFP expression in TCRβ^+ Eomes$^+$ SP8 from C57/B6 WT RagGFP (left) and CCR7 KO x RagGFP C57/B6 (right) mice, with graphical representation of numbers of RagGFP$^-$ (left) and RagGFP$^+$ (right) TCRβ^+ Eomes$^+$ SP8 in C57/B6 WT RagGFP (dark green bars) and CCR7 KO x RagGFP C57/B6 (light green bars) mice.

Data is taken from 3 separate experiments with n=5 WT RagGFP and n=6 CCR7 KO x RagGFP mice. Each data point represents an individual mouse, with bars plotting the mean and error bars representing the SEM. Statistical significance was determined using Independent Student's T-test, with (***) representing $P<0.001$, and (ns) representing no significance.

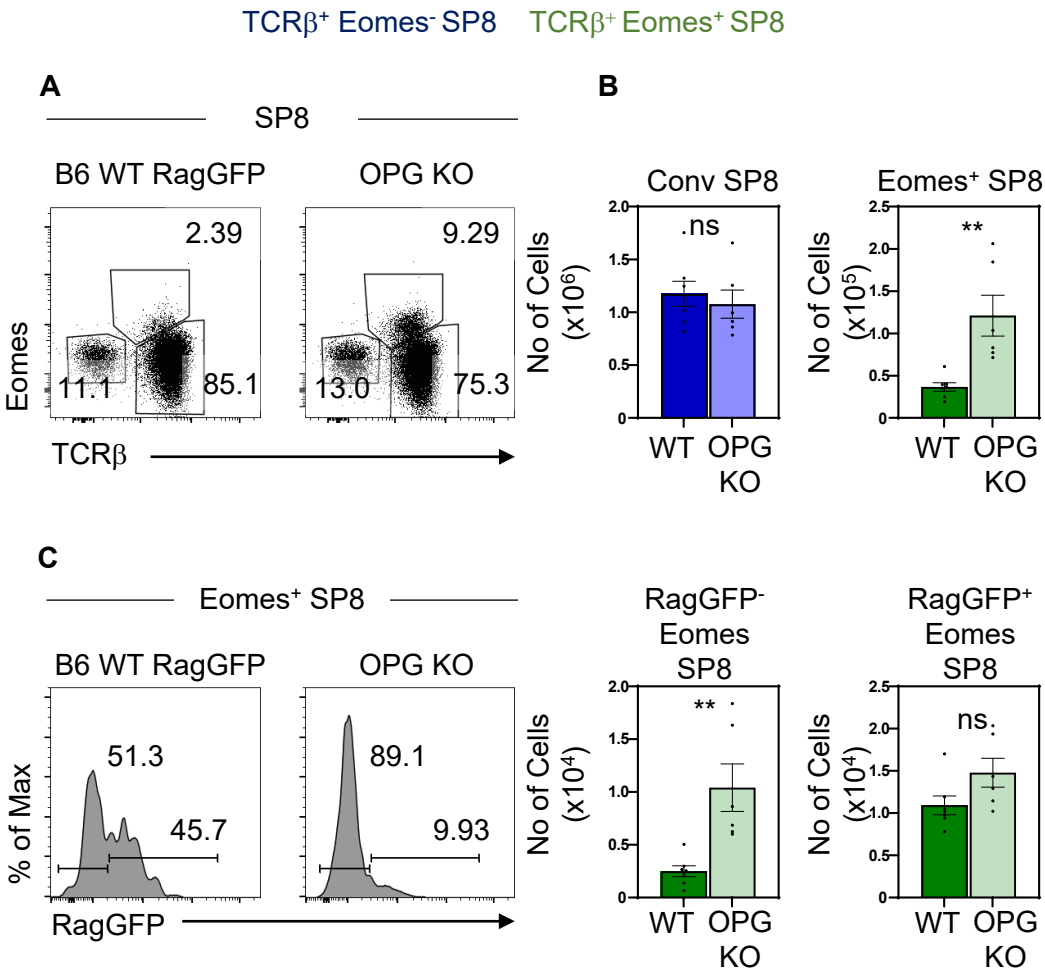
TCRβ+ Eomes- SP8
TCRβ+ Eomes+ SP8
A
SP8
B6 WT RagGFP
OPG KO
2.39
9.29
11.1
85.1
13.0
75.3
Eomes
TCRβ
B
Conv SP8
Eomes+ SP8
No of Cells (x10^6)
No of Cells (x10^5)
ns
**
WT
OPG KO
C
Eomes+ SP8
B6 WT RagGFP
OPG KO
51.3
45.7
89.1
9.93
% of Max
RagGFP
RagGFP- Eomes SP8
RagGFP+ Eomes SP8
No of Cells (x10^4)
**
ns
WT
OPG KO

Figure 5.9. OPG KO mice show Specific Increase in RagGFP$^-$ Eomes$^+$ SP8

Thymuses were harvested from WT RagGFP C57/B6 and OPG KO x RagGFP C57/B6 mice and mechanically disaggregated for FACS analysis of thymocyte subpopulations

(A) Representative FACS plots identifying SP8 subpopulations in C57/B6 WT RagGFP (left) and OPG KO x RagGFP C57/B6 (right) mice.

(B) Graphical representation of numbers of TCRβ^+ Eomes$^-$ SP8 (left) and TCRβ^+ Eomes$^+$ SP8 (right), in C57/B6 WT RagGFP (dark bars) and OPG KO x RagGFP C57/B6 (light bars) mice.

(C) Representative histogram plots of RagGFP expression in TCRβ^+ Eomes$^+$ SP8 from C57/B6 WT RagGFP (left) and OPG KO x RagGFP C57/B6 (right) mice, with graphical representation of numbers of RagGFP$^-$ (left) and RagGFP$^+$ (right) TCRβ^+ Eomes$^+$ SP8 in C57/B6 WT RagGFP (dark green bars) and OPG KO x RagGFP C57/B6 (light green bars) mice.

Data is taken from 3 separate experiments with n=7 WT RagGFP and n=6 OPG KO x RagGFP mice. Each data point represents an individual mouse, with bars plotting the mean and error bars representing the SEM. Statistical significance was determined using Independent Student's T-test, with (**) representing $P<0.01$, and (ns) representing no significance.

5.3 DISCUSSION

During T-cell development a number of non-conventional cells emerge within the thymus, including nTreg, iNKT cells, and Eomes^{+} innate-memory CD8 T-cells. The latter population have been shown to develop both in the periphery and intrathymically, however beyond a well-reported reliance on the availability of IL-4 within the thymus, the factors controlling their development within the thymus remains somewhat unclear. We therefore looked to explore their thymic development and how this is controlled. We identified these innate-memory SP8 within the thymus using expression of Eomes, comparing them to Eomes^{-} TCRβ^{+} SP8 that are almost entirely made up of cSP8. Characterising this population in WT RagGFP mice on a C57/B6 background showed that the relatively small proportion of Eomes^{+} innate-memory SP8 within the thymus are largely newly generated RagGFP^{+} cells. Furthermore, the newly generated RagGFP^{+} Eomes^{+} innate-memory SP8 had distinct M1 and M2 maturational populations, with a higher proportion of M2 than Eomes^{-} TCRβ^{+} SP8, and a lower level of RagGFP at both the M1 and M2 stages. This older and more mature phenotype suggests that innate-memory SP8 emerge late in the M1 stage of development, but beyond this continue their progression through maturational stages in the same manner as Eomes^{-} TCRβ^{+} SP8. This similarity in the maturation of Eomes^{+} SP8 and cSP8 is in line with previous reports showing that Eomes^{+} SP8 exist within M1 and M2 populations (52). Furthermore Eomes^{+} SP8 have been shown to continue their maturation extrathymically, upregulating expression memory-phenotype markers CD44 and CD122 only once they leave the thymus, shown through an accumulation of Eomes^{+} SP8 with FTY720 treatment, but no such accumulation of CD44^{+} CD122^{+}

cells. Interestingly this also suggests that innate-memory Eomes$^+$ SP8 generated in the thymus leave in an S1PR1-dependent manner, further mirroring cSP8 (52).

Key to the development of Eomes$^+$ innate-memory SP8 is IL-4, with the size of this population within the SP8 compartment being directly linked to the availability of IL-4. The main source of this IL-4 to support the development of Eomes$^+$ SP8 within the thymus is PZLF-expressing iNKT2 (274). In keeping with what has been reported, we found a significant increase in the size of the thymic Eomes$^+$ SP8 population in Balb/c mice when compared to C57/B6, owing to the larger iNKT2 population within Balb/c mice. Similarly, in CD1d KO mice that lack iNKT, and IL-4Rα KO mice which lack the ability to respond to IL-4, we see a dramatic loss in Eomes$^+$ SP8 (272–274), made even more striking by the fact both mice are on a Balb/c background, yet have Eomes$^+$ SP8 populations more similar to WT C57/B6 mice. Interestingly, however, is the lack of effect seen on the Eomes$^-$ TCRβ^+ SP8. Whilst there is a decrease in the number of cSP8 in Balb/c mice compared to C57/B6, it is significantly smaller than the increase in the Eomes$^+$ population, and therefore the change in distribution between Eomes$^-$ TCRβ^+ SP8 and Eomes$^+$ SP8 between the two strains cannot be caused by a divergence of Eomes$^-$ TCRβ^+ SP8 to Eomes$^+$ SP8 as a result of increased IL-4 availability during T-cell development. Further confirming this, in both CD1d and IL-4Rα KO mice the Eomes$^-$ TCRβ^+ SP8 population was unchanged, showing that the reduction in Eomes$^+$ SP8 in these models is not due to an increased number of cSP8 maintaining a conventional phenotype as a result of a lack of IL-4.

That Eomes$^+$ SP8 but not Eomes$^-$ TCRβ^+ SP8 thymocytes are affected by differences in IL-4-availibility within the thymus suggests that the role IL-4 plays in Eomes$^+$ innate

memory SP8 development is not the conversion of conventional cells towards this non-conventional lineage. This may suggest that IL-4 supports the new generation of Eomes$^+$ innate memory SP8 within the thymus during SP thymocyte selection. By breeding Balb/c mice to WT RagGFP mice on a C57/B6 background we were able to determine the RagGFP status of a dramatically expanded Eomes$^+$ SP8 thymocyte population due to increased IL-4 availability. Interestingly the large majority of Eomes$^+$ SP8 within Balb/c RagGFP mice were RagGFP$^-$, suggesting that whilst there are likely more newly generated RagGFP$^+$ Eomes SP8 within Balb/c mice, they do not account for most of the significant increase in the size of the Eomes$^+$ population. Such an increase in RagGFP$^-$ cells within the thymus would often likely be attributed to recirculating cells from the periphery, or long-term resident cells, both of which being populations that will have lost expression of RagGFP as they have aged (227). Aside from this aging however, RagGFP expression can also be lost through rapid proliferation. Such proliferation could explain why the significantly larger population of cells within Balb/c mice are mainly RagGFP$^-$. Despite this, Eomes$^+$ SP8 from the thymuses of Balb/c expressed significantly lower levels of Ki67, a cell cycle protein used to measure levels of proliferation (275). This suggests that IL-4 does not influence the development of Eomes$^+$ SP8 through extensive proliferation, further confirmed by our observation that there is no difference in Ki67 expression in Eomes$^+$ SP8 between WT Balb/c mice and both CD1d and IL-4Rα KO mice.

It is known that IL-4 provided by iNKT2 directly influences the size of the Eomes$^+$ innate-memory SP8 population, how this effect is carried out remains unclear. These data show that it is not through a conversion of cSP8 to Eomes$^+$ SP8, new generation of Eomes$^+$ SP8, or the induction of extensive proliferation of this population. Whilst the

direct effect IL-4 has on innate-memory SP8 has not been reported, it has been shown to have an interesting effect on naïve CD8 T-cells within the periphery. Upon TCR stimulation in the presence of IL-4, CD8 T-cells showed extended survival and protection from apoptosis compared to those stimulated without IL-4 (278–280). This extended survival was attributed to increased activation of signalling pathways downstream of the IL-4-receptor complex such IRS-2/PI-3 K/protein kinase B and Jak/STAT pathways in CD8 T-cells, in conjunction with a lower level of activity within the SOCS pathway compared to CD4 T-cells, which acts to inhibit these pathways (280). Furthermore, separate work has shown that IL-4 can act to maintain Bcl2 expression in CD8 T-cells following TCR-stimulation (278). As Bcl2 acts to suppress apoptosis, this provides further evidence for a unique role of IL-4 in the survival of CD8 T-cells. Whilst this work outlines this role in CD8 T-cells responding to their cognate antigen in a conventional manner, it presents an interesting function of IL-4 signalling in CD8 T-cells. It may suggest that the increased availability of IL-4 seen in Balb/c models acts to support the survival of those CD8 thymocytes that are selected to become Eomes^{+} innate-memory SP8 within the thymus. Recent work has shown that specific TCRs with a moderate affinity for self-antigen are selected within the thymus to becomes Eomes^{+} SP8 (52). In conjunction with a role of IL-4 in the survival of CD8 thymocytes, it may be possible that the same number of thymocytes are selected with Eomes^{+} innate-memory-bound TCRs in C57/B6 and Balb/c models, and it is the availability of IL-4 present that determines the amount that survive selection in the thymus and go on to form thymic and peripheral populations. Although this role of IL-4 would fit with the fact we do not see any higher degree of proliferation or conversion from conventional cells in Balb/c mice, how this may fit with the increase in RagGFP^{-}

cells still remains unclear. If Eomes$^+$ SP8 are simply more likely to survive following selection when IL-4 availability is increased, we would expect an increase in RagGFP$^+$ cells as the population would be newly generated during thymic selection. That we see a greater increase in the RagGFP$^-$ population would instead imply greater proportion of recirculating or resident cells rather than newly produced cells within the thymus. Questions still remain, therefore, around the intricacies of the relationship between IL-4 and Eomes$^+$ innate-memory SP8 in the thymus.

The importance for the thymus medulla in Eomes$^+$ innate-memory SP8 development is shown both through the presence of these cells within the M1 and M2 medullary populations (52,228), and also through their requirement for iNKT2 shown to be localised to medullary areas (91,276). Whether these cells require interaction with other cells within the medulla beyond those with iNKT2-supplied IL-4 has not been determined. We specifically looked to determine the requirement for interactions with mTEC in the development of Eomes$^+$ innate-memory SP8 within the thymus. Interestingly, we found that both a limited access to mTEC following selection in CCR7 KO mice (100,204), and increased availability of mTEC in OPG KO mice (93) had no significant impact on the new generation of RagGFP$^+$ Eomes$^+$ SP8, suggesting that the development of these cells does not rely on interactions with mTEC. Both CCR7 KO and OPG KO mice are on a C57/B6 background where it is known the size of the Eomes$^+$ SP8 population in the thymus is relatively small. It would therefore be interesting to determine whether mTEC interactions play any role in the development of the expanded Eomes$^+$ population in Balb/c mice alongside the known role of IL-4.

Whilst newly generated RagGFP$^+$ Eomes$^+$ SP8 are unchanged with altered access to mTEC, there was a surprisingly significant increase in RagGFP$^-$ Eomes$^+$ SP8 in both

CCR7 KO and OPG KO mice. Such an increase in recirculating cells, but no effect on the newly produced population has been previously reported within both CCR7 KO and OPG KO mice. Treg are a population that require the thymus medulla for their development, shown in $Relb^{-/-}$ mice (207), however when access to mTEC is limited in CCR7 KO mice, or mTEC availability increased in OPG KO mice, new generation of nTreg is unchanged, but there is a significantly increased $RagGFP^{-}$ Treg population of likely recirculated cells from the periphery (93,246). Whilst the relevance of the role these recirculated cells within the thymus remains unclear, the fact they appear in increased numbers in both of these models is thought to be owing to niche availability. As OPG KO mice have roughly a 3-fold increase in mTEC numbers, with no apparent effect on newly generated cells, this increased availability of mTEC is hypothesised to provide more niches for recirculating Treg to fill (93). Similarly, the impairment on SP thymocytes to translocate to the medulla in CCR7 KO mice (100) is thought to reduce competition for these medullary niches which recirculated Treg subsequently occupy (246). The increase in $RagGFP^{-}$ $Eomes^{+}$ SP8 that we see in both CCR7 and OPG KO mice could therefore be explained by an increased recirculating population from the periphery as a result of greater niche availability within the thymus medulla. This would suggest that as well as IL-4, the availability of mTEC determines the size of the $Eomes^{+}$ innate-memory SP8 population in the thymus, primarily through controlling the size of the recirculating population. Importantly it was reported that iNKT susbets are unaffected in OPG KO mice (93), and that the numbers of all subsets were in fact reduced in CCR7 KO mice (281), showing the effect we see in both models is mTEC-dependant, and not an indirect effect through and increase in iNKT like has been reported in previous gene-KO models (51). Furthermore, that this increased

recirculated Eomes$^+$ SP8 population doesn't impact the development of newly generated Eomes$^+$ SP8 in the thymus also mirrors the effects seen in Treg, whereby RagGFP$^+$ Treg were largely unaffected (93,246). This would suggest that whilst mTEC regulate the recirculation of both of these non-conventional lineages to the thymus, the presence of both populations does not affect development of new cells through competition for factors such as IL-2 and IL-4.

Together this chapter investigates the development and role of Eomes$^+$ innate-memory SP8 within the thymus. We have emphasised the complexity of relationship between these cells and the availability for IL-4, demonstrating that IL-4 does not promote the increase in new generation of Eomes$^+$ SP8, the proliferation of these cells, nor the conversion of conventional cells to this non-conventional lineage. Nonetheless the direct relationship between the availability of IL-4 within the thymus and the size of Eomes$^+$ SP8 remains clear to see. We have also shown that whilst availability of mTEC does not alter the new generation of Eomes$^+$ SP8, it does control their recirculation from the periphery, similar to what has been seen with Treg.

CHAPTER 6: GENERAL DISCUSSION

6.1 The Requirement for Defining Conventional Single Positive Thymocytes

This thesis aimed to determine the differences between the thymic maturation and egress of cSP4 and cSP8, how different factors provided within the thymus are differentially required for cSP4 and cSP8 development, and how non-conventional SP8 develop. Fundamental to realising these aims is the accurate definition of truly conventional SP thymocytes, removing non-conventional lineages from the analysis that may disrupt this definition. Through studying the literature, it is clear that such accurate definition within the SP4 lineage has become convention, removing $CD25^+$ Treg, thymic iNKT, and $RagGFP^-$ recirculated cells (228). Whilst this work successfully uses this definition of conventional cells to define stages in post selection maturation that are both phenotypically and functionally separate from one another, it fails to take into account heterogeneity within the SP8 population (51,52). By constructing an extensive flow cytometry panel, we were able to isolate and remove the same non-conventional lineages removed by Xing et al. (228), but also to identify $CD8\alpha\alpha$ IEL, and $Eomes^+$ innate memory SP8. Crucially, removing these lineages from our analysis allowed us to confidently define the maturation and egress in cSP thymocytes.

Whilst the size of these non-conventional populations in WT B6 mice are all relatively small in comparison to the larger conventional populations we aimed to analyse, the importance of their isolation was exemplified by our work to define the non-conventional $Eomes^+$ SP8 population. Even the relatively small populations of $Eomes^+$ SP8 in B6-background WTRagGFP showed a distinct phenotype from cSP8, representing both older and more mature cells with a higher proportion of $RagGFP^-$ recirculating populations. More striking was the variation in the size of this population between different mouse strains. Owing to their increased number of IL-4-producing

PZLF^{+} iNKT2, WT Balb/c mice have a significantly larger number of Eomes^{+} SP8 (273,274), and we show this to be around 48-fold larger than in B6 mice. The fact that this non-conventional population is so drastically expanded in Balb/c mice to the extent to which the large majority, around 70%, of total SP8 are Eomes^{+} SP8 and only around 20% are cSP8 outlines the extent to which this population interferes with analysis of the SP8 lineage in Balb/c WT mice. Furthermore, we saw an expansion of Eomes^{+} SP8 in CCR7$^{-/-}$ and OPG$^{-/-}$ mice. The identification of Eomes^{+} innate memory SP8 within the thymus was initially aided by the observation of its expansion in different KO models, such as interleukin-2-inducible T-cell kinase KO (ITK$^{-/-}$) (282) and KLF2$^{-/-}$ mice (272), before it was shown that in fact an increase in IL-4-producing cells was the root-cause of such expansion (51,272,283). Whilst the expansion of Eomes^{+} SP8 in the OPG$^{-/-}$ and CCR7$^{-/-}$ mouse models we observed does not appear to be caused by an increase in IL-4 producing iNKT (93,281), in combination with a number of previous studies that show an increase in Eomes^{+} SP8 in different KO models (51) our data exemplifies the importance of separating this population from cSP8.

The importance of accurate definition and isolation of cSP8 and non-conventional populations such as Eomes^{+} SP8 works two-fold. Firstly, it will ensure that the assumptions drawn from experiments observing the effect that experimental models may have on cSP8 within the thymus are accurate and don't unintentionally include any potential effects the model may have on on Eomes^{+} SP8. Accurate isolation and separation of these populations would also further the understanding of Eomes^{+} SP8 development within the thymus. Whilst the link between IL-4 and Eomes^{+} SP8 generation is clear and can explain the increase in Eomes^{+} SP8 in Balb/c mice and a number of KO models, the increase we see in CCR7$^{-/-}$ and OPG$^{-/-}$ implicates a

previously undefined role for mTEC interactions in determining the size of the Eomes$^+$ SP8 population. Further work using such of Eomes$^+$ SP8 in different models may help to understand this link, and as such the dynamics and factors involved in generation of Eomes$^+$ SP8 in the thymus, further elucidating this poorly understood population.

6.2 The Balance of CD4 and CD8 T-cells is Established by Thymic Selection, and Maintained Through Maturation and Egress

Our analysis of the post-selection maturation of cSP4 and cSP8 lineages alongside one-another allowed us to accurately track the ratio at which these cells progress through their thymic development and subsequently egress into the periphery. Crucial to this was the use of the previously identified DP3 population, known to contain exclusively CD8-committed cells that are yet to downregulate the CD4 coreceptor (201). By further investigating this population we identified the earliest SM and M1 populations that are missing from conventional analysis of the cSP8 population, contained within the DP3 population. By subsequently including this DP3 population in our analysis of cSP8 we were able to draw the maturation and egress of cSP4 and cSP8 in line with one another from selection through to the periphery. By analysing the ratio of CD4:CD8 thymocytes from SM, the earliest maturational stage following the selection of SP thymocytes, through to RTE in the periphery, we found that the CD4:CD8 T-cell ratio described in the periphery of around 1:1 - 2:1 (249) is present throughout thymic development. This observation again demonstrates the importance of the full definition of the SP thymocyte populations, including DP3 as the earliest SP8-committed cells. Previous analysis of the CD4:CD8 ratio within the thymus has described CD4 dominance within the ratio, but often at a higher proportion of CD4 thymocytes at around 4:1 (250). Such a difference in the ratio between the thymus and

the periphery would imply that other processes throughout T-cell development dictate the 2:1 ratio, but in fact the inclusion of the DP3 population provides evidence that this is not the case.

That the CD4:CD8 ratio established in the earliest cSP thymocyte populations implicates selection in determining this ratio. Previous work has implicated selection in the skewing of the CD4:CD8 ratio towards CD4 T-cells (250). Here, through the use of inducible Zap70$^{-/-}$, MHC I, and MHC II deficient mice to inform intricate mathematical modelling of cell death, maturation, and egress, it was estimated how efficiently CD4 and CD8 thymocytes progress through the DP1, DP2, and DP3 stages to ultimately give rise to SP thymocytes (250). Interestingly, the model predicted that within the DP2 stage, a larger proportion of MHC I restricted cells underwent cell death through negative selection compared to MHC II restricted cells. This was then confirmed using Bax^{huCD2} mice, where overexpression of Bax increases apoptotic stress in thymocytes. The DP2 population, and subsequently the DP3 and CD8 compartment was more sensitive to this apoptotic stress, skewing the ratio further towards CD4 thymocytes (250). Such evidence strongly suggests that MHC I committed cells are more susceptible to apoptosis through negative selection than MHC II committed cells at the same stage in development. This difference in susceptibility to negative selection, termed ‘asymmetric cell death’, ultimately leads to the bias towards CD4 over CD8 thymocytes. This would indeed fit with our data describing the CD4:CD8 ratio being established immediately following selection of SP thymocytes, suggesting that the factor within thymocyte selection that determines this CD4 bias is negative selection induced cell death, and specifically MHC I restricted thymocytes’ increased susceptibility to this.

Despite this role of negative selection in determining the CD4:CD8 ratio, other possible factors involved in the selection of SP thymocytes may contribute to the establishment of the CD4:CD8 ratio observed. During the selection of DP thymocytes, these cells undergo commitment to either the CD4 or CD8 SP thymocyte lineage. A number of different mechanisms behind this lineage commitment have been suggested, supplying a number of both classical and alternative models (186–188,190,191), however what remains clear is that recognition either MHC I-presented or MHC II-presented peptide complexes underpin the lineage decision between these thymocytes becoming CD8 or CD4 T-cells respectively. Given that the recognition of specific MHC-complexes by TCR is crucial to deciding the fate of developing thymocytes and therefore potentially the balance between CD4 and CD8 thymocytes, it may be an inherent feature of TCRs to have a bias for recognition of MHC II over MHC I specific peptides, hence committing more thymocytes to the CD4 lineage. Whilst random recombination of the V(D)J regions of the TCR looks to ensure there is a vast array of TCR-specificities during selection that may rule out such bias, that bias for MHC molecules exists within TCRs prior to selection events, has long been considered.

The coevolutionary model of TCR specificity for MHC complexes suggests that these molecules have evolved alongside one-another, and that within the germline-encoded complementary determining regions (CDR) 1 and 2 structures of the TCR there are multiple MHC-recognising regions, providing a bias for MHC recognition despite random TCR-rearrangement (284,285). The bias of TCRs towards MHC has been displayed using T-cell hybridoma experiments expressing specific TCRs. One such study utilised MHC I^oII^o mice to obtain pre-selection TCRs, before showing that 30%

of these TCRs recognised at least one of the 8 MHC molecules they were presented with. Given the relatively low number of MHC molecules presented for recognition in this study, it was therefore suggested that any given TCR is likely to recognise one of the multitude presented in the thymus (286). More recent work used retroviral transduction of TCR^- T-cell hybridomas with specific TCRs to measure their reactivity with different peptide presentation in the context of MHC molecules, measured through IL-2 production (287). As well as their cognate antigen, the TCRs responded to null peptides previously shown to provide no response, and with peptides that had their TCR-exposed residues mutated, termed ‘shaved’ (287). Combined, this evidence suggests that TCR specificity for MHC itself was providing the response and subsequent production of IL-2. If such recognition for MHC molecules in general is encoded into germline regions of the TCR, it is perhaps possible that there may be similar regions that recognise conserved aspects of either MHC I or MHC II molecules. If this was the case, the bias for commitment to the CD4 over the CD8 lineage that we observe in the CD4:CD8 ratio in the thymus may be determined by an increased frequency of such regions recognising MHC II over MHC I within TCRs, hence providing TCRs with an inherent bias for MHC II over MHC I. Many hybridoma studies used to determine the bias of TCRs for MHC use MHC II on APC to determine this recognition (285–287). Replication of such studies comparing the reactivity with MHC I and MHC II complexes by pre-selection TCRs may determine whether this inherent bias for MHC II over MHC I exists, elucidating further factors contributing to the balance of CD4 and CD8 T-cells established in the thymus.

Another interesting factor that has been reported to contribute towards lineage decision is the strength of signalling provided during selection. One theory of commitment to the

CD4 or CD8 lineage suggests that stronger TCR-signalling during thymocyte selection directs commitment to the CD4 lineage, whilst weaker signals lead to the CD8 lineage (188). The basis of this is differences between signalling via the CD4 and CD8 co-receptors. The intracellular domain of CD4 is known to associate stronger with Lck than that of the CD8 coreceptor, hence leading to stronger signals when engaged with TCR-signalling (189). This difference in signal strength was argued to be the basis of lineage choice through use of transgenes whereby the CD8 coreceptor expresses the intracellular tail of the CD4 coreceptor, hence providing TCR engagement supported by CD8 the strength of that provided by the CD4 coreceptor (188). However, whilst initial reports suggested this led to greater CD4-commitment with use of such transgene, supporting the strength-of-signal model, later studies showed that such a model also increased the number of DP thymocytes prompted to commit to the CD8 lineage, suggesting the increased strength of signalling is not specific to CD4 commitment (288). Whilst the role strength of signalling play in the choice between the CD4 and CD8 lineage may remain unclear, that engagement via the CD4 coreceptor provides stronger TCR signalling during selection provides another aspect of selection that may determine the balance of the CD4:CD8 ratio. If a threshold of TCR signalling is required during selection for thymocytes to receive survival signals and be positively selected, such stronger signalling via CD4's increased association with $p56^{Lck}$ would suggest it is easier for thymocytes engaging with MCH II complexes via their TCR and, importantly, CD4 to reach this threshold and therefore survive. Thymocytes expressing TCRs capable of recognising MHC I on the other hand are less likely to receive adequate signalling, and as such undergo death by neglect, simply due to the relatively lower $p56^{Lck}$ association. This possibility is supported through use of the CD8-CD4

cytosolic tail transgene. When signalling via the CD8 coreceptor was boosted in this model, the number of CD8 thymocytes and peripheral CD8 T-cells increased dramatically, presumably through a larger number successfully passing through positive selection (288). It is possible, therefore, that following random V(D)J rearrangement the number of TCRs capable of recognising MHC I and MHC II complexes when entering selection at the DP stage are relatively even, however those that recognise MHC II are more likely to receive the level of TCR signalling upon engagement required to survive. Such a possibility works along the same lines as that proposed by the Seddon group (250), however rather than increased susceptibility to negative selection in MHC I restricted cells causing the skew towards CD4, it would be a higher success rate of positive selection in MHC II restricted cells.

Whilst the exact cause for the CD4:CD8 ratio amongst the multitude of factors involved in selection and lineage commitment remains unclear, our work outlines that it is in fact selection that establishes the ratio at around 2:1. Importantly, that this ratio is established immediately following the selection of SP thymocytes and carried through thymic maturation, ordered egress via the PVS, and ultimately presence in the periphery highlights the thymus' control and maintenance of this balance. The way in which the thymus controls thymocyte maturation and egress has been defined as a 'conveyor belt' mechanism, whereby cells progress through sequential maturational populations as they gain functional maturity and egress competence before the most mature cells are preferentially selected for thymic egress (98,228). Whilst the data described in this thesis describes how this conveyor belt controls the cSP8 lineage for the first time, it also highlights the how these processes are controlled separately in cSP4 and cSP8 to maintain the balance within the CD4:CD8 ratio. cSP8 thymocytes

represent older cells at the most mature stages of thymocyte maturation, egress via the PVS, and ultimately within the periphery. If a conveyor belt that controlled maturation and egress was universal for both cSP4 and cSP8, it would therefore select more cSP8 than cSP4 owing to their more mature status. That the CD4:CD8 ratio is maintained from selection through this maturation and egress suggests that the most mature cSP4 and cSP8 are chosen separately for egress via the PVS into the periphery. These two separate conveyor belts work separately from one another, but in the same manner to ensure that cSP4 and cSP8 undergo and ordered maturation and egress whilst maintaining perfect balance between the two.

6.3 Long-term Implications of BMT on Thymus Structure and Function

The standard treatment for a number of haemotological conditions, including cancers, is ablative therapy follow by BMT (253). For this therapy to succeed in re-establishing a functioning immune system including a sufficient T-cell compartment donor stem cells must undergo thymopoeisis within the host thymus (258). Recent work has suggested that the therapy itself may hinder such recovery, highlighting a failure in recovery specific to mTEC following the ablative therapy that precedes BMT (261). Importantly this has functional implications, with mice displaying a break down in tolerance as a result of a loss of negative selection and nTreg generation following the loss of mTEC (261). We therefore looked to utilise our definition of post-selection maturation and thymic egress in cSP4 and cSP8 to ask whether these processes are also affected by the failure of mTEC recovery following BMT, selecting the d28 timepoint as at this stage mice are reported to show a recovery of cTEC but not mTEC (261). Interestingly this analysis showed that in fact post-selection maturation is largely unaffected by the lack of mTEC recovery seen in d28 BMT mice. This lack of

requirement for mTEC interactions for the maturation of cSP thymocytes is consistent with previous work determining the maturation of SP thymocytes in Relb$^{-/-}$ that lack mTEC, and in CCR7$^{-/-}$ and *plt/plt* mice where SP thymocytes cannot translocate to the medulla, showed that maturation occurs as normal without these medullary interactions (100,204,207). This work therefore acts to further confirm the lack of requirement for interaction with mTEC that post-selection maturation has despite the fact that cSP thymcoytes undergo this maturation within the medulla following their selection and preceding their egress.

Our analysis of d28 BMT mice did however identify further failures in the recovery of thymic structure following irradiation. Beyond the failure in mTEC recovery, specialised endothelium within the thymus, TPEC, were also shown at a lower number in d28 BMT mice than that seen in control mice, whilst other endothelial populations were unaffected. These TPEC are shown to be associated with the trafficking of cells in and out of the thymus, controlling entry of progenitors and egress of mature cells (98,164,263). Furthermore, these processes have been suggested to be controlled by further subpopulations within TPEC based on BST-1 expression (263). Both the BST-1^{LO} 'homing vessels' and BST-1^{HI} 'egress vessels' were significantly reduced in d28 BMT mice, showing that whilst this failure in recovery is specific to TPEC, it does not discriminate between further TPEC subsets. We observed the repercussions of the failure of TPEC to recover post-BMT in the form of an accumulation of the most mature thymocytes in d28 BMT. This indicated that the lack of these specialised egress vessels restricted the number of egress points available to egress-competent thymocytes, causing their build up within the thymus. Whilst our own analysis provides evidence of the consequences of the loss of egress-specific vessels following BMT,

the effect of the loss of entry-specific vessels could be assessed using the recruitment of progenitor cells to the thymus. Whilst previous work has not assessed this in the context of TPEC and BMT, the relationship between BMT recovery and progenitor recruitment has been studied. In fact, it was previously shown that progenitor recruitment and subsequently numbers of ETP following BMT is reduced to the extent where the niche of progenitor cells within the thymus is still unsaturated 10-weeks after therapy (289). Furthermore, LTβR was separately shown to support the recruitment of progenitors to the thymus following BMT, with anti-LTβR agonist boosting the levels of donor-derived cells (165). TPEC are known to be an LTβR-dependent population, with specific endothelial loss of LTβR resulting in a significant reduction in TPEC (98,164,263). As such, the previous studies describing the lack of progenitor recruitment to the thymus following BMT and the role of LTβR in supporting this process work in line with the data presented here, suggesting that a loss of BST-1^{LO} TPEC following BMT results in reduced recruitment of progenitors, and is recovered through provision of anti-LTβR agonists to stimulate the re-emergence of the TPEC population.

Interestingly, whilst we see clear signs of an accumulation in d28 BMT mice, this accumulation is relatively minor, with no significant loss of GFP to indicate substantial aging on accumulating cells, and no change in the number of measurable RTE within the spleen. Whilst the former may be explained through insufficient time for a significant accumulation to occur given normal thymopoeisis only returns around d21 (261), the lack of change in peripheral RTE is likely a result of the current model. T-cells that enter the periphery following BMT are entering a lymphopenic environment following the ablative lethal irradiation provided during the therapy, and as such undergo

peripheral expansion in response (255,257). Expansion of cells expressing RagGFP leads to a loss of fluorescence through cell divisions, and therefore in RTE which already have low levels of GFP expression by nature such expansion would cause complete loss of expression. It is therefore likely that a number of cells contained within the RagGFP^{-} fraction of donor-derived splenic T-cells are in fact RTE that have lost GFP expression due to expansion.

Future work to better understand RTE in a BMT setting could look to combat the issue of defining the population using a number of different techniques. Firstly, it would be possible to examine the peripheral blood from BMT mice through a number of early time points to ‘catch’ the first donor-derived cells that leave the thymus. Such experiment may not necessarily require the use of RagGFP to define RTE as the first wave of donor-derived T-cells present in the periphery would be identified through congenic labelling and already known to be RTE as they would be the only donor T-cells present. Alternatively, rather than isolating the first RTE that have left the thymus and not had the chance to expand in response to lymphopenia, experiments could aim to provide a ‘normal’ periphery for RTE to enter following BMT, avoiding lymphopenic expansion entirely. This would involve performing a BMT as normal, but as well as reconstituting host mice with stem cells from donor bone marrow, supplementing them with mature T-cells from the periphery of donor mice. This would provide a complete peripheral T-cell compartment in the host mice, meaning that cells exported from the thymus are entering a periphery mirroring that of a steady-state mouse. Whilst such a model would solve the issue of peripheral expansion in response to lymphopenia, it would potentially have its own flaws. Although the reason for recirculating cells within the thymus remains unclear, that they exist is evident through study of populations in

the thymus using RagGFP mice (93,227,246). By supplementing BMT mice with mature T-cells from donor mice, these cells could recirculate from the periphery and into the thymus, a phenomenon that would not normally occur owing to the reduced peripheral compartment following BMT. This potential thymic presence of peripheral T-cells would therefore not be representative of a BMT model and may have implications on the recovery of stromal populations in the thymus. This is made ever more important by the role of 'thymic cross-talk' in the development of the thymic stroma associated with failures in recovery following BMT in the form of mTEC (89,90) and TPEC (164,263). It could be possible that as well as filling the periphery, these mature T-cells may support the recovery of these stromal populations in the thymus upon recirculation via thymic crosstalk. As such, this provides interesting avenues to further expand on the understanding of the thymus's response to BMT in terms of early-output and RTE, but models would have to be careful not to artificially disrupt the changes in the thymic microenvironment that are already associated with BMT.

This analysis of the implications of BMT on thymic structure and function works to supplement previous studies that have outlined other failures in recovery of the thymus following BMT. The thymus' role in re-establishing a complete immune system and subsequently ensuring an efficient and successful BMT therapy is clear, and therefore a better understanding of how the thymus responds to the BMT is crucial to ensuring its function is best supported to achieve successful therapeutic outcomes.

6.4 Concluding Remarks

In summary, this thesis aimed to understand the post-selection maturation and thymic egress of cSP8 to the same degree as cSP4, to determine how these processes are affected following structural changes in the thymus post-BMT, and how the thymus controls the development of non-conventional lineages excluded by conventional analysis. Our work provides an accurate characterisation of truly conventional SP8 by isolating non-conventional lineages, whilst also providing a novel definition of the earliest stages of cSP8 maturation within the DP3 population. Interestingly this definition reveals that thymic selection establishes the CD4:CD8 ratio that is carried through maturation and egress into the periphery. We further used this understanding of cSP4 and cSP8 alongside one another to determine whether loss of mTEC following BMT alters maturation and egress of these populations. Instead, we showed that a failure in the recovery of not mTEC, but TPEC disrupts thymocyte egress following BMT, further supplementing the growing understanding of the consequences of BMT within the thymus. This presents an interesting avenue to further explore, with the aim of completely mapping thymic structure and the functional consequences following BMT. We finally explored the thymic development of Eomes^{+} SP8, highlighting the complexity of this population, with further work needed to fully understand both their generation and their role within the thymus.

REFERENCES

1. Brodin P, Davis MM. Human immune system variation. Nat Rev Immunol. 2017;17(1):21–9.

2. Janeway CA, Medzhitov R. Innate immune recognition. Annu Rev Immunol. 2002;20(2):197–216.

3. Brubaker SW, Bonham KS, Zanoni I, Kagan JC. Innate Immune Pattern Recognition: A Cell Biological Perspective. Annu Rev Immunol [Internet]. 2015 Mar 21;33(1):257–90.

4. Gasteiger G, D'osualdo A, Schubert DA, Weber A, Bruscia EM, Hartl D. Cellular Innate Immunity: An Old Game with New Players. J Innate Immun. 2017;9(2):111–25.

5. Hayashi F, Smith KD, Ozinsky A, Hawn TR, Yi EC, Goodlett DR, et al. The innate immune response to bacterial flagellin is mediated by Toll-like receptor 5. Nature. 2001;410(6832):1099–103.

6. Mancuso G, Gambuzza M, Midiri A, Biondo C, Papasergi S, Akira S, et al. Bacterial recognition by TLR7 in the lysosomes of conventional dendritic cells. Nat Immunol. 2009;10(6):587–94.

7. Kawasaki T, Kawai T. Toll-like receptor signaling pathways. Front Immunol. 2014;5(SEP):1–8.

8. Noris M, Remuzzi G. Overview of complement activation and regulation. Semin Nephrol [Internet]. 2013;33(6):479–92.

9. Xie CB, Jane-Wit D, Pober JS. Complement Membrane Attack Complex: New Roles, Mechanisms of Action, and Therapeutic Targets. Am J Pathol [Internet]. 2020;190(6):1138–50.

10. Griffith JW, Sokol CL, Luster AD. Chemokines and chemokine receptors: Positioning cells for host defense and immunity. Annu Rev Immunol. 2014;32:659–702.

11. Häger M, Cowland JB, Borregaard N. Neutrophil granules in health and disease. J Intern Med. 2010;268(1):25–34.

12. Galli SJ, Borregaard N, Wynn TA. Phenotypic and functional plasticity of cells of innate immunity: Macrophages, mast cells and neutrophils. Nat Immunol. 2011;12(11):1035–44.

13. Marshall JS, Warrington R, Watson W, Kim HL. An introduction to immunology and immunopathology. Allergy, Asthma Clin Immunol [Internet]. 2018;14(s2):1–10.

14. Pieper K, Grimbacher B, Eibel H. B-cell biology and development. J Allergy Clin Immunol [Internet]. 2013;131(4):959–71.

15. Jung D, Alt FW. Unraveling V(D)J Recombination: Insights into Gene Regulation. Cell. 2004;116(2):299–311.

16. Loder F, Mutschler B, Ray RJ, Paige CJ, Sideras P, Torres R, et al. B cell

development in the spleen takes place in discrete steps and is determined by the quality of B cell receptor-derived signals. J Exp Med. 1999;190(1):75–89.

17. Stavnezer J, Guikema JEJ, Schrader CE. Mechanism and regulation of class switch recombination. Annu Rev Immunol. 2008;26:261–92.

18. Kranich J, Krautler NJ. How Follicular Dendritic Cells Shape the B-Cell Antigenome. Front Immunol [Internet]. 2016 Jun 21;7:225.

19. Bonilla FA, Oettgen HC. Adaptive immunity. J Allergy Clin Immunol [Internet]. 2010;125(2 SUPPL. 2):S33–40.

20. Ciofani M, Knowles GC, Wiest DL, von Boehmer H, Zúñiga-Pflücker JC. Stage-Specific and Differential Notch Dependency at the αβ and γδ T Lineage Bifurcation. Immunity. 2006;25(1):105–16.

21. Bromley SK, Iaboni A, Davis SJ, Whitty A, Green JM, Shaw AS, et al. The immunological synapse and CD28-CD80 interactions. Nat Immunol. 2001;2(12):1159–66.

22. Kaiko GE, Horvat JC, Beagley KW, Hansbro PM. Immunological decision-making: How does the immune system decide to mount a helper T-cell response? Immunology. 2008;123(3):326–38.

23. Allison JP, Havran WL. The immunobiology of T cells with invariant γδ antigen receptors. Annu Rev Immunol. 1991;9(1):679–705.

24. Born WK, Kemal Aydintug M, O'brien RL. Diversity of γδ T-cell antigens. Cell Mol Immunol. 2013;10(1):13–20.

25. Dong C. Cytokine Regulation and Function in T Cells. Annu Rev Immunol. 2021;39:51–76.

26. Zhu J, Paul WE. CD4 T cells : fates , functions , and faults ASH 50th anniversary review CD4 T cells : fates , functions , and faults. Immunobiology. 2009;112(5):1557–69.

27. Mosmann TR, Cherwinski H, Bond MW, Giedlin MA, Coffman RL. Two types of murine helper T cell clone. I. Definition according to profiles of lymphokine activities and secreted proteins. J Immunol [Internet]. 1986 Apr 1;136(7):2348–57.

28. Szabo SJ, Kim ST, Costa GL, Zhang X, Fathman CG, Glimcher LH. A novel transcription factor, T-bet, directs Th1 lineage commitment. Cell. 2000;100(6):655–69.

29. Swain SL, Weinberg AD, English M, Huston G, Huston G. IL-4 directs the development of Th2-like helper effectors. J Immunol. 1990;145(11):3796–806.

30. Jenkins SJ, Ruckerl D, Thomas GD, Hewitson JP, Duncan S, Brombacher F, et al. IL-4 directly signals tissue-resident macrophages to proliferate beyond homeostatic levels controlled by CSF-1. J Exp Med. 2013;210(11):2477–91.

31. Weaver CT, Harrington LE, Mangan PR, Gavrieli M, Murphy KM. Th17: An

Effector CD4 T Cell Lineage with Regulatory T Cell Ties. Immunity. 2006;24(6):677–88.

32. Kim CH, Rott LS, Clark-Lewis I, Campbell DJ, Wu L, Butcher EC. Subspecialization of CXCR5+ T cells: B helper activity is focused in a germinal center-localized subset of CXCR5+ T cells. J Exp Med. 2001;193(12):1373–81.

33. Nurieva RI, Chung Y, Hwang D, Yang XO, Kang HS, Ma L, et al. Generation of T Follicular Helper Cells Is Mediated by Interleukin-21 but Independent of T Helper 1, 2, or 17 Cell Lineages. Immunity. 2008;29(1):138–49.

34. Sakaguchi S, Sakaguchi N, Asano M, Itoh M, Toda M. Immunologic self-tolerance maintained by activated T cells expressing IL-2 receptor alpha-chains (CD25). Breakdown of a single mechanism of self-tolerance causes various autoimmune diseases. J Immunol. 1995 Aug 1;155(3):1151–64.

35. Moran AE, Holzapfel KL, Xing Y, Cunningham NR, Maltzman JS, Punt J, et al. T cell receptor signal strength in Treg and iNKT cell development demonstrated by a novel fluorescent reporter mouse. J Exp Med. 2011;208(6):1279–89.

36. Chen WJ, Jin W, Hardegen N, Lei KJ, Li L, Marinos N, et al. Conversion of Peripheral CD4+CD25- Naive T Cells to CD4+CD25+ Regulatory T Cells by TGF-β Induction of Transcription Factor Foxp3. J Exp Med. 2003;198(12):1875–86.

37. Fontenot JD, Gavin MA, Rudensky AY. Foxp3 programs the development and function of CD4+CD25+ regulatory T cells. Nat Immunol. 2003 Apr 3;4(4):330–6.

38. Asseman C, Mauze S, Leach MW, Coffman RL, Powrie F. An essential role for interleukin 10 in the function of regulatory T cells that inhibit intestinal inflammation. J Exp Med. 1999;190(7):995–1003.

39. Fahlén L, Read S, Gorelik L, Hurst SD, Coffman RL, Flavell RA, et al. T cells that cannot respond to TGF-β escape control by CD4+ CD25+ regulatory T cells. J Exp Med. 2005;201(5):737–46.

40. Qureshi OS, Zheng Y, Nakamura K, Attridge K, Manzotti C, Schmidt EM, et al. Trans-Endocytosis of CD80 and CD86: A Molecular Basis for the Cell-Extrinsic Function of CTLA-4. Science (80-) [Internet]. 2011 Apr 29;332(6029):600–3.

41. Gondek DC, Lu LF, Quezada SA, Sakaguchi S, Noelle RJ. Cutting Edge: Contact-Mediated Suppression by CD4 + CD25 + Regulatory Cells Involves a Granzyme B-Dependent, Perforin-Independent Mechanism . J Immunol. 2005;174(4):1783–6.

42. Brunkow ME, Jeffery EW, Hjerrild KA, Paeper B, Clark LB, Yasayko S ann, et al. Disruption of a new forkhead/winged-helix protein, scurfin, results in the fatal lymphoproliferative disorder of the scurfy mouse. Nat Genet [Internet]. 2001 Jan;27(1):68–73.

43. Blum JS, Wearsch PA, Cresswell P. Pathways of Antigen Processing. Annu Rev Immunol [Internet]. 2013 Mar 21;31(1):443–73.

44. Zhang N, Bevan MJ. CD8+ T Cells: Foot Soldiers of the Immune System. Immunity. 2011;35(2):161–8.

45. Obar JJ, Lefrançois L. Early Signals during CD8 + T Cell Priming Regulate the Generation of Central Memory Cells. J Immunol [Internet]. 2010 Jul 1;185(1):263–72.

46. Kaech SM, Ahmed R. Memory CD8+ T cell differentiation: Initial antigen encounter triggers a developmental program in naïve cells. Nat Immunol. 2001;2(5):415–22.

47. Khanna KM, McNamara JT, Lefrançois L. In Situ Imaging of the Endogenous CD8 T Cell Response to Infection. Science (80-) [Internet]. 2007 Oct 5;318(5847):116–20.

48. Curtsinger JM, Lins DC, Mescher MF. Signal 3 determines tolerance versus full activation of naive CD8 T cells: Dissociating proliferation and development of effector function. J Exp Med. 2003;197(9):1141–51.

49. Takemoto N, Intlekofer AM, Northrup JT, Wherry EJ, Reiner SL. Cutting Edge: IL-12 Inversely Regulates T-bet and Eomesodermin Expression during Pathogen-Induced CD8 + T Cell Differentiation . J Immunol. 2006;177(11):7515–9.

50. Pearce EL, Mullen AC, Martins GA, Krawczyk CM, Hutchins AS, Zediak VP, et al. Control of Effector CD8+ T Cell Function by the Transcription Factor Eomesodermin. Science (80-). 2003;302(5647):1041–3.

51. Jameson SC, Lee YJ, Hogquist KA. Innate Memory T cells. Adv Immunol. 2015;126:173–213.

52. Miller CH, Klawon DEJ, Zeng S, Lee V, Socci ND, Savage PA. Eomes identifies thymic precursors of self-specific memory-phenotype CD8+ T cells. Nat Immunol. 2020;21(May).

53. Goadsby PJ, Kurth T, Pressman A. Present Yourself! By MHC Class I and MHC Class II Molecules. Trends Immunol. 2016;35(14):1252–60.

54. Cresswell P, Bangia N, Dick T, Diedrich G. The nature of the MHC class I peptide loading complex. Immunol Rev. 1999;172:21–8.

55. Neefjes J, Jongsma MLM, Paul P, Bakke O. Towards a systems understanding of MHC class i and MHC class II antigen presentation. Nat Rev Immunol. 2011;11(12):823–36.

56. Klein L, Kyewski B, Allen PM, Hogquist KA. Positive and negative selection of the T cell repertoire: What thymocytes see (and don't see). Nat Rev Immunol. 2014;14(6):377–91.

57. Ghosh P, Amaya M, Mellins E, Wiley DC. The structure of an intermediate in class II MHC maturation : CLIP bound to HLA-DR3. Nature. 1995;378:457–62.

58. Joffre OP, Segura E, Savina A, Amigorena S. Cross-presentation by dendritic cells. Nat Rev Immunol. 2012;12(8):557–69.

59. Linsley PS, Brady W, Grosmaire L, Aruffo A, Damle NK, Ledbetter JA. Binding of the B cell activation antigen B7 to CD28 costimulates T cell proliferation and interleukin 2 mRNA accumulation. J Exp Med. 1991;173(3):721–30.

60. Yoshinaga SK, Whoriskey JS, Khare SD, Sarmiento U, Guo J, Horan T, et al. T-cell co-stimulation through B7RP-1 and ICOS. 1999;1:827–32.

61. Keir ME, Butte MJ, Freeman GJ, Sharpe AH. PD-1 and its ligands in tolerance and immunity. Annu Rev Immunol. 2008;26:677–704.

62. Hubo M, Trinschek B, Kryczanowsky F, Tuettenberg A, Steinbrink K, Jonuleit H. Costimulatory molecules on immunogenic versus tolerogenic human dendritic cells. Front Immunol. 2013;4(APR):1–14.

63. MILLER J. Immunological Function of the Thymus. Lancet. 1961 Sep;278(7205):748–9.

64. Gordon J, Manley NR. Mechanisms of thymus organogenesis and morphogenesis. Development. 2011;138(18):3865–78.

65. Vaidya HJ, Briones Leon A, Blackburn CC. FOXN1 in thymus organogenesis and development. Eur J Immunol. 2016;46(8):1826–37.

66. Gordon J, Patel SR, Mishina Y, Manley NR. Evidence for an early role for BMP4 signaling in thymus and parathyroid morphogenesis. Dev Biol [Internet]. 2010 Mar;339(1):141–54.

67. Gordon J, Bennett AR, Blackburn CC, Manley NR. Gcm2 and Foxn1 mark early parathyroid- and thymus-specific domains in the developing third pharyngeal pouch. Mech Dev. 2001;103(1–2):141–3.

68. Anderson G, Takahama Y. Thymic epithelial cells: working class heroes for T cell development and repertoire selection. Trends Immunol. 2012 Jun;33(6):256–63.

69. Abramson J, Anderson G. Thymic epithelial cells. Annu Rev Immunol. 2017;35:85–118.

70. Griffith A V., Fallahi M, Nakase H, Gosink M, Young B, Petrie HT. Spatial Mapping of Thymic Stromal Microenvironments Reveals Unique Features Influencing T Lymphoid Differentiation. Immunity [Internet]. 2009 Dec;31(6):999–1009.

71. Rossi SW, Jenkinson WE, Anderson G, Jenkinson EJ. Clonal analysis reveals a common progenitor for thymic cortical and medullary epithelium. Nature. 2006;441(7096):988–91.

72. Bleul CC, Corbeaux T, Reuter A, Fisch P, Mönting JS, Boehm T. Formation of a functional thymus initiated by a postnatal epithelial progenitor cell. Nature [Internet]. 2006 Jun 10;441(7096):992–6.

73. Nehls M, Kyewski B, Messerle M, Waldschütz R, Schüddekopf K, Smith AJH, et al. Two Genetically Separable Steps in the Differentiation of Thymic Epithelium. Science (80-) [Internet]. 1996 May 10;272(5263):886–9.

74. Nowell CS, Bredenkamp N, Tetélin S, Jin X, Tischner C, Vaidya H, et al. Foxn1 regulates lineage progression in cortical and medullary thymic epithelial cells but is dispensable for medullary sublineage divergence. PLoS Genet. 2011;7(11).

75. Blackburn CC, Augustine CL, Li R, Harvey RP, Malin MA, Boyd RL, et al. The nu gene acts cell-autonomously and is required for differentiation of thymic epithelial progenitors. Proc Natl Acad Sci U S A. 1996;93(12):5742–6.

76. Ripen AM, Nitta T, Murata S, Tanaka K, Takahama Y. Ontogeny of thymic cortical epithelial cells expressing the thymoproteasome subunit β5t. Eur J Immunol. 2011;41(5):1278–87.

77. Ohigashi I, Zuklys S, Sakata M, Mayer CE, Zhanybekova S, Murata S, et al. Aire-expressing thymic medullary epithelial cells originate from β5t-expressing progenitor cells. Proc Natl Acad Sci U S A. 2013;110(24):9885–90.

78. Ribeiro AR, Rodrigues PM, Meireles C, Di Santo JP, Alves NL. Thymocyte Selection Regulates the Homeostasis of IL-7–Expressing Thymic Cortical Epithelial Cells In Vivo. J Immunol. 2013;191(3):1200–9.

79. Baik S, Jenkinson EJ, Lane PJL, Anderson G, Jenkinson WE. Generation of both cortical and Aire+ medullary thymic epithelial compartments from CD205+ progenitors. Eur J Immunol. 2013;43(3):589–94.

80. Alves NL, Takahama Y, Ohigashi I, Ribeiro AR, Baik S, Anderson G, et al. Serial progression of cortical and medullary thymic epithelial microenvironments. Eur J Immunol. 2014;44(1):16–22.

81. Ohigashi I, Zuklys S, Sakata M, Mayer CE, Hamazaki Y, Minato N, et al. Adult Thymic Medullary Epithelium Is Maintained and Regenerated by Lineage-Restricted Cells Rather Than Bipotent Progenitors. Cell Rep [Internet]. 2015;13(7):1432–43.

82. Mayer CE, Žuklys S, Zhanybekova S, Ohigashi I, Teh HY, Sansom SN, et al. Dynamic spatio-temporal contribution of single β5t+ cortical epithelial precursors to the thymus medulla. Eur J Immunol. 2016;46(4):846–56.

83. Hamazaki Y, Fujita H, Kobayashi T, Choi Y, Scott HS, Matsumoto M, et al. Medullary thymic epithelial cells expressing Aire represent a unique lineage derived from cells expressing claudin. Nat Immunol. 2007;8(3):304–11.

84. Sekai M, Hamazaki Y, Minato N. Medullary thymic epithelial stem cells maintain a functional thymus to ensure lifelong central T cell tolerance. Immunity [Internet]. 2014;41(5):753–61.

85. Baik S, Sekai M, Hamazaki Y, Jenkinson WE, Anderson G. Relb acts downstream of medullary thymic epithelial stem cells and is essential for the emergence of RANK+ medullary epithelial progenitors. Eur J Immunol. 2016;46(4):857–62.

86. Burkly L, Hession C, Ogata L, Reilly C, Marconl LA, Olson D, et al. Expression of relB is required for the development of thymic medulla and dendritic cells. Nature. 1995;373(6514):531–6.

87. Kadouri N, Nevo S, Goldfarb Y, Abramson J. Thymic epithelial cell heterogeneity: TEC by TEC. Nat Rev Immunol [Internet]. 2020;20(4):239–53.

88. Rossi SW, Kim MY, Leibbrandt A, Parnell SM, Jenkinson WE, Glanville SH, et al. RANK signals from CD4+3- inducer cells regulate development of Aire-expressing epithelial cells in the thymic medulla. J Exp Med. 2007;204(6):1267–72.

89. Hikosaka Y, Nitta T, Ohigashi I, Yano K, Ishimaru N, Hayashi Y, et al. The Cytokine RANKL Produced by Positively Selected Thymocytes Fosters Medullary Thymic Epithelial Cells that Express Autoimmune Regulator. Immunity [Internet]. 2008 Sep;29(3):438–50.

90. Desanti GE, Cowan JE, Baik S, Parnell SM, White AJ, Penninger JM, et al. Developmentally Regulated Availability of RANKL and CD40 Ligand Reveals Distinct Mechanisms of Fetal and Adult Cross-Talk in the Thymus Medulla. J Immunol. 2012;189(12):5519–26.

91. White AJ, Jenkinson WE, Cowan JE, Parnell SM, Bacon A, Jones ND, et al. An Essential Role for Medullary Thymic Epithelial Cells during the Intrathymic Development of Invariant NKT Cells. J Immunol. 2014;192(6):2659–66.

92. Akiyama T, Shimo Y, Yanai H, Qin J, Ohshima D, Maruyama Y, et al. The Tumor Necrosis Factor Family Receptors RANK and CD40 Cooperatively Establish the Thymic Medullary Microenvironment and Self-Tolerance. Immunity. 2008;29(3):423–37.

93. Mccarthy NI, Cowan JE, Nakamura K, Bacon A, Baik S, White AJ, et al. Osteoprotegerin-Mediated Homeostasis of Rank+ Thymic Epithelial Cells Does Not Limit Foxp3+ Regulatory T Cell Development. J Immunol. 2015;195(6):2675–82.

94. Boehm T, Scheu S, Pfeffer K, Bleul CC. Thymic Medullary Epithelial Cell Differentiation, Thymocyte Emigration, and the Control of Autoimmunity Require Lympho–Epithelial Cross Talk via LTβR. J Exp Med [Internet]. 2003 Sep 1;198(5):757–69.

95. Wu W, Shi Y, Xia H, Chai Q, Jin C, Ren B, et al. Epithelial LTβR signaling controls the population size of the progenitors of medullary thymic epithelial cells in neonatal mice. Sci Rep. 2017;7(March):1–11.

96. Cosway EJ, Lucas B, James KD, Parnell SM, Carvalho-Gaspar M, White AJ, et al. Redefining thymus medulla specialization for central tolerance. J Exp Med. 2017;214(11):3183–95.

97. Martins VC, Boehm T, Bleul CC. Ltbr Signaling Does Not Regulate Aire-Dependent Transcripts. J Immunol. 2008;181(1):400–7.

98. James KD, Cosway EJ, Lucas B, White AJ, Parnell SM, Carvalho-Gaspar M, et al. Endothelial cells act as gatekeepers for LTβRdependent thymocyte emigration. J Exp Med. 2018;215(12):2984–93.

99. Gray D, Abramson J, Benoist C, Mathis D. Proliferative arrest and rapid turnover

of thymic epithelial cells expressing Aire. J Exp Med. 2007;204(11):2521–8.

100. Ueno T, Saito F, Gray DHD, Kuse S, Hieshima K, Nakano H, et al. CCR7 signals are essential for cortex-medulla migration of developing thymocytes. J Exp Med. 2004;200(4):493–505.

101. Lkhagvasuren E, Sakata M, Ohigashi I, Takahama Y. Lymphotoxin β Receptor Regulates the Development of CCL21-Expressing Subset of Postnatal Medullary Thymic Epithelial Cells. J Immunol. 2013;190(10):5110–7.

102. Metzger TC, Khan IS, Gardner JM, Mouchess ML, Johannes KP, Krawisz AK, et al. Lineage Tracing and Cell Ablation Identify a Post-Aire-Expressing Thymic Epithelial Cell Population. Cell Rep [Internet]. 2013 Oct;5(1):166–79.

103. Miller CN, Proekt I, von Moltke J, Wells KL, Rajpurkar AR, Wang H, et al. Thymic tuft cells promote an IL-4-enriched medulla and shape thymocyte development. Nature [Internet]. 2018 Jul 18;559(7715):627–31.

104. Lucas B, White AJ, Cosway EJ, Parnell SM, James KD, Jones ND, et al. Diversity in medullary thymic epithelial cells controls the activity and availability of iNKT cells. Nat Commun [Internet]. 2020;11(1):1–14.

105. Plotkin J, Prockop SE, Lepique A, Petrie HT. Critical Role for CXCR4 Signaling in Progenitor Localization and T Cell Differentiation in the Postnatal Thymus. J Immunol. 2003;171(9):4521–7.

106. Zlotoff DA, Sambandam A, Logan TD, Bell JJ, Schwarz BA, Bhandoola A. CCR7 and CCR9 together recruit hematopoietic progenitors to the adult thymus. Blood. 2010;115(10):1897–905.

107. Gossens K, Naus S, Corbel SY, Lin S, Rossi FMV, Kast J, et al. Thymic progenitor homing and lymphocyte homeostasis are linked via s1p-controlled expression of Thymic p-selectin/ccl25. J Exp Med. 2009;206(4):761–78.

108. Scimone ML, Aifantis I, Apostolou I, Von Boehmer H, Von Andrian UH. A multistep adhesion cascade for lymphoid progenitor cell homing to the thymus. Proc Natl Acad Sci U S A. 2006;103(18):7006–11.

109. Bunting MD, Comerford I, Seach N, Hammett M V., Asquith DL, Körner H, et al. CCX-CKR deficiency alters thymic stroma impairing thymocyte development and promoting autoimmunity. Blood [Internet]. 2013;121(1):118–28.

110. Ulvmar MH, Werth K, Braun A, Kelay P, Hub E, Eller K, et al. The atypical chemokine receptor CCRL1 shapes functional CCL21 gradients in lymph nodes. Nat Immunol. 2014;15(7):623–30.

111. Heinzel K, Benz C, Bleul CC. A silent chemokine receptor regulates steady-state leukocyte homing in vivo. Proc Natl Acad Sci U S A. 2007;104(20):8421–6.

112. Lucas B, White AJ, Ulvmar MH, Nibbs RJB, Sitnik KM, Agace WW, et al. CCRL1/ACKR4 is expressed in key thymic microenvironments but is dispensable for T lymphopoiesis at steady state in adult mice. Eur J Immunol. 2015;45(2):574–83.

113. Koch U, Fiorini E, Benedito R, Besseyrias V, Schuster-Gossler K, Pierres M, et al. Delta-like 4 is the essential, nonredundant ligand for Notchl during thymic T cell lineage commitment. J Exp Med. 2008;205(11):2515–23.

114. Buono M, Facchini R, Matsuoka S, Thongjuea S, Waithe D, Luis TC, et al. A dynamic niche provides Kit ligand in a stage-specific manner to the earliest thymocyte progenitors. Nat Cell Biol. 2016;18(2):157–67.

115. Balciunaite G, Ceredig R, Fehling HJ, Zúñiga-Pflücker JC, Rolink AG. The role of Notch and IL-7 signaling in early thymocyte proliferation and differentiation. Eur J Immunol. 2005;35(4):1292–300.

116. Janas ML, Varano G, Gudmundsson K, Noda M, Nagasawa T, Turner M. Thymic development beyond β-selection requires phosphatidylinositol 3-kinase activation by CXCR4. J Exp Med. 2010;207(1):247–61.

117. Murata S, Sasaki K, Kishimoto T, Niwa S i., Hayashi H, Takahama Y, et al. Regulation of CD8+ T Cell Development by Thymus-Specific Proteasomes. Science (80-). 2007 Jun 1;316(5829):1349–53.

118. Nitta T, Murata S, Sasaki K, Fujii H, Ripen AM, Ishimaru N, et al. Thymoproteasome Shapes Immunocompetent Repertoire of CD8+ T Cells. Immunity [Internet]. 2010;32(1):29–40.

119. Takada K, Van Laethem F, Xing Y, Akane K, Suzuki H, Murata S, et al. TCR affinity for thymoproteasome-dependent positively selecting peptides conditions antigen responsiveness in CD8+ T cells. Nat Immunol. 2015;16(10):1069–76.

120. Honey K, Nakagawa T, Peters C, Rudensky A. Cathepsin L regulates CD4+ T cell selection independently of its effect on invariant chain: A role in the generation of positively selecting peptide ligands. J Exp Med. 2002;195(10):1349–58.

121. Bowlus CL, Ahn J, Chu T, Gruen JR. Cloning of a novel MHC-encoded serine peptidase highly expressed by cortical epithelial cells of the thymus. Cell Immunol. 1999;196(2):80–6.

122. Gommeaux J, Grégoire C, Nguessan P, Richelme M, Malissen M, Guerder S, et al. Thymus-specific serine protease regulates positive selection of a subset of CD4+ thymocytes. Eur J Immunol. 2009;39(4):956–64.

123. Nedjic J, Aichinger M, Emmerich J, Mizushima N, Klein L. Autophagy in thymic epithelium shapes the T-cell repertoire and is essential for tolerance. Nature. 2008;455(7211):396–400.

124. Liu H, Jain R, Guan J, Vuong V, Ishido S, La Gruta NL, et al. Ubiquitin ligase MARCH 8 cooperates with CD83 to control surface MHC II expression in thymic epithelium and CD4 T cell selection. J Exp Med. 2016;213(9):1695–703.

125. Wekerle H, Ketelsen UP. Thymic nurse cells-Ia-bearing epithelium involved in T-lymphocyte differentiation? Nature. 1980;283(5745):402–4.

126. Nakagawa Y, Ohigashi I, Nitta T, Sakata M, Tanaka K, Murata S, et al. Thymic nurse cells provide microenvironment for secondary T cell receptor α

rearrangement in cortical thymocytes. Proc Natl Acad Sci U S A. 2012;109(50):20572–7.

127. Kozai M, Kubo Y, Katakai T, Kondo H, Kiyonari H, Schaeuble K, et al. Essential role of CCL21 in establishment of central selftolerance in T cells. J Exp Med. 2017;214(7):1925–35.

128. Derbinski J, Schulte A, Kyewski B, Klein L. Promiscuous gene expression in medullary thymic epithelial cells mirrors the peripheral self. Nat Immunol [Internet]. 2001 Nov 15;2(11):1032–9.

129. Danan-Gotthold M, Guyon C, Giraud M, Levanon EY, Abramson J. Extensive RNA editing and splicing increase immune self-representation diversity in medullary thymic epithelial cells. Genome Biol [Internet]. 2016;17(1):1–13.

130. Takahama Y, Ohigashi I, Baik S, Anderson G. Generation of diversity in thymic epithelial cells. Nat Rev Immunol. 2017;17(5):295–305.

131. Cloosen S, Arnold J, Thio M, Bos GMJ, Kyewski B, Germeraad WTV. Expression of tumor-associated differentiation antigens, MUC1 glycoforms and CEA, in human thymic epithelial cells: Implications for self-tolerance and tumor therapy. Cancer Res. 2007;67(8):3919–26.

132. Anderson MS, Venanzi ES, Klein L, Chen Z, Berzins SP, Turley SJ, et al. Projection of an immunological self shadow within the thymus by the aire protein. Science (80-). 2002;298(5597):1395–401.

133. Ramsey C. Aire deficient mice develop multiple features of APECED phenotype and show altered immune response. Hum Mol Genet. 2002 Feb 1;11(4):397–409.

134. Nagamine K, Peterson P, Scott HS, Kudoh J, Minoshima S, Heino M, et al. Positional cloning of the APECED gene. Nat Genet. 1997;17(4):393–8.

135. Chuprin A, Avin A, Goldfarb Y, Herzig Y, Levi B, Jacob A, et al. The deacetylase Sirt1 is an essential regulator of Aire-mediated induction of central immunological tolerance. Nat Immunol. 2015;16(7):737–45.

136. Derbinski J, Gäbler J, Brors B, Tierling S, Jonnakuty S, Hergenhahn M, et al. Promiscuous gene expression in thymic epithelial cells is regulated at multiple levels. J Exp Med. 2005;202(1):33–45.

137. Takaba H, Morishita Y, Tomofuji Y, Danks L, Nitta T, Komatsu N, et al. Fezf2 Orchestrates a Thymic Program of Self-Antigen Expression for Immune Tolerance. Cell. 2015 Nov;163(4):975–87.

138. Lei Y, Ripen AM, Ishimaru N, Ohigashi I, Nagasawa T, Jeker LT, et al. Aire-dependent production of XCL1 mediates medullary accumulation of thymic dendritic cells and contributes to regulatory T cell development. J Exp Med. 2011;208(2):383–94.

139. Li J, Park J, Foss D, Goldschneider I. Thymus-homing peripheral dendritic cells constitute two of the three major subsets of dendritic cells in the steady-state thymus. J Exp Med. 2009;206(3):607–22.

140. Wu L, Shortman K. Heterogeneity of thymic dendritic cells. Semin Immunol. 2005;17:304–12.

141. Ardavin C, Wu L, Li CL, Shortman K. Thymic dendritic cells and T cells develop simultaneously in the thymus from a common precursor population. Nature [Internet]. 1993 Apr 17;362(6422):761–3.

142. Schlenner SM, Madan V, Busch K, Tietz A, Läufle C, Costa C, et al. Fate Mapping Reveals Separate Origins of T Cells and Myeloid Lineages in the Thymus. Immunity. 2010;32(3):426–36.

143. Liu K, Victora GD, Schwickert TA, Guermonprez P, Meredith MM, Yao K, et al. In Vivo Analysis of Dendritic Cell Development and Homeostasis. Science (80-) [Internet]. 2009 Apr 17;324(5925):392–7.

144. Cosway EJ, Ohigashi I, Schauble K, Parnell SM, Jenkinson WE, Luther S, et al. Formation of the Intrathymic Dendritic Cell Pool Requires CCL21-Mediated Recruitment of CCR7+ Progenitors to the Thymus. J Immunol. 2018;201(2):516–23.

145. Gallegos AM, Bevan MJ. Central Tolerance to Tissue-specific Antigens Mediated by Direct and Indirect Antigen Presentation The Journal of Experimental Medicine. J Exp Med. 2004;200(8):1039–1049.

146. Perry JSA, Lio CWJ, Kau AL, Nutsch K, Yang Z, Gordon JI, et al. Distinct Contributions of Aire and Antigen-Presenting-Cell Subsets to the Generation of Self-Tolerance in the Thymus. Immunity [Internet]. 2014 Sep;41(3):414–26.

147. Hadeiba H, Lahl K, Edalati A, Oderup C, Habtezion A, Pachynski R, et al. Article Plasmacytoid Dendritic Cells Transport Peripheral Antigens to the Thymus to Promote Central Tolerance. Immunity. 2012;36(3):438–50.

148. Baba T, Nakamoto Y, Mukaida N, Alerts E. Crucial Contribution of Thymic Sirp α+ Conventional Dendritic Cells to Central Tolerance against Blood-Borne Antigens in a CCR2-Dependent Manner. J Immunol. 2009;183:3053–63.

149. Bonasio R, Scimone ML, Schaerli P, Grabie N, Lichtman AH, von Andrian UH. Clonal deletion of thymocytes by circulating dendritic cells homing to the thymus. Nat Immunol. 2006;7(10):1092–100.

150. Bhandoola A, Sambandam A. From stem cell to T cell: One route or many? Nat Rev Immunol. 2006;6(2):117–26.

151. Krueger A. Thymus Colonization: Who, How, How Many? Arch Immunol Ther Exp (Warsz) [Internet]. 2018;66(2):81–8.

152. Bhandoola A, von Boehmer H, Petrie HT, Zúñiga-Pflücker JC. Commitment and Developmental Potential of Extrathymic and Intrathymic T Cell Precursors: Plenty to Choose from. Immunity. 2007;26(6):678–89.

153. Ikuta K, Weissman IL. Evidence that hematopoietic stem cells express mouse c-kit but do not depend on steel factor for their generation. ProcNatlAcadSci, USA. 1992;89(4):1502–6.

154. Adolfsson J, Borge OJ, Bryder D, Theilgaard-Mönch K, Åstrand-Grundström I, Sitnicka E, et al. Upregulation of Flt3 Expression within the Bone Marrow Lin−Sca1+c-kit+ Stem Cell Compartment Is Accompanied by Loss of Self-Renewal Capacity. Immunity [Internet]. 2001 Oct;15(4):659–69.

155. Kondo M, Weissman IL, Akashi K. Identification of clonogenic common lymphoid progenitors in mouse bone marrow. Cell. 1997;91(5):661–72.

156. Sitnicka E, Bryder D, Theilgaard-Mönch K, Buza-Vidas N, Adolfsson J, Jacobsen SEW. Key role of flt3 ligand in regulation of the common lymphoid progenitor but not in maintenance of the hematopoietic stem cell pool. Immunity. 2002;17(4):463–72.

157. Schwarz BA, Bhandoola A. Circulating hematopoietic progenitors with T lineage potential. Nat Immunol. 2004;5(9):953–60.

158. Schwarz BA, Sambandam A, Maillard I, Harman BC, Love PE, Bhandoola A. Selective Thymus Settling Regulated by Cytokine and Chemokine Receptors. J Immunol. 2007;178(4):2008–17.

159. Umland O, Mwangi WN, Anderson BM, Walker JC, Petrie HT. The Blood Contains Multiple Distinct Progenitor Populations with Clonogenic B and T Lineage Potential. J Immunol. 2007;178(7):4147–52.

160. Saran N, Łyszkiewicz M, Pommerencke J, Witzlau K, Vakilzadeh R, Ballmaier M, et al. Multiple extrathymic precursors contribute to T-cell development with different kinetics. Blood. 2010;115(6):1137–44.

161. Lind EF, Prockop SE, Porritt HE, Petrie HT. Mapping precursor movement through the postnatal thymus reveals specific microenvironments supporting defined stages of early lymphoid development. J Exp Med. 2001;194(2):127–34.

162. Wu L, Kincade PW, Shortman K. The CD44 expressed on the earliest intrathymic precursor population functions as a thymus homing molecule but does not bind to hyaluronate. Immunolfy Lett. 1993;38:69–75.

163. Rossi FMV, Corbel SY, Merzaban JS, Carlow DA, Gossens K, Duenas J, et al. Recruitment of adult thymic progenitors is regulated by P-selectin and its ligand PSGL-1. Nat Immunol. 2005;6(6):626–34.

164. Shi Y, Wu W, Chai Q, Li Q, Hou Y, Xia H, et al. LTβR controls thymic portal endothelial cells for haematopoietic progenitor cell homing and T-cell regeneration. Nat Commun. 2016;7.

165. Lucas B, James KD, Cosway EJ, Parnell SM, Tumanov A V., Ware CF, et al. Lymphotoxin β Receptor Controls T Cell Progenitor Entry to the Thymus. J Immunol. 2016;197(7):2665–72.

166. Calderón L, Boehm T. Three chemokine receptors cooperatively regulate homing of hematopoietic progenitors to the embryonic mouse thymus. Proc Natl Acad Sci U S A. 2011;108(18):7517–22.

167. Shah DK, Zúñiga-Pflücker JC. An Overview of the Intrathymic Intricacies of T Cell Development. J Immunol. 2014;192(9):4017–23.

168. Porritt HE, Gordon K, Petrie HT. Kinetics of steady-state differentiation and mapping of intrathymic-signaling environments by stem cell transplantation in nonirradiated mice. J Exp Med. 2003;198(6):957–62.

169. Trampont PC, Tosello-Trampont AC, Shen Y, Duley AK, Sutherland AE, Bender TP, et al. CXCR4 acts as a costimulator during thymic β-selection. Nat Immunol. 2010;11(2):162–70.

170. Porritt HE, Rumfelt LL, Tabrizifard S, Schmitt TM, Zúñiga-Pflücker JC, Petrie HT. Heterogeneity among DN1 prothymocytes reveals multiple progenitors with different capacities to generate T cell and non-T cell lineages. Immunity. 2004;20(6):735–45.

171. Masuda K, Kakugawa K, Nakayama T, Minato N, Katsura Y, Kawamoto H. T Cell Lineage Determination Precedes the Initiation of TCR β Gene Rearrangement . J Immunol. 2007;179(6):3699–706.

172. Dudley EC, Petrie HT, Shah LM, Owen MJ, Hayday AC. T cell receptor β chain gene rearrangement and selection during thymocyte development in adult mice. Immunity. 1994;1(2):83–93.

173. Davis MM, Bjorkman PJ. The T cell receptor genes and T-cell recognition. Nature. 1988;334:395–402.

174. Fehling HJ, Krotkova A, Saint-Ruf C, von Boehmer H. Crucial role of the pre-T-cell receptor α gene in development of αβ but not γδ T cells. Nature [Internet]. 1995 Jun 29;375(6534):795–8.

175. Yamasaki S, Ishikawa E, Sakuma M, Ogata K, Sakata-Sogawa K, Hiroshima M, et al. Mechanistic basis of pre-T cell receptor-mediated autonomous signaling critical for thymocyte development. Nat Immunol. 2006;7(1):67–75.

176. Irving BA, Alt FW, Killeen N. Thymocyte development in the absence of pre-T cell receptor extracellular immunoglobulin domains. Science (80-). 1998;280(5365):905–8.

177. Falk I, Nerz G, Haidl I, Krotkova A, Eichmann K. Immature thymocytes that fail to express TCRβ and/or TCRγδ proteins die by apoptotic cell death in the CD44-CD25- (DN4) subset. Eur J Immunol. 2001;31(11):3308–17.

178. Taghon T, Yui MA, Pant R, Diamond RA, Rothenberg E V. Developmental and molecular characterization of emerging β- and γδ-selected pre-T cells in the adult mouse thymus. Immunity. 2006;24(1):53–64.

179. Ciofani M, Zúñiga-Pflücker JC. The thymus as an inductive site for T lymphopoiesis. Annu Rev Cell Dev Biol. 2007;23:463–93.

180. Starr TK, Jameson SC, Hogquist KA. Positive and Negative Selection of T Cells. Annu Rev Immunol. 2003;21(1):139–76.

181. Witt CM, Raychaudhuri S, Schaefer B, Chakraborty AK, Robey EA. Directed migration of positively selected thymocytes visualized in real time. PLoS Biol. 2005;3(6):1062–9.

182. Dzhagalov I, Phee H. How to find your way through the thymus: a practical guide for aspiring T cells. Cell Mol Life Sci [Internet]. 2012 Mar 14;69(5):663–82.

183. Brandle D, Muller C, Rulicke T, Hengartner H, Pircher H. Engagement of the T-cell receptor during positive selection in the thymus down-regulates RAG-1 expression. Proc Natl Acad Sci U S A. 1992;89(20):9529–33.

184. Sun Z, Unutmaz D, Zou YR, Sunshine MJ, Pierani A, Brenner-Morton S, et al. Requirement for RORγ in thymocyte survival and lymphoid organ development. Science (80-). 2000;288(5475):2369–73.

185. Ma A, Pena JC, Chang B, Margosian E, Davidson L, Alt FW, et al. Bclx regulates the survival of double-positive thymocytes. Proc Natl Acad Sci U S A. 1995;92(11):4763–7.

186. Singer A, Adoro S, Park JH. Lineage fate and intense debate: myths, models and mechanisms of CD4- versus CD8-lineage choice. Nat Rev Immunol. 2008 Oct;8(10):788–801.

187. Seong RH, Chamberlain JW, Parnes JR. Signal for T-cell differentiation to a CD4 cell lineage is delivered by CD4 transmembrane region and/or cytoplasmic tail. Nature. 1992;356(6371):718–20.

188. Itano A, Salmon P, Kioussis D, Tolaini M, Corbella P, Robey E. The cytoplasmic domain of CD4 promotes the development of CD4 lineage T cells. J Exp Med [Internet]. 1996 Mar 1;183(3):731–41.

189. Wiest DL, Yuan L, Jefferson J, Benveniste P, Tsokos M, Klausner RD, et al. Regulation of T cell receptor expression in imrnature CD4+CD8+ thymocytes by p56lck tyrosine kinase: Basis for differential signaling by CD4 and CD8 in immature thymocytes expressing both coreceptor molecules. J Exp Med. 1993;178(5):1701–12.

190. Yasutomo K, Doyle C, Miele L, Germain RN. The duration of antigen receptor signalling determines CD4+ versus CD8+ T-cell lineage fate. Nature. 2000;404(6777):506–10.

191. Brugnera E, Bhandoola A, Cibotti R, Yu Q, Guinter TI, Yamashita Y, et al. Coreceptor reversal in the thymus: Signaled CD4+8+ thymocytes initially terminate CD8 transcription even when differentiating into CD8+ T cells. Immunity. 2000;13(1):59–71.

192. Singer A. New perspectives on a developmental dilemma: The kinetic signaling model and the importance of signal duration for the CD4/CD8 lineage decision. Curr Opin Immunol. 2002;14(2):207–15.

193. Davis CB, Killeen N, Crooks MEC, Raulet D, Littman DR. Evidence for a stochastic mechanism in the differentiation of mature subsets of T lymphocytes. Cell. 1993;73(2):237–47.

194. Chan SH, Cosgrove D, Waltzinger C, Benoist C, Mathis D. Another view of the selective model of thymocyte selection. Cell. 1993;73(2):225–36.

195. Yu Q, Erman B, Bhandoola A, Sharrow SO, Singer A. In vitro evidence that

cytokine receptor signals are required for differentiation of double positive thymocytes into functionally mature CD8+ T cells. J Exp Med. 2003;197(4):475–87.

196. Sun G, Liu X, Mercado P, Jenkinson SR, Kypriotou M, Feigenbaum L, et al. The zinc finger protein cKrox directs CD4 lineage differentiation during intrathymic T cell positive selection. Nat Immunol. 2005;6(4):373–81.

197. He X, Dave V, Zhang Y, Hua X, Nicolas E, Xu W, et al. The zinc finger transcription factor Th-POK regulates CD4 versus CD8 T-cell lineage commitment. Nature [Internet]. 2005;433(7028):826–33.

198. Taniuchi I, Osato M, Egawa T, Sunshine MJ, Bae SC, Komori T, et al. Differential requirements for Runx proteins in CD4 repression and epigenetic silencing during T lymphocyte development. Cell. 2002;111(5):621–33.

199. Sato T, Ohno SI, Hayashi T, Sato C, Kohu K, Satake M, et al. Dual functions of runx proteins for reactivating CD8 and silencing CD4 at the commitment process into CD8 thymocytes. Immunity. 2005;22(3):317–28.

200. Jenkinson SR, Intlekofer AM, Sun G, Feigenbaum L, Reiner SL, Bosselut R. Expression of the transcription factor cKrox in peripheral CD8 T cells reveals substantial postthymic plasticity in CD4-CD8 lineage differentiation. J Exp Med. 2007;204(2):267–72.

201. Saini M, Sinclair C, Marshall D, Tolaini M, Sakaguchi S, Seddon B. Regulation of Zap70 expression during thymocyte development enables temporal separation of CD4 and CD8 repertoire selection at different signaling thresholds. Sci Signal. 2010;3(114).

202. Yin X, Ladi E, Chan SW, Li O, Killeen N, Kappes DJ, et al. CCR7 Expression in Developing Thymocytes Is Linked to the CD4 versus CD8 Lineage Decision. J Immunol. 2007;179(11):7358–64.

203. Kurd N, Robey EA. T-cell selection in the thymus: a spatial and temporal perspective. Immunol Rev. 2016 May;271(1):114–26.

204. Kurobe H, Liu C, Ueno T, Saito F, Ohigashi I, Seach N, et al. CCR7-dependent cortex-to-medulla migration of positively selected thymocytes is essential for establishing central tolerance. Immunity. 2006;24(2):165–77.

205. Norment AM, Bogatzki LY, Gantner BN, Bevan MJ. Murine CCR9, a Chemokine Receptor for Thymus-Expressed Chemokine That Is Up-Regulated Following Pre-TCR Signaling. J Immunol. 2000;164(2):639–48.

206. Choi YI, Duke-Cohan JS, Ahmed WB, Handley MA, Mann F, Epstein JA, et al. PlexinD1 Glycoprotein Controls Migration of Positively Selected Thymocytes into the Medulla. Immunity. 2008 Dec;29(6):888–98.

207. Cowan JE, Parnell SM, Nakamura K, Caamano JH, Lane PJL, Jenkinson EJ, et al. The thymic medulla is required for Foxp3+ regulatory but not conventional CD4+ thymocyte development. J Exp Med. 2013;210(4):675–81.

208. Dzhagalov IL, Chen KG, Herzmark P, Robey EA. Elimination of Self-Reactive T

Cells in the Thymus: A Timeline for Negative Selection. PLoS Biol. 2013;11(5).

209. Klein L, Jovanovic K. Regulatory T cell lineage commitment in the thymus. Semin Immunol [Internet]. 2011;23(6):401–9.

210. Daniels MA, Teixeiro E, Gill J, Hausmann B, Roubaty D, Holmberg K, et al. Thymic selection threshold defined by compartmentalization of Ras/MAPK signalling. Nature. 2006;444(7120):724–9.

211. McNeil LK, Starr TK, Hogquist KA. A requirement for sustained ERK signaling during thymocyte positive selection in vivo. Proc Natl Acad Sci U S A. 2005;102(38):13574–9.

212. Gong Q, Cheng AM, Akk AM, Alberola-lla J, Gong G, Pawson T, et al. Disruption of T cell signaling networks and development by Grb2 haploid insufficiency. Nat Immunol. 2001;2(1):29–36.

213. Stritesky GL, Xing Y, Erickson JR, Kalekar LA, Wang X, Mueller DL, et al. Murine thymic selection quantified using a unique method to capture deleted T cells. Proc Natl Acad Sci U S A. 2013;110(12):4679–84.

214. Burchill MA, Yang J, Vogtenhuber C, Blazar BR, Farrar MA. IL-2 Receptor β-Dependent STAT5 Activation Is Required for the Development of Foxp3 + Regulatory T Cells . J Immunol. 2007;178(1):280–90.

215. Lio CW, Hsieh CS. A 2 step process for thymic Treg development. Immunity [Internet]. 2008;28(1):100–11.

216. Tai X, Erman B, Alag A, Mu J, Kimura M, Katz G, et al. Foxp3 Transcription Factor Is Proapoptotic and Lethal to Developing Regulatory T Cells unless Counterbalanced by Cytokine Survival Signals. Immunity [Internet]. 2013 Jun;38(6):1116–28.

217. Weih F, Carrasco D, Durham SK, Barton DS, Rizzo CA, Ryseck RP, et al. Multiorgan inflammation and hematopoietic abnormalities in mice with a targeted disruption of RelB, a member of the NF-κB/Rel family. Cell. 1995;80(2):331–40.

218. McCaughtry TM, Baldwin TA, Wilken MS, Hogquist KA. Clonal deletion of thymocytes can occur in the cortex with no involvement of the medulla. J Exp Med. 2008;205(11):2575–84.

219. Cosway EJ, James KD, Lucas B, Anderson G, White AJ. The thymus medulla and its control of αβT cell development. Semin Immunopathol. 2021;43(1):15–27.

220. Ramsdell F, Jenkins M, Dinh Q, Fowlkes BJ, Ramsdell F, Jenkins M, et al. The majority of CD4 + 8- thymocytes are functionally immature. J Immunol [Internet]. 1991;147(6):1779–85.

221. Reichert RA, Weissman IL, Butcher EC. Phenotypic analysis of thymocytes that express homing receptors for peripheral lymph nodes. J Immunol [Internet]. 1986;136(10):3521–8.

222. Takahama Y. Journey through the thymus: Stromal guides for T-cell

development and selection. Nat Rev Immunol. 2006;6(2):127–35.

223. Carlson CM, Endrizzi BT, Wu J, Ding X, Weinreich MA, Walsh ER, et al. Kruppel-like factor 2 regulates thymocyte and T-cell migration. Nature. 2006;442(7100):299–302.

224. Feng C, Woodside KJ, Vance BA, El-Khoury D, Canelles M, Lee J, et al. A potential role for CD69 in thymocyte emigration. Int Immunol. 2002;14(6):535–44.

225. Yu W, Nagaoka H, Jankovic M, Misulovin Z, Suh H, Rolink A, et al. Continued RAG expression in late stages of B cell development and no apparent re-induction after immunization. Nature. 1999;400(6745):682–7.

226. Boursalian TE, Golob J, Soper DM, Cooper CJ, Fink PJ. Continued maturation of thymic emigrants in the periphery. Nat Immunol. 2004;5(4):418–25.

227. McCaughtry TM, Wilken MS, Hogquist KA. Thymic emigration revisited. J Exp Med. 2007;204(11):2513–20.

228. Xing Y, Wang X, Jameson SC, Hogquist KA. Late stages of T cell maturation in the thymus involve NF- kappa B and tonic type I interferon signaling. Nat Immunol. 2016;17(5).

229. Allende ML, Dreier JL, Mandala S, Proia RL. Expression of the Sphingosine 1-Phosphate Receptor , S1P 1 , on T-cells Controls Thymic Emigration. J Biol Chem. 2004;279(15):15396–401.

230. Cowan JE, McCarthy NI, Parnell SM, White AJ, Bacon A, Serge A, et al. Differential Requirement for CCR4 and CCR7 during the Development of Innate and Adaptive αβT Cells in the Adult Thymus. J Immunol. 2014;193(3):1204–12.

231. Staton TL, Habtezion A, Winslow MM, Sato T, Love PE, Butcher EC. CD8+ recent thymic emigrants home to and efficiently repopulate the small intestine epithelium. Nat Immunol. 2006;7(5):482–8.

232. Fabre S, Carrette F, Chen J, Lang V, Semichon M, Denoyelle C, et al. FOXO1 Regulates L-Selectin and a Network of Human T Cell Homing Molecules Downstream of Phosphatidylinositol 3-Kinase. J Immunol. 2008;181(5):2980–9.

233. Bai A, Hu H, Yeung M, Chen J. Krüppel-Like Factor 2 Controls T Cell Trafficking by Activating L-Selectin (CD62L) and Sphingosine-1-Phosphate Receptor 1 Transcription. J Immunol. 2007;178(12):7632–9.

234. Bankovich AJ, Shiow LR, Cyster JG. CD69 suppresses sphingosine 1-phosophate receptor-1 (S1P1) function through interaction with membrane helix 4. J Biol Chem. 2010;285(29):22328–37.

235. Zachariah MA, Cyster JG. Neural crest-derived pericytes promote egress of mature thymocytes at the corticomedullary junction. Science (80-). 2010;328(5982):1129–35.

236. Rosen H, Alfonso C, Surh CD, McHeyzer-Williams MG. Rapid induction of medullary thymocyte phenotypic maturation and egress inhibition by nanomolar

sphingosine 1-phosphate receptor agonist. Proc Natl Acad Sci U S A. 2003;100(19):10907–12.

237. Brinkmann V, Davis MD, Heise CE, Albert R, Cottens S, Hof R, et al. The immune modulator FTY720 targets sphingosine 1-phosphate receptors. J Biol Chem [Internet]. 2002;277(24):21453–7.

238. Yagi H, Kamba R, Chiba K, Soga H, Yaguchi K, Nakamura M, et al. Immunosuppressant FTY720 inhibits thymocyte emigration. Eur J Immunol. 2000;30(5):1435–44.

239. Bréart B, Ramos-Perez WD, Mendoza A, Salous AK, Gobert M, Huang Y, et al. Lipid phosphate phosphatase 3 enables efficient thymic egress. J Exp Med. 2011;208(6):1267–78.

240. Zamora-Pineda J, Kumar A, Suh JH, Zhang M, Saba JD. Dendritic cell sphingosine-1-phosphate lyase regulates thymic egress. J Exp Med. 2016;213(12):2773–91.

241. Scollay R, Godfrey DI. Thymic emigration: conveyor belts or lucky dips? Immunol Today. 1995;16(6):268–73.

242. James KD, Jenkinson WE, Anderson G. T-cell egress from the thymus : Should I stay or should I go ? J Leukoc Biol. 2018;104:275–84.

243. White AJ, Baik S, Parnell SM, Holland AM, Brombacher F, Jenkinson WE, et al. A type 2 cytokine axis for thymus emigration. J Exp Med. 2017;214(8):2205–16.

244. Ueno T, Hara K, Willis MS, Malin MA, Höpken UE, Gray DHD, et al. Role for CCR7 ligands in the emigration of newly generated T lymphocytes from the neonatal thymus. Immunity. 2002;16(2):205–18.

245. James KD, Legler DF, Purvanov V, Ohigashi I, Takahama Y, Parnell SM, et al. Medullary stromal cells synergize their production and capture of CCL21 for T-cell emigration from neonatal mouse thymus. Blood Adv. 2021;5(1):99–112.

246. Cowan JE, McCarthy NI, Anderson G. CCR7 Controls Thymus Recirculation, but Not Production and Emigration, of Foxp3+ T Cells. Cell Rep [Internet]. 2016;14(5):1041–8.

247. Jin R, Aili A, Wang Y, Wu J, Sun X, Zhang Y, et al. Critical role of SP thymocyte motility in regulation of thymic output in neonatal Aire-/- mice. Oncotarget. 2017;8(1):83–94.

248. Heinen P, Wanke F, Moos S, Attig S, Waisman A, Kurschus FC, et al. Improved Method to Retain Cytosolic Reporter Protein Fluorescence While Staining for Nuclear Proteins. 2014;(3).

249. Sprent J, Schaefer M. Antigen-presenting cells for unprimed T cells. Immunol Today [Internet]. 1989 Jan;10(1):17–23.

250. Sinclair C, Bains I, Yates AJ, Seddon B. Asymmetric thymocyte death underlies the CD4:CD8 T-cell ratio in the adaptive immune system. Proc Natl Acad Sci [Internet]. 2013 Jul 30;110(31):E2905–14.

251. Sim BC, Aftahi N, Reilly C, Bogen B, Schwartz RH, Gascoigne NRJ, et al. Thymic skewing of the CD4/CD8 ratio maps with the T-cell receptor α-chain locus. Curr Biol. 1998;8(12):701–4.

252. Cheroutre H, Lambolez F, Mucida D. The light and dark sides of intestinal intraepithelial lymphocytes. Nat Rev Immunol. 2011;11(7):445–56.

253. Chabannon C, Kubal J, Bondanza A, Dazzi F, Pedrazzoli P, Toubert A, et al. Hematopoietic stem cell transplantation in its 60s: A platform for cellular therapies. Sci Transl Med. 2018;10(436):1–11.

254. CONGDON CC, URSO IS. Homologous bone marrow in the treatment of radiation injury in mice. Am J Pathol. 1957;33(4):749–67.

255. Storek J, Zhao Z, Lin E, Berger T, McSweeney PA, Nash RA, et al. Recovery from and consequences of severe iatrogenic lymphopenia (induced to treat autoimmune diseases). Clin Immunol [Internet]. 2004 Dec;113(3):285–98.

256. Tan JT, Ernst B, Kieper WC, LeRoy E, Sprent J, Surh CD. Interleukin (IL)-15 and IL-7 jointly regulate homeostatic proliferation of memory phenotype CD8+ cells but are not required for memory phenotype CD4+ cells. J Exp Med. 2002;195(12):1523–32.

257. Mackall CL, Bare C V, Granger LA, Sharrow SO, Titus JA, Gress RE. Thymic-independent T cell regeneration occurs via antigen-driven expansion of peripheral T cells resulting in a repertoire that is limited in diversity and prone to skewing. J Immunol [Internet]. 1996;156(12):4609–16.

258. Hakim FT, Memon SA, Cepeda R, Jones EC, Chow CK, Kasten-Sportes C, et al. Age-dependent incidence, time course, and consequences of thymic renewal in adults. J Clin Invest. 2005;115(4):930–9.

259. Krenger W, Blazar BR, Holländer GA. Thymic T-cell development in allogeneic stem cell transplantation. Blood. 2011;117(25):6768–76.

260. Douek DC, Vescio RA, Betts MR, Brenchley JM, Hill BJ, Zhang L, et al. Assessment of thymic output in adults after haematopoietic stem-cell transplantation and prediction of T-cell reconstitution. Lancet. 2000;355(9218):1875–81.

261. Alawam AS, Cosway EJ, James KD, Lucas B, Bacon A, Parnell SM, et al. Failures in thymus medulla regeneration during immune recovery cause tolerance loss and prime recipients for auto-GVHD. J Exp Med. 2021;219(2).

262. Kelly RM, Goren EM, Taylor PA, Mueller SN, Stefanski HE, Osborn MJ, et al. Short-term inhibition of p53 combined with keratinocyte growth factor improves thymic epithelial cell recovery and enhances T-cell reconstitution after murine bone marrow transplantation. Blood. 2010;115(5):1088–97.

263. Xia H, Zhong S, Zhao Y, Ren B, Wang Z, Shi Y, et al. Thymic Egress Is Regulated by T Cell-Derived LTβR Signal and via Distinct Thymic Portal Endothelial Cells. Front Immunol. 2021;12(July):1–17.

264. Zhang SL, Wang X, Manna S, Zlotoff DA, Bryson JL, Blazar BR, et al.

Chemokine treatment rescues profound T-lineage progenitor homing defect after bone marrow transplant conditioning in mice. Blood. 2014;124(2):296–304.

265. Hogquist K, Georgiev H. Recent advances in iNKT cell development. F1000Research. 2020;9:1–10.

266. Bendelac A, Lantz O, Quimby ME, Yewdell JW, Bennink JR, Brutkiewicz RR. CD1 Recognition by Mouse NK1 + T Lymphocytes. Science (80-) [Internet]. 1995 May 12;268(5212):863–5.

267. Goldrath AW, Bogatzki LY, Bevan MJ. Naive T cells transiently acquire a memory-like phenotype during homeostasis-driven proliferation. J Exp Med. 2000;192(4):557–64.

268. Murali-Krishna K, Ahmed R. Cutting Edge: Naive T Cells Masquerading as Memory Cells. J Immunol. 2000;165(4):1733–7.

269. Cho BK, Rao VP, Ge Q, Eisen HN, Chen J. Homeostasis-stimulated proliferation drives naive T cells to differentiate directly into memory T cells. J Exp Med. 2000;192(4):549–56.

270. Min B, McHugh R, Sempowski GD, Mackall C, Foucras G, Paul WE. Neonates support lymphopenia-induced proliferation. Immunity. 2003;18(1):131–40.

271. Akue AD, Lee JY, Jameson SC. Derivation and Maintenance of Virtual Memory CD8 T Cells. J Immunol [Internet]. 2012 Mar 15;188(6):2516–23.

272. Weinreich MA, Odumade OA, Jameson SC, Hogquist KA. T cells expressing the transcription factor PLZF regulate the development of memory-like CD8+ T cells. Nat Immunol. 2010;11(8):709–16.

273. Lai D, Zhu J, Wang T, Hu-Li J, Terabe M, Berzofsky JA, et al. KLF13 sustains thymic memory-like CD8+ T cells in BALB/c mice by regulating IL-4-generating invariant natural killer T cells. J Exp Med. 2011;208(5):1093–103.

274. Lee YJ, Holzapfel KL, Zhu J, Jameson SC, Hogquist KA. Steady-state production of IL-4 modulates immunity in mouse strains and is determined by lineage diversity of iNKT cells. Nat Immunol. 2013;14(11):1146–54.

275. Scholzen T, Gerdes J. The Ki-67 protein: From the known and the unknown. J Cell Physiol. 2000;182(3):311–22.

276. Lee YJ, Wang H, Starrett GJ, Phuong V, Jameson SC, Hogquist KA. Tissue-Specific Distribution of iNKT Cells Impacts Their Cytokine Response. Immunity [Internet]. 2015;43(3):566–78.

277. Mendiratta SK, Martin WD, Hong S, Boesteanu A, Joyce S, Van Kaer L. CD1d1 mutant mice are deficient in natural T cells that promptly produce IL-4. Immunity. 1997;6(4):469–77.

278. Riou C, Dumont AR, Yassine-Diab B, Haddad EK, Sekaly RP. IL-4 influences the differentiation and the susceptibility to activation-induced cell death of human naive CD8+ T cells. Int Immunol. 2006;18(6):827–35.

279. Morrot A, Hafalla JCR, Cockburn IA, Carvalho LH, Zavala F. IL-4 receptor expression on CD8+ T cells is required for the development of protective memory responses against liver stages of malaria parasites. J Exp Med. 2005;202(4):551–60.

280. Acacia de Sa Pinheiro A, Morrot A, Chakravarty S, Overstreet M, Bream JH, Irusta PM, et al. IL-4 induces a wide-spectrum intracellular signaling cascade in CD8 + T cells . J Leukoc Biol. 2007;81(4):1102–10.

281. Wang H, Hogquist KA. CCR7 defines a precursor for murine iNKT cells in thymus and periphery. Elife. 2018;7:1–20.

282. Atherly LO, Lucas JA, Felices M, Yin CC, Reiner SL, Berg LJ. The Tec Family Tyrosine Kinases Itk and Rlk Regulate the Development of Conventional CD8 + T Cells. Immunity. 2006;38(July):79–91.

283. Felices M, Yin CC, Kosaka Y, Kang J, Berg LJ. Tec kinase Itk in γδT cells is pivotal for controlling IgE production in vivo. Proc Natl Acad Sci U S A. 2009;106(20):8308–13.

284. Garcia KC, Adams JJ, Feng D, Ely LK. The molecular basis of TCR germline bias for MHC is surprisingly simple. Nat Immunol. 2009;10(2):143–7.

285. Krovi SH, Gapin L. Revealing the TCR bias for MHC molecules. Proc Natl Acad Sci U S A. 2016;113(11):2809–11.

286. Zerrahn J, Held W, Raulet DH. The MHC reactivity of the T cell repertoire prior to positive and negative selection. Cell. 1997;88(5):627–36.

287. Parrish HL, Deshpande NR, Vasic J, Kuhns MS. Functional evidence for TCR-intrinsic specificity for MHCII. Proc Natl Acad Sci U S A. 2016;113(11):3000–5.

288. Bosselut R, Feigenbaum L, Sharrow SO, Singer A. Strength of signaling by CD4 and CD8 coreceptor tails determines the number but not the lineage direction of positively selected thymocytes. Immunity. 2001;14(4):483–94.

289. Zlotoff DA, Zhang SL, De Obaldia ME, Hess PR, Todd SP, Logan TD, et al. Delivery of progenitors to the thymus limits T-lineage reconstitution after bone marrow transplantation. Blood. 2011;118(7):1962–70.